Sediment Erosion in Hydro Turbines

Hari Prasad Neopane

This thesis is submitted to
Faculty of Engineering Science and Technology,
Norwegian University of Science and Technology (NTNU)
in partial fulfilment of the requirement of the degree of Doctor of Philosophy
Trondheim
Norway
March 2010

SUMMARY

Sediment erosion is caused by the dynamic action of sediment flowing along with water impacting against a solid surface. Hydraulic turbine components operating in sediment-laden water are subject to abrasive and erosive wear. This wear not only reduces the efficiency and the life of the turbine but also causes problems in operation and maintenance, which ultimately leads to economic losses. This is a global operation and maintenance problem of hydropower plants. The high sediment concentration combined with high percentage of quartz content in water causes severe damage to hydraulic turbine components. Withdrawal of clean water from the river for power production is expensive due to design, construction and operation of sediment settling basins. Even with the settling basins, 100 % removal of fine sediments is almost impossible and uneconomical.

A number of factors can influence the process of sediment erosion damage in hydro turbine components. The erosion intensity depends on the sediment type and its characteristics (shape, size, hardness, concentration etc.), hydraulic design and operating conditions of turbine (flow rate, head, rotational speed, velocity, acceleration, turbulence, impingement angle etc.), and material used for the turbine components. All these factors are needed to be considered for predicting the erosion. Therefore, dealing with sediment erosion problems requires a multidisciplinary approach. More research and development is needed to investigate the relationship between the particle movement and erosion inside a turbine and to establish the operating strategy for the turbine operating in sediment-laden water.

In order to achieve the main objective of this PhD study, the overall research methodology adopted for this work 'sediment erosion in hydro turbines' include; experimental studies, numerical simulation, and field studies. This research work is based on result from laboratory experiment, and numerical simulation.

A previously made test rig (Thapa, 2004), was reviewed and modified to create a strong swirl flow in curved path. This flow was found similar to the flow between the guide vane outlet and the runner inlet of a Francis turbine. The flow in the guide vane cascade was simulated in order to verify the particle separation process and to investigate the relation of the velocity and the drag coefficient with different shape and size of the particle. There was a provision to introduce particles, with sizes ranging from 1 to 10 mm, and to observe the motion of the particles from Plexiglas windows located on the cover of the tank using a high-speed digital camera. When a particle is flowing in swirl flow, drag force and centrifugal force are two major forces influencing the particle equilibrium. The equilibrium of these two forces provides a critical diameter of the particle. While, a particle larger than the critical diameter move away from the centre and hit the wall, a particle smaller than the critical diameter flows along with the water, and ultimately sinks. For critical diameter, the particle continues to rotate in the turbine. Different shapes and sizes of particles were tested with the same operating conditions

and found that triangularly shaped particles were more likely to hit the suction side of the guide vane cascade. Furthermore, this study supports the concept of separation of particles from streamlines inside the test rig, which led to the development of an operating strategy for a Francis turbine processing sediment-laden water. This study also permitted experimental verification of the size and the shape of a particle as it orbits in the turbine, until either the velocity components are changed or the particle became smaller.

The steady state numerical simulations were carried out on the Cahua power plant Francis turbine design, mainly at two operating conditions with varying particle size, shape, and concentration using ANSYS CFX. The predictions of erosion, based on the Lagrangian calculation of particle paths in a viscous flow, are described for stay vanes, guide vanes, and runner vanes of a Francis turbine, for which the results of the field tests have been available for verification. The flow simulation was obtained through use of a commercially available computational fluids dynamics (CFD) code, namely ANSYS CFX. The code utilizes a finite-volume, multi-block approach to solve the governing equations of fluid motion numerically on a user-defined computational grid. The flow solution procedure first generates the computational grid. A pre-processor is available in the software to perform this task. Second, the solution option such as inlet and boundary conditions, turbulence model, and discretization scheme, are specified. The final step is running the flow solver to generate the actual flow field simulation.

Sediment erosion analysis of a Francis turbine gives an indication of relative erosion intensity and critical zones of erosion damage of the turbine components. The most realistic numerical prediction of erosion is found on a turbine blade. The highest velocities and accelerations occurred at outlet of the runner blade and more erosion was predicted especially at the pressure side of the blade outlet and at the lower cover. Furthermore, unexpected sediment erosion was found at the suction side of the guide vane where concept of critical diameter can be utilized. It has been concluded that if the particle size in the water is more than critical particle sizes, the turbine should not be operated at low guide vane opening.

The numerically obtained erosion pattern and the field test observation and inspection at Cahua Francis turbine components are in good qualitative agreement. The encouraging agreement shows that, for this application, numerical simulation really can be used in a predictive manner. This information may serve as an input in an early stage of turbine design process to identify the regions where special surface treatment is necessary in order to increase the lifetime of the components for new hydropower projects involving risks of sediment erosion.

The size of a particle is inversely proportional to the velocity of the particle, and it was determined that spherically shaped particles had higher settling velocities than particles with other shapes. However, non-spherical shape of the particles will tend to have lower settling velocities because both decreases in spheroid and increases in angularity tend to decrease velocities. Moreover, larger cross-sectional areas tend to be directed perpendicular to the transport path. As a result, higher coefficient of drag, higher

rotational motion and more separation of flow are likely to occur and hence more erosion rate was predicted. The roles played by the shape of the particle significantly affect erosion rate prediction inside the Francis turbine components.

Furthermore, it has been found that the erosion process is strongly dependent on the particle size, shape, concentration, and operating conditions of the turbine. The reduction of the erosion is not only linked to the reduction of particle velocity but also is linked to the reduction of separation of flow, which further depends on shape, size, and concentration of the particle. The significant reduction of erosion rate can be achieved by operating turbine at best efficiency point. The full load operation reduced efficiency, increased turbulence, and increased relative velocity of flow at outlet of the blades.

The present knowledge and findings, although may not be enough to deal with this problem completely, can be utilised to achieve one major step forward in sediment erosion prediction and prevention.

PREFACE AND ACKNOWLEDGEMENTS

The research presented in this thesis was mainly carried out at Waterpower Laboratory, Department of Energy and Process Engineering, Norwegian University of Science and Technology (NTNU), Norway, during the period from February 2007 to March 2010.

Professor Ole Gunnar Dahlhaug has been my main supervisor. His theoretical and practical knowledge in the field of hydropower has been huge source of help and inspiration during the course of study. He inspired me to start my academic and professional carrier in the field of hydropower in general, and sediment erosion in particular. I am indebted to him, who has not only been an advisor to me but also a guardian putting tireless efforts to guide, arrange financial support, field work, and ensuring a conducive environment for my study at Waterpower Laboratory. Furthermore, I would like to thank him for making this study possible, for valuable discussions, and for guiding me in the right direction at the time when I was lost.

I would like to acknowledge sincerely to Professor Hermod Brekke, Professor Arne Kjølle, Professor Torbjørn Nielsen, and Associate Professor Morten Kjeldsen, for their valuable suggestions, support, and cooperation during my study.

I would like to thank staffs of the Waterpower Laboratory Bård Brandåstrø, Joar Grilstad, Ellef Bakken, Trygve Opland, Halvor Haukvik, Idun Schjerven Østgård, for their help to find out and set up earlier test rig at the laboratory, to modify the test rig and finally to conduct the experiments. Similarly, I would like to thank Wenche Johansen for her help not only to provide all the necessary logistic support to complete my work but also to keep track of all my deadlines and others administrative challenges. In addition, her cooperation and friendly behaviour created a homely environment at Waterpower Laboratory. I would also like to thank Eugen Uthaug for helping and providing the relevant computer software throughout my study.

My sincere thanks go to the Kathmandu University and then the Department of Mechanical Engineering for allowing me to pursue this study at NTNU. I would like to thank especially Dr. Bhola Thapa, Professor and dean, school of engineering, for his help, cooperation and guidance throughout the study. He is the one who motivated me to continue the research in this field. I have used his PhD experimental set up at the beginning of my experimental work and then modified the same set up for the rest of my experiment. It has been a pleasure working with this experimental set up at Waterpower Laboratory. Moreover, he has always been available with me for discussion and guidance to accomplish the objective of this study.

In addition, I would like to thank Dr. Bhupendra Bimal Chhetri, Associate Professor, at Department of Electrical and Electronics Engineering, KU, for his help to correct language mistakes during final phase of my writing. It has been pleasure to have his comments on right time.

The discussions and interactions with the colleagues at the Waterpower Laboratory have been very fruitful. Many thanks go to PhD fellows, Pål-Tore Selbo Storli, Jørgen Ramdal, Einar Kobro, Håkon Hjort Francke, and Lars Frøyd. I would also like to thank, Mette Eltvik, former master degree student and present research assistant at the Waterpower Laboratory, for her help especially in Turbo Grid generation and CFD simulation. It has been always pleasure to discuss with her regarding sediment erosion issues and their challenge.

I wish to express my heartfelt gratitude to the State Education Loan Fund (Lånekassen), Norway, for partly supporting my living expenses during my stay at Trondheim. I would like to thank Anette Moen, Coordinator of Quota Programme, Ragnhild Brakstad, Turid Bræk, and Gro Johnsen, staffs at the office of international relations, NTNU for their administrative arrangements for loan fund and residence permit issues for me and my family. I am equally indebted to Energy Norway (former EBL) for their additional financial support during my study. I would like to thank and acknowledge all Nepalese colleagues those who were here during my study period for supporting me, and for my family.

I declare that this study is my own work and outside inputs are referenced at the relevant places. I am sure that there will be some errors, for which I take absolute responsibility. This is a small step towards achieving sediment erosion prediction and prevention in hydraulic turbine components in hydropower plants. I do believe that this work will encourage many researchers to put their knowledge and efforts in order to achieve the significant contribution against sediment erosion problem.

I wish to thank my wife Radhika and two lovely sons Sushant and Hardik, whose presence, patience, smiles and moral support always encouraged me to complete my work on time. I would like to thank my brother Tulsi for his cooperation and continued support towards my home responsibilities during my absence in Nepal.

Last but not the least, I dedicate this work to my loving parents, Aama and Baba. I am always grateful to them and now I am here in this position because of their hard work, continued support, encouragement and blessing.

Hari Prasad Neopane

PhD Candidate
Waterpower Laboratory
Department of Energy and Process Engineering (EPT)
Faculty of Engineering Science and Technology (IVT)
Norwegian University of Science and Technology(NTNU)
Trondheim
Norway
March, 2010

TABLE OF CONTENTS

LIST OF FIGURES

LIST OF TABLES

NOMENCLATURE

Symbols

Symbol	Description	Unit	Symbol	Description	Unit
F_D	Drag force	N	S_1	Coefficient of sediment concentration	-
C_D	Drag coefficient	-	S_2	Coefficient of sediment hardness	-
A_p	Projected area	m^2	S_3	Coefficient of sediment particle size	-
U	Peripheral velocity	m/s	S_4	Coefficient of sediment particle shape	-
F_B	Buoyancy force	N	M_r	Coefficient of wear resistance of base material	-
F_C	Centrifugal force	N	W	Erosion rate	mm/yr
F_R	Rotation force	N	W_c	Cutting wear	mm/yr
F_E	External force	N	W_C	Corrosion rate	mm/yr
m	Mass of the particle	kg	W_D	Deformation wear	mm/yr
d_c	Critical dia. of particle	m	W_t	Total wear (cutting and deformation)	mm/yr
d_p	Diameter of particle	m	W_T	Total wear rate (erosion and corrosion)	mm/yr
g	Gravity	m/s^2	R	Radius of curvature of surface	m
r	Radius	m	C	Velocity of particle	m/s
r_p	Radius of particle	m	V	Volume of particle	m^3
C_m	Meridional velocity component	m/s	N	Number of abrasive particles	-
V_p	Particle impact velocity	m/s	K_{mat}	Material constant	-
P	Plastic flow stress	N/m^2	K_{env}	Environmental constant	-
M	Total mass of material	kg	KT	Maximum particle velocity	m/s
S	Abrasive depth	mm	K_m	Material factor	-
h	Net head	m	k	Coefficient of discharge	-
n_s	Specific speed	rpm	C_u	Peripheral velocity component	m/s
h_{tot}	Total enthalpy	J	Y^+	Dimensionless distance from the wall	-
B	Sum of body force	N	Q	Flow rate	m^3/s
P	Pressure	Pa	U_S	Slip velocity	m/s
F_P	Pressure gradient force	N	F_{VM}	Force due to virtual mass	N
U_F	Under relaxation factor	-	C_μ	Constant	-
n	Speed	rpm	D	Characteristic dimension of machine	m
$\overline{U}$	Mean velocity	m/s	$f(\alpha)$	Function of impingement angle	-
U	$\overline{U}+u$	m/s	$f(V_{PN})$	Function of velocity of particle	-
$\underline{U}$	Reduced peripheral velocity	m/s	$R_{e,p}$	Particle Reynolds's number	-
k_1	Shape constant	-	k_2	Hardness constant	-
c	Concentration of sediment	ppm	k_3	Abrasive resistance coefficient	-

Greek Symbols

ρ	Density of fluid	kg/m3	λ	Turbine coefficient	-
ω	Angular velocity	red/s	φ	Diffusion of turbulence stress	W/kg
η_h	Hydraulic efficiency	-	ϕ	Viscous stress	N/m²
σ	Normal stress	N/m²	τ	Shear stress	N/m²
ε	Turbulence eddy dissipation	m2/s3	Ω	Speed number	-
η	Efficiency	-	β	Blade angle	degree
γ	Impact angle	rad	γ_0	Maximum Impact angle	rad
μ	Dynamic viscosity	Kg/N-m	μ_{eff}	Effective viscosity	kg/N-m
ν	Kinematic viscosity	m²/s	μ_t	Turbulent viscosity	kg/N-m
π	Constant	-	κ	Turbulence kinetic energy	m²/s²
α_0	Maximum Guide vane angle	degree	α	Guide vane/ Impingement angle	degree

Sub-symbols

m	Refers to meridional direction	$\bullet$	Refers to vector dot product
n	Refers to net value	∇	Refers to del vector operator
p	Refers to particle	$\otimes$	Refers to dyadic operator
u	Refers to the peripheral direction	$\propto$	Refers to directly proportional
r	Relative value	h	Refers to hydraulic
*	Refers to best efficiency point of turbine	a	Refers to average grain size
°	Refers to the full load of the turbine	x	Concentration exponent
1	Refers to the inlet of the turbine runner	y	Size exponent
2	Refers to the outlet of the runner	z	Characteristic velocity exponent
f	Refers to fluid	∂	Refers to partial derivative

Abbreviations

AISI	American Iron and Steel Institute
ADB	Asian Development Bank
BPC	Butwal Power Company Limited
BEP	Best Efficiency Point
BHEL	Bharat Heavy Electricals Limited
CFD	Computational Fluids Dynamics
CPU	Central processing unit
CAT	Catchment Area Treatment
DNS	Direct Numerical Simulation
EPT	Department of Energy and Process Engineering
EDA	Effective desilting arrangements
FL	Full Load
GoN	Government of Nepal
HPP	Hydropower Plant
HB	Brinell Hardness Number
IEC	International Electro-Technical Commission
IVT	Faculty of Engineering Science and Technology
JHP	Jhimruk Hydropower Plant
KU	Kathmandu University
MUSIG	Multiple Size Group
MSDM	Micro-Scale Dynamic Model
MoWR	Ministry of Water Resources
NTNU	Norwegian University of Science and Technology
N-S	Navier-Stokes
NEA	Nepal Electricity Authority
PL	Particle load
PPM	Parts per million
RANS	Reynolds Averaged Navier-Stokes
RMS	Root mean square
RoR	Run- of -River
SST	Shear Stress Transport
SN-Power	Statkarft Norfund Power Invest
SRE	Silt resistant equipment
URANS	Unsteady Reynolds Averaged Navier-Stokes equations
VHN	Vickers Hardness Number

Chapter 1
Introduction

1.1 BACKGROUND

1.1.1 General

Nepal, where the author comes from, is situated in South Asia on the lap of mighty Himalayas, and possesses enormous water resources, which is one of the major resources for technological, social and economic development of the nation. The energy supply and demand characteristics have a great role to play in order to attain sustainable development in the country. Thus, meeting Nepal's current energy demand would help foster higher economic growth. On the other hand, energy demand of the country increases not only due to the increases in population but also due to the gradual industrial development and modernization of society. However, Nepal has one of the lowest per-capita energy consumption rates in the world. Less than one third of the country's population has access to electricity. In the rural areas, where most people live, has even less access to the electricity. According to recent report of Asian Development Bank (ADB), the demand for power in Nepal has increased steadily with an annual average growth rate of 8.5 % over the past decade, and it is estimated to grow at least by 10 % annually until 2020. Moreover, the current energy generation trend shows that meeting this projected energy demand is possible due to huge water resources available for hydropower development.

The total estimated hydropower potential of the nation is about 83,000 MW and out of which about 43,000 MW is estimated to be economically feasible (MoWR, 2003). So far, Nepal has been able to exploit about 2 % of the economically feasible hydropower potential. This shows a huge scope for hydropower development in the country. The total installed capacity of the country is about 680 MW, of which about 84 % is produced from Run-of-River (RoR) hydropower plants. Therefore, RoR hydropower plants are the main sources of electricity in the country. Among the different sources of energy, hydropower is considered economical, non-polluting and environmental friendly renewable source of energy.

The overview of hydropower potential in different River basins in Nepal is presented in Table 1-1.

Table 1-1 Hydropower potential in different river basins in Nepal (MoWR, 2003)

Main river basins	Small river power potential (GW)	Major river power potential (GW)	Total power potential (GW)	Economically feasible power potential (GW)
Sapta Kosi	3.6	18.75	22.35	10.86
Sapta Gandaki	2.7	16.95	20.65	5.27
Karnali and Mahakali	3.5	32.68	36.18	25.1
Southern	1.04	3.07	4.11	0.88
Country Total	10.84	72.45	83.29	42.13

Furthermore, there is a huge potential for hydropower development in Himalayan region in general. However, there are also technical challenges for hydropower development due to erosion and sedimentation problem. The climatic and physical conditions are highly responsible for the erosion and sedimentation problem in the region. The tropical climate, immature geology, and intense seasonal rainfall, are the main reasons for this problem. As a result, the Rivers in this region transport substantial amount of sediments during the monsoon.

According to Naidu, 1999, about 20 billion tones of earth material are carried to the sea each year by Rivers and Streams throughout the world, of which nearly 6 billion tones is from the Indian subcontinent alone. Southeast Asia contributes two thirds of the world's total sediment transport to oceans (http://www.gemswater.org/atlas-gwq/solids-e.html) [accessed on, 31 August 2009]. Handling sediments in hydropower projects has therefore been a problem.

The management of the hydropower projects for achieving higher efficiency of hydraulic turbines is an important factor. Hence, this problem has become primary concern for the safety, reliability and longer life of the RoR hydropower projects. Many of the Himalayas sites in Asia and South America's sites in Andes, are examples of large regions where, the problem of erosion and sedimentation is challenging. From the global perspective, the RoR hydropower projects are becoming popular due to relatively less environmental impacts than reservoir type of projects. Recent research has indicated that the benefits of Run-of-River projects can be valued much more highly than they used to be considered, because of environmental consequences.

Both types of hydropower projects (storage as well as Run-of-River) suffer from sediment erosion problems, however the nature of problem is different. The storage projects suffer from reservoir capacity depletion over time due to sediment deposition. On the contrary, the RoR projects, which do not have room for storage of sediments, suffer from excessive wear of the turbines from the first year of operation itself. The sediment erosion of turbines causes losses in revenue due to losses in energy generation and increase in maintenance costs. Dealing with sediment has, therefore been a great challenge while developing hydropower projects in sediment-loaded rivers (Bishwakarma, 2008).

1.1.2 Sediment erosion problems

Sediment erosion problem is a global operation and maintenance problem of hydropower plants. Hydraulic turbine components operating in sediment-laden water are subject to abrasive and erosive wear. This wear not only reduces efficiency and life of the turbine but also causes problems in operation and maintenance, and ultimately leads to economic losses. Many hydropower plants built on sediment-loaded rivers have faced serious problems of sediment erosion during the first years of operation itself. The 12 MW Jhimruk hydropower plant (JHP) built in Nepal can be taken as an example.

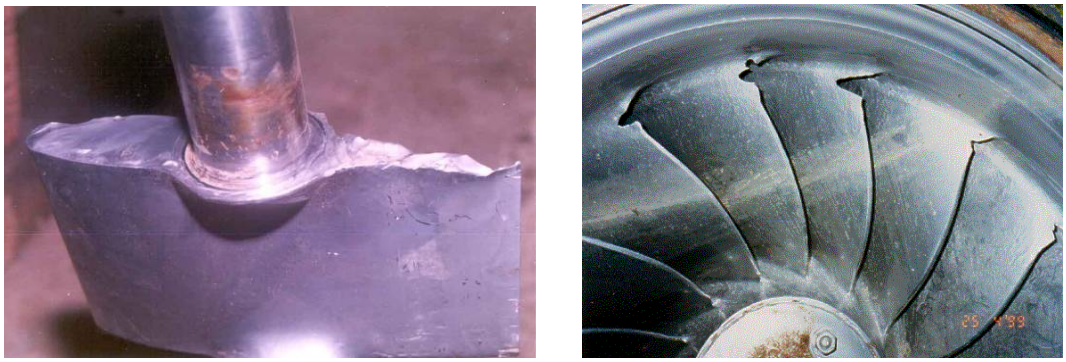

(a) Guide vanes (b) Turbine runner

Figure 1-1 Sediment erosion at Jhimruk hydropower plant, Nepal

The photographs presented in Figure 1-1 illustrate the extent of sediment erosion in guide vane cover and the runner blades after operating during a single monsoon. The sediment study conducted in this power plant indicated that, the sediment concentration exceeds 4,000 ppm for about 15 % of the monsoon. The average content of quartz in the sediment is found to be above 60 % (Basnyat, 1999).

Similarly, 22 MW Cahua hydropower plant built in Peru can be taken as another example of excessive sediment erosion. The photographs presented in Figure 1-2, also illustrate the extent of sediment erosion in guide vanes and turbine runner. These photographs were taken during inspection visit from NTNU in April 2009. The sediment study conducted in this power plant indicated that, the sediment concentration exceeded 120,000 tons of sediment only after six weeks of operation. The average content of quartz particles in the sediment was found to about 35 % and feldspar was found about 30 %.

(a) Guide vanes

(b) Turbine runner

Figure 1-2 Sediment erosion at Cahua hydropower plant, Peru

The high sediment concentration combined with high percentage of quartz and feldspar, which are harder than the turbine material (hardness 6-7 in Moh's scale), was the main causes of excessive sediment erosion in the hydraulic machinery operating in these power plants. During monsoon season, a large amount of sediment (as high as 50,000 ppm) is carried by Rivers and it becomes difficult to remove all these sediments before passing through the turbine, and causes severe damage to the turbine components.

1.2 MOTIVATION FOR THIS RESEARCH

There are huge technical challenges to develop new hydropower projects involving risks of sediment erosion. The declining performance of hydro turbines has become one of the major technical issues in the development of hydropower plants. Sediment transport from the rivers is a natural phenomenon, it neither can be completely controlled, it nor can be completely avoided; it should however be managed. Withdrawal of the clean water from the river for power production is expensive due to design, construction and

operation of sediment settling basins. Even with the settling basins, 100 % removal of fine sediments is impossible and uneconomical (Thapa, 2004). A 3-dimentioanal approach is desirable to encounter sediment problems in hydropower plants (Naidu, 1999), namely, catchment area treatment (CAT) for reduction of sediment load, effective desilting arrangements (EDA) for prevention of sediment, and sediment resistant equipment (SRE) for withstanding the sediment.

The sediment erosion of turbine runners is a complex phenomenon, which depends upon different parameters such as silt size, hardness and concentration, velocity of water, and base material properties. The efficiency of the turbine decreases with the increase in the sediment wear and finally breakdown of hydro turbines results. Various researchers have conducted experiments to study the effect of these parameters on sediment wear, but most of these experiments are on small-size samples in different types of test rigs to simulate the flow conditions in the turbine. However, actual flow conditions and the phenomenon of sediment wear are too complex to simulate (Padhy et al., 2008)

Extensive research has been done to develop a wear model in terms of the material properties involved but little attention has been given to clarify the influence of fluid motion, especially in the turbulent flow regime. Over the years, many models have been proposed for many different situations. Unfortunately, most models are co-relational in nature and therefore system specific. They only work for the particular material pair, contact geometry, operating condition and range, and the particular environment and lubricant. The available equations are so confusing that few designers can use any of them to predict product life with confidence. The complexity of wear and the large number of parameters affecting the outcome are the primary reasons for this situation.

Furthermore, several attempts have been made to minimize the loss of material due to erosion. While they have proved successful elsewhere, they have not much success in Himalayan region. Development in the areas of control of sediment from reaching the turbine and protective coating on the surfaces, prone to erosion, has been the main area of research. Very little has been done for developing erosion resistant flow passage design. The problem blows multi-folds as the sediment mainly consists of quartz (60 – 90 %) which is extremely hard and causes severe erosion damage.

A study carried out at the Department of Mechanical Engineering, Kathmandu University, Nepal, shows that all rivers that flow through Nepal have sediment load and high concentration of quartz (Thapa, 2004). This means that all turbines installed in these rivers will experience sediment erosion. This study also revealed that the intensity of erosion rate is no longer directly proportional to the percentage of quartz content of the sediment. As a result, a few instances have been noticed where the intensity of damages at different power plants were not identical. While components at a particular power plant eroded very fast, damages to components at other power plants were insignificant. This leads one to believe that large numbers of factors influences the process of erosion damage (Naidu, 1999). In addition, they are jointly responsible for predicting sediment erosion damage in the turbine components. There is strong need to study and identify the effect of different shape and size of the sediment particle to predict the erosion rate

correctly. Therefore, dealing with sediment erosion problems requires a multidisciplinary approach. More research and development is needed to investigate the relationship between the particle movement and the erosion inside the turbine.

1.3 OBJECTIVE OF THIS STUDY

The main objective of this study is to investigate the relationship between the particle movement and erosion inside the Francis turbine and to establish the operating strategy for Francis turbine operating in sediment-laden water. In order to achieve the main objective the following specific activities have been carried out during this study period:

- Develop and build a laboratory test rig that can facilitate the testing of particle to study the separation process in fluid flow in curved path
- Conduct experiment of the particle in the laboratory test rig to study the forces acting on particle in rotational motion and to investigate the drag coefficient and velocity relation with respect to different size, and shape of the particles
- Perform numerical simulation on a Cahua power plant Francis turbine design and describe the prediction of the erosion for stay vanes, guide vanes, and runner vanes for which the results of the field tests are available for verification
- Identify critical zones of erosion and investigate empirical relations based upon particle shape, size, concentration, and operating conditions

1.4 STUDY METHODOLOGY

The overall study methodology adopted for this research work includes experimental studies, numerical simulation, and field studies. A previously made test rig (Thapa, 2004), was reviewed and modified to create a strong swirl flow in curved path. This flow was found similar to the flow between the guide vane outlet and the runner inlet of a Francis turbine. The flow in the guide vane cascade was simulated in order to verify the particles separation process and to investigate the velocity and the drag coefficient relations based upon different shape and size of the particle. Then, numerical simulations on a Cahua Francis turbine design were carried out, mainly at two operating conditions with varying particle size, shape, and concentration in ANSYS CFX 11. The predictions of erosion, based on the Lagrangian calculation of particle paths in a viscous flow, have been described for different components of the Francis turbine. The numerically obtained erosion patterns were compared with the field studies at Cahua hydropower plant, in Peru. The experimentally obtained velocities and drag coefficients relations were utilised for the validations of numerical simulations.

1.5 SCOPE OF STUDY

The scope of this research is not only to improve the Francis turbine components operating in sediment-laden water subject to sediment erosion through design modification but also to identify the regions where special surface treatment is necessary in order to increase the lifetime of the components for new hydropower projects involving risks of sediment erosion. This is pursued by achieving the objectives mentioned in the previous section. This research focuses only on the role of sediment characteristics in fluid dynamics, even though the erosion primarily depends on both sediment characteristics and material used for the turbine components.

This sediment erosion research in hydraulic machinery in general and the Francis turbine in particular, is aimed to contribute the knowledge for:

- operation strategy of hydropower plants
- selection and design of turbine
- selection of appropriate material for turbine construction and maintenance
- maintenance of eroded turbine and maintenance scheduling

Hence, all technical, managerial and economical aspects are supposed to be considered in this kind of study but only technical aspect has been studied extensively in present work. It is believed that if a Francis turbine designer combines the hydraulic design and coating of the critical parts, a significant reduction of erosion can be achieved, but detail analysis of this aspect is out of the scope of this research work.

1.6 OUTLINE OF THE THESIS

This thesis is organized in eight chapters. Some chapters include their own conclusions. An extensive literature review regarding the various form of wear and its mechanisms caused by contact between a particle and a surface is presented in Chapter 2. The sediment erosion types in hydraulic machinery components and the field observation at Cahua hydropower plant is considered in Chapter 3. Chapter 4 is dedicated to the laboratory studies of particle velocity measurement in highly swirl conditions similar to turbine flow in curved path. It also includes a brief description of the developed test rig, concept of critical diameter of particle inside a turbine, and experimental analysis. The governing equations of fluid, particle equation of motion and two erosion models are briefly presented in Chapter 5. A description of CFD computational model similar to Cahua power plant Francis turbine design along with solution methods is included in chapter 6. The simulations results and discussions are presented in Chapter 7. Finally, the conclusions and recommendations for further work are given in Chapter 8. The auto generated turbine rotor reports and three publications are included in the appendices.

Chapter 2
Literature Review

This chapter presents extensive literature review regarding the various forms of wear and its mechanisms caused by contact between a particle and a surface. Furthermore, factors responsible for sediment erosion with controlling parameters, and general erosion model are also included.

2.1 INTRODUCTION

Sediment erosion is a phenomenon of mechanical wear of components. This is due to the dynamic action of sediment flowing along with water impacting against a solid surface of hydraulic components. Therefore, sediment flowing along with water passing through the turbine is the root cause of sediment erosion in turbine components. The mechanical wear in hydraulic machinery is mainly due to the suspended sediment in water, which is subjected to kinetic energy, the force of gravity, viscosity, turbulence, centrifuge and cavitation. Even if minor abrasion may take place in certain parts of hydro turbines, erosion is the main caused of the damage.

Erosion occurs in a wide range of machinery (Thapa, 2004). The blades of gas turbines are subjected to erosion from high velocity solid particle, and those of steam turbines from liquid droplets (Tabakoff, 1995). The military aircrafts and missiles experience both sand and rain erosion. The problem of hydro-abrasive erosion of hydraulic machinery is not limited to hydroelectric plants. Similar problems to those encountered in hydroelectric work are also prevalent in the mining industry, dredging work, and waste disposal. Even though erosion is normally harmful for the machine components, the same mechanism has beneficial use in unconventional manufacturing techniques. Some common examples of beneficial applications of erosion mechanism are water jet machining, sand blasting, erosive drilling and rock cutting (Finnie, 1960).

2.2 MECHANISMS OF SOLID PARTICLE EROSION

In general, there are wide ranges of material degradation mechanisms. However, it can be classified into three basic categories: mechanical, chemical and thermal actions, which are considered the root causes of material separation as debris in erosion, but

mechanisms for reaching to those actions are different (Thapa, 2004). Figure 2-1 illustrates the different action of solid particle erosion and its mechanisms. Stachowiak and Batchelor, 1993, have discussed the different possible mechanisms for solid particle erosion. From the subject point of view of sediment erosion damage caused by the suspended solid particle in hydraulic machinery, only four solid particle erosion i.e., abrasive erosion, surface fatigue, brittle fracture, and ductile deformation are mainly applicable.

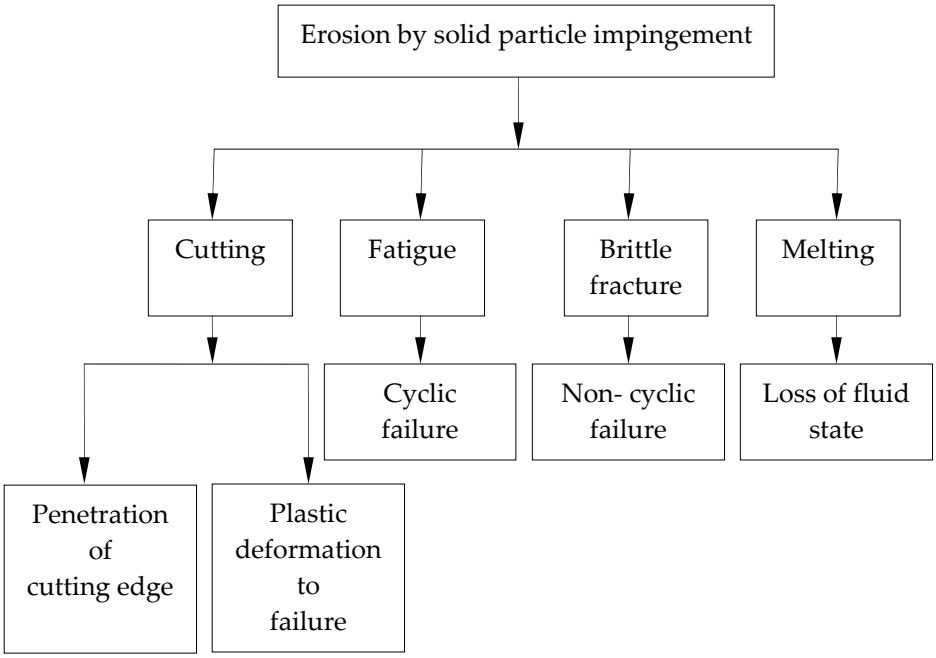

Figure 2-1 Mechanisms of solid particle erosion

2.3 ABRASIVE AND EROSIVE WEAR

Abrasive wear is the loss of material by the passage of hard particles over a surface. This wear occurs whenever a solid object is loaded against particles of a material that have equal or greater hardness. The abrasive wear involves processes such as micro cutting, fatigue, grain detachment and brittle fracture. Erosive wear is caused by the impact of solid and liquid particles on a surface. Erosive wear can resemble abrasive wear when hard solid particles of microscopically visible size are eroding agent, the angle of impingement is low and the impingement speed is of the order of 100 m/s. For all other conditions, wear mechanisms not resembling abrasive wear become dominant. For particle of microscopically visible size and an impingement speed of the order of 100 m/s, wear at the high impingement angles proceeds by a combination of plastic deformation and fatigue or by cracking for brittle materials.

2.3.1 Mechanism of abrasive wear

Generally, abrasive wear by grits or hard asperities closely resembled cutting by a series of machine tools or a file. However, microscopic examination has revealed that the cutting process is only approximated by the sharpest of grits and many other more indirect mechanisms are involved. The particles or grits may remove material by micro cutting, micro fracture, pullout of individual grains or accelerated fatigue by repeated deformations as illustrated in Figure 2-2.

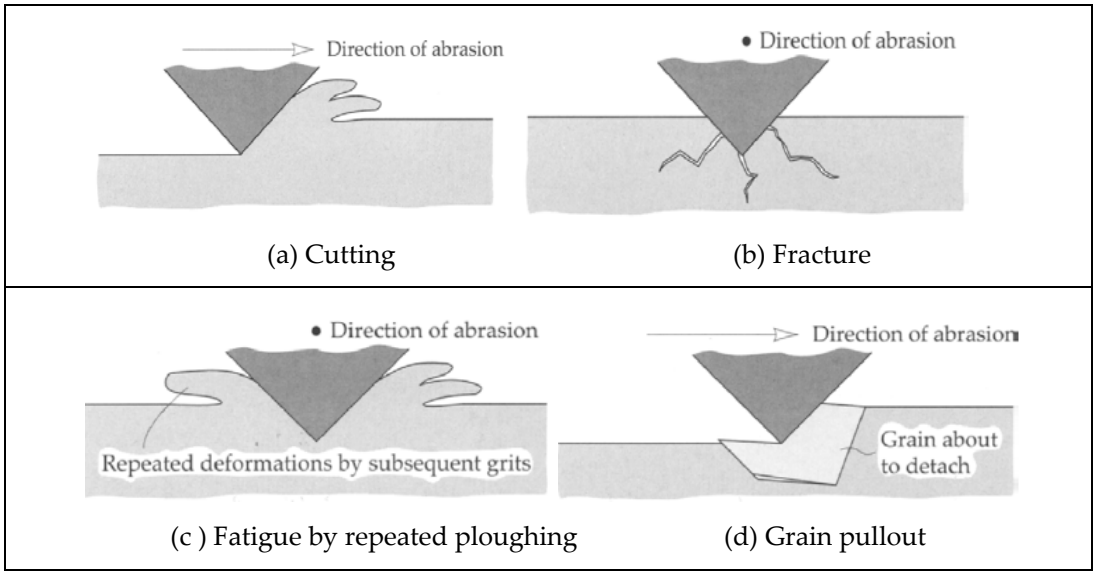

Figure 2-2 Mechanisms of abrasive wear (Stachowiak and Batchelor, 1993)

The first mechanism illustrated in Figure 2-2 a, is cutting, which represents the classic model where a sharp grit or hard asperity cuts the softer surface. The material that is cut is removed as wear debris. When the abraded material is brittle, e.g., ceramic, fracture of the worn surface may occur (Figure 2-2 b). In this instance, wear debris is the result of crack convergence. When a ductile material is abraded by a blunt grit, then cutting is unlikely and the worn surface is repeatedly deformed (Figure 2-2 c). In this case, wear debris is the result of metal fatigue. The last mechanism illustrated (Figure 2-2 d) represents grain detachment or grain pullout. This mechanism applies mainly to ceramics, where the boundary between grains is relatively weak. In this mechanism, the entire grain is lost as wear debris.

Abrasive wear has the virtue of being possibly the easiest of the wear mechanism to suppress completely if adequate materials are available. Rapid abrasive wear only occurs when the ratio of particle hardness to materials hardness is greater than 1.2. When the ratio of particle hardness to material hardness is less than 1.2, abrasive wear declines rapidly but does not cease entirely until the material hardness is greater than the particle

hardness by a similar factor of 1.2. It is observed that when the particles have equal hardness to the material, some scratching and wear of the material occurs although damage to the particles by crushing and plastic deformation is extensive.

2.3.2 Mechanisms of erosive wear

Erosive wear involves several wear mechanisms, which are largely controlled by the particle material, the angle of impingement, the impact velocity and the particle size. If the particle is hard and solid then it is possible that a process similar to abrasive wear will occur. Where liquid particles are the erodent, abrasion does not take place and the wear mechanisms involved are the result of repetitive stresses on impact.

The term erosive wear refers to an unspecified number of wear mechanisms, which occur when relatively small particles impact against mechanical components. This definition is empirical by nature and relates more to practical considerations than to any fundamental understanding of wear. The known mechanisms of erosive wear are illustrated in Figure 2-3.

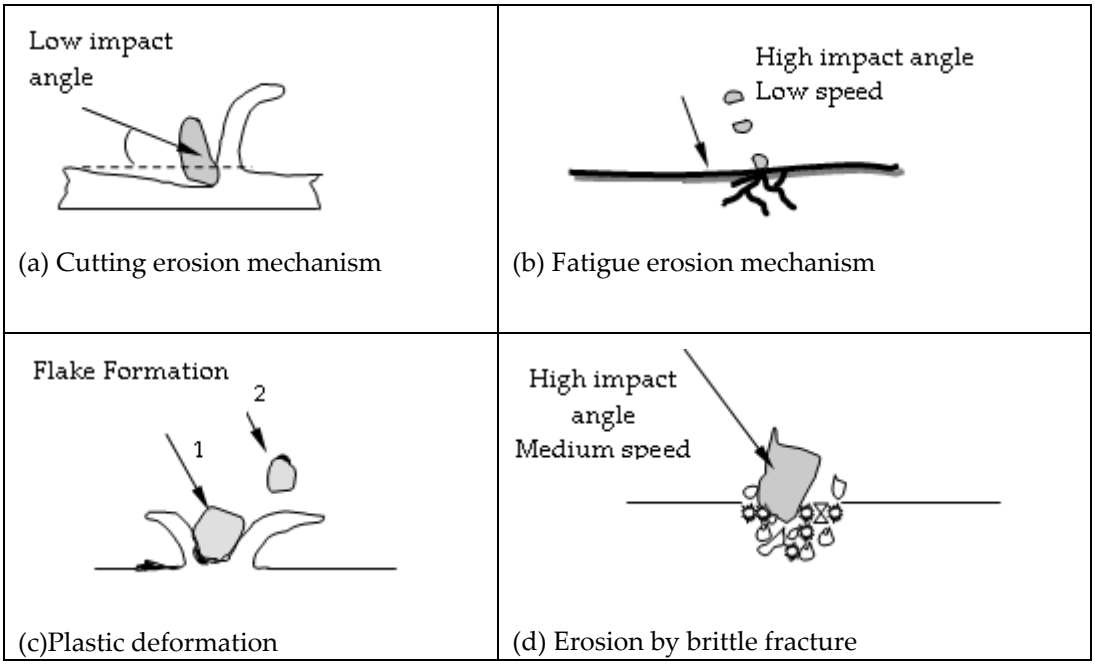

(a) Cutting erosion mechanism

(b) Fatigue erosion mechanism

(c)Plastic deformation

(d) Erosion by brittle fracture

Figure 2-3 Mechanisms of erosive wear (Stachowiak and Batchelor, 1993)

2.3.2.1 Cutting erosion

As illustrated in Figure 2-3 a, when particles strike the surface at low impact angle and removal of material by cutting action, the erosion mechanism is called abrasive erosion. The abrasive grits roll or slide when they strike on the surface and cause erosion by

abrasion or cutting mechanism. The material is removed by scouring or scrapping by sharp edges of the particles forming short track-length scars.

2.3.2.2 Surface fatigue

As illustrated in Figure 2-3 b, surface fatigue erosion mechanism occurs, when the particles strike the surface with large impact angle but at low speed. This mechanism of erosion is similar to wear due to surface fatigue on rolling surfaces. The surface cannot be plastically deformed. Instead, the surface becomes weak due to fatigue action and cracks are initiated in surface after repeated hitting. The particles will be detached from the surface after several strikes.

2.3.2.3 Plastic deformation

As illustrated in Figure 2-3 c, plastic deformation of the surface takes place due to formation of the flakes around the striking point when the particles strike the elastic surface with medium speed and large impact angle. With repeated strike on the flakes, the material will detach as debris.

2.3.2.4 Brittle fracture

As illustrated in Figure 2-3 d, when particles strike the brittle surface with large impact angle in medium velocity, brittle fracture erosion takes place. If the particles are sharp, then brittle fragmentation is more likely to occur and the particles detach from the material by subsurface cracking.

2.4 CONTROLLING PARAMETERS FOR EROSIVE WEAR

The mechanisms of erosive wear are not constant but are controlled by the angle of impingement of a particle, its speed, its size and the phase of material that constitutes the particles. The angle of impingement is the angle between the eroded surface and the trajectory of the particle immediately before impact, as shown in Figure 2-4. A low angle of impingement favours wear processes similar to abrasion because the particles tend to track across the worn surface after impact. A high angle of impingement causes wear mechanisms, which are typical in erosion.

The speed of the erosive particle has a very strong effect on the wear process. If the speed is very low, then stresses at impact are insufficient for plastic deformation to occur and wear proceeds by surface fatigue. When the speed is increased, for example, to 20 m/s, it is possible for the eroded material to deform plastically on particle impact. In this regime, which is quite common for many engineering components, wear may occur by repetitive

plastic deformation. If the eroding particles are blunt or spherical then thin plates of worn material form on the worn surface because of extreme plastic deformation. If the particles are sharp, then cutting or brittle fragmentation is more likely. Brittle materials, on the other hand, wear by subsurface cracking. At very high particle speeds, melting of the impacted surface might even occur (C. S. Yust and R. S. Crouse, 1975). The angle of impingement and the other listed parameters are illustrated schematically in Figure 2-4.

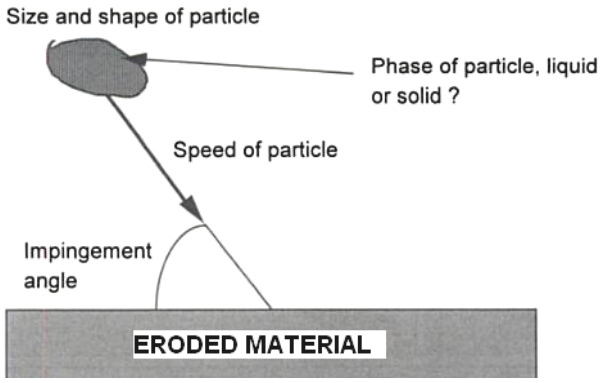

Figure 2-4 Physical and material parameters for controlling erosive wear (Batchelor et al., 2002)

There are two modes of erosive wear, called the ductile mode of erosive wear (at moderate particle speeds) and the brittle mode of erosive wear. The ductile mode of erosive wear depends on tangential movement of the impingement particle across the eroded surface for wear particle to be produced by searing or cutting. This tangential movement is favoured by a very small angle of impingement as opposed to normal impact. However, the angle of impingement is zero, there will be no kinetic energy of impact between particle and worn surface to initiate indentation by the particle and chip formation. A maximum in the ductile mode of erosive wear is usually found close to an angle of 30 °, which represents a compromise between the requirements of tangential particle movement and impact energy. For the brittle mode of erosive wear, the maximum in erosive wear occur around 90 °, where the kinetic energy of impact is at a maximum. The wear rates as a function of impingement angle for the brittle and ductile modes of erosive wear are shown schematically in Figure 2-5 .

Erosive wear by liquid particles is mostly limited to the brittle mode, where the rate of wear is far more sensitive to particle velocity than when solid particles are involved. For liquids, erosive wear is observed to be proportional to approximately the 5^{th} power of impact velocity while for solids wear, it is proportional to the square of impact velocity approximately (Batchelor et al., 2002). Material with high toughness are usually the most effective at resisting erosive wear, as hard materials are often too brittle to be wear resistant. The size of the particle is critical to wear resistance as small particles, e.g. 8 μm average sizes tend to erode by ductile shearing of the worn material. This characteristic is

observed because brittleness depends on the presence of at least one defect in the deformed volume. Since the deform volume decreases in proportion to particle size, erosive wear at small particle sizes is more likely to be ductile than erosion at large particle sizes, where the apparent brittleness of the worn material is higher. High hardness materials are therefore more likely to be effective in resisting erosive wear by small particles, whereas tough materials are suitable for larger particles of 50 μm sizes and larger.

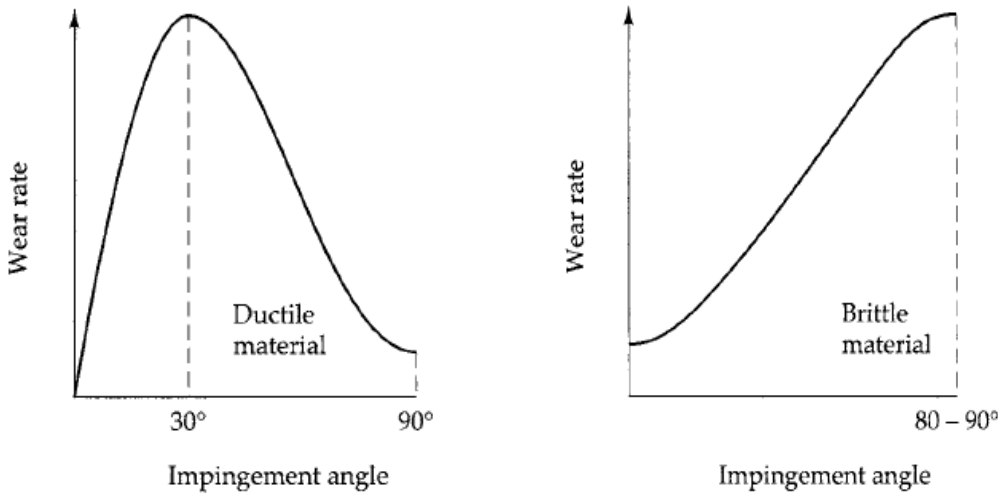

Figure 2-5 Contrast in dependence on impingement angle for brittle and ductile modes of wear (Stachowiak and Batchelor, 2006)

2.5 SEDIMENT

River sediments flowing along with water passing through the turbine are the reasons why the sediment erosion in hydraulic turbine components occurs. The river sediments are in the form of clay, silt, sand and gravel with specific gravity approximately 2.6. In the river hydraulics, sediment particles are classified in to bed load and suspended load based on transport of sediment. All the particles, which move close to the bed by sliding, rolling or jumping are called bed load. These particles have much lower velocity than flowing water, whereas all those particles, which are carried away in suspension by flowing water, are called suspended load and they have more or less same velocity as the flowing water. Fraction of suspended load is settled down in the settling basins or reservoirs and rest will pass through turbines causing erosion of components.

Sediments are made of fragmentation of rock due to chemical and mechanical weathering. The sediments in river are mixtures of different particle sizes as shown in Table 2-1. This is a sand fraction of the sediment, which causes turbine erosion. The sand

fraction can be further classified in to fine (0.06 - 0.2 mm), medium (0.2 - 0.6 mm) and coarse (0.6 - 2 mm).

Table 2-1 Classification of river sediment (Lysne et al., 2003)

Particle	Clay	Silt	Sand	Gravel	Cobbles	Boulders
Size (mm)	<0.002	0.002 - 0.06	0.06 - 2	2 - 60	60 - 250	>250

2.6 FORCES ACTING ON THE PARTICLES

The fluid flow influence the particle velocity and direction, and several forces are also acting on the particle for stabilizing and destabilizing its position on its path through the turbine. The particle will be affected mainly two different force categories (Lysne et al., 2003).

- Stabilizing forces: This is due to viscous and gravity forces that retard movements of the particles and have stabilizing effects
- Destabilizing forces: This is due to centrifugal and coriolis forces that slide the sediment along the bed with a low velocity, called bed load. The turbulence force will cause irregular movement in the fluid and the particles as they move in the same direction as the fluid surrounding them.

When particles move along curved path, the centrifugal force and, if the system is rotating (including global rotations), the Coriolis force are pertinent destabilizing forces. Exact interactions between all associated factors are complicated for numerical analysis. Sediment transport analysis may give indication on location of attack on turbine, which can be useful to focus on an optimal location of erosion resistant coating in turbine.

2.6.1 Drag and lift forces

The drag force works in the direction of the main flow, and the lift force in the transverse direction. The forces are proportional to the square of the flow velocity.

$$F_D = \frac{1}{2} \cdot C_D \cdot A_P \cdot \rho \cdot U^2$$ **Equation 2-1**

$$F_L = C_L \cdot A_P \cdot \rho_f \cdot U^2$$ **Equation 2-2**

2.6.2 The buoyancy force

The buoyancy force is an effect of the difference between the density of the fluid and particles. The gravity effect influences the particle motion.

$$F_B = \frac{\pi}{6} \cdot {d_P}^3 \cdot \left(\rho_P - \rho_f\right) \cdot g \qquad \textbf{Equation 2-3}$$

2.6.3 Rotation force

The sum of coriolis and centripetal forces is the rotation force acting in a rotating domain.

$$F_R = m \cdot \left(-2 \cdot \omega \cdot U_P - \omega \cdot \omega \cdot r_P\right) \qquad \textbf{Equation 2-4}$$

2.6.4 Turbulence force

Eddies are formed in an irregular flow due to shearing action inside the flow. Eddies will form and dissipate irregularly, and this disorderly flow is called turbulence effect.

2.7 FACTORS RESPONSIBLE FOR SEDIMENT EROSION

Since the sediment erosion damage is due to the dynamic action of sediment against a solid surface, characteristics of the sediment, fluids (carrying sediments) and base material are jointly responsible for sediment erosion (Thapa, 2004).

- Characteristics of the sediment (shape, size, hardness, concentration, material etc.),
- Characteristics of fluids (velocity, acceleration, impingement angle, medium of flow, temperature, turbulence etc.) and,
- Characteristics of the base material (chemistry, elastic property, hardness, surface morphology etc.)

2.7.1 Characteristics of the sediment

Particle characteristics are important but relatively poorly researched aspect of the erosion problem (Stachowiak and Batchelor, 2006). It is known that hard particles cause higher wear rates than soft particles (Goodwin et al., 1969 - 70). The sharpness of the particle has also been recognized as accelerating erosive wear (Bahadur et al., 1990). Both of these parameters have been included in numerical models of erosive wear (Stachowiak et al., 1987). The ratio of particle hardness to substrate hardness seems to be a controlling parameter (Stachowiak et al., 1987). The significance of particle hardness becomes apparent when the hardness of some erosive, for e.g., alumina, are compared to that of standard materials such as mild steel. In this instance, the ratio of particle to substrate hardness is about 10. The effect of particle hardness on wear depends on the particular mode of erosive wear taking place, e.g., ductile or brittle. In the brittle mode, the effect of particle hardness is much more pronounced than in the ductile mode (Stachowiak et al., 1987).

It is impossible to isolate hardness completely from other features of the particle such as its shape. Even if the particle is hard but relatively blunt then it is unlikely to cause severe erosive wear. A blunt particle has a mostly curved surface approximating to a spherical shape while a sharp particle consists of flat areas joined by corners with small radii, which are critical to the process of wear.

Variations in particle size in the range typical to engineering applications can cause fundamental changes in the erosion mechanism. A series of erosion tests on glass, steel, graphite and ceramics revealed that as particle size was increased from 8.75 μm to 127 μm in diameter, the mode of erosion changed from ductile to brittle. This caused the erosive wear peak to move from 30 ° to 80 ° impingement angle and even more significantly resulted in a dramatic increase in erosive wear rates as shown in Figure 2-6 (Sheldon and Finnie, 1966). In both cases, silicon carbide impinging at a speed of 152 m/s was used as the erosive agent.

It can also be seen from Figure 2-6 that particle size not only affects the wear rate but drastically alters the ranking of materials in terms of wear resistance. When the small particles were used as the erosive agent, the materials ranked according to their wear resistance are in the following order: high-density alumina > annealed aluminium > plate glass > high-density magnesia > graphite and hardened steel. In this case, apart from the annealed aluminium, erosive wear rate depends on the hardness of the material. Work hardening of the aluminium could be significant in this instance. On the other hand, when the large particles were used as the erosive agent, the order changes to annealed aluminium > hardened steel > high-density alumina > high-density magnesia > plate glass > graphite. Therefore, in this case toughness of the material is important. Materials, which are neither tough nor hard, e.g., graphite, show inferior erosion resistance.

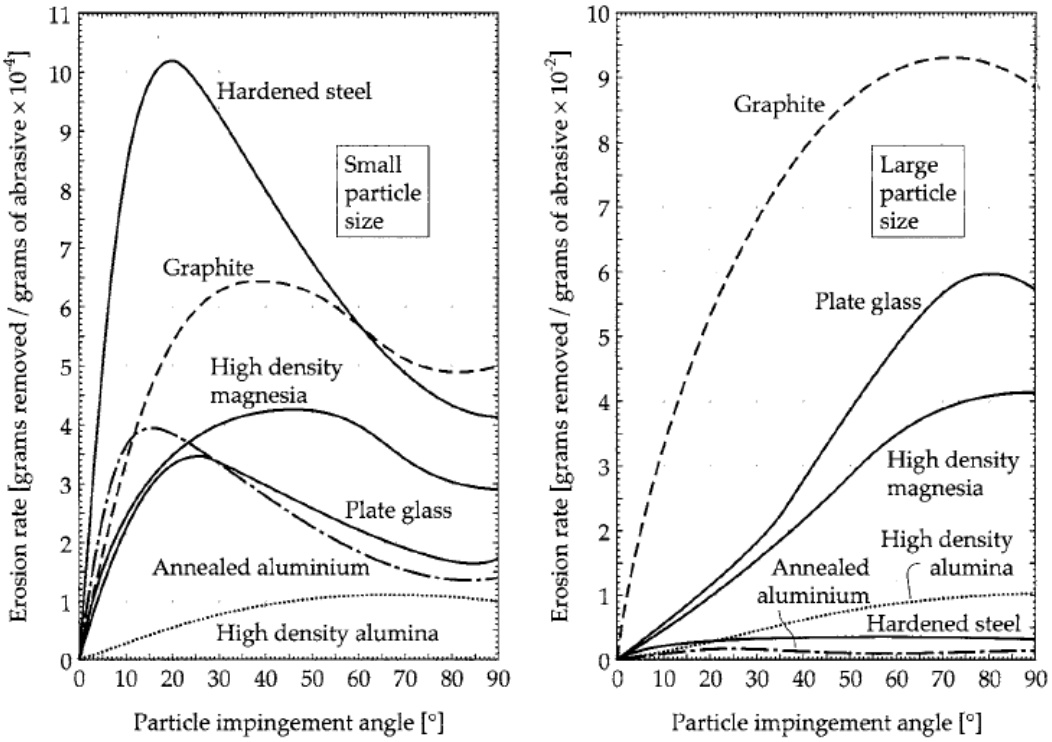

Figure 2-6 Effect of particle size on mode and rates of erosive wear (Hojo et al., 1986)

The change in wear modes is believed to be a consequence of the average spacing of defects, e.g., holes or cracks in a solid. If the impinging particles are very small, then only a minority of the impingement sites will coincide with a defect. The impingement site is a zone of highly stressed material directly beneath the particle on impact and similar in size to the particle. Plastic deformation is encouraged by an absence of defects and is the predominant mode of metal removal for small particles. Since repeated plastic deformation is required to remove material, this form of wear is relatively slow. For larger eroding particles, a defect is usually present in the impingement site and material removal by brittle processes is therefore favoured. Since crack formation is rapid the brittle mode of erosion can be a very destructive form of wear.

The incubation period of erosive wear refers to the period from the start of erosion to the onset of measurable positive wear. During the incubation period, wear either may be negligible or may appear to be negative. This latter characteristic is caused by eroding particles becoming trapped in the worn material. The incubation period is generally believed to relate to the accumulation of subsurface damage, e.g., cracks or strained materials that are the precursors of wear particle release. Once the incubation period has passed, wear usually proceeds at a constant rate.

2.7.1.1 Size and shape of the particle

The intensity of erosion is directly proportional to the size of the particles. Particle sizes above 0.2 to 0.25 mm are extremely harmful. It has been found that large size sediment particles (above 0.25 mm) even with hardness lesser than 5 on Moh's scale cause wear. Similarly fine silt even with size less than 0.05 to 0.1 mm, containing quartz wears out the underwater parts. The fine sediment can also be dangerous if the turbine is operating under high head. Sharp and angular particles cause more erosion in comparison to rounded ones.

Based upon the information available from literature survey conducted on abrasive wear in hydraulic machinery by Truscott, 1972, Beregoron, 1950, and Wiedenorth, 1970, state that, in general, the absolute wear rate increases with grain size and sharpness. Wellinger, 1958, and Worster, 1955, state that wear is directly proportional to size for sliding or grazing abrasion, but is independent of size for direct impact. Goodwin's tests, 1970, show that the erosion rate for impact abrasion becomes constant only above a certain grain size (about 50 - 100 μm depending on velocity). Stauffer, 1956, also states that the relative wear of metals decreases with increasing size, but gives no results. Bergeron, 1952, found from tests on Aluminum Bromide (Al-Br), that wear was proportional to $(\text{size})^{0.75}$, but he stated that for general application, wear was proportional to size × function of coefficient of friction, densities, and size / surface curvature ratio. Wellinger, 1958, shows the effects of particle shape on impact abrasion and states that angular grains cause about twice the wear compared to rounded ones. Goodwin, 1970, also discusses erosiveness of particles, and defines a shape-factor; he states that hardness and sharpness are interrelated. Wiedenroth's wear tests, 1970, on a small dredge pump impeller, using a lacquer removal technique, show differences in the blade wear pattern depending on grain size (i.e. sand or gravel).

Particle size can be characterized mainly in two basic dimension, mass and length. For a given velocity, the kinetic energy of particle is directly proportional to mass and mass of spherical particle is proportional to $(\text{diameter})^3$.

Sheldon and Finnie, 1966, observed the change of ductile mode of erosion to brittle mode when particle size is changed from small to larger. In the experiment with small and larger size particles, maximum erosion rate shifted from impact angle 30 ° to 80 °. Small size particles have more cutting effect while bigger particles deform material by elastic deformation and fatigue. The erosion rate ranking depends on hardness in case of erosion due to small particles, whereas, in case of large particles, it is dependent on toughness of material. Most often, non-cohesive natural sediments are characterized in term of particle diameter in river hydraulics. This method can be acceptable for other particles that have shape and density similar to natural sediments. Sediment particle sizes are defined in terms of sedimentation diameter, standard fall diameter, and nominal diameter or sieve diameter. Sedimentation diameter of a particle is the diameter of sphere that has the same specific gravity of 2.65 and has the same terminal settling velocity as the given particle in the same fluid under the same condition.

Generally, particle shapes are described qualitatively such as round, angular and semi-round based on visual observation. The basic shapes found in the nature are generally uniform, but due to several reasons, actual shapes of particles are sharp and complex, which cannot be described in simple mathematical terms.

The shape of the particle is a good indicator of erosion process, for instance, irregular shape with sharp edge increases erosion rate, whereas, blunt particles with round edges are less erosion rate in general. Most of the erosion models have incorporated the effect of shape; hence, quantification of the shape parameter is essential for the estimation of erosion by solid particles. Together with some of the approaches suggested by Bahadur and Badruddin, 1990, roundness factor and other statistical parameters are also used to describe the shape of the particles. Correlating the ductile erosion with cutting by single point cutting tool, the shape of particles can also be defined in term of Rake angle, which is the angle between the front face of particle and normal to the target surface. Winter and Hutchings, 1975, also used this concept. H. Drolon et al., 2000, used multi-scale roughness descriptor technique, based on harmonic wavelet transform for sediment particle analysis. Stachowiak, 2000, used Spike Parameter-Linear Fit based on projected particle boundary and Spike Parameter-Quadratic Fit based on curve fitting for major boundary to describe the angularity of the particles and studied their relation with erosion rate. These parameters are based on representing the particle boundary by set of triangles, which is directly related to particle erosivity. Chen and Li, 2003, simulated erosion using computer model (Micro-scale dynamic model, MSDM), and investigated the difference in erosion rate by three basic shapes: triangle, square and circle. The highest erosion loss in single particle impact is by triangular particle followed by circular and square. This observation is in agreement with stresses induced by contact area. The erosion loss changes when square particle is rotated at 45 ° and contact becomes the smallest. In reality, several particles strike the surface and the ranking of erosion will be different. In this case, erosion by square shape particle is bigger than circular, because of plastic deformation after subsequent strikes is in a larger area. In general, the erosion rate by triangular or square particles may be 1.5 times higher than the circular particles. Shrestha and Sandeep, 2005, studied shape feature extraction and pattern recognition of sand particles and their impact on hydraulic turbines. A systematic approach to the problem was identified. Sand particles were collected from the erosion sensitive power plants and its digital images were acquired. Software was developed on MATLAB 6.5 platform to extract the exact shape of sand particles collected. These shapes were further been analyzed by artificial neural network. This network was first trained for the known input and known output. After that, it was trained for unknown input and known output. Finally these networks can recognize any shape given to it and gives the shape which is nearest to the seven predefined shape. The software was trained for seven types of shapes with shape number 1 to 7 in increasing number of sharp edges. The shape with shape number seven is having large number of sharp edges, and is considered as most erosive where as shape with shape number one is having round edges and considered as the least erosive.

2.7.1.2 Hardness of the particle

The intensity of the erosion is also directly proportional to the hardness of particles (irrespective of sizes). Those particles have a hardness value above 5 in Moh's scale are considered harmful. Incidentally, most of the Himalayan sediment contains more than 70 % Quartz particles on average with hardness value 7 in Moh's scale. Hence, hardness of the particle is a highly influencing factor in the erosion rate.

Truscott, 1972, mentioned that both Wehinger's, 1958, and Stauffer's, 1956, laboratory tests show that, for metals in general, wear increases rapidly once the particle hardness exceeds that of the metal, for both scouring and impact abrasion. Beyond this, the wear rate may become constant, or even reduce, with increasing abrasive hardness. Stauffer noted that the wear resistance of a 13 % Cr cast steel was only slightly better than that of the unalloyed reference steel, whereas it is usually considerably better in practice; he suggests this might have been due to the excessive hardness of the test abrasive. From tests with various grades of very fine sand (< 200 μm) under dry conditions, Goodwin et al., 1970, found that erosion varied as hardness, and depended on the amount of quartz present. The stronger is an abrasive particle, the deeper it is pressed into the surface before it is broken and the heavier is the resulting wear. The mechanical strength, σ, is determined as

$$\sigma = \frac{4 \cdot N}{\pi \cdot d^2} \qquad \textbf{Equation 2-5}$$

Where, N is the load producing destruction of a single abrasive grain and d is its diameter. The values of σ rises with reduction in d because of the scale effect (Kragelsky, 1985).

2.7.1.3 Concentration

The sediment concentration is one of the dominating factor influencing erosive wear rates. Concentration is the total mass (or volume) of imparting particles present in the unit mass (or volume) of the fluid. Sometimes, it also called the particle flux rate, or the mass of the imparting material per unit area and time. It can also be represented in terms of percentage of particles in a given fluid mass (or volume). Especially for river sedimentation, concentration is usually expressed in grams per litre (g/l). However, often parts per million (ppm) by weight is used, which is equivalent to mg/l, with the approximation of 1,000 ppm equal to 1 kg/ m^3 of water being normal usage (1,000 ppm is equivalent to 0. 1 %).

Erosive wear rate is proportional to the concentration up to a certain limiting value of the wear. This limit has been observed in many studies and is believed to be the result of interference between rebounding particles and arriving particles. It is also possible for wear rates to decrease marginally when the limiting flux is exceeded.

There is surprisingly little quantitative information on the effect of solids concentration. It is generally accepted that wear increases with concentration. Bak, 1966, and Antunes, 1966, consider this relationship to be direct. Bergeron, 1952, from tests on Al-Br., suggested that this applies only to small amounts of solids, but for larger values, wear increases more slowly; his theory states that wear times no. of grains per unit surface area is dependent on concentration and flow pattern. Arnold and Hutchings, 1989, found that the limiting particle flux rate is highly variable, ranging from as low as 100 kg/m^{2}s for elastomer to as high as 10,000 kg/m^{2}s for erosion against metals by large particles (Stachowiak and Batchelor, 2006). Mostly erosion rate is considered linearly proportional to concentration. Bjordal, 1995, found relations for different metals and coatings as follows. Erosion rate $\propto$ concentration$^{0.25 \text{ to } .27}$

However, for most of the materials, when tested for longer period, this value is close to unity. Hence, considering erosion rate direct proportional to concentration with respect to velocity is a satisfactory approximation.

2.7.2 Characteristics of fluids

The main characteristics of fluids include velocity and acceleration of water carrying sediment, impingement angle, media of the flow, temperature, and turbulence. The effect of each characterises on erosive wear is important.

2.7.2.1 Velocity of water carrying sediment

The intensity of erosion is normally proportional to the cube of the velocity of water, carrying sediment particles in suspended condition. This seems true of Francis runners. Any decrease in velocity therefore would substantially reduce the erosion damage. For instance, 10 % decrease in water velocity would reduce erosion at least by 27 % (Naidu, 1999). Laboratory experiments conducted at corporate R and D, BHEL, Hyderabad, India, by utilizing rotating disc apparatus with sediment concentration 75,000 ppm on an AISI 304 steel test piece proved that the sediment erosion rate increased in proportion to V from 1.75 to 2.4. The same experiment also revealed that the reduction in sediment erosion rate was 200 to 280 % when the particle sizes, were reduced by half. Sediment erosion rate (W) can be generally governed by the formula,

$$W \propto S_1 \cdot S_2 \cdot S_3 \cdot S_4 \cdot M_r \cdot V^n \qquad \textbf{Equation 2-6}$$

Where, S_1 = coefficient of sediment concentration, S_2 = coefficient of sediment hardness, S_3 = coefficient of sediment particle size, S_4 = coefficient of sediment particle shape, M_r = coefficient of wear resistance of base material, and V^n = relative velocity of water.

Based on experience of some hydropower stations in Latin America, following values of exponent n have been suggested: n = 3 for Francis runner, n = 3 for Guide vanes and pivot ring liners, n = 2.5 for Pelton nozzles, and n = 1.5 for Pelton runner buckets.

In actual practice, material damage due to plastic deformation and cutting occur simultaneously and the ratio of these damage mechanisms depends on the velocity of particle and the impingement angle together with other parameters. Up to certain velocity, also referred as critical velocity or threshold velocity, the particle cannot skid in the surface due to friction and cutting action does not take place. Yabuki et al., 1999, found this critical velocity for silica sand and carbon steel pair as 2.5 m/s for 0.26 mm particles. As the velocity increases higher than critical velocity, both cutting and plastic deformation component increases, which amplify the erosion rate drastically. The modes of erosion also vary depending on the velocity of the particles. At low velocity, the particles do not have enough energy to erode the material by cutting action, but elastic deformation or fatigue effect may be observed.

Most often quoted expression for relation between erosion and velocity of particle is Erosion $\propto$ Velocity^n, where the values of exponent n vary depending on material and other operating conditions. Considering the impact of particles due to kinetic energy as cause of material removal, theoretically, value of n is 3. However, the view and the finding of different researchers on the value of this exponent n are not alike. Truscott, 1971, reported different values of the exponent, for instance n = 1.4 for steel St37 to n = 4.6 for rubber tested on sandblast apparatus. The value of the exponent will be lower in the case of combined effect of corrosion and erosion with higher corrosion intensity. However, sudden increase in this value can be observed in some velocity range when corrosion scales are removed. In the combined case of solid particle erosion and cavitation, Zhang et al., 1996, found the erosion rate proportional to peripheral speed of disc with exponent value in between 3 - 4.5 for non-metallic coatings.

Similarly, Arnold and Hutchings, 1990, found the velocity exponent for unfilled elastomer in between 2.9 and 5.1 for impingement angle 30 ° and 90 ° respectively. It may be due to particle erosion at higher velocity is more significant than synergy due to cavitation and erosion. Daun et al., 2002, observed different values for different type of test rig for instance n = 2.5 ~ 3.0 for rotary type stand, n = 1.8 ~ 2.7 for disc stands, and n = 2.0 ~ 2.2 for water jet impact. There are big differences in values of the velocity exponent and it is difficult to have uniformity in erosion rate prediction and simulation.

Most often, particle velocity is considered same as the fluid velocity, which is estimated based on continuity equation (Wood, 1999). This is not true in actual practice because generally particle velocity is less than the fluid velocity. Zahavi and Schmitt, 1981, found sand velocity one third of air velocity in jet type of erosion test rig. The accuracy of particle velocity is important in erosion models, but measurement of that is difficult in practice. Chevallier and Vannes, 1995, have mentioned light speed photography, optic gates and double rotating disc for measurement of particle velocity. Bjordal, 1995, used the velocity based on rotational speed of specimen. In the experimental part of this

research, velocity of the particles will be computed by considering continuity equation of the mixture.

2.7.2.2 Impingement angle

The impingement angle is defined as the angle between the eroded surface and the trajectory of the particle just before impacting a solid surface. If the particles are moving parallel to the surface, impingement angle is almost 0 ° and hence only minor erosion may take place. When particles are moving normal to the surface the impingement angle is 90 °.

There are differences in the ways of presenting the relation of erosion rate with respect to impingement angle. Bhushan, 2002, showed that the maximum erosion rate for brittle material is higher than that for ductile material. On the other hand, Matsumura and Chen, 2002, have shown higher erosion rate for ductile material. Similarly, Bhushan, 2002, has shown no erosion up to certain low impingement angles and on contrary, Stachowiak and Batchelor, 1993, have shown erosion rate (about 10 % of maximum) even at zero degree impingement. These differences in the presentation could be due to way of defining the impingement angle of actual particles. Normally the jet angle is considered as impingement angle of particles for practical purpose, but that is not the true impact angle. The flow of particle in the straight pipe or parallel plates can be considered to have impingement angle zero but even in such flow, erosion can be expected. In such cases, if the flow is turbulent, the particles could be dancing or oscillating within the boundary layer in the direction normal to the flow and hence effective impingement could be even close to 90 °.

2.7.2.3 Effect of erosion media on erosive wear

Most erosive agents are conveyed by a medium, e.g., water or air. A mixture of erosive particles and liquid medium is known as slurry. The characteristics of the medium have a surprisingly strong effect on the final wear rate. Controlling factors relate to the bulk properties of the medium, i.e., viscosity, density and turbulence, and to its microscopic properties such as corrosivity and lubrication capacity. It has been shown that small additions of lubricants to erosive slurries can significantly reduce wear (Levy et al., 1987). The ability of the liquid medium to provide cooling during particle impingement is also important (levy et al., 1987). In terms of bulk properties, the drag forces imposed by viscous slurry on the erosive particles can affect wear by altering the impingement angle. This is demonstrated schematically in Figure 2-7(Hojo et al., 1986).

It can be seen that the increased particle drag forces, imposed by more viscous medium, shift particle impingement to the sides of the eroding cylinder. The effect of the medium is to alter the location and the form of wear since the impingement angle is reduced by the shift to the cylinder sides. The medium-induced reduction in impingement angle causes an increase in abrasion-type mechanisms of erosive wear. If an estimation of wear rates in a real machine is required, then a comprehensive analysis of the particle trajectories is essential. For example, an analysis performed for the inlet blades of a gas turbine gave an excellent agreement between predicted and actual location of wear spots (Tabakoff, 1987). An example of erosive particle trajectories between gas turbine blades is shown in Figure 2-8.

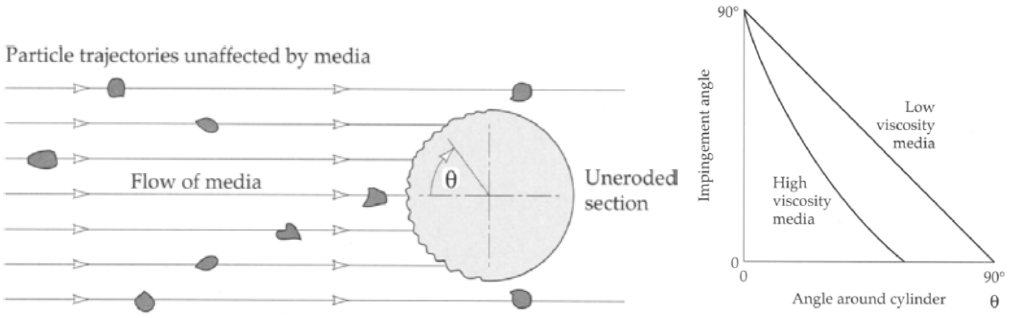

(a) Low viscosity media

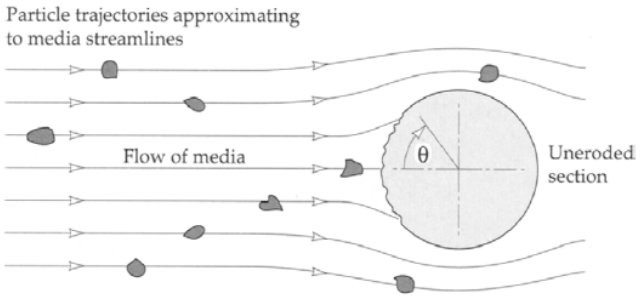

(b) High viscosity media

Figure 2-7 Effect of medium on impingement angle by erosive particles (Stachowiak and Batchelor, 2006)

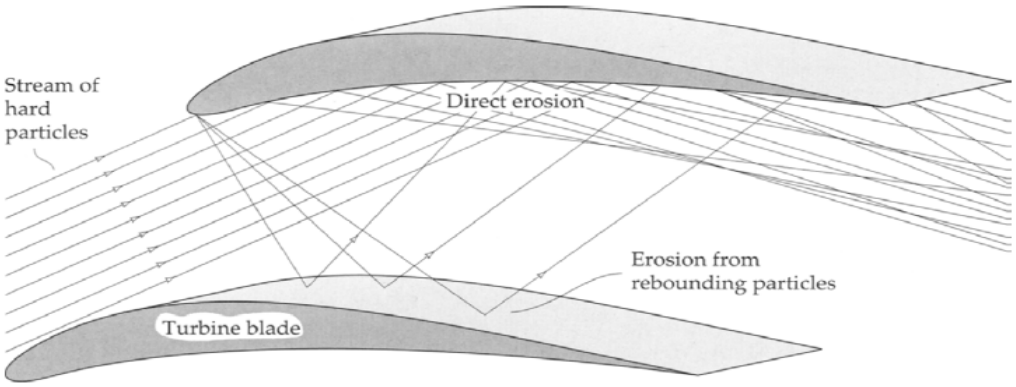

Figure 2-8 Example of particle trajectory analysis to predict erosive wear (Stachowiak and Batchelor, 2006)

The effect of a medium is assessed in terms of the 'collision efficiency', which is the ratio of particles that actually hits a wearing surface to the theoretical number of particle impacts in the absence of any medium. It was found that the collision efficiency declines from a limiting value of 1 for large particles, e.g., 750 μm size, to less than 0.1 for small particles of 75 - 90 μm size, at medium viscosities of 0.005 Pa (H. Mcl et al., 1991). The reduction in collision efficiency is due to the viscous medium sweeping the particles past the wearing surface. The erosive wear rate was found to closely follow the same trend as collision efficiency, which indicates that the primary effect of a liquid medium is to divert particles from the wearing surface. Increasing particle velocity reduces the influence of medium, so that at high slurry velocities, only large particles are affected by the medium's viscosity (H. Mcl et al., 1991).

2.7.2.4 Effect of temperature on erosive wear

From the sediment erosion in hydraulic machinery point of view, temperature alone cannot give any problem however; in general, this can influence the erosion rate and mechanism of erosive wear. The primary effect of temperature is to soften the eroded material and increase wear rates. The effects of temperature on erosion of stainless steel are shown in Figure 2-9 (Levy et al., 1986). The erosive agent is silicon carbide impinging stainless steel at a speed of 30 m/s in a nitrogen atmosphere. It is not until temperatures higher than 600 ~ are reached when the erosion rate showed significant increase. This temperature coincides with the softening point of the steel. There is a strong correlation between the mechanical properties of the material at the temperature of erosion and wear rate as shown in Figure 2-10 (Y. Shida et al., 1985).When high temperature erosion of metals occurs in an oxidizing medium, corrosion can take place and it further accelerates wear. Material is removed from the eroding surface as a relatively brittle oxide and this process of wear can be far more rapid than the erosion of ductile metal. At sufficiently

high temperatures, however, the underlying metal does not come into contact with the impinging particles because of the thick oxide layer present (Stephenson et al., 1986) and then, oxidation rates, not mechanical properties, control the erosive wear.

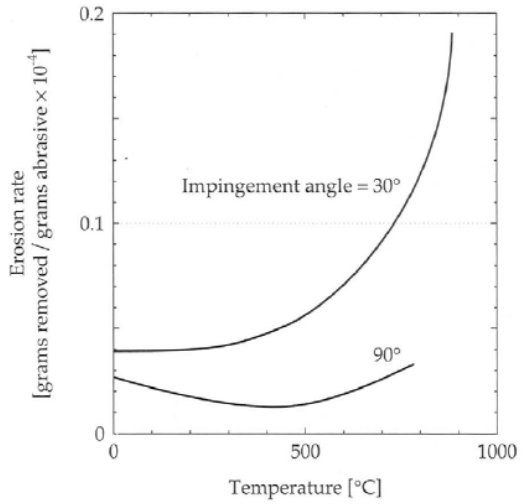

Figure 2-9 Effect of temperature on the erosive wear rate of stainless steel (Stachowiak and Batchelor, 2006)

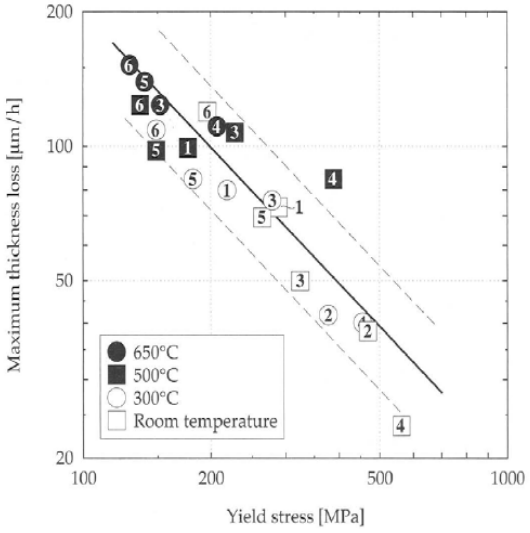

Figure 2-10 Relationship between mechanical properties of materials and erosion rate at elevated temperature (Y. Shida et al., 1985):

(1) Carbon steel, (2) 1.2Cr-1Mo-v steel, (3) 2.25Cr-1Mo steel, (4) 12Cr-1 Mo-V steel, (5) 304 steel and (6) alloy 800

2.7.2.5 Effect of turbulence on erosive wear

Turbulence of the medium accelerates erosive wear, as particle impingement is more likely to occur in turbulent flow than in laminar flow, where the medium tends to draw the particles parallel to the surface (S. Dosanjh at el., 1985). The difference between particle behaviour in laminar and turbulent flow of the medium is illustrated in Figure 2-11.

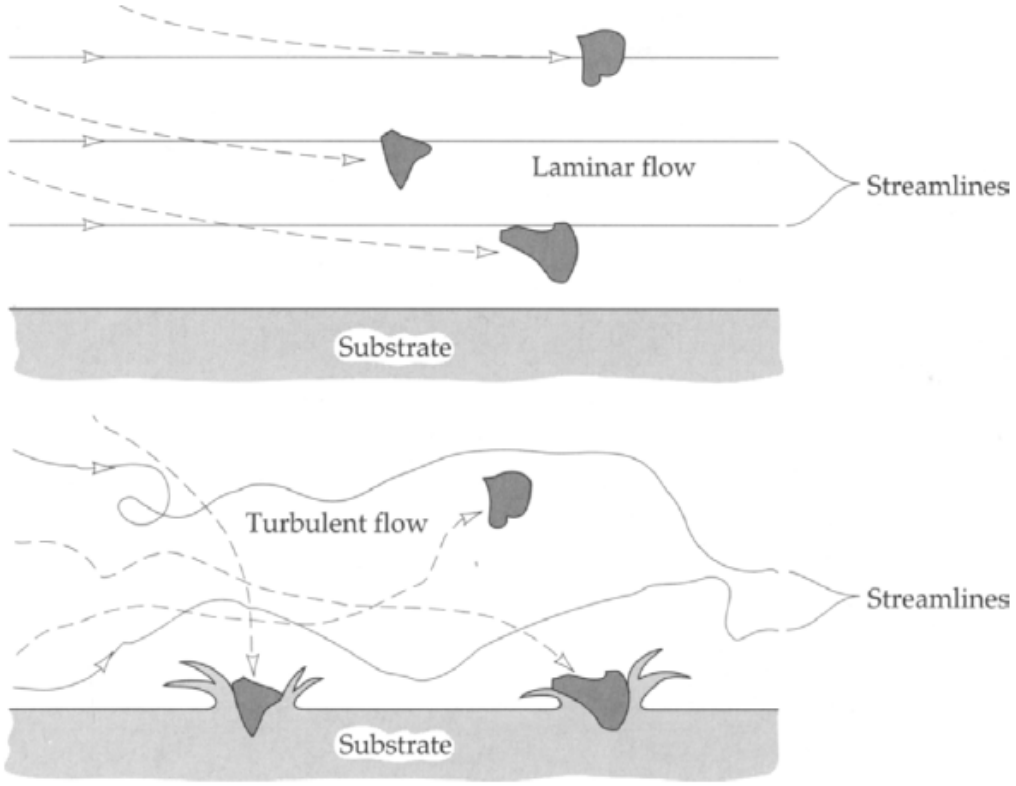

Figure 2-11 Effect of flow on erosive wear (Stachowiak and Batchelor, 2006)

2.7.3 Characteristics of the base material

The material used for the turbine components is equally important factor in the sediment erosion damage. Hardness of the material, its chemical composition, microstructure and its work hardening property influence the intensity of erosion. The choice of the material for a particular component is to be made considering its ability to meet the functional requirements like impact strength and ability to withstand cyclic loading in addition to its wear resistance.

Experience has shown that it is sufficient for components, which are not very susceptible to abrasion, such as spiral casings, nozzle pipes and draft tubes, to be made of plain

structural steel or castings of adequate strength, if their wetted surfaces are protected by a tough, elastic coating. Various epoxy and polyurethane based plastics have proved very suitable for this purpose. These coating materials are recommended for new components and even for eroded parts after suitable pre-treatment. Experience also indicates that the erosion resistance of stainless steel is very good compared to other materials. Stainless steel is stainless because of a thin layer of chromium oxide on their surfaces. The film of chromium oxide is also responsible for the resistance of stainless steels to oxidation. It is therefore necessary that stainless steels have a minimum of 12 % chromium. In addition to chromium, stainless steels also have other alloying elements like carbon, Nickel, Manganese, Molybdenum, Silicon and in some cases, Titanium and Columbium (Niobium).

2.7.3.1 Erosive wear resistance of materials

Material characteristics exert a strong effect on erosive wear and have been extensively studied. In a similar manner to abrasive wear, it is found that improvements in mechanical properties do not always coincide with superior erosive wear resistance. For example, erosive wear rates may increase when a material is deliberately hardened. The difficulty with material optimization for wear reduction is that the characteristics of erosive wear as well as the material characteristics control the wear rate. An illustration of this rule is provided by the comparison of the relative erosion resistance of metals as a function of impingement angle. When the impingement angle is shallow, a hardened steel shows lower wear than a soft steel; the converse is true at high impingement angles. This is illustrated in Figure 2-12, where the erosive wear rate, at two different impingement angles of 15 ° and 90 °, is shown as a function of material hardness for various metals and grades of steel hardness (K-H. Zum et al., 1987). The abrasive used was silicon carbide of diameter about 1 mm impinging at a velocity of 30 m/s. At the shallow impingement angle, it is evident that the hardness and work-hardening ability of materials suppress a quasi-abrasive process of wear. In this case, materials can be rated according to the hardness of the pure metal. It can be seen from Figure 2-12 that, at an impingement angle of 15 °, the most wear resistant metal is cobalt while the second worst is copper. When the impingement angle is 90 °, the ranking of materials changes significantly and copper has the second best while cobalt has the third worst wear resistance. Heat treatment of steel to increase hardness improves erosive wear resistance at low impact angles but lessens the erosive wear resistance at high impact angles. To summarize, the effects of small differences in, for example, hardness or alloy content between similar materials cannot be viewed in isolation from the overall system characteristics of erosive wear. In order to define a material's erosive wear resistance it is only useful to consider broad classes of materials, e.g., polymers, ceramics and metals, where distinctive differences are present and are not obscured by the effects of variables such as velocity or impingement angle. There is no general recipe for a high level of erosive wear resistance. Because of the two different erosive wear protection mechanisms that can take place, high wear resistance can be achieved by more than one type of

material. In some cases, the material can be extremely hard and tough so that the impacting particle is unable to make any impression on the surface. This is the approach adapted when developing metallic or ceramic erosion resistant materials. Alternatively, the material can be tough but with an extremely low elastic modulus so that the kinetic energy of the particles is harmlessly dissipated. These contrasting wear protection mechanisms are illustrated in Figure 2-13.

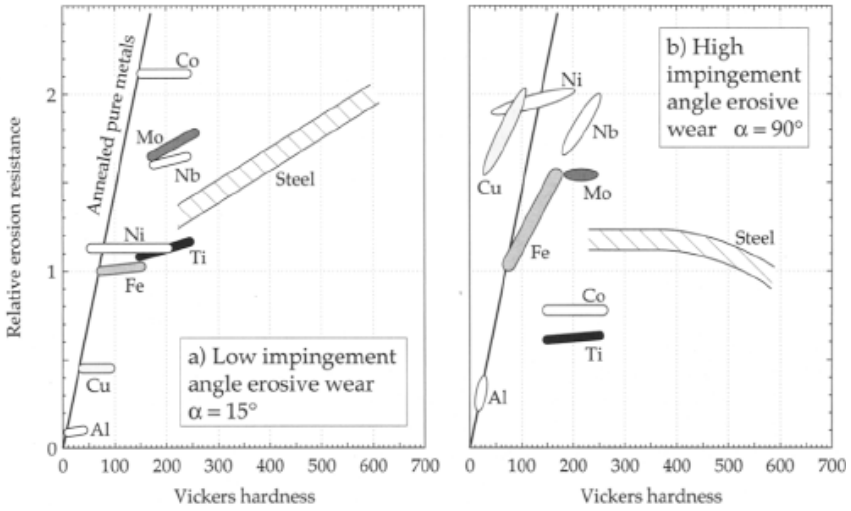

Figure 2-12 Effect of primary material characteristics and erosion parameters on erosive wear rate (Zum et al., 1987)

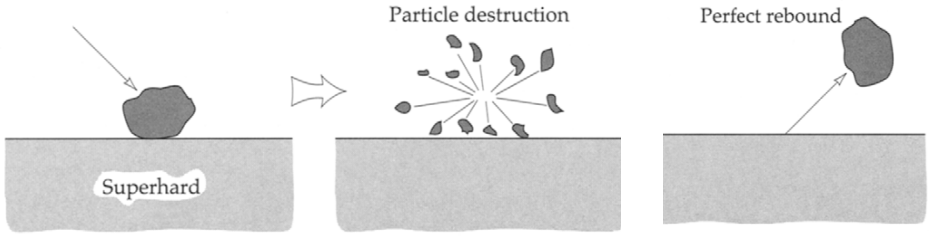

Super hard material to resist erosion

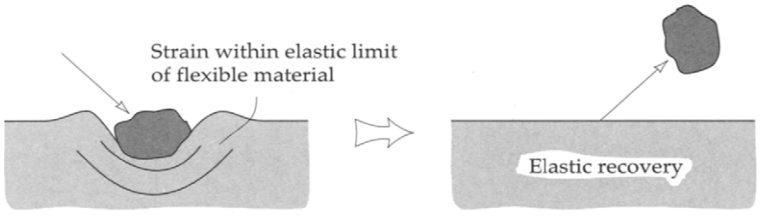

Elastic Energy absorption

Figure 2-13 Comparison of the high and low elastic modulus modes of erosive wear protection (Stachowiak and Batchelor, 1993).

Rubber is generally believed to provide good erosion resistance by elastic absorption of particle energy although this has not been demonstrated experimentally. It has been shown that the first particle impact causes no visible damage to a rubber surface and that wear depends on slow fatigue processes (Arnold and Hutchings, 1990). Unfilled rubber shows good erosive wear resistance but surprisingly it is not resistant to abrasive wear (Arnold and Hutchings, 1990). The choice of erosion resistant material may also be compromised by other considerations such as operating temperature or material transparency. Clearly, temperatures in excess of 200 °c preclude polymers from service, but if a transparent material is required for a specific application then metals are not particularly useful. For example, materials for aircraft windscreens, apart from being transparent, are required to be resistant to high-speed erosion by sand, dust and rain (Rao and Buckley, 1986). The relative merits and demerits of metals, polymers and ceramics as erosive wear resistant materials are summarized in Table 2-2.

Table 2-2 Relative qualities of erosive wear resistant materials (Batchelor et.al., 1993)

Material	Relative qualities regarding erosive wear resistance
Metals	Large range of toughness and hardness to suit any particle or impingement angle. Prone to high temperature corrosion, and softening effects; corrosive media also harmful.
Ceramics	Very hard and increasingly tougher grades available. Resistant to high temperatures and corrosive media. Poor erosive wear resistance when brittle mode prevails.
Polymers	Tough polymers and rubbers provide good erosion resistance even in corrosive media. Usage is restricted however by a relatively low temperature limit.

It was found that the erosive wear of steels shows the classical ductile erosion characteristic, i.e., a maximum wear rate at a low impingement angle of 30 ° with subsurface and surface cracking (Levy, 1987). This suggests that the erosive wear resistance of steels is limited by a lack of ductility. For very soft erosive particles such as coal, the inclusion of carbides promotes wear resistance slightly (Sargent and Saigal, 1986). Alloying of steel or cast iron to obtain a microstructure containing a significant amount of retained austenite is an effective means of reducing erosive wear. Bahadur et al., 1990, adding about 2.5 wt % of silicon to 0.7 wt % carbon steel or about 0.45 wt % of silicon to 2.54 wt % cast iron results in good erosive wear resistance. The optimum heat treatment of this steel or cast iron includes a relatively long austempering time where all the martensite is removed and only retained austenite and bainitic ferrite are present. Generally, ductility rather than hardness should be enhanced in steels for improved erosive wear resistance.

2.8 WEAR THEORY

There are many different terms are used to define the wear. Wear can be classified and characterized in several ways (Thapa, 2004). Several authors give different expressions of wear and its rate, based upon their wear test results. The wear/erosion rate (mm/year) is often expressed as functions of the velocity of the particles and proportional to V^n. The velocity exponent n for pure erosion in between 3 to 4 has most often been reported. Since wear rate is a function of velocity, this means that the relative importance of erosion depends on the flow rate. Further, it depends on material hardness, grain size, solids concentration and temperature. The one most often quoted expression of wear is (Truscott, 1972),

$$Wear \propto (Velocity)^n \qquad \textbf{Equation 2-7}$$

Where, the index n may vary depending on the material and other factors involved; the most common value appears to be 3 (Truscott, 1972).

Some more detailed analyses consider wear as affected by the forces and velocities acting on a particle in a liquid flow. Bovet, 1958, states that wear is directly proportional to abrasive power (P_f) of a particle impinging on a surface (mentioned by Truscott, 1972), and

$$P_f = \frac{\mu \cdot V \cdot (\rho_s - \rho_1) \cdot c^3}{R_p} \qquad \textbf{Equation 2-8}$$

Where, μ = coefficient of friction between particle and surface, V = volume of particle ϱ_s = density of particle, ϱ_1 = density of liquid, c = velocity of particle, R = radius of curvature of surface.

In a much more involved analysis, but starting with the same basic assumption, Bergeron, 1952, develops a complicated expression based on the statement.

$$Wear \propto (accleration\ of\ main\ flow) \cdot (coefficient\ of\ friction) \cdot (thickness\ of\ particle\ layer) \cdot (solid - liquid\ density\ difference) \cdot (flow\ velocity)$$

He thus takes account of the difference between the solid and liquid velocities. He attempts to predict wear rates in similar pumps handling solids with varying properties, with simplified assumptions such as pure sliding of the particles over the surface, from the initial expression:

$$Wear \propto \frac{U^3 \cdot (P - \rho) \cdot d^3 \cdot p \cdot K}{D} \qquad \textbf{Equation 2-9}$$

Where, U = characteristic velocity of liquid, P = density of particles, ϱ =density of liquid, d = diameter of particles (assumed spherical), D = characteristic dimension of machine, p = no. of particles/unit surface area, and K = experimental coefficient depending on abrasive nature of particles.

Bitter, 1963, in a fundamental study of erosion phenomena, but strictly for dry conditions, gives expressions for cutting and deformation wear, also based on energy considerations and the type of material eroded, i.e., whether brittle or ductile.

A few authors also develop expressions for pump service life. Both Bak, 1966, and Bergeron, 1952 (Truscott, 1972), consider this in terms of pump total head for given conditions. Vasiliev, 1970, gives a somewhat involved method, based on statistical analysis of pump wear tests, to predict life based on a specified maximum permitted wear.

It is perhaps debatable whether these more complex theories can be used to predict absolute wear rates with any certainty; most involve empirical constants and other parameters difficult to determine for an actual machine (Truscott, 1972). In fact, Bergeronlo, 1952, admits that some of the assumptions made may be questionable. However, such theories are of some value in predicting likely trends in wear rates when only one or two of the relevant factors are altered (Truscott, 1972).

When considering a stationery plate as a unit of area with flow normally to its face surface by a uniform steady liquid stream, it becomes possible to derive the mathematical relationship representing the mass laws of hydro abrasive erosion. Daun et al., 2002, gave relation of erosion and kinetic energy. He stated that without regard to the deterioration pattern, the place erosion developed under the action on its surface of a single solid particle E' is proportional to the kinetic energy possessed by this moving particle, i.e.

$$E' = \alpha \cdot \frac{m \cdot c^2}{2} \qquad \textbf{Equation 2-10}$$

where, m is mass of the particle, c is average particle velocity of translation, and α is coefficient defined by the flow conditions, the material of the particle and the plate, as well as other factors. The number N of abrasive particles containing with the plate surface for time interval t can be defined by the expression:

$$N = \beta \cdot \varepsilon \cdot v \cdot t \qquad \textbf{Equation 2-11}$$

Where, β is coefficient dependent on the flow conditions around the plate and conveying capabilities of the flow, v is mean velocity of the flow, ε is the particle concentration. The plate erosion for time interval t is as follows:

$$E = E' \cdot N = \alpha \cdot \beta \cdot \frac{m \cdot c^2}{2} \cdot \varepsilon \cdot v \cdot t \qquad \textbf{Equation 2-12}$$

It can be assumed that velocity c of the solid particles suspended in the flows is proportional to flow speed v, i.e. $c = \gamma \cdot v$, therefore, equation 2.12 will be,

$$E = \alpha \cdot \beta \cdot \gamma^2 \cdot \frac{m \cdot \varepsilon \cdot v^3}{2} \cdot t$$

or

$$E = k \cdot m \cdot \varepsilon \cdot v^3 \cdot t$$ **Equation 2-13**

Equation (2.13) shows that the abrasive erosion of stationery component passed by a liquid flow with solid particles suspended varies in direct proportion to the mass of particles, their volumetric concentration, the 3rd power of the flow velocity and duration of the effect exerted by the flow. This is the theoretical evaluation of abrasion intensity. In practice, a large number of additional factors complicate the erosion of hydraulic machines. Moreover, there is no extra mathematical dependence, for the time being to define them.

2.9 EROSION MODELS

Mathematical models of erosion are useful for designing of hydraulic turbine components, sediment settling basin and optimization of hydropower plant operation in Sediment-laden River. Most often, individual particle dynamics are used for developing erosion models. Empirical and statistical relations are also often developed from experiments and field experiences. However, studies are heading toward numerical modelling and simulations, the importance of analytical models are increasing day by day (Thapa, 2004). Truscott, 1972, has found that the most often quoted expression for erosion is proportional to (velocity)^n.

Extensive research has been done to develop a wear model in terms of the material properties involved but little attention has been given to clarify the influence of fluid motion, especially in the turbulent flow regime (Humphry, 1990). Over the years, many models have been proposed for many different situations. Unfortunately, most models are co-relational in nature and therefore system specific. They only work for the particular material pair, contact geometry, operating condition and range, and the particular environment and lubricant. The available equations are so confusing that few designers can use any of them to predict product life with confidence. The complexity of wear and the large number of parameters affecting the outcome are the primary reasons for this situation.

However, several fundamental studies of erosion behaviours for different conditions are found while reviewing the available literatures, only general erosion model and some erosion models that have been developed for hydraulic machinery applications, is discussed here.

2.9.1 General erosion model

The actual mechanism of the erosive wear is not yet clearly understood. Hence, simple, reliable and generalized model for erosion is not yet developed for engineering purpose. Most common expression for the erosive wear is based on experimental experience and they are generally expressed as a function of the factors that associated with erosive wear.

The most often quoted expression is Wear $\propto$ (Velocity)^n where index may vary upon the factors (Thapa and Dahlhaug, 2003). The simplest way of writing equation for erosion is:

Erosion = f (operating condition, properties of particles, properties of base material)

Generally, this expression is given as a function of velocity, material hardness, particle size, and concentration. Bardal, 1985, describes the most general formula for pure erosion as,

$$W = K_{mat} \cdot K_{evn} \cdot c \cdot V^n \cdot f(\alpha) \qquad \textbf{Equation 2-14}$$

Here, W is erosion rate (material loss) in mm/year, K_{mat} is material constant and K_{env} is constant depending on environment, c is concentration of particles and f(a) is function of impingement angle α. V is the velocity of particle and n is the exponent of velocity.

2.9.2 Erosion models for hydraulic machinery

Many erosion models are developed for specific purpose or condition (Thapa, 2004). For example, Bitter's model is developed for dry condition, hence it is not clear whether this equation realistically predict erosion rate for wet condition or not. Few researchers have presented models specifically for hydraulic machinery. Truscott, 1972, presented the equation of Bergeron, 1952, to predict the erosion rate of pump with simplified assumptions such as pure sliding of spherical particles over the surface.

$$W \propto \frac{V^2}{D} \cdot (\rho_p - \rho) \cdot d^3 \cdot p \cdot K \qquad \textbf{Equation 2-15}$$

Where, V is the characteristic velocity of liquid, D is the characteristic dimension of the machine, ϱp is density of particle, d is diameter of particle, p is number of particles per unit surface area, ϱ is density of liquid and K is experimental coefficient depending upon nature of abrasive particles. This equation is depends on experimental coefficient, which is dependent on abrasive nature of particles.

Daun et al., 2002, established the equation for surface erosion based on impact effect of particles considering kinetic energy of single particle. They have anticipated deviation on erosion estimated by equation due to uncertainties like non-homogeneous particles, variable concentration, continuous alteration and pulsation of velocities and pressure, non-uniform flow distribution and so on. On the contrary, to laboratory tests, Tsuguo, 1999, established the relationship of factors concerning erosion of turbines based on 8 years erosion data of 18 hydropower plants. The repair cycle of turbine is determined according to calculation of turbine erosion from equation, which gives erosion rate in term of loss of thickness per unit time (w).

$$W = \lambda \cdot c^x \cdot a^y \cdot k_1 \cdot k_2 \cdot k_3 \cdot V_{Char}^z \qquad \textbf{Equation 2-16}$$

Where 'λ' is turbine coefficient at eroded part; 'c' is the concentration of suspended sediment, and V is the characteristic velocity. The term 'a' is average grain size coefficient based on unit value for grain size 0.05 mm. The terms k_1 and k_2 are shape and hardness

coefficient of sand particles and k_3 is abrasion resistant coefficient of material. The x, y and z are exponent values for concentration, size coefficient and velocity respectively. The value of x and y are close to the unity and any deviation of this linear proportionality is determined from plot of wear versus parameter. The values of z are proposed for different turbine components based on relation between relative velocity and erosion. Minimum value of n is proposed as 1.5 for Pelton bucket and maximum value is 3 for Francis turbine runner. Similarly, for Francis turbine guide vanes and Pelton turbine needle, this value is proposed as 2.5.

IEC 2008, recommended the following theoretical model of abrasion rate in order to demonstrate how different critical aspects impact the particle abrasion rate in the turbine.

dS/dt = f(particle velocity, particle concentration, particle physical properties, flow pattern, turbine material properties, other factors)

However, this formula being of little practical use, several simplifications are introduced. The first simplification is to consider the several variables as independent as follows:

dS/dt = f(particle velocity) . f(particle concentration) . f(particle physical properties, turbine material properties) . f(particle physical properties) . f(flow pattern) . f(turbine material properties) . f(other factors)

This simplification is not proven. Nevertheless, based on literature studies and experience, it is felt that this simplification is justified for hydraulic machines. Finally, IEC suggested the following expression with additional simplifications and new variable.

$$S = W^3 \cdot PL \cdot K_m \cdot K_f$$

Equation 2-17

Where, S is abrasive depth in mm, W is characteristic velocity, PL is particle load which is obtained by particle concentration integrated over the time, K_m is material factor and K_f is flow factor.

2.10 CONCLUSION

The abrasive and erosive wear was initially thought to consist of one or two relatively simple mechanisms, but it is now realized that many processes are involved and some of them are not yet well understood. Most of the common expressions for erosive wear models for hydraulic machinery are based upon the experimental experience only. The sediment erosion damage of mechanical components is due to the dynamic action of sediment flowing along with water, which involves different forces and many other influencing factors that make the erosion mechanism further complex. More research and development is needed to understand the actual mechanisms of particle movement and erosion inside the hydraulic machines.

Chapter 3
Sediment Erosion in Hydraulic Machinery

This chapter presents the sediment erosion types in hydraulic machinery components based upon an extensive literature review and the field observation at Cahua hydropower plant. It includes some recommended methods to minimize the effect of sediment erosion in turbine components. An alternative design of a Francis turbine in sediment-laden water is also briefly discussed.

3.1 INTRODUCTION

Hydraulic turbines mainly divided into two groups: Impulse and Reaction. This classification is based upon the principle of energy conversion. Pelton and Turgo are examples of Impulse turbines. Francis, Kaplan and Bulb turbine are examples of reaction turbines. The cross flow turbines are two stage impulse turbine used for smaller units.

In general, a number of factors influence the development of sediment erosion process of hydraulic machinery. These factors include mean velocity of particles, mass of the particle, concentration of the abrasive particles in a liquid flow, grain size and shape of the particles and angle of attack at which the particles collide with the surface etc. In practice, a large number of additional factors involved and further complicated the erosion of hydraulic machinery. In addition, there is no exact mathematical dependence, for the time being, to define them. Variable concentration and structural in homogeneity of suspended particles, continuous alternation and pulsation of both velocities and pressure during the motion of the flow, and variance in operation, and design features of hydraulic machinery itself, caused the actual pattern of the erosion more complicated and different (Duan et al.,2002).

Most often, it is difficult to distinguish the exact type of erosion on the hydraulic machinery. Duan et al., 2002, have described the erosion of hydraulic turbines in six categories as shown in Table 3-1 based upon the visual appearance. This classification could be use to evaluate the hydraulic patterns.

Table 3-1 Turbine erosion categories (Duan et al., 2002)

S.N.	Type	Description
1	Metallic luster	A Shining surface with no traces of paint, scale or rust
2	Fine-scaly erosion	A surface with rare, separately located and skin-deep minute scales
3	Scale erosion	A surface entirely covered with skin-deep fine scale
4	Large-sized scaly erosion	A surface entirely covered with deep and enlarged scales
5	In-depth erosion	A surface covered with deep and long channels
6	Through hole or entire erosion	Out of the material

Similarly, B.S. Mann, 1999, collected data on wear patterns of different sediment affected hydro turbine components at various hydropower stations in India in order to analyse the wear patterns. This was compared with the data available with some foreign hydropower stations from Switzerland, Pakistan, and China. It was observed that the wear patterns have a resemblance and there is a significant relevance to the flow characteristics of all the power stations. The wear pattern on a particular component is found to be similar.

As mentioned by Thapa, 2004, Matsumura and Chen, 2002, classified the erosion condition in Reaction turbines in three categories, as I, II and III, based upon difference in flow velocity and impingement angle of particle. This classification is shown in Table 3-2, which was developed based on erosion test of specimens located at different turbine components. From this classification, it is not possible to interpret the different type of erosion on the same component of turbine, for example, the turbine blade, can have different type of erosion at leading edge and trailing edge.

Table 3-2 Classification of erosion (Matsumura and Chen, 2002)

Type of erosion	Location	Flow velocity	Impingement angle
I	Spiral casing Draft tube	Low	Small
II	Runner blade Guide vane	High	Small
III	Wearing ring	High	Large due to vortex and turbulence

Brekke, 2002, classified the sediment erosion in hydraulic machinery into three different categories, namely, micro erosion, secondary flow vertex erosion, and acceleration erosion.

Micro erosion is found on the surface of turbine components where fine particles with grains size less than 60 μm are moving at very high velocity. High shear stress in the boundary layers gives high rotational motion to these particles causing several ripples in

the direction of flow. The patterns with such erosion are also compared as fish scale or orange peel. Such type of erosion can appear in guide vane and runner blade in a Francis turbine towards outlet and in the needle of a Pelton turbine.

Obstacles in the flow field or secondary flow in the corners of conduits causes secondary flow vortex erosion. Any obstruction in the flow field causes secondary flow and horseshoe vortex is generated around the cylindrical obstacles like guide vane leading edge. Similarly the needle of the Pelton wheel have vortex behind the ribs supporting needle and hence vortex erosion takes in the straight line downstairs the ribs. The vortices in the corner of conduits like guide vanes-facing plates and blades-band also cause this type of erosion. Such vortices and secondary flow are caused by combined effect of boundary layer and change in flow acceleration. The design of hydraulic machinery working in the range of high Reynolds numbers, (10^6 - 10^8) will normally be exposed all three types of erosion.

3.2 IMPULSE TURBINE: PELTON

Generally, Pelton turbines are designed for low speed number, range from 0.1 to 0.2, the velocity in the jets will be higher than 100 m/s. The acceleration of the particles in the buckets will normally be more than 50,000 m/s^2, which depends on the size of the buckets and head of the turbine. The high velocity and acceleration of particles at the buckets are main reasons for the sediment erosion. Brekke, 2002, categorized the Pelton turbine components into four groups in order to study the sediment erosion phenomenon. Those are inlet system, nozzle system, turbine runner and the wheel pit.

3.2.1 Inlet system

Inlet system consists of manifold and valve. The velocity at inlet system is normally maintained low. Brekke, 2002, provided the following velocity relations in order to design the inlet system of the Pelton turbines.

At inlet manifold, $C = k_i \cdot \sqrt{2 \cdot g \cdot h}$ [$0.08 < k_i > 0.1$] **Equation 3-1**

At valve, $C = k_v \cdot \sqrt{2 \cdot g \cdot h}$ [$0.095 < k_v > 0.12$] **Equation 3-2**

At nozzle, $C = k_n \cdot \sqrt{2 \cdot g \cdot h}$ [$k_n > 0.99$] **Equation 3-3**

Because of the low operating velocity at the inlet, the inlet system or pipes will have only moderate effect of sediment. Hence, application of high erosion resistance rubber, and

epoxy based coating or paint may prevent erosion in such pipes. Slight erosion of this system does not affect the performance of the turbine by any means, but severe erosion in bifurcation and bends is likely to increase the leakage and in worst-case rupture of pipe. Regular inspection and maintenance should be carried out to prevent any catastrophic effect.

3.2.2 Nozzle system

Nozzle system includes nozzle ring and needle. High head Pelton turbine, for example, 1,200 m head can have jet velocity up to 150 m/s. Such a high velocity can damage both the nozzle and the needle. The flow is accelerated from the outlet of fins supporting needles up to nozzle tip and all the pressure energy available in the water is converted into kinetic energy. High velocity combined with the needle geometry creates strong turbulence in the boundary layer close to needle tip. The fine particles bombarding due to turbulence strikes the needle surface several times and severe erosion can be seen in short time. Cavitation can follow in a short interval of time and severe damage of the needle can take place. The nozzle tips are relatively sharp and less than 1 mm contact between nozzle and needle are maintained to reduce cavitation damage and to obtain highest possible efficiency. This makes the nozzle tip vulnerable to sand erosion. If nozzle diameter increases by 5 % due to erosion at tip, the turbine will run at 10 % load even if needle is at closed position. It may affect entire control system of the power plant.

The photographs presented in Figure3-1 illustrate the extent of sediment erosion in Pelton turbine nozzle and needle. These photographs were taken from the lecturer notes provided by professor Ole Gunnar Dahlhaug, NTNU.

(a) Nozzle needle, Mel, Norway

(b) Nozzle ring, Andhi Khola, Nepal

Figure 3-1 Sediment erosion at Pelton turbine nozzle and needle

The protection of needle and nozzle surface by applying ceramic-metallic coatings may help to improve erosion resistance. Ceramic coating is not very effective in case of larger size particles. There is very little scope to improve the erosion resistance of needle and nozzle by hydraulic design, but maintainability can be improved by designing replaceable nozzles tip.

3.2.3 Pelton turbine runner

Peltion turbine runner consists of splitter, bucket tip and bucket surface. Sediment erosion can be found in all components however, the nature of erosion is different. In high head Pelton turbines, the absolute acceleration range normal to the surface could be 50,000 - 100,000 m/s^2. Such a high acceleration is the main reason of sediment erosion in turbine buckets, which has a strong effect on separation of particles from streamline. The characteristics of damage due to fine and coarse sediment are different. With coarse particles, most of the damages are in the area where the jet directly hits at the bucket surface. Surface damage is observed due to the hammering action and not due to the cutting action by sharp edge. Long scars are also seen in the flow direction in each side of the bucket splitter but no damage is observed at the root of the bucket. Splitters and entrance lips are most severely damaged portion of the buckets, because of direct hitting of particles. The photographs presented in Figure 3-2 illustrate the extent of sediment erosion in Pelton turbine buckets and splitter.

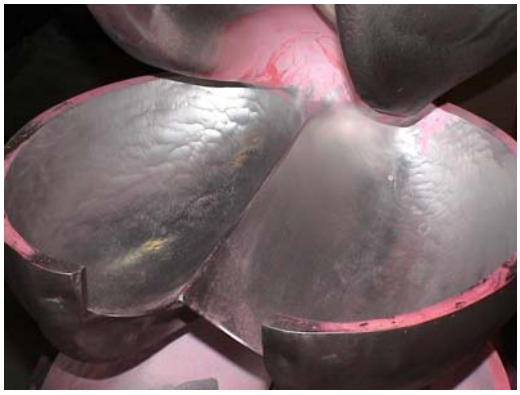

(a) Bucket surface, Khimti, Nepal

(b) Splitter, Rangjung, Bhutan

Figure 3-2 Sediment erosion at Runner buckets

The acceleration of particles normal to the flow direction separates the particles from the flow direction and such accelerating particle strikes the surface causing collision in the water conduit surface. Large particles, for instance higher than 0.5 mm, cause severe damage in the Pelton turbine bucket.

Fine particles may glide along with water inside the bucket and strike the surface toward outlet edge, causing severe erosion around the outlet. Due to distortion of bucket profiles near the outlet, but not at the edge where the acceleration is zero, the direction of flow changes bending inward and strike backside of following bucket with braking effect. This phenomenon is schematically explained in Figure 3-3

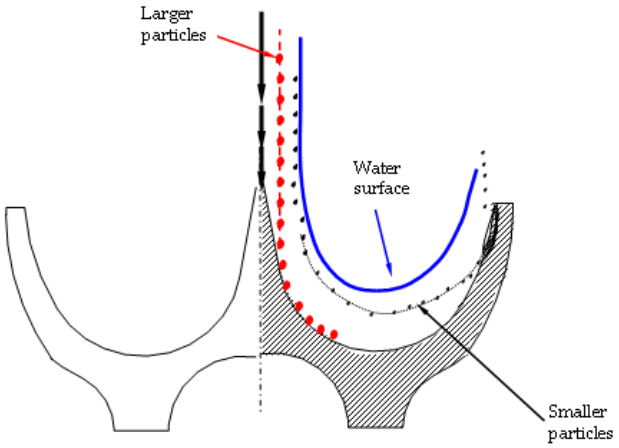

Figure 3-3 Illustration of separation of particle in a Pelton bucket (Thapa and Brekke, 2004)

Thapa and Brekke, 2004, have drawn some conclusions based upon the different hydropower plants erosion patterns observations:

- If the particles are fine (silts), then there will be erosion on the needle but not much erosion in the buckets
- If the particles are coarse (sand), then there will be erosion in the buckets and there is less erosion of needles
- With medium size particles, both needle and bucket will be eroded

3.2.4 Criteria for Pelton turbine design

Sediment erosion problem cannot be solved completely by hydraulic design alone however, this can be minimised to some extent. The three basic criteria for the design of Pelton turbine to minimize the effect of sand erosion are as follows (Brekke, 2002).

- The radius of curvature should be as large as possible at the location where flow direction changes
- The number of jets should be as low as possible
- The hydraulic radius of the bucket and nozzle size should be large. This brings minimum sand particles in contact with the surface

3.3 REACTION TURBINE: FRANCIS

Generally, Francis turbines are designed for speed number, range from 0.2 to 1.5. High head Francis turbines are mostly affected by sediment erosion. For the high head type of Francis turbine, approximately 50 % of energy is converted in to kinetic energy at guide vane and remaining 50 % is retained as pressure energy. The inlet velocity could reach up to 85 - 95 m/s on high head turbines. Hence, guide vane faces high absolute velocity. The runner outlet has highest relative velocity. The velocity at the runner outlet is normally selected around 40 m/s during design to ensure flow of water out of the turbine. Brekke, 2002, categorized the Francis turbine components in to four groups in order to study the sediment erosion phenomenon. Those are inlet system, guide vanes system, runners and labyrinth seals, draft tubes, and shaft seals.

3.3.1 Inlet system: Stay vane

Inlet system of Francis turbine consists of manifold, valves, bypass system, spiral casing and stay vanes. Compared to inlet valve of Pelton turbine, its inlet valve will face 50 % less pressure during closing due to pressure created by spinning runner. Hence inlet valve of Francis turbine have rubber seal against movable steel seal, which has better erosion resistance. It is important to make bypass system larger in order to create higher possible pressure in the spiral casing before opening the valve seals because lower pressure in the spiral casing during opening will increase the damage of the valve seals and bypass valve seals. Hence, bypass system in the Francis turbine has to be stronger than Pelton turbine to create higher pressure in spiral casing. The starting pressure in the guide vane system gives indication of leakage due to sand erosion. The velocity at spiral casing is higher than Pelton turbine manifold because of shorter distance between inlet valve and guide vanes. The velocity at the inlet of the spiral casing is almost same as the meridional velocity at the runner outlet and inlet of valve.

The stay vanes have the main purpose of keeping the spiral casing together. The dimensions have to be given due to the stresses in the stay vanes. The vanes are designed so that the flow is not disturbed, and they direct the flow into the turbine. Because of the secondary flow in the spiral casing, an incorrect flow angle towards the top and the bottom region of inlet of stay vanes in traditional design often cause secondary flow erosion in high head turbines. Similar phenomenon has been observed at Cahua power

plant, where paint and material are removed due to the erosion at the stay vane inlet as shown in Figure 3-4 (a).

(a) Inlet of stay vane

(b) Typical ring grooves near leading edge

Figure 3-4 Erosion at stay vane at Cahua power plant

The corrosion followed by removal of paint accelerates the erosion rate. However, modern parallel stay rings reduces incorrect flow and minimizes erosion at stay vane inlet. Under normal condition, erosion resistant paints can be used in spiral casing and stay vane, but for high head turbines, stainless steel stay vanes can be used to reduce the effect of sediment erosion. The mid height of the leading edge part is exposed to less erosion intensity. Near the upper and lower cover at the inlet, ring-shaped erosion grooves, as shown in Figure 3-4 (b), were observed (Mette Eltvik, 2009).

3.3.2 Guide vane system

The guide vane system is highly affected by sediment erosion due to highest absolute velocity and acceleration. For high head turbines, the relative velocity head $(C^2/2g)/H_n$ for guide vane increases from 10 % at guide vane inlet to 50 % at runner inlet. At normal speed, pressure drop across the guide vane will be approximately 40 % of net head at full load and 50 % at small opening, which is one of the reason for cross flow and hence erosion takes place at the junction of guide vanes and facing plates. The main reason for cross flow is the pressure difference. The erosion of guide vane due to sand laden water can be classified in following four categories (Brekke, 2002):

- Turbulence erosion at the outlet region and facing plate due to high velocity of fine grain sand
- Secondary flow erosion in the corner between guide vane and facing plates due to fine and medium size particles, which makes horseshoe grooves in the facing plates following contours of guide vanes
- Leakage erosion at the clearance between guide vane and facing plate due to local separation and turbulence increasing the horseshoe vortex in the suction

side. The leakage also causes local separation and turbulence at the pressure side at inlet and suction side at outlet of guide vanes causing even a deep groove at the bottom and top of the guide vanes

- Acceleration erosion is caused by separation of large particles from the streamlines of main flow due to rotation of water in front of the runner. This acceleration of particle is normal to the streamline and strikes guide vane surface causing severe erosion. This acceleration also creates secondary flow causing erosion at the corner between the guide vanes and the facing plates by fine particles

In Cahua power plant, as shown in Figure 3-5 (a), more erosion is observed near the transitional zone to the lower cover, due to the high acceleration and absolute velocity in the guide vane cascade. The acceleration erosion in the guide vane in reaction turbine can be reduced by designing the flow with smoothest possible acceleration. The stay vane outlet angle should be carefully chosen so that guide vane will be in neutral position in normal operation condition. Similarly, reduction of clearance between guide vane and facing plate avoid cross flow and secondary flow. Metal sealing are used to reduce gap between guide vane and facing plates with the intention to improve efficiency, but this could be more destructive once damage of such seal commence. The turbulence and secondary flow create dangerous galling in facing plates. It destroys flow pattern and reduces turbine efficiency. The covers will be exposed to erosion since the acceleration normal to the streamline creates secondary flow, especially at the corners between the facing plates and guide vane as clearly seen in Figure 3-5 (b). This effect occurs because of the horseshoe vortex and heavy erosion grooves are observed.

(a) Eroded guide vanes

(b) Horseshoes vortex of facing plates

Figure 3-5 Erosion at guide vane and facing plates at Cahua power plant

The guide vane clearance for new turbine is recommended roughly 0.1 - 0.3 mm in pressurized condition, which is dependent on deflection of the head cover. Low initial dry clearance in the order of 0.05 to 0.1 mm may give low clearance in pressurized condition, but such a low dry clearance may cause abrasion and adhesion between guide vane and facing plates. The facing plates can be improved by cladding underneath the

guide vanes, but the difference in hardness between guide vanes and facing plates should be maintained to avoid galling of the surface. The hardness of 16Cr5Ni Guide vanes with 350-400 HB and facing plate of 17Cr1Ni with 300 HB is an example of appropriate combination, which avoids galling and abrasion. The necessary tolerance and surface finish at the mating part of guide vane and facing plate should also be maintained to get rid of these problems. The maintainability of the facing plate is often improved by designing replaceable layer to save maintenance time and expensive bulk material.

3.3.3 Runner

In the runner, the highest relative velocity occurs at outlet region while the highest absolute velocity and accelerations may be found at the inlet of the blade. Hence, impact due to kinetic energy is small compared to force exerted by large accelerating particle. Contrary to this, the relative velocity is the highest at the outlet of the runner blade. Hence, turbulence erosion due to fine sand is always susceptible at the trailing edge of the blade. Also because of high relative velocity, most of the particles will move towards outer diameter in the runner outlet and hence more effect of erosion is seen there. Inlet region of the runner is sensitive to incorrect pressure distribution between pressure and suction side and any separation caused by this may cause severe local erosion at the inlet due to fine grain sand. Cross flow from the hub to the shroud caused by incorrect blade leaning will also increase the so-called horseshoe vortex in the blade roots. The erosion at runner outlet of Cahua power plant is shown in Figure 3-6.

(a)Erosion at runner outlet

(b) Erosion at pressure side of blade

Figure 3-6 Erosion at runner at Cahua power plant

The improvement of blade leaning and correct blade loading at inlet may improve performance of Francis turbine against erosion. The splitter blades at the inlet of runner help to reduce damage of flow around leading edge at off design operation, which ultimately improves the resistance to sand erosion and cavitation. Incorrect blade leaning may lead to cross flow between hub to band and such cross flow may intensify erosion effect together with other loss associated with it.

3.3.4 Labyrinth seals

The velocity in labyrinth is in order of 45 m/s for high head turbine. Labyrinth seals having small clearance and working with coarse sand may also have erosion as well as abrasion effect. The efficiency of a labyrinth seal is inversely proportional to clearance gap. Hence, gaps should be made the smallest possible to have minimum leakage, but it has to be sufficiently large to avoid any direct contact between rotating and stationary part. The clearance between the stationary and rotating parts is varied between 0.25 to 1.0 mm depending on the size of the turbine. The turbulence erosion due to fine sand is always susceptible in the labyrinth seal because of high velocity in its surrounding. The rotating labyrinth seals are made up of steels to achieve longer life, while stationary seals are normally made of softer materials such as bronze. The replacement cost for the stationary seal is cheaper. However, in the case of high sediment concentration, even the stationary seals can be made up of steel, which has higher erosion resistance than softer material.

3.3.5 Draft tube

The draft tube section closer to runner will be exposed to the highest velocity because of high absolute velocity of water coming out of runner and some sediment erosion effect can be anticipated. Apart from this portion, sediment erosion is normally no problem in draft tube.

3.3.6 Shaft seal

Mechanical shaft seal will be damaged if the sand-laden water is exposed to it. The damage could be due to more abrasion than erosion. Shaft seals are normally made up of carbon rings, bronze and steels with lower hardness compared to shaft material. Apart from selection of erosion and abrasion resistance material for seals, insertion of pressurized clean water in the shaft seal also avoids wear.

3.4 TURBINE DESIGN

The following IEC guidelines explain some recommended methods to minimize particle abrasion and the effects thereof, by modifications to design for clean water. It should be understood that every hydraulic power plant is a compromise between several requirements. While it is possible to design a unit to be more resistant against particle abrasion, this may adversely, affect other aspects of the turbine. Some examples are:

- Thicker runner blades may result in decreased efficiency and increased risk of vibrations from von Karman vortices.
- Fewer runner blades (in order to improve the access to the blade surfaces for thermal spray surface treatment) may result in reduced cavitation performance.
- Abrasion resistant coatings may initially result in increased surface roughness, which may reduce the efficiency.
- Reduced runner blade overhang may result in reduced cavitation performance, which in turn may reduce the output that can be achieved for a turbine upgrade.
- Many abrasion resistance design features will increase the total cost of the power plant.

The optimum combination of abrasion resistant design features must be considered and selected for each site based on its specific conditions.

3.4.1 Hydraulic design of turbine

3.4.1.1 Selection of type of machine

It is advantageous to select a type of machine that has low water velocity that can easily be serviced and that can easily be coated with abrasion resistant coatings. Some general guidelines are; in the choice between a vertical shaft Kaplan and a Bulb; the Kaplan will normally have lower velocity. The serviceability and ease of coating is approximately equal between the two. In the choice between a Kaplan and a Francis, the Francis will normally have lower velocity. On the other hand, the Kaplan runner has better access for applying abrasion resistant coatings. The serviceability is approximately equal between the two. In the choice between a Francis and a Pelton, the Francis will normally have lower maximum velocity. However, the parts in a Pelton turbine that are subject to the maximum velocity (i.e. the needle tips and seat rings) are small and have better access for applying abrasion resistant coatings. The Pelton turbine is also easier to service.

3.4.1.2 Specific speed

For the same plant, lower specific speed machines are normally bigger and have lower water velocities in the runner outlet. However, the water velocities are not lower in the guide vanes and in the runner inlet. For Kaplan, Bulb and low head Francis turbines, most of the abrasion damage will be in the runner, so the specific speed is important. For high head Francis turbines, much of the abrasion damage will be in the guide vane apparatus, so the specific speed is not so important. For Pelton turbines, the water velocity does not depend on the specific speed. However, a lower number of jets is beneficial for a Pelton turbine since the buckets will be larger which in turn gives less water acceleration in the buckets and thus less abrasion damage. A lower number of jets will automatically result in a lower specific speed.

3.4.1.3 Variable speed

Even though variable speed machines are not frequent, they are less prone to cavitation, even under a wide head range operation. Due to this characteristic, the variable speed machine may better resist particle abrasion.

3.4.1.4 Turbine submergence

Cavitation and abrasion will mutually reinforce each other. For this reason, it is recommended that the turbine submergence is higher for plants where abrasion is expected.

3.4.1.5 Runner blade overhang

In case of Francis runner refurbishment, there is sometimes a need to increase the turbine output significantly. One way to do that is to extend the runner band inside the draft tube cone, in order to increase the blade area and to improve the cavitation performance. However, this creates additional turbulences at the top of draft tube cone that will increase metal removal if particles are present in water. A secondary effect of the overhang blades is to create a lower pressure zone downstream of the runner band seal, thus creating higher seal leakage and more particle abrasion at the band seal.

3.4.1.6 Thicker runner blades and guide vanes

Increased runner blade thickness, particularly at the outflow edge, gives some extra margin before the removal of material on the runner blades becomes critical for the structural integrity of the runner. A thicker blade design should be done with care. The thicker blade may result in decreased efficiency and increased risk of vibrations from von Karman vortices. In addition, the risk of cavitation damage on the runner band, downstream of the blade, may increase.

3.4.2 Mechanical design of turbine

If abrasion is expected and the turbine type is defined, not only the hydraulic design but also the mechanical design can take some precautions to reduce the abrasion rate and to allow easy maintenance or replacement of the abraded parts. Generally, for the design, the area exposed to the abrasive wear should be as small as possible. As well, discontinuities and sharp transitions or direction change of the flow should be avoided. The turbine shaft seal should have rubber rigs in place of carbon rings and its design should be such as to allow dismantling and replacement in the shortest possible time. The thickness of the runner blade in the area prone to erosion should be increased. These areas are mainly at runner outlet. Increasing the wall thickness is a method to increase the overhaul interval of a component due to abrasion. For structural components, which

do not influence the efficiency, the wall thickness can be increased in critical areas to avoid early failure of the component due to higher stresses.

The material selection for components, which are subject to abrasive wear, is another important criterion. Generally, weldable stainless steel materials are preferred. If both corrosive and abrasive attack anticipated then stainless steel is preferred. Considering the larger hardness, martensitic steel is preferred over austenitic steel. Furthermore, shaft seal with clean sealing water is recommended. Normally, shaft seals in units, which are operated with water and, which contains abrasive particles, have to be fed with clean sealing water. It must be avoided that the contact surface or the wearing surface get contact with the abrasive particles.

3.4.3 Operation of turbine

Operation of a turbine at part load and full load is marked by reduced efficiency, increased flow turbulence and higher relative flow velocities at turbine runner outlet. Presence of secondary flows and accompanying vortices lead to increased local velocities. Since such flow conditions are conducive to increased sediment erosion, attempt should be made to avoid such operations when water carries excessive sediment.
The following actions are recommended for consideration during operation of the units.

- Shut down units at higher particle concentration periods. This may avoid considerable wear on the unit for a small amount of lost production. Especially for run of river schemes, where large variation in particle concentration can happen very fast this strategy can be useful.

- Minimize amount of debris passing through unit. Large solid items, for example logs, gravel (larger than 2 mm), etc. may damage the hydraulic surfaces and any abrasion resistant coatings. Damage to hydraulic surfaces may increase the turbulence of the flow, which will increase the abrasion damage. This is especially important for high head Francis and Pelton units, since the water velocities are very high and these units rely on smooth hydraulic surfaces to keep the turbulence low.

- Do not operate the unit in case the abrasion damage jeopardizes the safety of operation. As the abrasion damage progresses, the unit will eventually become unsafe to operate. This could for example be due to seal leakage increasing so much that the axial thrust exceeds allowable limits or that the remaining material thickness of some component falls below acceptable minimum thickness. Regular inspections of critical components should be made at least every year and inspection results must be compared with predefined acceptance criteria.

- Avoid low load operation as much as possible. Low load operations are the worst operating conditions with respect to abrasion for most components and turbine types.

- Close inlet valve at shutdown. With a turbine at standstill and the water shut off only by the guide vanes, the water leaking past the guide vane clearances will have very high velocity, close to the free spouting velocity. This will cause abrasion wear in the guide vane apparatus. By closing the inlet valve, this abrasion is eliminated. To close the inlet valve is especially important for high head units.

- Hard coatings are very sensitive to cavitation. Thus, in machines with such coatings all operating conditions that lead to cavitation must be avoided and strictly stick to the recommended operating range for the turbine.

3.5 ALTERNATIVE DESIGN OF FRANCIS TURBINE

A few instances have been noticed where under identical conditions of sediment, the intensity of damages at different hydropower stations were not identical. While components at a particular power station eroded very fast, damages to components at other power stations were insignificant. This leads one to believe that equipment design has a role to play in influencing the intensity of erosion (Naidu, 1999).

The author earlier designed a Francis turbine for sediment-laden water that considering the erosion of the Francis turbine occurs mainly at the outlet of the guide vanes and at the outlet of the runner blades. In order to reduce the erosion rate of the turbine, the absolute velocity at the inlet of the runner and the relative velocity at the outlet of the runner have to be reduced. In this study, the flow and head were kept constant while the speed, inlet peripheral velocity and outlet runner blade angle were changed according to Table 3-3.

Table 3-3 Variable input parameters

Speed	rpm	n	750	600	500	433	375	333	300	275
Inlet peripheral Velocity, reduced	-	$\underline{U_1}$	0.71	0.74	0.77	0.8	0.83	0.86	0.89	0.92
Outlet blade angle	degree	β_2	17	19	21	23	25	27	29	31

The results show that the outlet diameter changes relatively little while the inlet diameter changes drastically. The reduction of the erosion at the outlet is more than at the inlet. This is shown in Figure 3-7. The inlet angle of the turbine has changed so that the design looks more like a pump-turbine. This means that the turbine will be larger than the traditional design.

The reduction of the erosion is linked to the reduction of the velocity and therefore the size of the turbine increases. This result in a higher price of the turbine, but it will reduce the maintenance costs during its lifetime. It has been shown from the calculation that the design of the runner can decrease the sand erosion but it is not possible to avoid this problem completely by design alone.

However, if a Francis turbine designer combines the hydraulic design and coating of the critical parts, a significant reduction of erosion can be achieved.

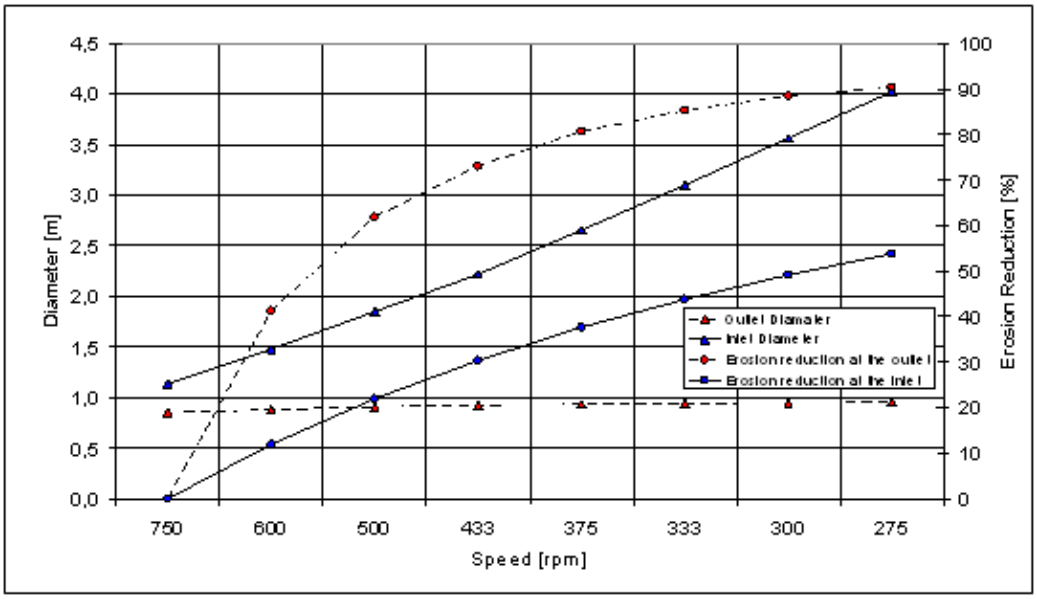

Figure 3-7 Variation of diameter for reduction of erosion

3.6 CONCLUSION

Sediment content of water can no more be overlooked in any phase of hydropower project implementation. This includes all the phases like, investigation, design, operation and maintenance, and refurbishment and upgrading. Due consideration of the problem at every stage, would effect economies on one hand and long-term solutions would emerge on the other hand. However, one solution in order to decrease the sediment erosion is to increase the size of the turbine, thereby increases the hydraulic radius of curvature, and thus decreases the accelerations. Furthermore, while it is possible to design a Francis turbine to be more resistant against sediment erosion, this may adversely, affect other aspects of the turbine. It should be understood that every hydraulic turbine is a compromise between several requirements.

Chapter 4
Particle Velocity Measurement in Swirl Flow, Laboratory Studies

This chapter presents the laboratory studies of particle velocity measurement in highly swirl conditions similar to turbine flow in curved path. It includes a brief description of the developed test rig, concept of critical diameter of particle inside a Francis turbine and experimental analysis.

4.1 BACKGROUND

4.1.1 General

Swirl flow can be used as a mechanism for separation of particles from the fluids creating a centrifugal force as in many separation processes. Solid particles of different shapes and sizes play a significant role in many separation processes. The separation of particles of different shapes and sizes depends upon the variations in behaviour of the particles when subjected to the action of moving fluid. A particle falling in an infinite fluid under the influence of gravity will accelerate until the resistance force that includes buoyancy and drag exactly balances the gravitational force. The constant velocity reached at that stage is called the terminal velocity. The resistive drag force depends upon an experimentally determined drag coefficient.

The separation of particles from streamline depends upon acceleration of particles, which further depends on profile and curvatures of runner blade and bucket. Together with several parameters affecting erosion rate (discussed in section 2.7), the modification in design in term of turbine size, profile and curvatures also play a vital role for reducing erosion rate. However, this aspect is not explored at large extent (Thapa, 2004).

There are very less literatures available for the separation of particles from streamline, which can directly apply to hydraulic turbines applications. However, some studies have been found in the field of particle transport and separation in erosion test rig together with cyclone separator and conveying of particles in process industry.

Chevallier and Vannes, 1995, carried out numerical and experimental study of interaction between particle and specimen. They studied the particle speed in non-uniform flow by generalizing Basset, Boussinesq and Oseen's expression that gives equilibrium of the particle. The added weight effect, effect of static and viscous pressure, Archimedes thrust and gravity force are neglected. When the ratio ρ/ρ_P is low ($<10^{-3}$), and if the particle and fluid acceleration are of the same order, those effects become negligible. After all these simplifications, the equation of motion of particles becomes,

$$\frac{\pi \cdot d^3}{6} \cdot \rho_p \cdot \frac{dV}{dt} = \frac{\pi}{8} \cdot d_p^2 \cdot \rho \cdot C_D \cdot \left(V - C\right) \cdot \left|V_p - C\right| \qquad \textbf{Equation 4-1}$$

Here, d_P is the diameter of the particle, ρ_P is the density of the particle, ρ is density of the fluid. The fluid velocity is C, and particle velocity is V. The coefficient of drag (C_D) is obtained from equation (Martin, 2008),

$$C_D = \frac{24}{R_{e,p}} \cdot \left(1 + 0.15 \cdot {R_{e,p}}^{0.687}\right) \qquad \textbf{Equation 4-2}$$

Similarly, Tabakoff et al. ,1991, used simplified governing equation of force of interaction of particle motion in the turbo-machinery flow with reference to cylindrical coordinates relative to frame of reference, fixed with respect to the rotating blades as shown below,

$$\overline{F} = \frac{3}{4} \cdot \frac{\rho}{\rho_p} \cdot \frac{C_D}{d} \cdot \left[\left(V_r - \frac{dr_p}{dt}\right)^2 + \left(V_\theta - \frac{d\left(r_p \cdot \theta_p\right)}{dt}\right)^2 + \left(V_z - \frac{dz_p}{dt}\right)^2\right]^{\frac{1}{2}} \cdot \left(\overline{V} - \overline{V_p}\right)$$

Equation 4-3

Here, r_P, θ_P and z_P define the particle location in cylindrical coordinates. Similarly, V_r, V_θ and V_z represent relative gas velocities in the radial, the circumferential and the axial directions respectively. This equation includes centrifugal force as well as Coriolis force. The forces due to gravity and inter particle interaction are negligible in the case of turbo machinery. The drag coefficient (C_D) is a function of particle Reynolds number. Deng et al., 2001, considered, $C_D = 0.44$ for large $R_{e,P}$ (> 500), and provided equation 4-4 for C_D for $R_{e,P}$ range, 0.2 – 500, which is almost same that of the values and the Reynolds number rages provided by Martin, 2008.

$$C_D = 24 \cdot \left({R_{e,p}}^{-1} + 0.167 \cdot {R_{e,p}}^{-\frac{1}{3}}\right) \qquad \textbf{Equation 4-4}$$

4.1.2 Characterization of non spherical particles

Particles in water may range in size from a few nanometres to few millimetres in dimension. Natural particles also have various shapes, including rod, plate, and sphere, with many variations in between, which make the treatment of the particle size difficult. The discussion is vastly simplified if the particles are considered spherical. In this case only one size parameter is needed (the diameter) and hydrodynamic properties are much more easily treated. Of course, non-spherical particles also occur in natural water, and some way of characterizing them is essential. A common concept is that of the equivalent sphere based on a chosen property of the particles (Gregory, 2006). For instance, an irregular particle has a certain surface area and the equivalent sphere could be chosen with the same surface area. The surface area of sphere with diameter d is $\pi \cdot d^2$. So, if the surface area of the non-spherical particle is known, the equivalent spherical diameter can easily be calculated. For an object of a given volume, the sphere has minimum surface area and the volume (or mass) of a given particle must be equal to or less than that of the sphere. Another common definition of equivalent spherical diameter is based on sedimentation velocity. In this case, from the sedimentation velocity and density of particle, the diameter of a sphere of the same material that would settle at the same rate can be calculated. This is sometimes called the Stokes equivalent diameter.

4.2 OBJECTIVE OF EXPERIMENT

The objectives of development of experimental set-up and conducting experiment are as follows:

- To study the particle separation process in the flow in the curved path
- To study the forces on the particle on rotational motion or swirl
- To investigate the velocity and the drag coefficient relations based upon different shape and size of the particle in swirl flow
- To establish an operating strategy for Francis turbine operating on sediment-laden water

4.2.1 Description of test rig and test procedure

A previously made test rig (Thapa, 2004), was reviewed and modified to create a strong swirl flow in curved path. This flow was found similar to the flow between the guide vane outlet and the runner inlet of a Francis turbine. The flow in the guide vane cascade was simulated in order to verify the particle separation process and to investigate the velocity and the drag coefficient relations based upon different shape and size of the particle. There was a provision to introduce particles, with sizes ranging from 1 to 10 mm,

into the swirl, and to observe the motion of the particles from Plexiglas windows located on the cover of the tank using a high-speed digital camera.

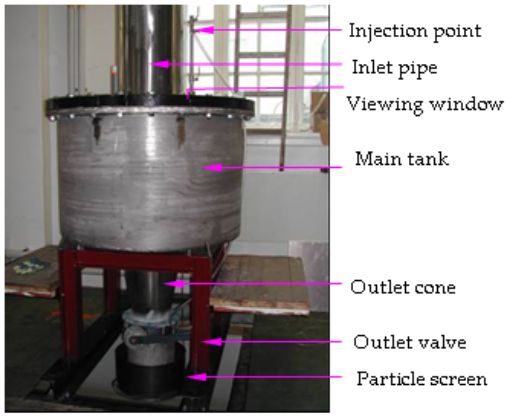

(a) Outside view

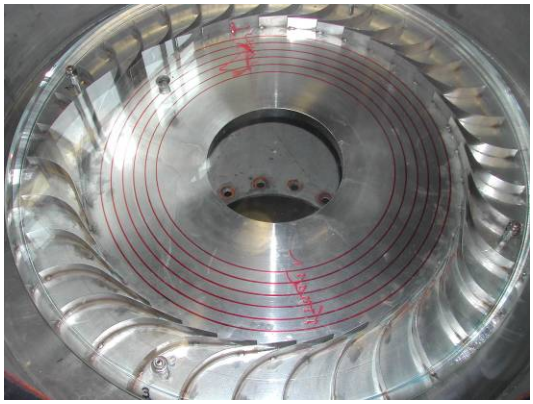

(b) Middle plate with vanes and Plexiglas

Figure 4-1 Photographs of test rig

The experimental set up, as shown in Figure 4-1, consisted of a main tank (1,100 mm diameter and 700 mm height), 400 mm diameter inlet pipe and outlet cone with valve. The main tank and other components of the test rig were designed and dimensioned for 50 m of head in order to carry out the experiment in high velocity. The main tank consisted of two compartments with a 250 mm diameter opening at the centre of the plate. This plate divides the main tank into two compartments. Thirty-six curved vanes, which resemble guide vanes of a Francis turbine, with a radius of 100 mm toward the inlet and 90 mm straight section toward the outlet, were fixed at a pitch circle diameter of 900 mm to the middle plate. This is shown in Figure 4.2. This arrangement was made in such a way that the inlet velocity direction should be almost in the radial direction and the outlet would be 10 ° to the tangent. Each vane cascade has 30 mm x 5 mm opening and altogether 36 numbers of vanes provide the total opening areas be about 5.4×10^{-6} m^2. These vanes were located in between the upper part of the middle plate and the bottom part of a 50 mm thick, 950 mm diameter transparent Plexiglas plate. Peripheral component (C_u) of absolute velocity can be obtained from the orientation of blade angle, which is fixed at 10 ° in this experimental set-up. However, this angle varies at different operating conditions in actual hydropower plant. The peripheral component is caused to create a centrifugal force of particle whereas the radial component is caused to create a drag force of particle. From this arrangement, the vanes caused swirl inside the tank, which further emulate the swirl flow created by guide vanes in a Francis turbine. The swirl flow in between the Plexiglas and the middle plate could be clearly observed from the top of the Plexiglas windows, which satisfied a free vortex relation towards vanes whereas; force vortex flow existed towards the centre of the tank. The edge of the Plexiglas was made uniform to ensure uniform flow.

The top cover of the tank was fitted with five transparent windows of Plexiglas. Four of those transparent windows of 160 mm diameter were located at 90 °, 180 °, 270 ° and 360° respectively at the pitch circle diameter 700 mm to observe the motion of the particles. The fifth window of 275 mm diameter was located at 315 ° at 700 mm pitch circle diameter to measure the velocity of the flow (after inserting a Pitot tube as shown in Figure 4-3) and to observe the velocity of particle. The particle injection point was located at 279 mm from the centre of the tank. The particle was released at the bottom of the Plexiglas through a 15 mm diameter pipe and valves arrangement as shown in exploded view in Figure 4-2. Particles up to 10 mm in diameter were tested in this experiment.

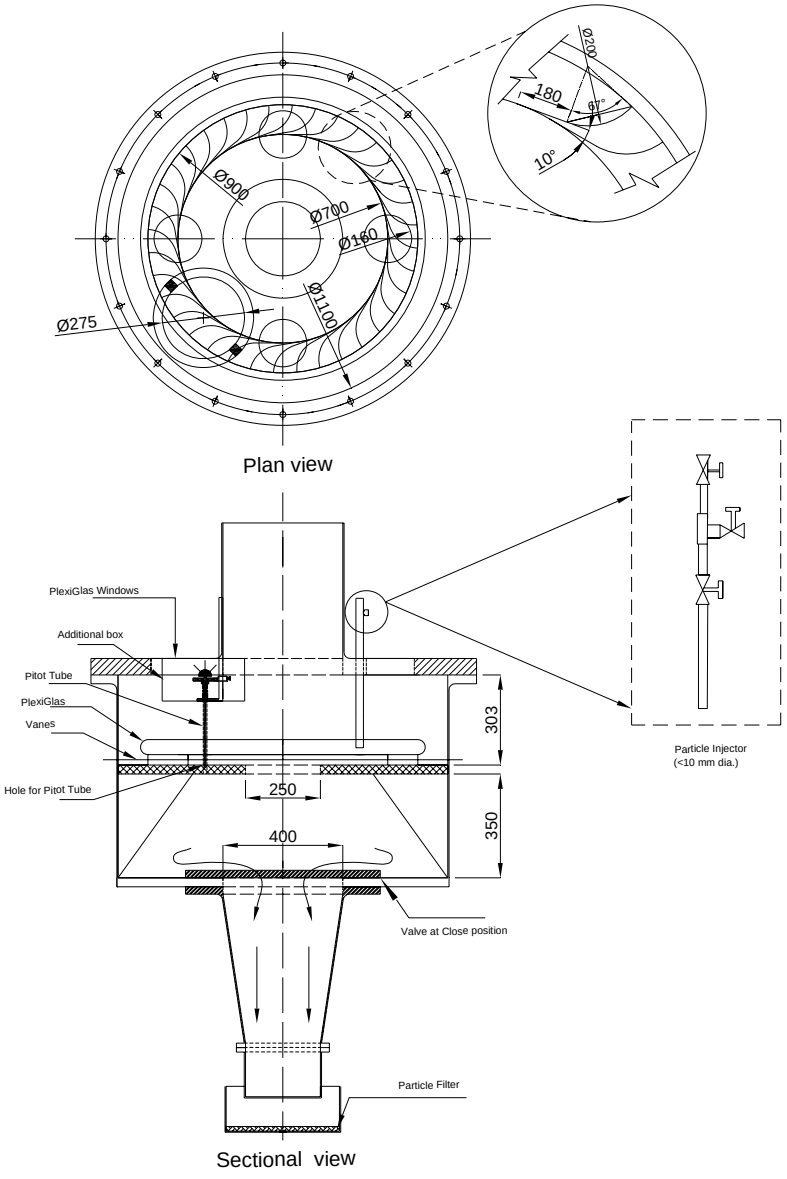

Figure 4-2 Schematic diagram of experimental set up

To release particle, first lower valve was closed and particle was inserted from the upper valve. Then upper valve was closed and lower valve was open. Once lower valve is opened, the particle sinks and drops in between Plexiglas and steel plate. Depending upon the velocity at the point of the injection, the particle either moves towards outer radius or follow flow direction heading towards outlet at the centre of the tank and ultimately sinks. A manometer was fitted into the injection pipe and valves arrangement in order to measure the inlet pressure of the tank in the swirl flow field. There were two additional manometers located in the system. One was connected to an air-bleeding valve located at 390 mm from the centre of the tank for measuring the inlet pressure, and another was fitted at the outlet of cone for measuring the pressure at the outlet. The flow rate was calculated with the help of an ultrasonic flow meter fitted in the inlet pipe.

Figure 4-3 Pitot tube for measuring the velocity of flow

4.2.2 Measurement of particle velocity

The main purpose of this experiment was to determine the velocity of the particle that would flow along with water in the given flow condition. To achieve this, firstly, the operating condition was set at a certain velocity level by controlling the valve opening. Then the particle was injected and the motion of the particle was observed through the Plexiglas windows with the help of the high-speed video camera.

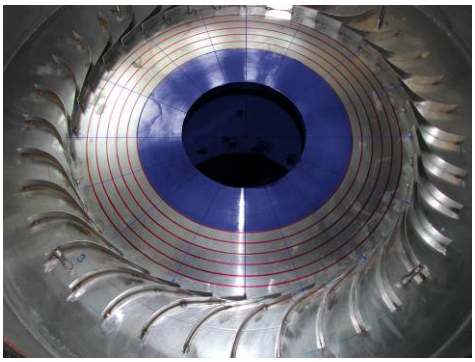

Figure 4-4 Photograph of middle plate with radial and angular markings

The particle images at different frame rate were saved and analysis was performed based upon the actual time required to move the particle from one fixed location to another fixed location. Location of the particle was identified based upon the radial and angular position of particle inside the test rig. In order to calculate the correct location of the particle inside the test rig, radial and angular markings were inscribed on the middle plate at diameters of 219 mm, 239 mm, 259 mm, 279 mm, 299 mm, 309 mm and 22.5 degrees interval respectively. Using these markings, six different circles and sixteen different angular lines could be clearly observed in the middle plate. Figure 4-4 illustrated the photograph of middle plate inside the test rig with radial and angular markings. A particle rotation radius and the angle traversed by the particle are needed to calculate the radial distance travel by the particle. Then the velocity of a particle was computed based upon the actual time obtained from the saved images to travel this radial distance, which is the rate of change of position of particle.

4.2.3 Visualization of particle motion

In order to find out the size of the particle which will flow along with water in a given flow condition, and to verify the validation of critical diameter expression that derived in Equation 4.7, six different particles having different densities were considered. The experiments were done based upon different shape and size of aluminium, brass, ceramic, plastic, sand and steel particles. Most of these particles rotating at low velocity can be clearly seen by naked eye. However, as the velocity of particle increase, it was not possible to visualize the location of particles in flow field by naked eye but the location of small particles at higher velocity was visualized by the high-speed video camera. The high-speed digital camera was used to compare the rotation radius for different shape and size of the particles at different operating conditions. The equilibrium condition was clearly observed with adjustment of flow and sizes of the particles for most of the samples except for plastic particles. Since the density of plastic particle is less than the density of water, most of these particles were floating on water. At equilibrium condition, the rotation radius of particle was observed very close to the injection radius of particle at 279 mm from the centre of the tank. The larger size of the particles that was assumed larger than critical diameter of particle on that particular operating condition was clearly observed by hitting the outer wall or suction side of the guide vane cascades in this experimental set up and the smaller size of the particle was observed clearly by its flow along with water and ultimately sinking.

4.2.4 Particle in swirl flow

When particles travel in swirling flow toward a turbine's outlet, which is located in the centre as shown in Figure 4-5, the particles will be exposed to two main forces. Centrifugal force $\left(F_c\right)$ moves the particles away from the centre, while the drag force $\left(F_D\right)$ pulls them toward the outlet, which is in the centre, or toward the runner in the

case of a Francis turbine (Thapa and Brekke, 2004). These two forces are given by the following equations.

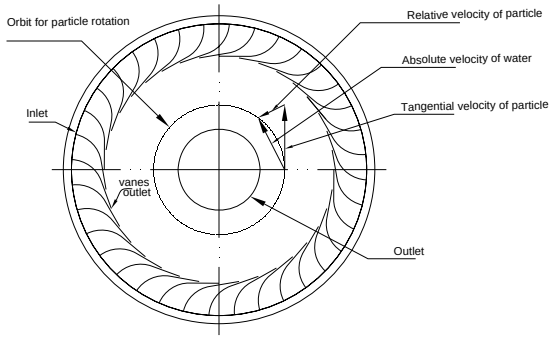

Figure 4-5 Illustration of particle flow in spiral swirl

$$F_c = \rho_p \cdot \frac{\pi \cdot d^3}{6} \cdot r \cdot \omega^2 = \rho_p \cdot \frac{\pi \cdot d^3}{6} \cdot \frac{C_u{}^2}{r}$$ **Equation 4-5**

$$F_D = \frac{1}{2} \cdot C_D \cdot \rho \cdot C_m{}^2 \cdot A_p$$ **Equation 4-6**

Following three conditions prevail in such case:

- Particle will stay at the orbit of radius r, if $F_c = F_D$
- Particle will strike outer wall, if $F_c > F_D$
- Particle will flow along with water towards the centre of the tank, if $F_c < F_D$

At equilibrium, these two forces balance each other and a particle of a given diameter will stay at an orbit of radius (r) until either the velocity component is changed or particles become smaller by fracture due to impact. The diameter of a particle (d) for the equilibrium condition is given by Equation 4-7. This is called the critical diameter.

$$d_c = \frac{3}{4} \cdot C_D \cdot \left(\frac{\rho}{\rho_p} \right) \cdot \left(\frac{C_m}{C_u} \right)^2 \cdot r$$ **Equation 4-7**

The drag force is caused by the relative velocity of particles in radial direction (i.e. towards the centre of the tank), and the centrifugal force is caused by the velocity of particle in tangential direction (i.e., away from the centre of the tank).

The phenomenon of particle motion discussed here is similar to swirl flow in between guide vane outlet and runner inlet of a reaction turbine. Once the larger particles enter in to the swirl flow it will be rotating and continuously hitting the suction side of the guide vanes. Direct application of this concept is on operating strategy for Francis turbines operating in sediment-laden water. Guide vane position can be manipulated to maintain a velocity ratio in a way that the particle of given size should flow along with the water.

A damage caused by the larger particles has been observed in Tokke hydropower plant in Norway. The damage on suction sides of guide vanes is clearly observed in Figure 4-6. The bigger particle sizes are settled down or removed before it enters the turbines. The unsettled bigger size particles, especially in the monsoon season, pass thorough turbines. The guide vanes of Francis turbine can have maximum angle as low as 12 ° at full load. Whereas this angle could go up to 40 ° in some of the turbine design.

Figure 4-6 Erosion damage of suction side of Tokke guide vane by large particles

The guide vane angles for some of Norwegian power plants are presented in Table 4-1. This inclination of guide vanes creates swirl flow in Francis turbine and the magnitude of swirl depends upon angle of inclination of guide vanes. Even though irregular shape of sand particles could have higher drag coefficient compared to spherical one, the observation from the test rig can be utilized for determining the size of particle, which will remain rotating in the swirl flow in between guide vane outlet and runner inlet. Any particles higher than this size hit the suction side of guide vane continuously and damage them severely.

Table 4-1 The guide vane maximum angle at full load condition

S.N.	Power plant	Specific Speed (n_s)	Maximum Guide vane angle at full load (a_0)
1	Skjærka	66	12
2	Nedre Vinstra	69	12
3	Hol I	72	13
5	Røssåga	104	18
6	Grønsdal	113	23
7	Nore II	198	34
8	Dynjafoss	208	27.5
9	Oltesvik	264	38.5
10	Iverland	269	31.5
11	Fiskumfoss	308	40.5
12	Fiskumfoss	308	36.5
13	Gravfoss	346	37
14	Solbergfoss	365	38

Particles larger than critical diameter will remain rotating in the swirl flow and hitting the guide vane wall but the particles smaller than critical size flows through turbines. The relation between critical diameter and runner inlet diameter is shown in Figure 4-7 a. This relation was obtained based upon drag coefficient of 0.1. At higher Reynolds number ($R_e > 10^6$), the drag coefficient is around 0.1 to 0.2. Similarly, the relation between particle size and drag coefficient for turbine of radius 1 m at inlet is shown in Figure 4-7 b. This figure indicates that the sand particles of diameter higher than 0.9 mm will stay rotating in the swirl flow and damage guide vanes positioned around 10 °. This figure also shows that smaller turbines are more prone to sand erosion because smaller turbines are having small critical diameter, for example particles as small as 0.7 mm may remain rotating in the turbines of inlet diameter 800 mm.

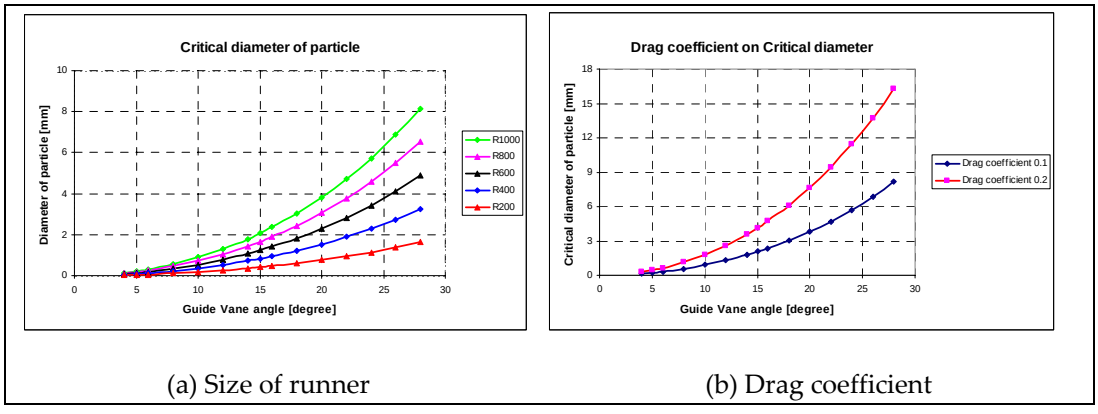

(a) Size of runner (b) Drag coefficient

Figure 4-7 Critical diameter relation based upon size of runner and drag coefficient

This result can be utilized as guidelines for operating strategy for Francis turbine operating in sediment-laden water. If the particle size flowing with water is larger than critical sizes of the particle, the turbine should not be operated at low guide vane opening.

4.2.5 Drag coefficient for particles

Drag coefficients and terminal velocities are important design parameters in many separation processes. Many equations have been developed and presented in literature relating the drag coefficient (C_D) to the Reynolds number (R_e) for particles of spherical shape falling at their terminal velocities. These correlations are of varying complexity and contain many arbitrary constants. Many of these correlations are listed in Gabitto and Tsouris, 2008. However, in the case of non-spherical particles, less information is found in literature. Gabitto and Tsouris, 2008, also mentioned that Heywood developed an approximate method for calculating the terminal velocity of non-spherical particle or for calculating its size from its terminal velocity. The method was an adaptation of his method for spheres. Several correlations have been proposed for C_D over the entire range, the one presented in Equation 4-8 is that of Haider et al., 1989, which is claimed to fit the data with a root mean square deviation of 0.024.

$$C_D = \frac{24}{R_{e,p}} \cdot \left(1 + 0.1806 \cdot {R_{e,p}}^{0.6459}\right) + \left(\frac{0.4251}{1 + \frac{6880.95}{R_{e,p}}} \right)$$

Equation 4-8

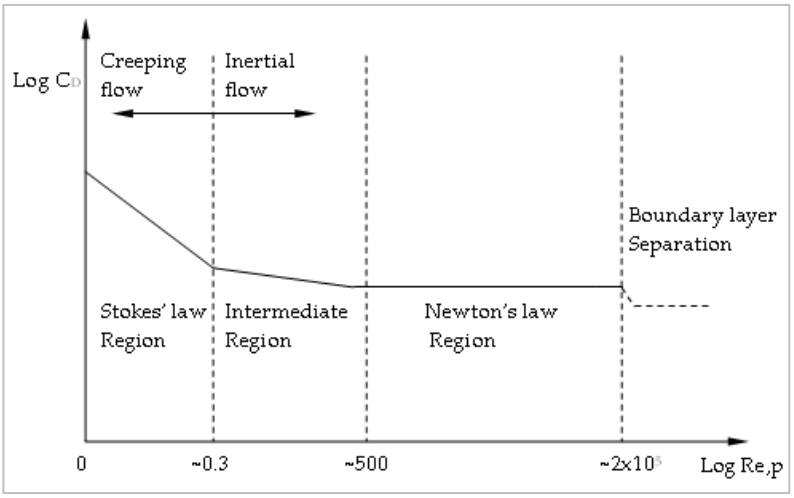

Figure 4-8 Standard drag curve for motion of particle in a fluid

At higher relative velocities, the inertia of the fluid begin to dominate (the fluid must accelerate out of the way of the particle). Analytical solution of the Navier-Stokes equations is not possible under these conditions. However, experiments give the relationship between the drag coefficient and the particle Reynolds number in the form of the so-called standard drag curve as shown in Figure 4-8. Four different regions are identified: the Stokes' law region, the Newton's law region in which drag coefficient is independent of Reynolds number, an intermediate region between the Stokes and Newton's regions; and the boundary layer separation region. The Reynolds number ranges and drag coefficient correlations for these regions are given in Table 4.2, (Martin, 2008)

Table 4-2 Reynolds number ranges for single particle drag coefficient correlations

Region	Stokes	Intermediate	Newton's law
$R_{e,p}$ *range*	< 0.3	$0.3 < R_{e,p} < 500$	$500 < \mathrm{Re},\ p < 2\times10^{5}$
C_D	$\frac{24}{R_{e,p}}$	$\frac{24}{R_{e,p}} \cdot \left(1 + 0.15 \cdot R_{e,p}^{\ 0.687}\right)$	≈ 0.44

As the Reynolds number increases, there will be a separation of flow field with the formation of vortex behind the body and further increase in Reynolds number causes unstable and unsteady wake formation.

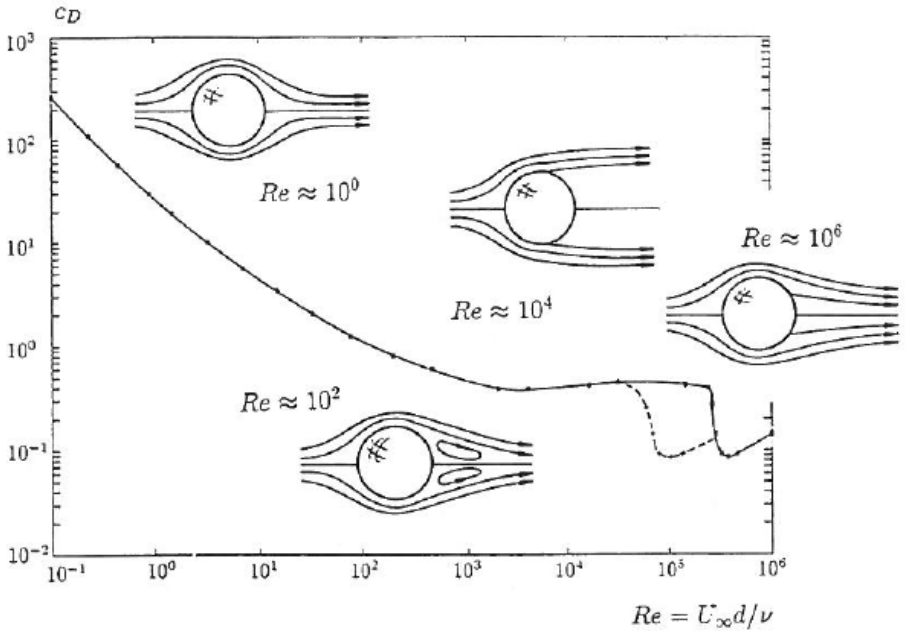

Figure 4-9 Drag coefficient of the sphere (Spurk, 1997)

The drag coefficient depends upon the flow pattern behind the object. However, for incompressible flow, the drag coefficient is only a function of particle Reynolds number

as shown in Figure 4-9. The sudden drop of value of C_D around Reynolds number 3 x10^5 is due to transition of laminar boundary layer on spherical surface to turbulent boundary layer. The shear stress in the turbulent boundary layer is larger; hence, fluid at outer layer is dragged close to the wall. This retards the flow separation and wake becomes narrower. The non-separated flow in the backside of the particle exerts force against the flow direction and hence C_D becomes smaller. This transition can occur in lower Reynolds number when the surface is made rougher. Sand particle surface being rougher than the regular spherical surface may have value of C_D in this region. The observation of Reynolds number at different flow condition and direction of flow components are presented in results and discussions section. The values of C_D from the experiment in the swirl flow are smaller than that shown by Spurk, 1997, because of measurement uncertainties and limitations of experimental study.

4.2.6 Uncertainties for the measurements

Due to the nature of physical measurements, it is impossible to measure a quantity without error. A measurement system is often made up of series of components, which are subjected to individual inaccuracy. Each of these individual uncertainties includes random and systematic errors. There are many uncertainties in laboratory experimental study, which combine to make this an imprecise prediction of drag coefficient for particle, including:

- The shape and size range distribution of the particle,
- The effect of the shape of non-spherical particles on their drag coefficient has proved difficult to define. This is probably due to difficulty in describing particle shape for irregular particles. The approached applied to define the irregular shape of the particle with its spheroid may not be sufficient in some cases,
- When many particles flow in a fluid in close proximity to each other the motion of each particle is influenced by the presence of the others. The simple analysis for the fluid particle interaction for a single particle is no longer valid but can be adapted to model the multiple particle system,
- While calculating the forces acting on the particle mainly centrifugal and drag forces were considered, however, the friction force may acting on the particle sliding on the surface of the middle plate then causes that particle slightly rotate. The rotation condition of the particle depends on characteristics of the particle and wall of the plate. If friction force is big enough the particle will rotate, otherwise, the particle will slide.

However, the value of drag coefficient around 0.1 to 0.2 could be appropriate for estimation of particle that will stay and rotating in the swirl flow at higher particle Reynolds number, where separation of particles from streamlines takes place.

4.3 RESULTS AND DISCUSSIONS

Velocities of particles of different sizes and shapes are shown in Figures 4-10 to 4-12. The velocity of the particle will increase if the velocity of water increases. Higher velocity of the particle was obtained at higher operating head. The size of the particle is inversely proportional to the velocity of the particle, and it depends upon the shape of the particle. Different shapes of particles were tested for different operating head, and it was determined that spherically shaped particles had higher settling velocities than particles with other shapes.

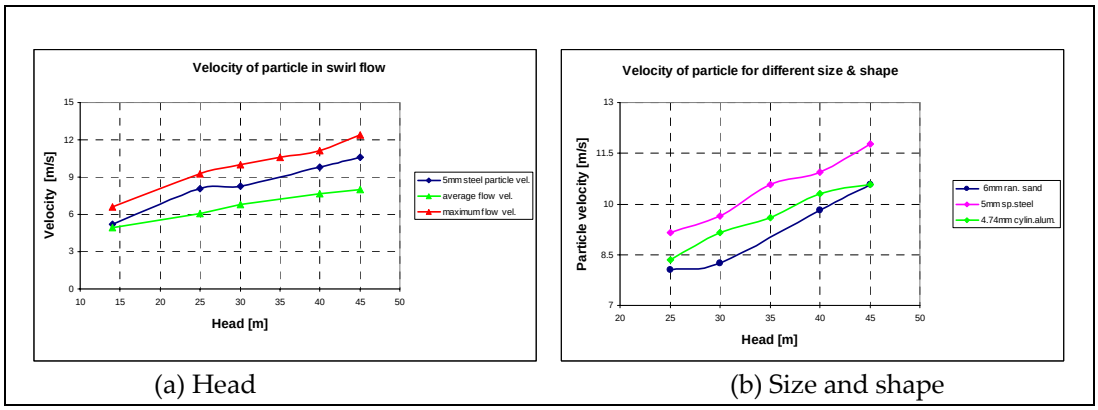

(a) Head (b) Size and shape

Figure 4-10 Particle velocity and head relation for different size and shape of particle

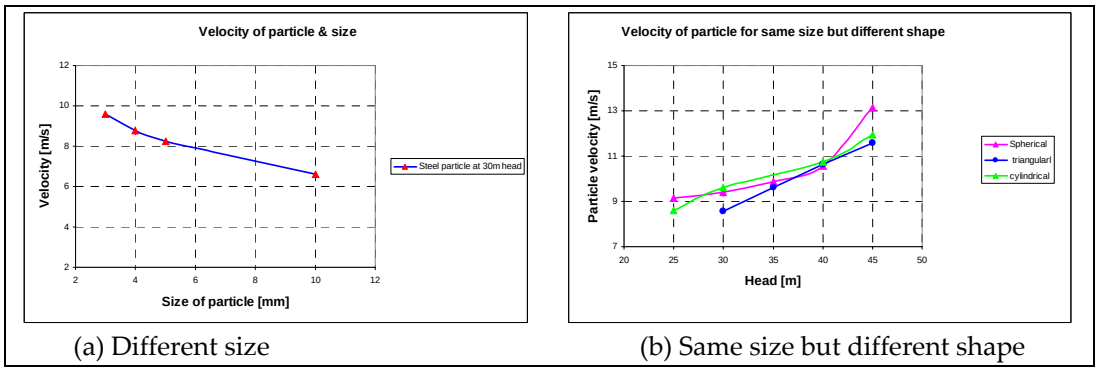

(a) Different size (b) Same size but different shape

Figure 4-11 Particle velocity for different sizes and same size with different shape

Many natural particles are usually in non-spherical shape. These particles will tend to have lower settling velocities because both decreases in spheroid and increases in angularity tend to decrease velocities. Furthermore, larger cross-sectional areas tend to be directed perpendicular to the transport path. As a result, higher coefficient of drag, higher rotational motion and more separation of flow likely to occur and hence more erosion rate is anticipated.

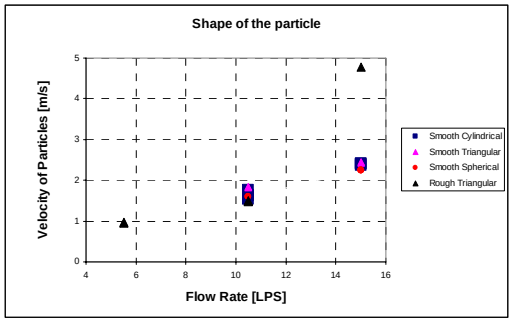

(a) Different particle with different shape

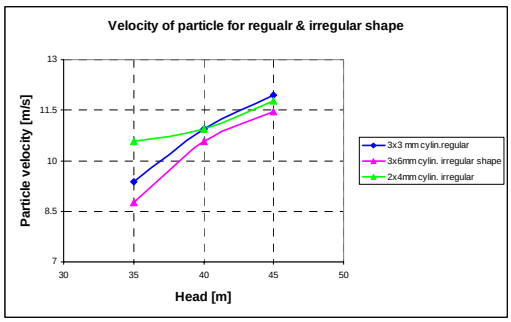

(b) Same particle with different shape

Figure 4-12 Particle velocity relation for same/different particle with different shape

If centrifugal force and drag force on the particle is equal, the particle will rotate exactly at the injecting radius, but if those forces do not balance each other, there will two possibilities. The particle either moves toward the inner radius and ultimately sinks or moves toward the outer radius and ultimately hits the sides of the vanes. The equilibrium condition was observed for a given particle after manipulating the flow velocity, verifying that the different forces were balanced in the test rig. This also revealed that the particle with a given diameter would stay at the orbit of the injecting radius until either the velocity components were changed or the particle became smaller by fracturing due to impact with the outer wall. Different shapes of particles were tested with the same operating conditions as shown in Figure 4-13, and it was determined that triangularly shaped particles were more likely to hit the suction side of the guide vane cascade. The radius at which the particle is moving, called rotation radius. This rotation radius also varied with different shapes of particles, which further supports the influence of shape factor for particle velocity calculation.

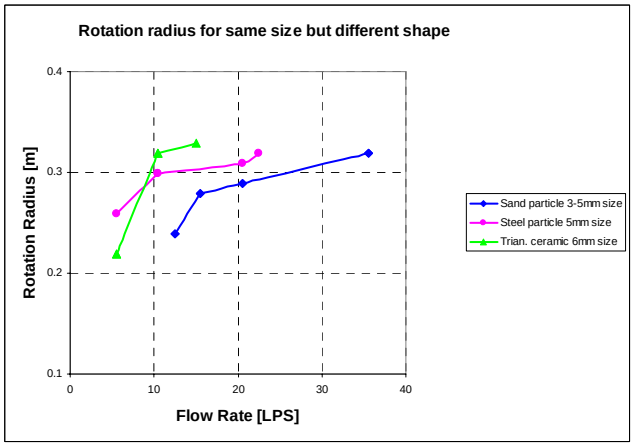

Figure 4-13 Rotation radius for particles of the same size but different shape

Drag coefficient was also calculated and plotted for different shapes and sizes of particle as shown in Figure 4-14 and 4-15.

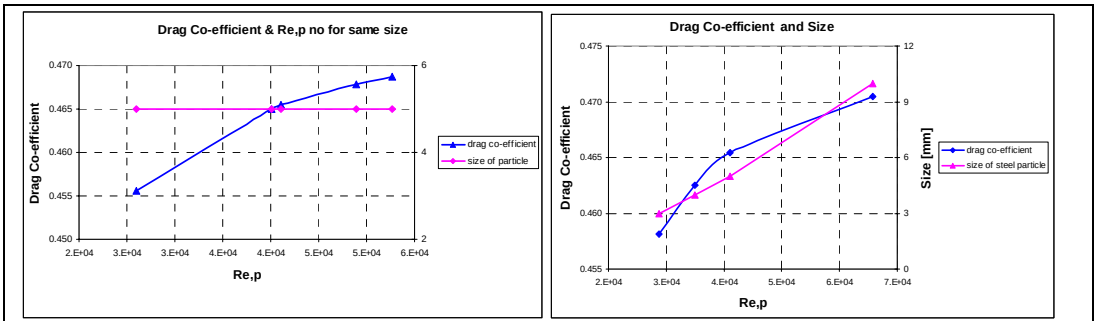

(a) Same size (b) Different size

Figure 4-14 Drag coefficient relation for same /different size of particle

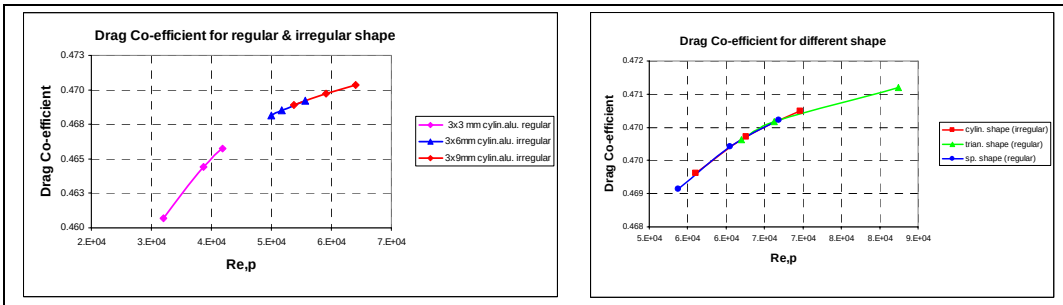

(a) Same particle different shape (b) Different particle different shape

Figure 4-15 Drag coefficient relation for regular and irregular shape of same/different particle

The drag coefficient C_D is a non-dimensional number that depends on the shape of the particle, the fluid kinematic viscosity, and the grain size. It has been found that the effect of the shape of non-spherical particles on their drag coefficient can be defined in terms of its spheroid. Moreover, shape affects drag coefficient far more in the intermediate and Newton's law regions than in the Stokes' law region. However, the variation of drag coefficient in the Newton's law region is not so significant, but the influence of size and shape of the particle has been clearly demonstrated. The result shows that the triangularly shaped particles have a higher drag coefficient than other shapes because the angular particles also tend to have lower settling velocity than the spherical ones.

Chapter 5
Computational Fluid Dynamics Theory

In this chapter, the governing equations of fluid, the particle equation of motion, and the two empirical erosion equations are briefly presented. The derivation of the governing equations is not included in this chapter, however, it can be found in many CFD books including ANSYS user guide, 2006.

5.1 INTRODUCTION

Computational Fluid Dynamics (CFD) is the analysis of systems, which involves fluid flow, heat transfer and other related physical processes by means of computer based simulation. It works by solving the equations of fluid flow over a region of interest, with specified boundary conditions of that region. ANSYS CFX is general-purpose CFD tool, which is used for the numerical simulation analysis that combines an advanced solver with powerful pre and post-processing capabilities. This is capable of modelling: steady state and transient flows, laminar and turbulent flows, subsonic, transonic and supersonic flows, heat transfer and thermal radiation, buoyancy, non-Newtonian flows, transport of non-reacting scalar components, multiphase flows, combustion, flows in multiple frames of reference, particle tracking, etc. Furthermore, this includes, an advanced coupled solver that is both reliable and robust, with full integration of problem definition, analysis, and results presentation and an intuitive and interactive setup process, using menus and advanced graphics features.

The CFX consists of five software modules that pass the information required to perform a CFD analysis. These are the mesh generation software, the pre-processor, the solver, the solver manager, and the post-processor.

5.2 GOVERNING EQUATIONS

The governing equations of fluid flow, which describe the processes of momentum, heat and mass transfer, are known as the Navier-Stokes equations. There are three different streams of numerical solution techniques: finite difference, finite volume method and spectral methods. The most common, and the CFX is based, is known as the finite volume technique. In this technique, the region of interest is divided into small sub-regions, called control volumes. The equations are discretized, and solved iteratively for each control volume. As a result, an approximation of the value of each variable at specific points throughout the domain can be obtained. In this way, one derives a full picture of the behaviour of the flow. The instantaneous equations of mass, momentum and energy conservation can be written as follows in a stationary frame (ANSYS, 2006).

The continuity equation:

$$\frac{\partial \rho}{\partial t} + \nabla \bullet \left(\rho \cdot U \right) = 0 \qquad \textbf{Equation 5-1}$$

The momentum equations:

$$\frac{\partial \left(\rho \cdot U \right)}{\partial t} + \nabla \bullet \left(\rho \cdot U \otimes U \right) = -\nabla p + \nabla \bullet \tau + S_M \qquad \textbf{Equation 5-2}$$

Where $\tau = \mu \cdot \left(\nabla \cdot U + \left(\nabla \cdot U \right)^r - \frac{2}{3} \cdot \delta \nabla \bullet U \right)$ **Equation 5-3**

The total energy equation:

$$\frac{\partial \left(\rho \cdot h_{tot} \right)}{\partial t} - \frac{\partial \rho}{\partial t} + \nabla \bullet \left(\lambda \cdot \nabla T \right) + \nabla \bullet \left(U \bullet \tau \right) + U \bullet S_M + S_E \qquad \textbf{Equation 5-4}$$

Where h_{tot} is the total enthalpy, related to the static enthalpy $h(T, p)$ by,

$$h_{tot} = h + \frac{1}{2} \cdot U^2 \qquad \textbf{Equation 5-5}$$

The term $\nabla \bullet \left(U \bullet \tau \right)$ represents the work due to viscous stress and is called the viscous work term. The term $U \bullet S_M$ represents the work due to external momentum sources and S_E is the energy source.

5.2.1 Two equation turbulence closure models

Two-equation turbulence models are widely used to provide a 'closure' to the time averaged Navier-Stokes equations. Two principle closure models exist commercially, are the $k-\varepsilon$ (*k*-epsilon) model and the shear stress transport (SST) model. The two-equation models are much more sophisticated than the zero equation models. In these equations both the velocity and the length scale are solved using separate transport equations. The detail of these equations is not considered in this section. This can be found in ANSYS user guides, 2006.

The $k-\varepsilon$ model has proven to be stable and numerically robust and has a well-established regime of predictive capability. For general-purpose simulations, the $k-\varepsilon$ model offers a good compromise in terms of accuracy and robustness; however, it can lack prediction accuracy for complex flow. Such complexities include rapid variations in flow area, flows with boundary layer separation, flows with sudden changes in the mean strain rate, flows in rotating fluids, flows over curved surfaces etc.

A Reynolds Stress model may be more appropriate for flows with sudden changes in strain rate or rotating flows, while the SST model may be more appropriate for separated flows.

5.3 PARTICLE EQUATION OF MOTION

The most widely applied method to determine the motion of the dispersed phase is by tracking a large number of individual particles in the flow field. This method is called Lagrangian tracking. In this method, each particle represents a sample of particles that follow an identical path, which describe the average behaviour of the dispersed phase. The CFD code contains a Lagrangian particle-tracking algorithm that numerically predicts trajectories of solid particles through the flow field. These calculations use information generated by the flow field simulation. The code also has the capability to couple the particle equation of motion, with the flow solution. Coupling the governing equations for the fluid and the particle allows effects, such as fluid displacement by particles and particles-induced turbulence, to be investigated. In many cases of engineering interest, especially solid /liquid flows, this coupling allows the investigation of particle concentration effects. However, at low particle concentrations, the particles do not affect the flow and this coupling is not necessary. While setting up the Lagrangian way particle model, the following assumptions are implied:

- Particle-particle interactions are neglected due to the low particle concentrations experienced.
- The particles are spherical. The physical properties of each phase are constants.
- The mean flow is steady. The turbulent flow is locally isotropic.
- The geometry modification caused by the removal of wall by the sand particles, are neglected

To derive a particle motion of equations, consider a discrete particle travelling in a continuous fluid medium. The forces acting on the particle, which affect the particle acceleration, are due to the difference in velocity between the particle and fluid, as well as to the displacement of the fluid by the particle. Basset, Boussinesq and Oseen derived the equation of motion for such a particle for a rotating reference frame (ANSYS, 2006):

$$m_P \cdot \frac{dU_P}{dt} = F_D + F_B + F_R + F_{VM} + F_P + F_{BA} \qquad \textbf{Equation 5-6}$$

Where, F_D is drag force acting on the particle, F_B is Buoyancy force due to gravity, F_R is forces due to domain rotation (centripetal and coriolis forces), F_{VM} is virtual (or added) mass force. This is the force to accelerate the virtual mass of the fluid in the volume occupied by the particle. This term is important when the displaced fluid mass exceeds the particle mass, such as in the motion of bubbles. F_P is pressure gradient force. This is the force applied on the particle due to the pressure gradient in the fluid surrounding the particle caused by fluid acceleration. It is only significant when the fluid density is comparable to or greater than the particle density. F_{BA} is Basset force or history term, which accounts for the deviation in flow pattern from a steady state. This term is not implemented in ANSYS CFX. The particle and fluid mass values are given by,

$$m_P = \frac{\pi}{6} \cdot {d_p}^3 \cdot \rho_p \qquad \textbf{Equation 5-7}$$

$$m_F = \frac{\pi}{6} \cdot {d_p}^3 \cdot \rho_F \qquad \textbf{Equation 5-8}$$

5.3.1 Drag force

The aerodynamic drag force on a particle is proportional to the slip velocity, U_S between the particle and the fluid velocity. This is given by,

$$F_D = \frac{1}{2} \cdot C_D \cdot \rho_F \cdot A_F \cdot |U_S| \cdot U_S = \frac{1}{2} \cdot C_D \cdot \rho_F \cdot A_F \cdot |U_F - U_P| \cdot (U_F - U_P)$$

Equation 5-9

Where, C_D is the drag coefficient and A_F is the effective particle cross section. The drag coefficient C_D is introduced to account for experimental results on the viscous drag of a

solid sphere. In the simplest form of equation of motion, the main term on the right hand side is the drag force that includes the consideration of both skin and form effects. The total drag force is most conveniently expressed in terms of the non-dimensional drag coefficient, as defined by the Schiller-Naumann correlation, which modifies this to ensure the correct limiting behaviour in the inertial regime by taking,

$$C_D = \max\left(\frac{24}{R_e}\cdot\left(1+0.15\cdot R_e^{\,0.687}\right),\ 0.44\right) \qquad \textbf{Equation 5-10}$$

However, this correlation has been developed based upon spherical shape of the particle; the trajectories of the non-spherical particles can be modelled through the application of shape factors, allowing non-uniform drag distribution and bounce characteristics to be classified.

5.3.2 Buoyancy force

The buoyancy force is the force on a particle immersed in a fluid. The buoyant force is equal to the weight of the displaced fluid and is given by,

$$F_B = \left(m_p - m_F\right)\cdot g = m_p\cdot\left(1-\frac{\rho_F}{\rho_p}\right)\cdot g = \frac{\pi}{6}\cdot d_p^3\cdot\left(\rho_p-\rho_F\right)\cdot g \qquad \textbf{Equation 5-11}$$

5.3.3 Rotation force

In a rotating frame of reference, the rotation term is an intrinsic part of the acceleration and is the sum of Coriolis and centripetal forces:

$$F_R = m_p\cdot\left(-2\cdot\Omega\cdot U_P - \Omega\cdot\Omega\cdot r_p\right) \qquad \textbf{Equation 5-12}$$

The implemented rotation term also contains contributions from the pressure gradient and the virtual mass force due to the domain rotation, which leads to the following final contribution of the rotation term.

5.3.4 Virtual or added mass force

This force is caused by the fact that the particle has to accelerate some of the surrounding fluid, leading to an additional drag, which has the following form:

$$F_{VM} = \frac{C_{VM}}{2} \cdot m_F \cdot \left(\frac{dU_F}{dt} - \frac{dU_P}{dt} \right)$$ **Equation 5-13**

If the virtual mass force is included, the coefficient C_{VM} is normally set to one. However, when the virtual mass force is not included, then C_{VM} effectively has the value zero, and R_{VM} is equal to one.

5.3.5 Pressure gradient force

The pressure gradient force results from the local fluid pressure gradient around the particle and is defined as,

$$F_P = -\frac{m_F}{\rho_F} \cdot \nabla P$$ **Equation 5-14**

This force is only important if large fluids pressure gradients exist and if the particle density is smaller than or similar to the fluid density. Neglecting diffusive and source terms in the steady state momentum equation, the pressure gradient can be replaced by the velocity gradient. Assuming a constant fluids density, the pressure gradient force can be written as,

$$Fp = m_F \cdot \left(U_F \cdot \nabla U_F - R_F \right) = m_p \cdot \frac{\rho_F}{\rho_p} \cdot \left(U_F \cdot \nabla U_F - R_F \right)$$ **Equation 5-15**

5.4 RESTITUTION COEFFICIENT FOR PARTICLES

The parallel and the perpendicular restitution coefficients describe the action of particles when they hit a wall. The reflected velocity of the particle is lower than the incoming velocity due to energy transfer. Energy is dissipated as heat, noise and target material deformation. This effect is described by the momentum-based restitution coefficient. The coefficient values of 1 describes an elastic collision, while values less than 1 describes an in-elastic collision. The parallel coefficient is usually equal to 1. The perpendicular coefficient will depend on the particle material. Particle that bounces off the walls will have a perpendicular coefficient close to 1, while particles that stick to walls will have a perpendicular coefficient of 0. In this simulation, the perpendicular and parallel coefficients of restitutions are chosen equal to 0.9 and 1 respectively.

5.5 BASIC EROSION MODEL

There are two erosion models available in ANSYS CFX, namely, Finnie and Tabakoff. The choice of one model over another is largely simulation-dependent. In general, the Tabakoff model provides more scope for customization with its larger number of input parameters. The erosion model can be set on a per-boundary or per-domain basis. When enabled for the domain, the domain settings will apply for all boundaries that do not explicitly have erosion model settings applied to them.

5.5.1 Model of Finnie

The wear of a wall due to the erosive effect of particle impacts is a complex function of particle impact, particle and wall properties. For nearly all metals, erosion is found to vary with impact angle and velocity according to the relationship (ANSYS, 2006)

$$E = k \cdot V_p^n \cdot f(\gamma)$$ **Equation 5-16**

Where, E is a dimensionless mass, V_p is the particle impact velocity and $f(\gamma)$ is a dimensionless function of the impact angle. The impact angle is the angle in radians between the approaching particle track and the wall. The value of the exponent, n, is generally in the range 2.3 to 2.5 for metals.

Finnie's model of erosive wear relates the rate of wear to the rate of kinetic energy of impact of particles on the surface, using $n = 2$

$$E = k \cdot V_p^{\,3} \cdot f(\gamma)$$ **Equation 5-17**

Where,

$$f(\gamma) = \frac{1}{3} \cdot Cos^2\gamma \qquad if\ \tan\gamma > \frac{1}{3}\text{, and}$$ **Equation 5-18**

$$f(\gamma) = Sin(2\gamma) - 3 \cdot Sin^2\gamma \qquad if\ \tan\gamma \le \frac{1}{3}$$ **Equation 5-19**

5.5.2 Model of Tabakoff and Grant

The Tabakoff erosion model requires the specification of five parameters (ANSYS, 2006). The k_{12} constant, 3 reference velocities and the angle of maximum erosion γ_0 must all be specified. Table 5-1 provides some values for the Tabakoff model coefficients for Quartz-Aluminium, Quartz-Steel and Coal-Steel.

Table 5-1 Coefficients for some materials using the Tabakoff erosion model

Variable	Coefficient	Value	Material
k_{12}	k_{12}	5.85 x 10^{-1}	Quartz- Aluminium
Ref Velocity 1	V_1	159.11 m/s	
Ref Velocity 2	V_3	194.75 m/s	
Ref Velocity 3	V_4	190.5 m/s	
Angle of Maximum Erosion	γ_0	25 degree	
k_{12}	k_{12}	2.93328 x 10^{-1}	Quartz - Steel
Ref Velocity 1	V_1	123.72 m/s	
Ref Velocity 2	V_3	352.99 m/s	
Ref Velocity 3	V_4	179.29 m/s	
Angle of Maximum Erosion	γ_0	30 degree	
k_{12}	k_{12}	-1.321448 x 10^{-1}	Coal - Steel
Ref Velocity 1	V_1	51.347 m/s	
Ref Velocity 2	V_3	87.57 m/s	
Ref Velocity 3	V_4	39.62 m/s	
Angle of Maximum Erosion	γ_0	25 degree	

In the erosion model of Tabakoff and Grant, the erosion rate E is determined from the following relation (ANSYS 2006):

$$E = k_1 \cdot f(\gamma) \cdot V_p{}^2 \cdot Cos^2\gamma \cdot \left[1 - R_T{}^2\right] + f(V_{PN}). \qquad \textbf{Equation 5-20}$$

Where,

$$f(\gamma) = \left[1 + k_2 \cdot k_{12} \cdot Sin\left(\gamma \cdot \frac{\pi/2}{\gamma_0}\right)\right]^2, \quad \textbf{Equation 5-21}$$

$$R_T = 1 - k_4 \cdot V_P \cdot Sin\gamma, \quad \textbf{Equation 5-22}$$

$$f(V_{P\,N}) = k_3 \cdot (V_P \cdot Sin\gamma)^4, \quad \textbf{Equation 5-23}$$

$$k_2 = \begin{cases} 1.0 & if\ \gamma \le 2 \cdot \gamma_0 \\ 0.0 & if\ \gamma > 2 \cdot \gamma_0 \end{cases} \quad \textbf{Equation 5-24}$$

Here, E is the dimensionless mass (mass of eroded wall material divided by the mass of particle). V_p is the particle impact velocity. γ is the impact angle in radians between the approaching particle track and the wall, and γ_0 is the angle of maximum erosion. k_1 to k_4, k_{12} and γ_0 are model constants and depend on the particle and wall material combination.

Chapter 6
CFD Simulation Model

In this chapter a description of computational model, similar to Cahua power plant Francis turbine design is presented, in which the governing equations will be solved and solution is obtained.

6.1 CAHUA HYDROPOWER PLANT (HPP)

Cahua hydropower plant is a Run-of-River hydropower plant built in Peru. It is located 60 km upstream the mouth of Pativilca River, which is about 200 km north of Lima. The construction of power plant was finished in 1967. SN-Power Norway purchased this power plant in 2003.

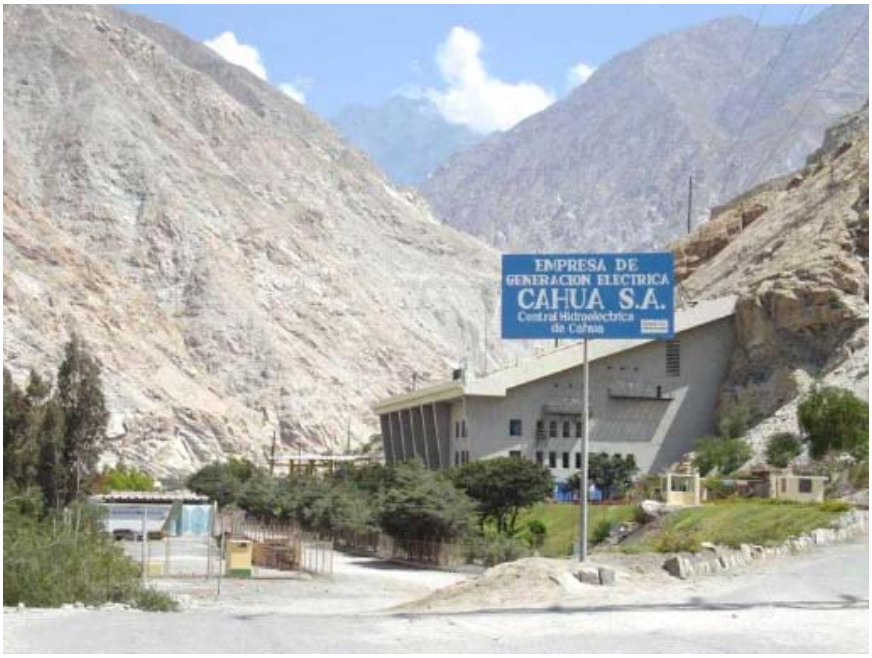

Figure 6-1 Cahua hydropower plant

There are two Francis turbines installed, which were originally delivered by Riva. Both Francis turbines composed of 20 stay vanes, 20 guide vanes and 17 runner blades. The rated power output is 42 MW, the gross head is 215 m, and the mass flow is 22 m^3/s.

The river carries large amount of sediments and has caused severe erosion damage on turbine components, mainly, turbine runner, guide vanes, and covers. The runner, guide vanes, and covers of the turbines are taken out every year and refurbished. The original turbines are operated at maximum 3 g/l (or 3,000 ppm) sediment concentration and the sediment that passes the turbine has about 35 % of quartz and 30 % of feldspar content on average. This means that the turbine has a maximum sediment load of 33 kg/s and 65 % of minerals are harder than the base material of turbine. This is the main reason of excessive sediment erosion in the hydraulic machinery operating in this power plant. Furthermore, the sediment study conducted at this power plant indicated that, the sediment concentration exceeds 120,000 tons of sediment, i.e. 33.06 kg/s only after six weeks of operation during intense monsoon period. Table 6-1 presents the sediment load of Cahua power plant for four monsoon periods. According to the engineers at the power plant, the turbine can take maximum 120,000 – 140,000 tons of sediment loads. If the load is even higher, the turbine parts gets eroded so much that welding and grinding is impossible.

Table 6-1 Sediment load of Cahua power plant (Ole et al., 2009)

Turbine	Turbine put in to service	Turbine taken out of service	Sediment load[tons]
1	16.04.2001	27.03.2002	165,6354
1	28.03.2002	02.05.2003	131,799
1	03.05.2003	29.05.2005	136,327
1	30.05.2005	01.07.2006	115,538
2	11.06.2001	28.07.2002	220,032
2	29.07.2002	13.07.2003	82,583
2	14.07.2003	19.04.2005	122,891
2	22.04.2005	01.07.2006	144,865

6.2 DESCRIPTION OF COMPUTATIONAL MODEL

The erosion prediction procedure mainly consists of three different models. These are, flow model, particle transport model, and erosion model. CFX code contains the ability to couple the equations governing fluid motion and the particle equation of motion.

The flow simulation contains the information necessary to perform all subsequent calculations. Velocity components, turbulence quantities (turbulence kinetic energy and dissipation rate), and carrier fluid properties (density and viscosity), are all contained within the flow field simulation. Once a simulated flow field is obtained, the solution is introduced with a large number of particles at the inlet of stay vanes. A large numbers of

particles are normally required in order to obtain a reasonable distribution and to reduce scatter in the erosion predictions. Each particle is tracked separately through the flow field. For each particle impingement, a set of empirical equations is applied. These erosion equations account for the impingement speed and angle, as well as the particle shape and the mechanical properties of the wall material.

In order to visualize erosion predictions in a convenient manner, predicted erosion data is transferred to a post-processor. This post-processor is used to generate contour plots of predicted erosion quantities. This allows not only the simultaneous examination of the flow solution, particle trajectories, and erosion predictions, but also provides the ability to identify areas of high erosion.

6.2.1 Flow model

The flow simulation was obtained through use of a commercially available computational fluids dynamics (CFD) code, namely ANSYS CFX. The code utilizes a finite-volume, multi-block approach to solve the governing equations of fluid motion numerically on a user-defined computational grid.

The flow solution procedure first generates the computational grid. A pre-processor is available in the software to perform this task. Second, the solution option such as inlet and boundary conditions, turbulence model, and discretization scheme, are specified. The final step is running the flow solver to generate the actual flow field simulation.

CFX contains several models for turbulence behaviour. Isotropic and non-isotropic turbulence models are available. In addition, multitudes of discretization schemes are available to obtain the most accurate flow solution possible. For this work, a differential Reynolds stress turbulence model, and Forward Euler implicit scheme, second order time in high-resolution advection scheme, with convergence criteria at 10^{-4} were used.

6.2.2 Mesh generation

A computational domain is necessary for the simulation of a Francis turbine. The computational domain was made based upon a Cahua Francis turbine design, which composed of stay vanes, guide vanes, and runner vanes, as shown in Figures 6-2. This domain corresponds to the water passages and can fully consider non-uniform flow field incoming from the stay vanes. Two computational domains, as shown in Figure 6-2 (a) and (b); were considered during simulation analysis, one based upon best efficiency point and another based upon full load conditions.

For each independent component, a hexahedral structure mesh was generated using Turbo Grid 11.0. The Turbo Grid was selected for meshing because this is a highly automated hexahedral mesh generator, specially designed for turbo-machinery applications.

The Grid generation relied on three different factors; namely, number of cells, Reynolds number, and turbulence model desired. Two equation turbulence models was chosen initially for grid generation but the Shear stress transport (SST) model gave the most realistic results, and it was decided to continue the simulation with this model only. Figure 6-2 shows single blade cascade computational model for three different vanes.

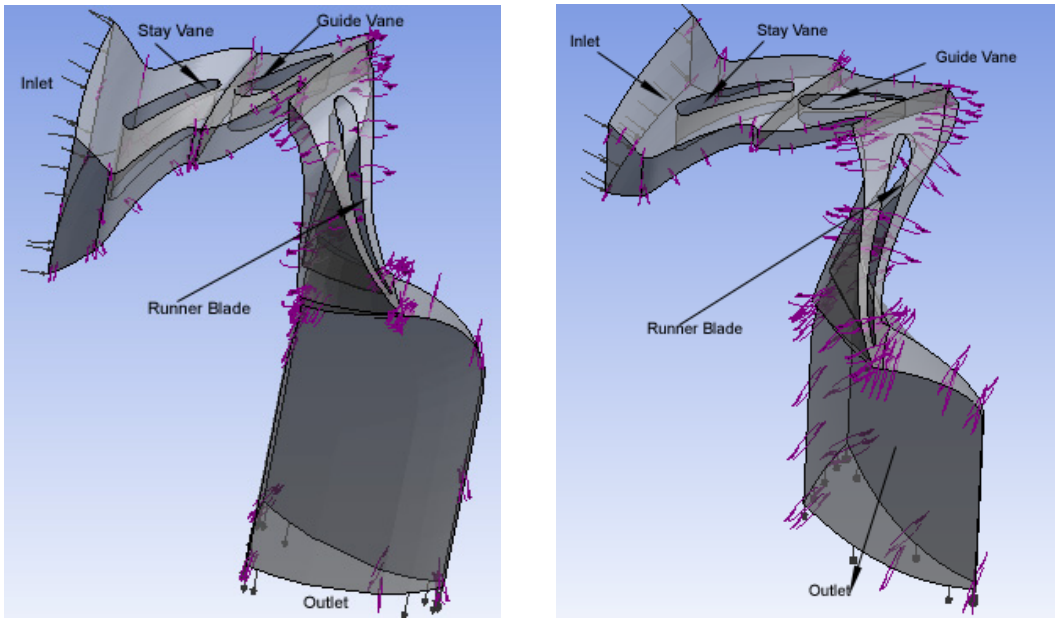

(a) BEP (b) Full load

Figure 6-2 A single blade cascade computational model for three vanes

To achieve a result with second order accuracy and sufficient numerical stability, a high-resolution scheme was applied for discretization of the grid. The grids used in these simulations have different mesh quality, as presented in Table 6-2. Since runner blade is more important than other components of turbine, higher numbers of nodes were observed in runner blade than guide vane and stay vane. At areas where the flow includes large gradients, the grid quality needs special attention.

Table 6-2 Mesh statistics of numerical models

Computational model	Vane	Number of nodes	Number of elements (hexahedra)
Full load (FL)	Runner blade	132,125	119,952
	Guide vane	110,345	100,800
	Stay vane	59,130	53,352
Best efficiency (BEP)	Runner blade	99,190	90,304
	Guide vane	72,565	65,472
	Stay vane	59,130	53,352

To get a smooth transition between the small and the large control volumes, an expansion factor of approximation 1.25 was used. The GTM files (mesh files) were directly imported into a Turbo machinery mode in pre-processor for defining simulation.

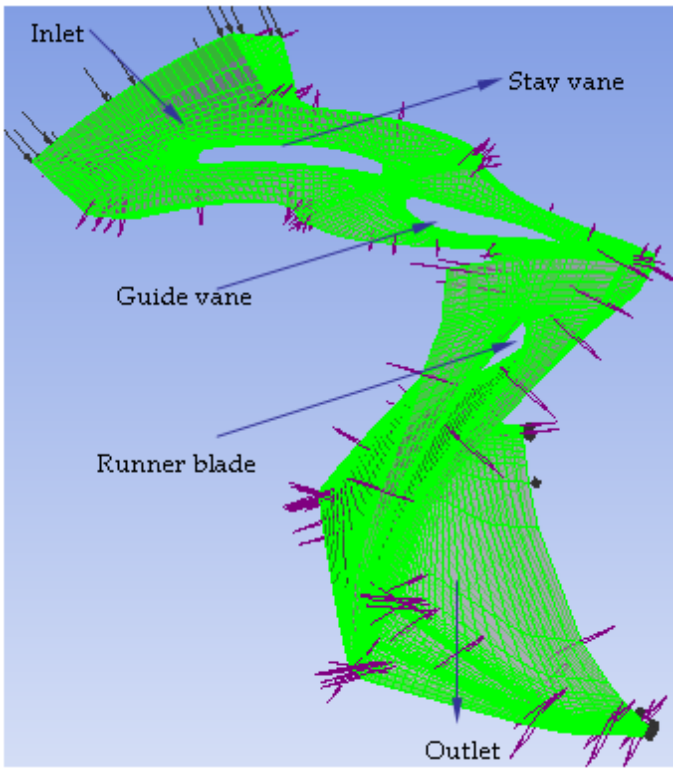

Figure 6-3 A single blade cascade mesh model for three vanes

6.2.3 Properties of sand

The density of sand particles used in the simulation needs to be defined in general mode. To calculate the effect of particles on continuous fluids, between 100 and 1,000 particles are usually required (ANSYS, 2006). However, if accurate information about the particle volume fraction or local forces on the wall boundaries is required, then a much larger number of particles are needed to be modelled. After creating a domain, full coupling or one-way coupling between the particle and continuous phase has to be chosen. Full coupling is needed to predict the effect of particles on the continuous phase flow field but has the higher computational cost than one-way coupling. One-way coupling simply predicts the particle paths during post processing based on the flow field, but without affecting the flow field. To optimize CPU usage, the two sets of identical particles were created. The first set is fully coupled and between 100 and 1,000 particles are used. This allows the particles to influence the flow field. The second set uses one-way coupling but

a much higher number of particles are used. This provides a more accurate calculation of the particle volume fraction and local forces on the wall. In inflow or in opening boundary, the particle velocity, injection position, diameter distribution, and mass flow rate are needed to be specified. Sand particles are uniformly injected at the stay vane inlet with the same conditions as the fluid. The particles will follow through the domains and exit at the outlet. The sand particles are defined as solid particles, and the size distribution is uniform in diameter. The turbulence dissipation force is activated, and the Schiller Naumann model is chosen to calculate the drag force acting on the particle. The two empirical erosion models, namely Finnie, and Tabakoff, were used for predicting erosion.

6.2.4 Boundary conditions

In a numerical simulation, it is impossible and unnecessary to simulate the whole system. Generally, the interesting regions with certain boundary conditions are sufficient to be chosen for conducting proper simulations. Numerical simulations also have to consider the physical processes in the boundary region. Different boundary conditions may cause quite different simulation results. Improper sets of boundary conditions may introduce nonphysical influences on the simulation system, while a proper set of boundary conditions can avoid that. So arranging the boundary conditions for different problems becomes very important. While at the same time, different variables in the environment may have different boundary conditions according to certain physical problems. If all residual are below their targeted criteria then convergences of equations will prevail. To improve the convergences of simulation and to obtain a convergence of solution with less numbers of iterations in relatively short interval of time, only one set of blades was considered in this simulation analysis. Generally, the meshed domains are imported into the pre-processor, and connected to each other by domain interfaces. The runner domain is a rotating domain, which is coupled to the stationary domain of guide vane and stay vane parts by so-called frozen rotor domain interfaces. In addition to these domain interfaces, inlet and outlet boundary conditions are defined. Fluid properties (density and viscosity) and particle properties (diameter distribution, density, and concentration) are also defined in the pre-processor. In the post-processor, there is a provision to assemble all components of a turbine. The two most interesting operating points were considered, at best efficiency point and at full load with guide vane angle of 16 ° and 22 ° respectively.

6.2.4.1 Inlet and outlet

When setting boundary conditions, ANSYS CFX best practices guide for Turbo machinery recommends specifying a total inlet pressure and mass flow outlet. This will give more appropriate calculation of the flow field than with the mass flow inlet condition for machines drawing fluid directly from a static reservoir. This may be valid for hydraulic pump simulation but in the case of radial turbine, the mass flow inlet and a

total pressure outlet were found more appropriate and robust than the total inlet pressure and mass flow outlet. In addition, this provides better performance of turbine, when looked at pressure distribution, y+ values, power output, head, and flow rate. Thus, the inlet condition was set as mass flow rate per passage with velocity components. The outlet pressure in this case is arbitrary and is usually set at zero or close to zero to reduce round off error. In this simulation, this was chosen equal to 1 atm. The detail boundary conditions with appropriate value are presented in Table 6-3.

Table 6-3 Boundary conditions

Variable	Value
Water density	997 kg/m^3
Quartz particle density	2.65 gm/cm^3
Diameter of the particle	15 μm to 2 mm
Inlet mass flow rate of water at BEP	540 kg/s
Inlet mass flow rate of water at full load	685 kg/s
Total pressure outlet	1 [atm.]
Inlet mass flow rate of particle	1 to 50 kg/s
Inlet flow direction at Stay vanes (α, r, θ)	0 , -0.4 , -0.9165

6.2.4.2 Wall

The covers, hub, shroud and vanes were defined as smooth walls with no-slip condition. The wall friction then decreases fluid velocities near the wall. The runner has an angular velocity 600 rpm, while the stay vane and guide vane are stationary domains. A periodic boundary condition was set to couple two adjacent blades. This simplified the computational model. When a particle reaches a symmetry plane boundary condition, it is reflected. If simulation includes any solid domains, then it needs to set particle options at the fluid-solid interface. To do this, first it needs to create the required fluid-solid domain interfaces, and then edit the automatically created interface boundary condition for the fluid side of the interface. The options on the fluid side of fluid-solid interfaces are specified in the same way as for wall boundaries.

Chapter 7
Simulation Result and Discussions

This chapter presents contour plots of erosion rate density on different components of the Francis turbine based upon the simulation results. The relationship between particle movement and erosion inside the turbine based upon the shape, size, and concentration of particle at two operating conditions namely, best efficiency point (BEP) and full load (FL) are compared and the results are discussed.

7.1 HYDRAULIC PERFORMANCE OF TURBINE

Turbines are always designed for specific conditions of head, speed and output. However, a turbine may actually be required to operate under conditions widely different from those it has been designed. It is, therefore, important to determine and have complete information about the performance of the turbine over a wide range of operating conditions. The hydraulic performance of a simulated turbine is presented in Figure 7-1. This is found in good agreement with the actual data obtained from the Cahua turbine. The auto generated hydraulic turbine reports of simulation analysis are presented in Appendix A and B.

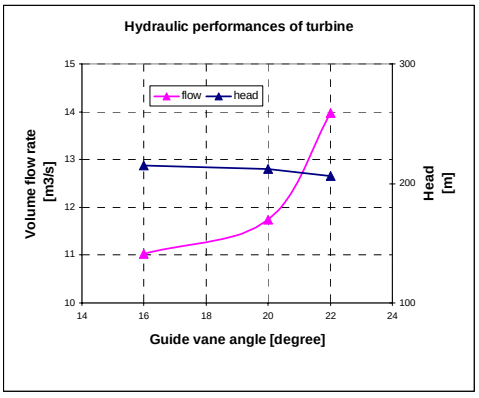

(a) Volume flow rate and guide vane angle

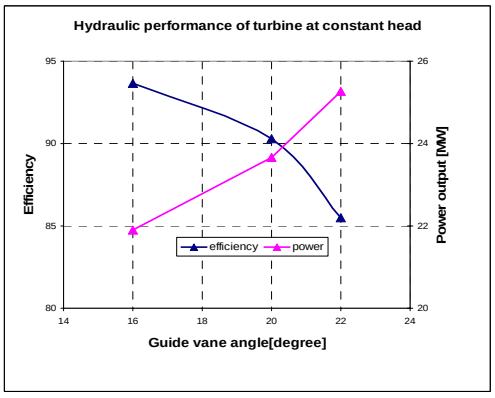

(b) Efficiency and guide vane angle

Figure 7-1 Hydraulic performance of turbine

7.2 SEDIMENT EROSION ON TURBINE COMPONENTS

An important consideration in these simulations is erosion to the different components of a turbine due to different shape and size of the sand particles. A good indication of erosion is given by the erosion rate density (kg/s/m^2) parameter, which corresponds to pressure and shear stress due to the flow. In order to visualize erosion predictions in a convenient manner, predicted erosion data is transferred to a post-processor. This post-processor is used to generate contour plots of predicted erosion quantities. This allows not only the simultaneous examination of the flow solution, particle trajectories, and erosion predictions, but also provides the ability to identify areas of high erosion. This can be seen as coloured spots. A Red colour indicates the highest value of erosion intensity, whereas a blue colour denotes the lowest intensity of erosion. The predicted erosion on different components can be used to better understand how parameters such as inlet conditions, fluids properties, flow rate, particle size & shape, concentration, and geometry, affect erosion behaviour.

7.2.1 Stay vane

Figure 7-2 (a-b) shows predicted erosion at stay vane and its surface. The mid height of the leading edge of stay vane is exposed to less erosion intensity. Near the upper and lower cover at the inlet, ring-shaped erosion grooves are observed, as seen in red colour in Figure 7-2 (a). On the blade surface, scattered erosion spots are observed at suction side. There is no erosion intensity observed at pressure side of vanes. This may be due to the boundary layer effect, which is caused by the initial velocity values at inlet of stay vanes or incorrect mesh properties. The boundary layer effect is one of the main limitations in many CFD turbulence models. These simulation results are found in agreement with Cahua turbine stay vanes as presented in Figure 3-2.

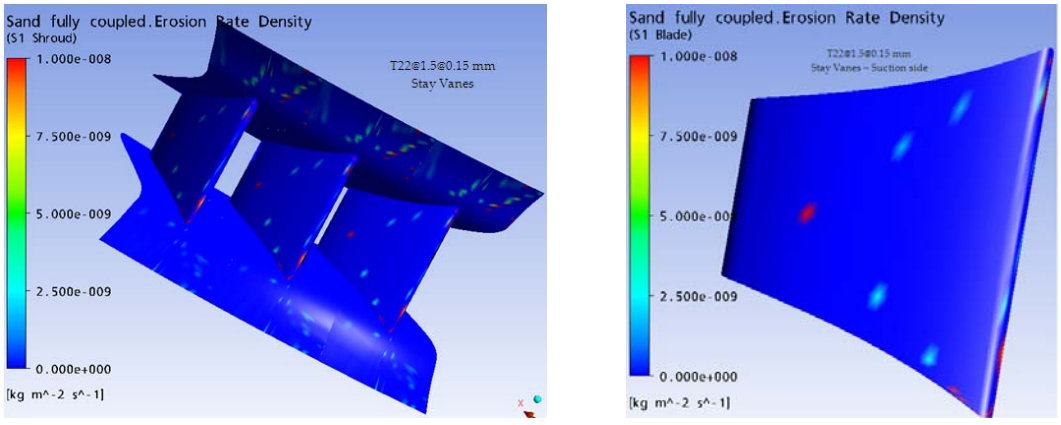

(a) Stay vanes with covers (b) Suction side of stay vane

Figure 7-2 Predicted erosion pattern on stay vanes

7.2.2 Guide vane

Figure 7-3 (a – b) shows the predictions of erosion rate density along the guide vane surface. The highest erosion is predicted on outlet regions and both covers. This is due to the turbulence erosion caused by high velocity with fine grain sand, which is in good agreement with the field test at Cahua, where significant surface deterioration was detected on the surface near the transitional zone to lower and upper cover. The particle velocity inside a turbine at both designed and maximum load conditions are presented in Figure 7-4 (a-b). The highest absolute velocity was observed at guide vane cascade and the highest relative velocity was observed at runner outlet surface. On the suction side of the vane, the simulations indicated relatively low erosion rate density on the surface towards the trailing edge whereas there is no erosion tendency found on the pressure side of the blades. This may be due to poor boundary conditions.

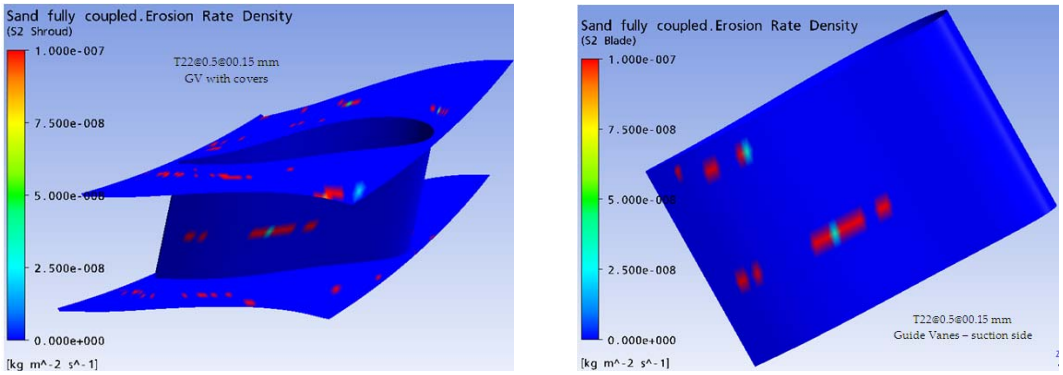

(a) Outlet and covers (b) Suction side

Figure 7-3 Predicted erosion pattern on guide vanes

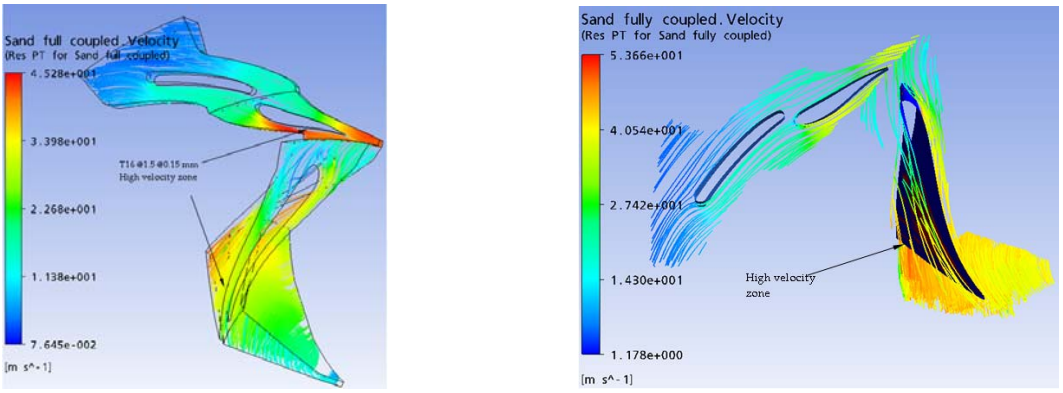

(a) Design load (b) Full load

Figure 7-4 Velocity of sand particle inside a turbine

Similar erosion tendency was observed at both design and off design conditions except at the leading edge of the vane, where surprisingly the highest erosion is predicted. This may be due to the combination of strong acceleration with bigger sizes of particle, and high velocity and strong turbulences with smaller sizes of particle. This creates secondary flow and strong vortex in the corners, and leads more erosion damage.

7.2.3 Runner blade

In the runner, the highest relative velocities occurred at the outlet regions while the highest accelerations may be found at or close to the blade inlet. Figures 7-5 (a- d) show the prediction of erosion on runner blade surface. The highest erosion is predicted at outlet blade surface than other component of turbine because the relative velocity is highest at the outlet of the blades. Hence, turbulence erosion due to fine sand particles is always susceptible at the trailing edge of the blades. In addition, because of high relative velocity, most of the particles will move towards outer diameter in the runner outlet and hence more effect of erosion is seen there. These simulations revealed that the outlet area of pressure side of the runner is highly exposed to erosion, which was found at the middle of the blade and towards the outlet area. This is due to the cross flow forming horseshoe vortices, which is caused by incorrect blade leaning. The incorrect blade leaning leads to cross flow between hub and shroud and such cross flow may intensify erosion effect. Minor erosion spots were also observed at the leading edge and at lower part of the outlet area on the suction side of the blades. The leading edge erosion is found due to the local accelerations.

The predicted erosion rate density on pressure side is more than on the suction side of the blade. This is even more in larger guide vane opening. The erosion rate density is more towards the outlet as compare to the inlet of the blade. This is due to the blade profile-tail vortex flow, which leads to higher erosion rate density in the blade outlet.

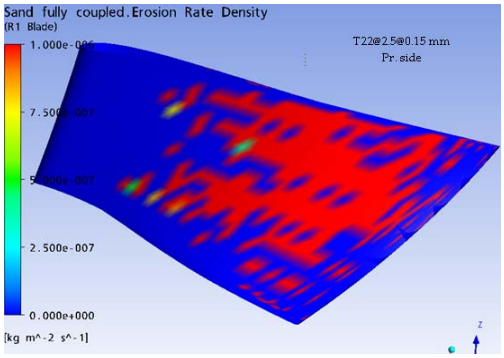

(a) Pressure side

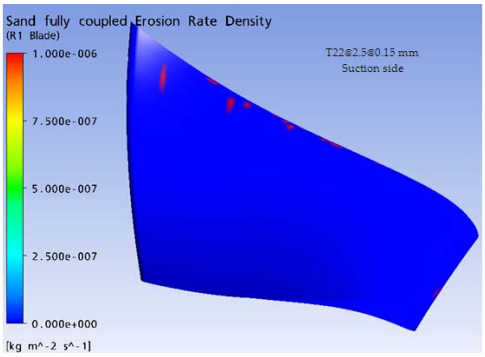

(b) Suction side

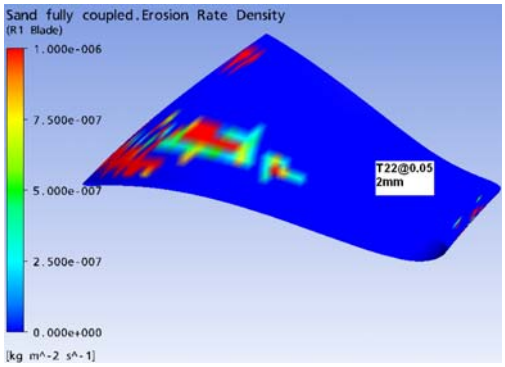

(c) Leading edge and trailing edge

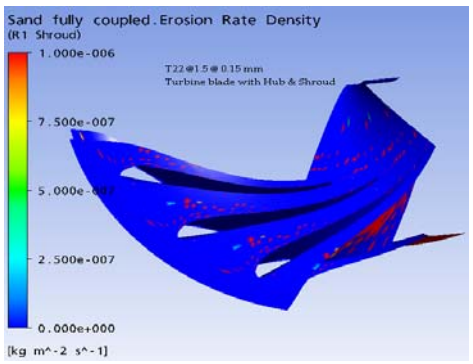

(d) Blade with hub and shroud

Figure 7-5 Predicted erosion pattern on turbine blades

7.3 EFFECT OF SEDIMENT CONCENTRATION ON EROSION

Based upon the simulation results obtained from Tabakoff erosion model, effects of sediment concentrations on erosion rate density on turbine blade are presented in Figure 7-6(a - d). In order to investigate the effect of sediment concentration on erosion, different sediment concentration rate were considered, while other parameters, i.e., sediment size, shape, operating condition of a turbine and impingement angle were kept constant. It can be observed from the figures that with the increase in concentration rate, the erosion rate density increases, although it is not the same at different guide vane openings.

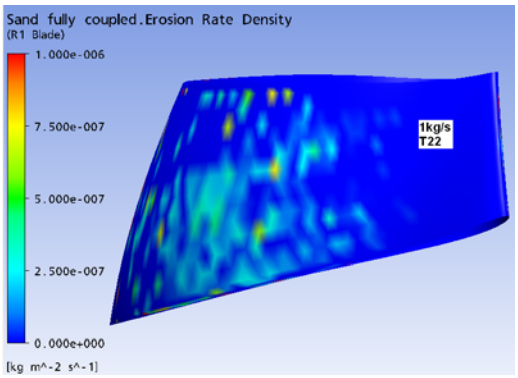

(a) 1 kg/s

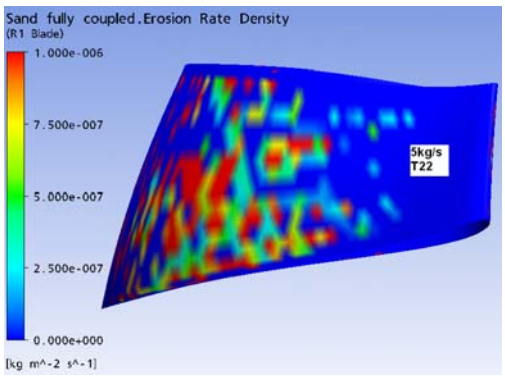

(b) 5 kg/s

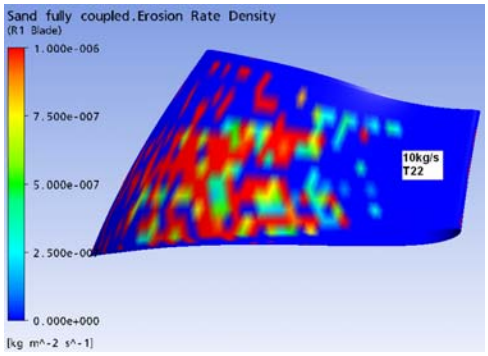

(c) 10 kg/s

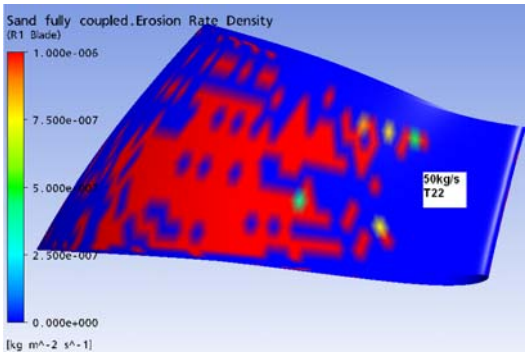

(d) 50 kg/s

Figure 7-6 Effect of concentration rate on erosion rate density of turbine blade

Additional simulations were performed with different sediment concentration rate at different guide vane opening i.e., 16 degree (BEP), 20 degree and 22 degree (full load) based upon Finnie erosion model. The variations of relative erosion rate density with concentration are presented in Figure 7 -7 (a - d). It can be seen from the figures that the relative erosion rate density increases almost linearly on increasing concentration rate. This shows that the erosion rate is constant for a given concentration and guide vane opening.

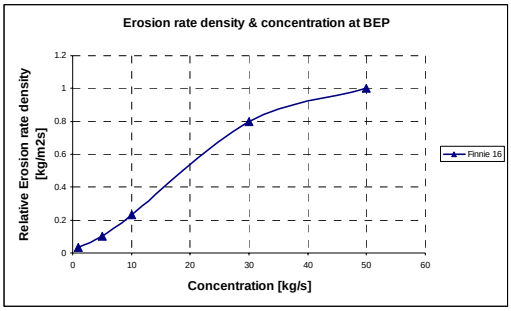

(a) Guide vane angle 16-degree

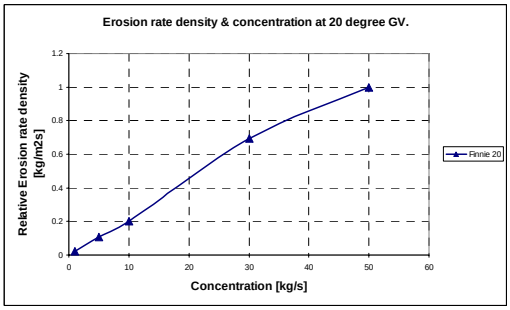

(b) Guide vane angle 20-degree

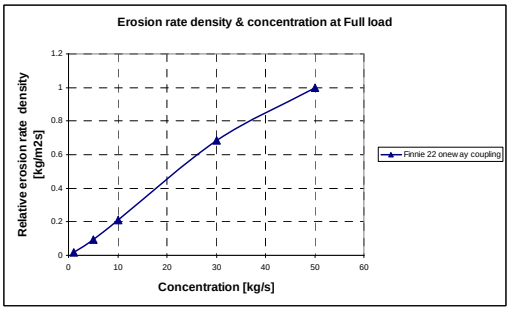

(c) Guide vane angle 22 degree (one-way coupled)

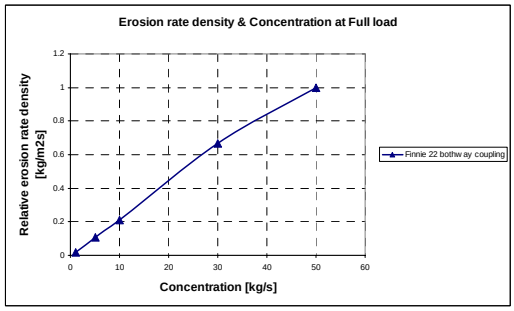

(d) 22 degree (both-way coupled)

Figure 7-7 Variation of relative erosion rate density with concentration

7.4 EFFECT OF SEDIMENT SIZE ON EROSION

Based upon the simulation results obtained from Finnie erosion model, effects of sediment sizes on erosion rate density on turbine blade are presented in Figure 7 -8 (a - d). In order to investigate the effect of sediment size on turbine blades, different sediment sizes were considered while other parameters, i.e., sediment concentration, shape factor of sediment, operating conditions of a turbine, and impingement angle were kept constant. It can be observed from the figures that within the range of sediment size i.e., 0.15 – 2 mm investigated, the erosion rate density increase with the increase in sediment size. However, the rate of increase of erosion rate density is not same for all sizes range and guide vane opening.

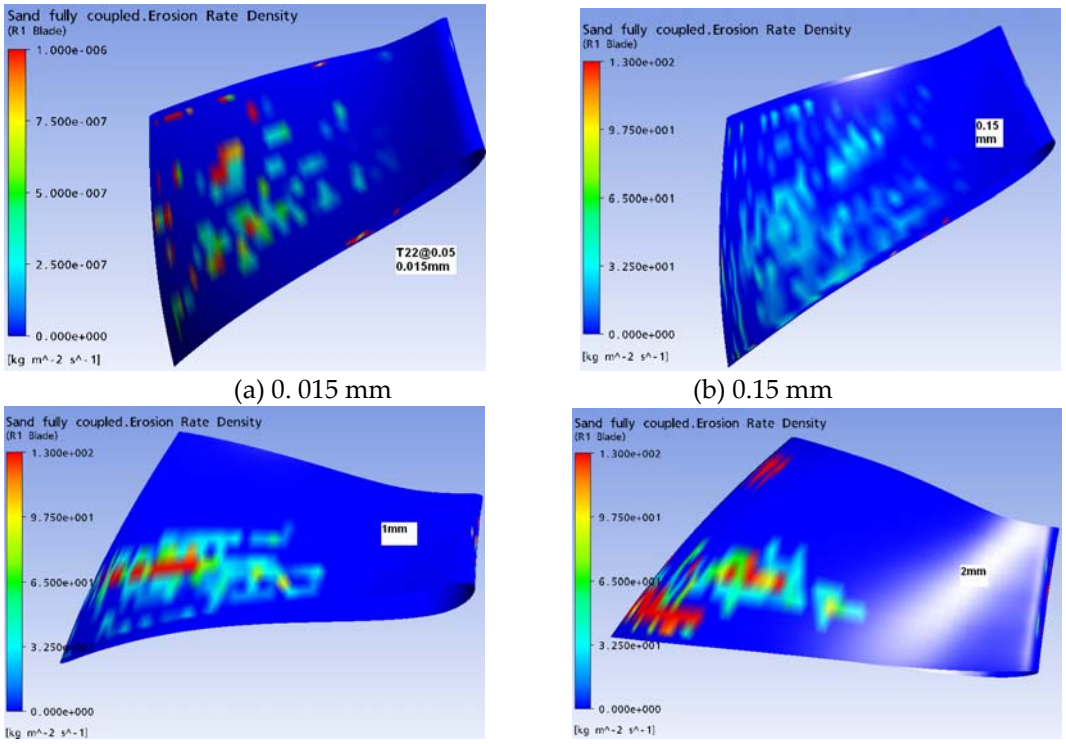

(a) 0. 015 mm (b) 0.15 mm

(c) 1 mm (d) 2 mm

Figure 7-8 Effect of sediment size on erosion rate density of turbine blade

Hence, additional simulations were performed at two guide vane opening i.e., at best efficiency point (16 degree) and at full load (22 degree). The variations of relative erosion rate density with mean sediment size are presented in Figure 7 -9 (a – b). It can be seen from the figures that the relative erosion rate density increases with sediment sizes. However, the erosion rate is not constant for all sizes range. For the particle smaller than 0.15 mm, owing to their light nature, they respond strongly to turbulences and thus gain the erosive energy, causing damage to the blade surface. In this range, the turbulence structure in the boundary layer dominates the erosion process. For larger particles sized

above 0.5 mm, the inertia force dominates their behaviour. They virtually do not respond to small turbulent structures. Their erosive power comes from the main flow where they are entrained. Owing to the significant momentum of these particles, they usually cause severe damage to the blade surface. For particles with size between these two extremes cases, a combined mode may exist subject to flow structure encountered, or one mode is more dominant than the other mode. They are likely to follow along the outer hydraulic contour of the blade, and their tendency for damage found progressively less. This further shows that the erosion rate is constant for a given size and guide vane opening.

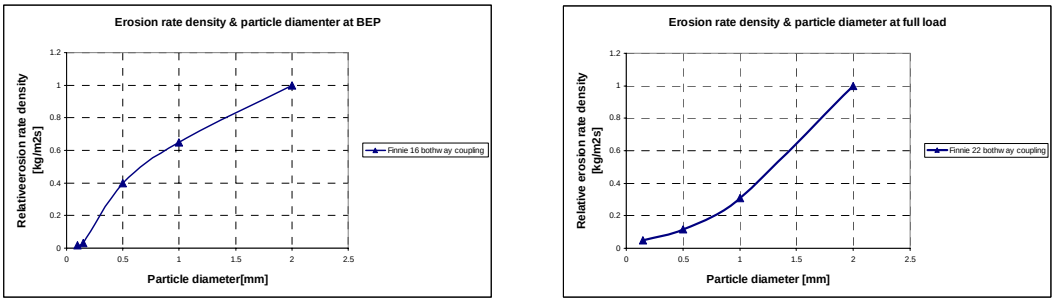

(a) BEP (b) Full load

Figure 7-9 Variation of relative erosion rate density with sediment size

7.5 EFFECT OF SEDIMENT SHAPE FACTOR ON EROSION

In order to investigate the effect of sediment shape on erosion, different shape factor of the particles i.e., 1, 0.75, 0.5 and, 0.25 were considered. Simulations were carried out at same concentration rates for both operating conditions while other influencing parameters were kept constant. The trajectories of the non-spherical particles can be modelled through the application of shape factors, allowing non-uniform drag distribution and bounce characteristics to be classified.

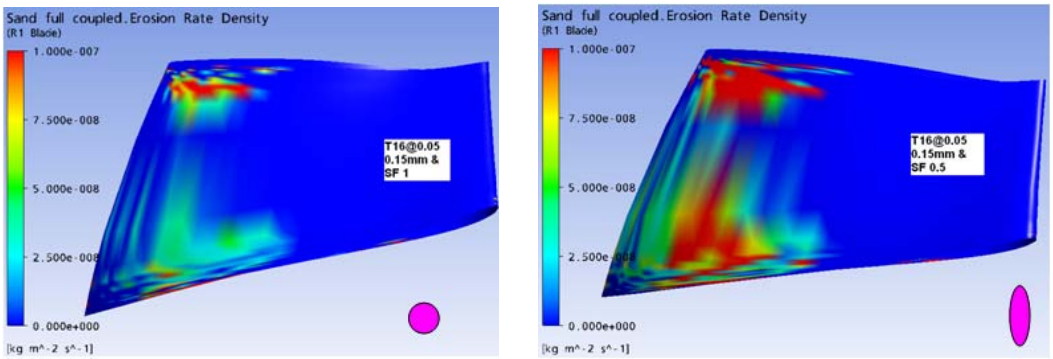

(a) Shape factor 1 (b) Shape factor 0.5

Figure 7-10 Effect of sediment shape factor on erosion rate density of turbine blade

A particle shape factor equals to one signifies that the shape of the particle is close to the spherical shape. In other words, it can be more or less regular shape of the particle. The lower value of shape factor gives the more irregular shape of the particle. Based upon simulations results obtained from Tabakoff erosion model, effects of shape factor on erosion rate density on turbine blade due to shape factor 1 and 0.5 are presented in Figure 7 -10 (a - b).

The figures show the prediction of erosion rate density along the blade surface at 16-degree guide vane opening which is at the maximum efficiency point. It can be clearly seen that maximum erosion occurs in the blade profile with shape factor of 0.5. The particle shape factor assumed spherical by default during simulations has value equal to 1. This always calculates the diameter of the particle from the mass of the particle divided by its density, assuming it is spherical. A cross sectional area factor can be included to modify the assumed spherical cross section area and to allow for non-spherical particles. This affects the drag force. The surface area factor is analogous to the cross sectional factor. For non-spherical particle, it is the ratio of the surface area to the surface area of spherical particle with the same equivalent diameter. This affects both mass transfer and heat transfer correlation and hence the erosion prediction. Similar erosion pattern is observed in each case. However, the blade profile area is highly affected and larger intensity of erosion rate is clearly observed in the case of non-spherical shape of the particle.

7.6 EFFECT OF OPERATING CONDITION ON EROSION

In order to investigate the effect of operating condition of turbine on erosion, simulations were carried out at mainly two operating points, i.e., at best efficiency and at full load conditions, while other influencing factors maintained constant. Based upon the simulation results obtained from Tabakoff erosion model, effects of operating conditions on erosion rate density on turbine blade are presented, as shown in Figure 7 -11 (a - d).

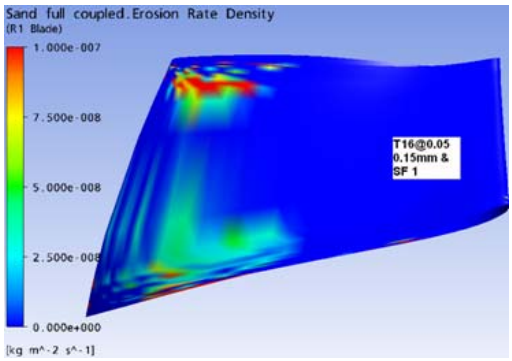

(a) BEP with shape factor 1

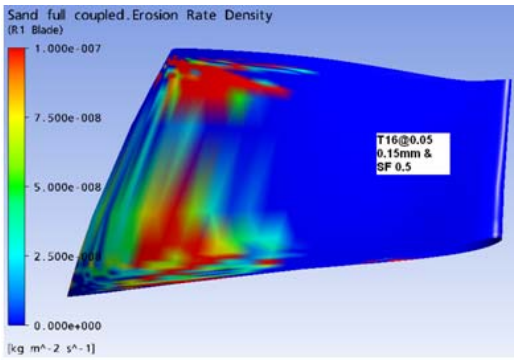

(b) BEP with shape factor 0.5

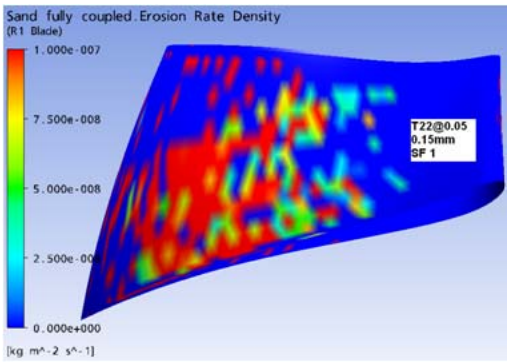

(c) Full load with shape factor 1

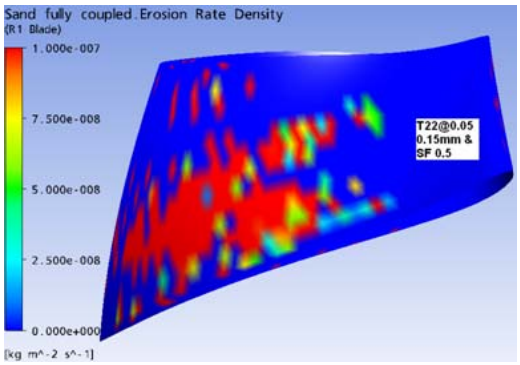

(d) Full load with shape factor 0.5

Figure 7-11 Effect of operating conditions on erosion rate density of turbine blade

These simulations revealed that the predicted erosion rate density at full load operation point is higher than at best efficiency operation point. This is due to increased flow turbulence and higher relative flow velocities at turbine runner outlet. Presence of secondary flows and accompanying vortices lead to increased local velocities, higher rotational motion and caused more separation of flow. Such flow conditions are conducive to increased erosion rate and hence more erosion rate density has been observed.

7.7 VALIDATION OF NUMERICAL SIMULATIONS

The experimental results discussed in section 4.3, and field studies at Cahua power plant discussed in section 3.3 are compared with CFD results to validate numerical simulations.

The velocity of particle was calculated in highly swirl conditions similar to turbine flow in curved path during experimental study, and it was determined that the size of the particle is inversely proportional to the velocity of the particle. Similarly, different sizes of spherically shaped particles, i.e., 0.015 mm, 0.05 mm, 0.15 mm, and 1 mm, were considered and velocities of those particles around a turbine blade were computed numerically. Figure 7-12 (a - d) shows the velocity for different size of the particle. It was found that higher velocity is obtained for smaller size of the particle and lower velocity is obtained for larger size of the particle. These simulations were carried out at same operating conditions keeping all other influencing parameters constant except the size of the particle. This is in agreement with the experimental results.

The experimental results further revealed that the velocity of particle also depends upon the shape of the particles. It was found that velocity of regular shape of the particle is higher than the other shapes of the particle. In order to compare this results, numerical simulations were performed on different shape and size of the particles, and it was

determined that spherically shaped particle had higher velocity than particle with other shapes. This can be clearly seen from Figure 7-13. These simulations were carried out at same operating conditions keeping all other influencing parameters constant except the shape of the particle.

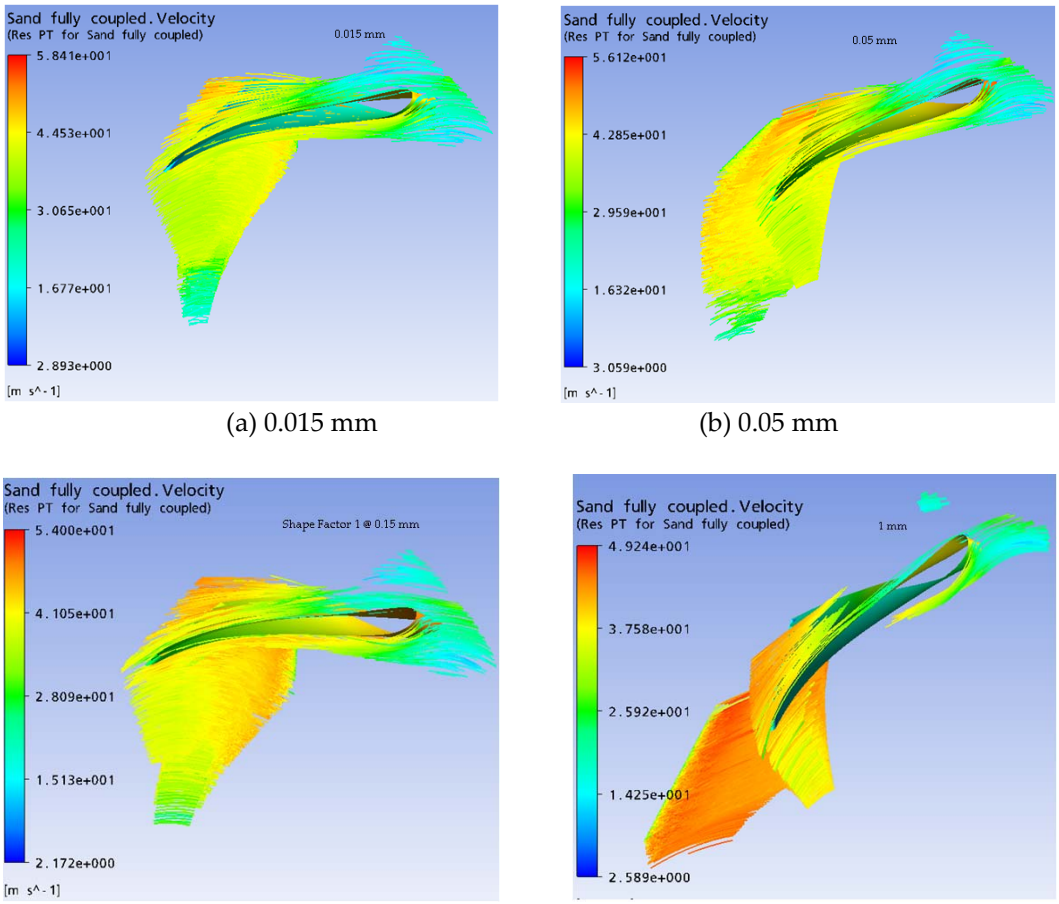

(a) 0.015 mm (b) 0.05 mm

(c) 0.15 mm (d) 1 mm

Figure 7-12 Particle velocity for different size around turbine blade

Generally, the erosion rate density increases when the velocity of particle increases. However, this has not occurred in the simulation analysis because of shape of the particle. Direct measurements of the erosion rate density from experimental analysis for comparison were not available; however, the drag coefficient of different shape of the particles, which were found from experimental analysis, can be utilized to verify the numerical predictions. The experiment results show that the triangularly shaped particles have higher drag coefficient than the other shapes.

This means that higher coefficient of drag caused higher drag force. The particle of given size flow along with the water and damage the blade surface. In general, many natural

particles are usually in non-spherical shape. These particles will tend to have lower velocities because both decrease in spheroid and increase in angularity tend to decrease velocities. The impact area of these particles on the eroded surface is relatively larger and tends to be directed perpendicular to the transport path. As a result, higher coefficient of drag, higher rotational motion and more separation of flow are likely to occur and hence more erosion rate is predicted.

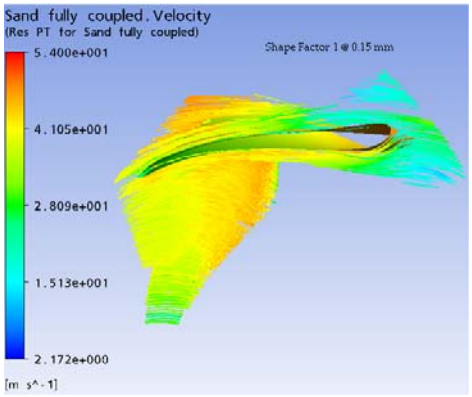

(a) Shape factor 1 and velocity

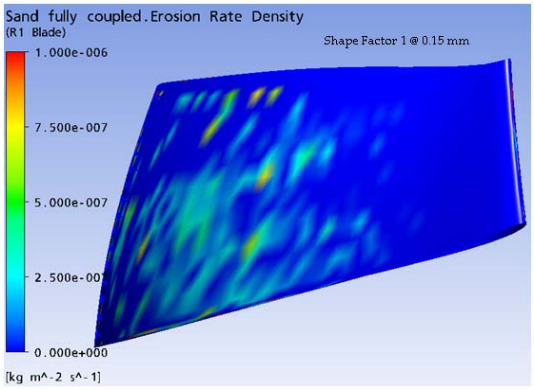

(b) Shape factor 1 and erosion rate

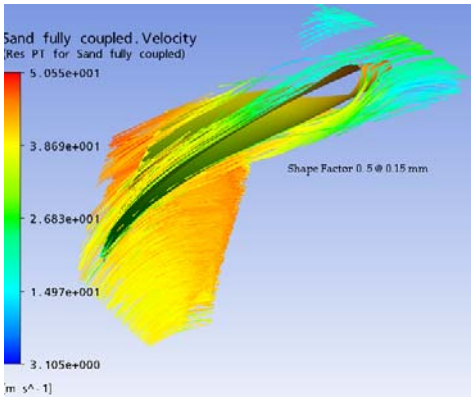

(c) Shape factor 0.5 and velocity

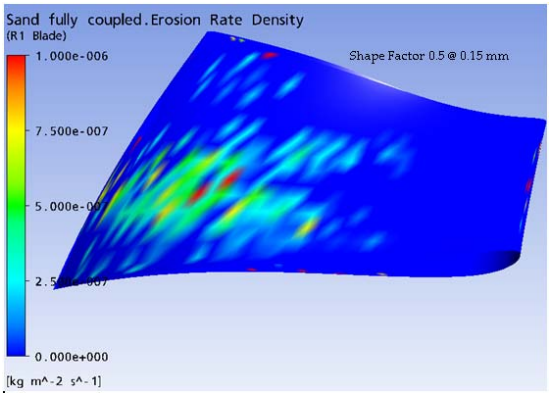

(d) Shape factor 0.5 and erosion rate

Figure 7-13 Particle velocity, shape factor and erosion rate around turbine blade

Furthermore, the numerically obtained erosion patterns, and similar field observations at Cahua power plant Francis turbine components discussed in section 7.2, are in good qualitative agreement for further validation of the numerical simulations.

Chapter 8
Conclusions and Recommendations for Further Work

8.1 CONCLUSIONS

Sediment erosion analysis of a Francis turbine gives an indication of relative erosion intensity and critical zones of erosion damage on the turbine components. The most realistic numerical prediction of erosion is found on a turbine runner blade. The highest velocities and accelerations occurred at outlet of the runner blade and more erosion was predicted especially at the pressure side of the blade outlet and at the shroud. Furthermore, unexpected sediment erosion was found at the suction side of the guide vane where concept of critical diameter can be utilized. It has been concluded that if the particle size in the water increases beyond critical particle sizes, the turbine should not be operated at low guide vane opening.

The numerically obtained erosion pattern and the field observation and inspection at Cahua power plant Francis turbine components are in good qualitative agreement. The encouraging agreement shows that, for this application, numerical simulation really can be used in a predictive manner. This information may serve as an input in an early stage of turbine design process to identify the regions where special surface treatment is necessary in order to increase the lifetime of the components for new hydropower projects involving risks of sediment erosion.

The velocity of a particle is inversely proportional to the size of the particle, and it was determined that spherically shaped particles had higher settling velocities than particles with other shapes. However, non-spherical shape of the particles will tend to have lower settling velocities because both decrease in spheroid and increase in angularity tend to decrease velocities. Moreover, larger cross-sectional areas tend to be directed perpendicular to the transport path. As a result, higher coefficient of drag, higher rotational motion and more separation of flow are likely to occur and hence more erosion rate is predicted. The roles played by shape of the particle significantly affect erosion rate prediction inside the Francis turbine components.

Furthermore, it has been found that the erosion process is strongly dependent on the particle size, shape, concentration, and operating conditions of the turbine. The reduction of the erosion is not only linked to the reduction of particle velocity but also is linked to the reduction of separation of flow, which further depends on the shape, size, and concentration of the particle. A significant reduction of erosion rate can be achieved by operating turbine at best efficiency point. The full load operations reduced efficiency, increased turbulence, and increased relative velocity of flow at outlet of the blade.

8.2 RECOMANDATIONS FOR FURTHER WORK

Sediment erosion problem in hydraulic machinery in general, and Francis turbine in particular, is one of the complex operation and maintenance problem that causes major challenges in the planning, design, operation and maintenance of hydropower projects in high sediment-laden Rivers. As discussed in section 2.7, there are large numbers of factors responsible for the sediment erosion damage inside the turbine. This research on sediment erosion in Francis turbine is one of the few attempts to address the problem area. The present knowledge and findings are not enough to deal with this problem completely but can be utilised to achieve one major step forward in erosion prediction and prevention. The ideas that were emerging during this study period are considered in this section. The following specific recommendations are made from the experience gained through this study, keeping a broader perspective on this specific problem.

Because of the simplicity of the empirical erosion model implemented in ANSYS CFX in steady state conditions, the present study demonstrated the relative erosion prediction on a qualitative basis. However, from the result provided, it is clear that the role of sediment characteristics and erosion pattern inside a turbine are addressed based upon the steady state conditions, which are quite different from the realistic operating conditions. Hence, a transient simulation analysis is recommended for predicting erosion on the turbine components, which was not possible during this study period due to the limitations in software and time.

The individual particles can be tracked throughout the computational domain, given knowledge of the flow field. However, in its basic form, CFX has no ability to produce erosion or particle impact data. To overcome such limitations, it is recommended that extensive FORTRAN routines have to be developed and embedded within CFX, allowing the relevant particle impact data to be computed, manipulated and displayed. The coefficient of restitution has to be modified to include the consideration of both impact angle and material type. Furthermore, validation of CFD by simplified lab test is, though challenging, also recommended.

It is recommended to carry out numerical simulation analysis including leakage flow in the guide vanes of Francis turbine because the losses due to the secondary leakage flow in the guide vanes represents a relatively large part of the total loss of the turbine

efficiency. This leakage flow arises due to the head covers deflection, which increases the gap between the guide vanes and the head covers, when it is pressurized. Moreover, when generating the grids, a tip- clearance can be added on the guide vane.

During this study, the drag coefficient and velocity relations were investigated with respect to different size and shape of the particles at fixed guide vanes position, i.e., at 16-degree guide vane opening. However, it is recommended to carry out more tests with adjustable vanes for statistical confidence. Furthermore, a rotational motion of the particle inside the flow field can also be included for assessing different forces acting on the particle so that the realistic expression for critical diameter of a particle other than spherical shape can be achieved.

It is recommended to carry out simulation analysis in CFD computational domain that corresponds to the water passages and can fully consider the non-uniform flow field incoming from the spiral casing so that better simulation of the flow can be achieved.

Hydraulic design modification is also recommended in a turbine runner to make them sediment friendly without much sacrificing the efficiency, size and cost parameters. This needs to be confirmed through model tests and numerical analysis.

REFERENCES

A. V. Levy, "The solid particle erosion behaviour of steel as a function of microstructure", Wear Vol. 68, 1981, pp. 269-287.

V. Levy, and G. Hickey, "liquid solid particle slurry erosion of steels", Wear Vol. 117, 1987, pp. 129 -158.

Al-Bukhaiti, M. A., S. M. Ahmed, F. M. F. Badran, and K. M. Emara, "Effect of impingement angle on slurry erosion behaviour and mechanisms of 1017 steel and high-chromium white cast iron", Wear Vol. 262, No. 9 - 10, 2007.

Anderson, J. D., "Computational Fluid Dynamics (The basics with applications)": McGraw-Hill Series in Mechanical Engineering, 1995.

ANSYS, Release 11.0 "Solver Theory Guide". 2006.

ANSYS, Release 11.0 "Turbo Grid Users Guide". 2006.

ANSYS, CFD online, "http://www.cfd-online.com"/, [Accessed on 31 August 2009].

Arnold, J. C., and I. M. Hutchings, "The mechanisms of erosion of unfilled elastomers by solid particle impact", Wear Vol. 138, 1990, pp. 33 - 46.

Avery, H. S., "Work hardening in relation to abrasion resistance", Material for mining industry symposium, editor: R. Q. Barr, Greenwich, conf. USA, Climax Molybdenum Co., Page 43 - 37, 1974.

Bahadur, S., and R. Badruddin, "Erodent particle characterization and the effect of particle size and shape on erosion", Wear Vol. 138, 1990, pp. 189 - 208.

Bajracharya, T. R., B. ,Acharya, C. B. Joshi, R. P. Saini, and O. G. Dahlhaug, "Sand erosion of Pelton turbine nozzles and buckets: A case study of Chilime hydropower plant", Wear Vol. 264, No. 3 - 4, 2008, pp. 177 - 184.

Basnyat, S., "Monitoring of sediment load and its abrasive effect in Jhimruk power plant", 1999, Proceedings, Optimum use of Run-of-River hydropower schemes, Trondheim, Norway.

Base, J. L., and K. G. Matthew, "Influence of structure on abrasive resistance of A1040 steel", Wear Vol. 14, Page 199 - 206, 1969.

Batchelor, A. W., L. N. Lam, and M. Chandrasekaran, "Materials degradation and its control by surface engineering": Imperial college press, 2002.

Bardal E., "Korrosjon og korrosjonsvern", 1985, Tapir, Trondheim (Norwegian)

Behera, U., P. J. Paul, K. Dinesh, and S. Jacob, "Numerical investigations on flow behaviour and energy separation in Ranque-Hilsch vortex tube", International journal of heat and mass transfer Vol. 51, No. 25 - 26, 2008, pp. 6077 - 6089.

Bergeron P. and Dollfus J., “The influence of nature of the pump mixture and hydraulic characteristics on design and installation of liquid/ solid mixture pump”, Proc. 5th conference on hydraulic turbines, 1952.

Bergeron P., “Similarity conditions for erosion caused by liquids carrying solids in suspension, application to centrifugal pump impellers”, La Houille Blanche, 5, 1950, B.H.R.A. translation T 408.

Bergeron P., “Consideration of the factors influencing wear due to hydraulic transport of solid materials”, 1952, Proc. 2nd conference on hydraulic transport and separation of solid materials.

Bergeron, S. Y., T. C. Vu, and A. P. Vincent, “Silt erosion in hydraulic turbines: The need for real- time numerical simulations”, 2002.

Bingley, M. S., and D. J. O'Flynn, “Examination and comparison of various erosive wear models", Wear Vol. 258, No. 1 - 4, 2005, pp. 511 - 525.

Bitter J. G. A., “A study of erosion phenomena”, 1962, part 1 and part II, Wear, Vol. 6, pp. 5- 21, and 169 – 190.

Bishwakarma, M. B., “Online sediment monitoring in RoR hydropower plants, PhD thesis”, Department of hydraulics and environmental engineering, Trondheim: NTNU, 2008.

Brekke, H., “A discussion of Pelton turbines versus Francis turbines for high head plants”, ASCE- IAHR/AIHR - ASME joint symposium on design and operation of fluid machinery, Colorado State University, Fort Collins, Colorado USA, 1978.

Brekke, H., E. Bardal, and R. T., "Norwegian research work on erosion resistive coating for water turbines", XVII IAHR symposium Beijing China, 1994.

Brekke, H., H. Wu, Y. L., and B. Y. Cai, “Design of hydraulic machinery working in sand laden water”. Book series on Hydraulic machinery, Vol.2 edited by Duan C. G. and Karelin V. Y., 2002.

Brown, G. J., "Erosion prediction in slurry pipeline tee-junctions", Applied mathematical modelling Vol. 26, No. 2, 2002, pp. 155 - 170.

Chevallier, P., and A. B. Vannes, "Effects on a sheet surface of an erosive particle jet upon impact", Wear Vol. 184, No. 1, 1995, pp. 87 - 91.

Chen Q. and Li D. Y., “Computer simulation of solid particle erosion”, 2003, Wear, Vol. 254, pp. 203- 210.

Clark, H. M., "On the impact rate and impact energy of particles in a slurry pot erosion tester", Wear Vol. 147, 1991, pp. 165 - 183.

Daun, C. G., Karelin, and W. Y., "Abrasive erosion and corrosion of hydraulic machinery published by Imperial College Press", 2002.

De Pellegrin, D. V., and G. W. Stachowiak, "Simulation of three-dimensional abrasive particles", Wear Vol. 258, No. 1 - 4, 2005, pp. 208 - 216.

Deng T., Bradley M. S. A. and Bingley M.S., "An investigation of particle dynamics within a centrifugal accelerator type erosion tester", 2001, Wear Vol., 247, pp., 55-65.

Desale, G. R., B. K. Gandhi, and S. C. Jain, "Effect of erodent properties on erosion wear of ductile type materials", Wear Vol. 261, No. 7 - 8, 2006, pp. 914 - 921.

Doby, M. J., A. F. Nowakowski, E. Nowak, and T. Dyakowski, "Numerical and experimental examination of swirl flow in a cylindrical container with rotating lids", Minerals engineering Vol. 20, No. 4, 2007, pp. 361 - 367.

Dosanjh, S., and J. A. C. Humphery, "The influence of turbulence on erosion by a particle laden fluid jet", Wear Vol. 102, 1985, pp. 303 - 330.

Edwards, J. K., and B. S. Mclaury, "Modelling solid particle erosion in elbows and plugged tees", Journal of Energy Resources Technology Vol. 123, 2001.

Eltvik Mette, "Sediment Erosion in Francis Turbines", 2009, Master thesis, NTNU

Escaler, X., E. Egusquiza, M. Farhat, F. Avellan, and M. Coussirat, "Detection of cavitation in hydraulic turbines", Mechanical Systems and Signal Processing Vol. 20, No. 4, 2006, pp. 983 -1007.

Fathy Hussein, M., and W. Tabakoff, "Computation and plotting of solid particle flow in rotating cascades", Computers & Fluids Vol. 2, No. 1, 1974, pp. 1 - 15.

Finnie, I., "Some observations on the erosion of ductile metals", Wear Vol. 19, No. 1, 1972, pp. 81 - 90.

Finnie, I., "Erosion of surfaces by solid particle", 1960, wear Vol. 3, pp. 87-102.

Forder, A., M. Thew, and D. Harrison, "A numerical investigation of solid particle erosion experienced within oilfield control valves", Wear Vol. 216, No. 2, 1998, pp. 184 - 193.

Gabitto, J., and C. Tsouris, "Drag coefficient and settling velocity for particles of cylindrical shape", Powder Technology Vol. 183, No. 2, 2008, pp. 314 - 322.

Gahr, K.-H. Z., "Microstructure and Wear of Materials, Elsevier, Amsterdam", 1981.

Goodwin, J. E., W. Sage, and G.P. Tilly, "Study of erosion by solid particles", Proc. Inst. Mech. Engrs., 1969 - 1970, pp. 279 - 289.

Gregory, J. (John), "Particles in water properties and processes", University College London England, 2006, CRC press, Taylor & Francis Group, p. 9-10

H. Drolon, F. Druaux, A. Faure, "Particles shape analysis and classification using the wavelet Transform", Pattern Recognition Letters, Volume 21, Issues 6-7, June 2000, Pages 473-482.

Haider, A., and O. Levenspiel, "Drag coefficient and terminal velocity of spherical and nonspherical particles", Powder Technology Vol. 58, No. 1, 1989, pp. 63 - 70.

Head, W. J., and M. E. Harr, "The development of a model to predict the erosion of materials by natural contaminants", Wear Vol. 15, 1970, pp. 1 - 46.

Hojo, H., K. Tsuda, and T. Yabu, "Erosion damage of polymeric material by slurry", Wear Vol. 112, 1986, pp. 17 - 28.

Honeycombe, R. W. K., "Steels, microstructure and properties, Edward Arnold (Publishers) Ltd." 1981.

IEC, "Hydraulic Machines - Guide for dealing with abrasive erosion in water, 62364", 2008.

I.V. Kragelsky, A.I. Zolotar, A. O. Sheiwekhman, “Theory of material wear by solid particle impact- a review”, Tribology, International Vol. 18, Issue 1, 1985 , pp. 3 - 11

Jin, H., F. Zheng, S. Li, and C. Hang, "The role of sand particles on the rapid destruction of the cavitation zone of hydraulic turbines", Wear Vol. 112, No. 2, 1986, pp. 199 - 205.

J. A. C. Humphrey, “Fundamental of fluid motion in erosion by solid particle impact”, International Journal of heat and fluid flow, vol.11, 1990.

Klujszo, L. A. C., P. K. Songfack, M. Rafaelof, and R.K. Rajamani, "Design of a stationary guide vane swirl air cleaner", Minerals Engineering Vol. 12, No. 11, 1999, pp. 1375 - 1392.

Klujszo, L. A. C., P. K. Songfack, M. Rafaelof, and R.K. Rajamani, "Design of a stationary guide vane swirl air cleaner", Minerals Engineering Vol. 12, No. 11, 1999, pp. 1375 - 1392.

L. Xu, and N. F. Kennon, "A study of the abrasive wear of carbon steels, Wear vol.148, Page 101 - 112." Wear, 1991.

Levy, A. V., N. Jee, and P. Yau, "Erosion of steels in coal solvent slurries", Wear Vol. 117, 1987, pp. 115 - 127.

Levy, A. V., and Y.- F. Man, "Surface degradation of ductile materials in elevated temperature gas particle streams ", Wear Vol. 111, 1986, pp. 173 - 186.

Li, J., T. Deng, M. S. Bingley, and M. S. A. Bradley, "Prediction of particle rotation in a centrifugal accelerator erosion tester and the effect on erosion rate", Wear Vol. 258, No. 1 - 4, 2005, pp. 497 - 502.

Li, S., "Cavitation enhancement of silt erosion-An envisaged micro model", Wear Vol. 260, No. 9 - 10, 2006, pp. 1145 - 1150.

Liu, X. B., L. D. Zhang, Z. Liang, and L. J. Cheng, "Numerical prediction of silt abrasive erosion in hydraulic turbine", Fluids Engineering Division Conference Volume 1, ASME, 1996.

Lysne, D., B. Clover, H. Støle, and E. Tesaker, "Hydraulic Design": Norwegian University of Science and Technology, Department of hydraulic and environmental engineering, 2003.

Mack, R., P. Drtina, and E. Lang, "Numerical prediction of erosion on guide vanes and in labyrinth seals in hydraulic turbines", Wear, 1999, pp. 685 - 691.

Mann, B. S., "Particle erosion--a new concept of flow visualization and boundary layer investigations of rotating machines at high Reynolds numbers", Wear Vol. 223, No. 1 - 2, 1998, pp. 110 - 118.

Mann, B. S., "High-energy particle impact wear resistance of hard coatings and their application in hydro turbines", Wear Vol. 237, No. 1, 2000, pp. 140 - 146.

Mann, B. S., and V. Arya, "Abrasive and erosive wear characteristics of plasma nitriding and HVOF coatings: their application in hydro turbines", Wear Vol. 249, No. 5 - 6, 2001, pp. 354 -360.

Mann, B. S., and V. Arya, "An experimental study to correlate water jet impingement erosion resistance and properties of metallic materials and coatings", Wear Vol. 253, No. 5 - 6, 2002, pp. 650 - 661.

Matsumura M. and Chen B.E., "Erosion resistant materials", In: Duan C. G. and Karelin V.Y. Eds., "Abrasive erosion and corrosion of hydraulic machinery", 2002, pp. 235- 314., Imperial college press, London.

Mazumder, Q. H., S. A. Shirazi, B.S. McLaury, J. R. Shadley, and E. F. Rybicki, "Development and validation of a mechanistic model to predict solid particle erosion in multiphase flow", Wear Vol. 259, No. 1 - 6, 2005, pp. 203 - 207.

Mazur, Z., R. Campos-Amezcua, G. Urquiza-Beltrán, and A. García-Gutiérrez, "Numerical 3D simulation of the erosion due to solid particle impact in the main stop valve of a steam turbine", Applied Thermal Engineering Vol. 24, No. 13, 2004, pp. 1877 - 1891.

Ministry of Water Resources, (MoWR) G. O. N., "Country report presented on 1st international summit on Sustainable use of water for energy", Kyoto, Japan, 2003.

Moore, M. A., "The relationship between the abrasive wear resistance, hardness and microstructure of ferritic materials", Wear Vol. 28 1974, pp. 59 - 68.

Moore, M. A., "Abrasive wear, ASM Material Science Seminar on Fundamentals of Friction and Wear of Materials", Pittsburgh, Pennsylvania, 1981.

Mosonyi, E., "Water power development, Budapest": Akademiai Kiado, 1965.

Naidu, D. B. K. S., "Developing Silt Consciousness in the minds of Hydro Power Engineers", Silting Problems in Hydro Power Plants, New Delhi, India, 1999.

NEA, "Nepal Electricity Authority Annual report", 2009.

Neopane, Hari Prasad, Ole. G. Dahlhaug, and M. Eltvik, "Numerical prediction of particle shape factor effect on sediment erosion in Francis turbine blades", 6th International conference on hydropower, Tromsø Norway, 2010.

Neopane, Hari Prasad, Ole. G. Dahlhaug, and B. Thapa, "Alternative Design of a Francis Turbine for sand-laden water", International Conference on Small Hydropower - Hydro Sri Lanka, (22 - 24 October) Sri Lanka, Kendy, 2007

Neopane, Hari Prasad, Ole. G. Dahlhaug, and B. Thapa, "Experimental examination of the effect of particle size and shape in hydraulic turbines", Waterpower XVI, Spokane, Washington, USA: HCI 2009.

Oka, Y. I., K. Okamura, and T. Yoshida, "Practical estimation of erosion damage caused by solid particle impact: Part 1: Effects of impact parameters on a predictive equation", Wear Vol. 259, No. 1 - 6, 2005, pp. 95 - 101.

Oka, Y. I., and T. Yoshida, "Practical estimation of erosion damage caused by solid particle impact: Part 2: Mechanical properties of materials directly associated with erosion damage", Wear Vol. 259, No. 1 - 6, 2005, pp. 102 - 109.

Ole, G. Dahlhaug., and B. Thapa, "Sand erosion in Francis turbine- a case study from Jhimruk power plant, Nepal", 22nd IAHR Symposium on Hydraulic Machinery and System, Stockholm, Sweden, 2004.

Ole Gunnar Dahlhaug, and P. E. Skåre, "Development of a sediment resistive Francis runner", Hydro 2009: Progress – Potential - Plans, Lyon, France: The international journal on hydropower & dam, 2009.

Padhy, M. K., and R. P. Saini, "A review on silt erosion in hydro turbines", Renewable and Sustainable Energy Reviews Vol. 12, No. 7, 2008, pp. 1974 - 1987.

Padhy, M. K., and R. P. Saini, "Effect of size and concentration of silt particles on erosion of Pelton turbine buckets", Energy Vol. 34, No. 10, 2009, pp. 1477 - 1483.

Rao, P. V., and D. H. Buckley, "Angular particle impingement studies of thermoplast materials at normal incidence", ASLE transactions Vol. 29, 1986, pp. 283 - 296.

Rhodes, M., “Introduction to Particle Technology”: Wiley, 2008.

Richardson, R. C. D., "The Abrasive Wear of Metals and Alloys", Inst. Mech. Engrs. Volume 182, Pt. 3A, Page 410 - 414, 1967, pp. 410 - 414.

Richardson, R. C. D., "Laboratory simulation of abrasive wear such as that imposed by soil," Inst. Mech. Engrs. Volume 182, Pt. 3A, Page 29 - 31, 1967.

Sandip Kumar Suman, and Bim Prasad Shrestha, “Shape feature extraction and pattern recognition of sand particles and their impact”, 2005, Proc. SPIE Vol. 5996

Sargent, G. A., and D. Saigal, "Erosion of Low-Carbon Steel by Coal Particles", ASLE Transactions Vol. 29, 1986, pp. 256 - 266.

Shah, S. M., S. Bahudur, and J. D. Verhoeven, "Erosion behaviour of high silicon bainitic structure II: high silicon steels", Wear Vol. 113, 1986, pp. 279 - 290.

Shah, S. M., J. D. Verhoeven, and S. Bahadur, "Erosion behaviour of high silicon bainitic structures,I: Austempered ductile cast iron", Wear Vol. 113, 1986, pp. 267 - 278.

Sheldon, G. L., and I. Finnie,"On the ductile behaviour of nominally brittle materials during erosive cutting", ASME Vol. 88B, 1966, pp. 387 - 392.

Sheldon, G.L., and A. Kanhere, "An investigation of impingement erosion using single particles", Wear Vol. 21, No. 1, 1972, pp. 195 - 209.

Shida, Y., and H. Fujikawa, "Particle erosion behaviour of boiler tube materials at elevated temperature", Wear Vol. 103, 1985, pp. 281 - 296.

Solero, G., and A. Coghe, "Experimental fluid dynamic characterization of a cyclone chamber", Experimental Thermal and Fluid Science Vol. 27, No. 1, 2002, pp. 87 - 96.

Spurk, J. H., Fluid Mechanics: Springer, 1997.

Stachowiak, G. W., and A. W. Batchelor, "Dimensional analysis modelling Tribological data", International conference, Melbourne, Australia: National conference publication, 1987.

Stachowiak, G. W., and A. W. Batchelor, "Abrasive, Erosive and Cavitation Wear", Engineering Tribology (3-Edition), Burlington: Butterworth-Heinemann, 2006, pp. 501 - 551.

Stachowiak, G. W., and A. W. Batchelor, Engineering Tribology, Elsevier, 1993

Stephension, D. J., J. R. Nicholls, and P. Hancock, "Particle surface interactions during the erosion of a gas turbine material (MarM002) by pyrolytic carbon particles", Wear Vol. 111, 1986, pp. 15 - 29.

Sugiyama, K., S. Nakahama, S. Hattori, and K. Nakano, "Slurry wear and cavitation erosion of thermal- sprayed cermets", Wear Vol. 258, No. 5-6, 2005, pp. 768 - 775.

T. Bovet, “Contribution to study of the phenomenon of abrasive erosion in the realm of hydraulic turbines”, 1958, Bull. Tech., Suisse Romande, Vol. 84, pp. 37-49.

Tabakoff, W., "Study of single stage axial flow compressor performance deterioration", Wear Vol. 119, 1987, pp. 51 - 61.

Tabakoff W. , Hamed A., and, Metwally M., “Effect of particle size distribution on particle dynamics and blade erosion in axial flow turbines”, 1991, ASME, Jr., of Engg. Gas and power, Vol. 113, pp. 607-615.

Tabakoff, W., "High-temperature erosion resistance of coatings for use in turbo machinery", Wear Vol. 186-187, No. Part 1, 1995, pp. 224 - 229.

Tabakoff, W., A. Hamed, and B. Beacher, "Investigation of gas particle flow in an erosion wind tunnel", Wear Vol. 86, No. 1, 1983, pp. 73 - 88.

Thapa, Bhola, "Sand erosion in hydraulic machinery, PhD thesis", Trondheim: Norwegian University of Science and Technology, Faculty of Engineering Science and Technology, Department of energy and process engineering, 2004.

Thapa, Bhola, and Brekke Hermod, "Effect of sand particle size and surface curvature in erosion of hydraulic turbine", IAHR symposium on hydraulic machinery and systems Stockholm, 2004.

Truscott, G. F., "A literature survey on abrasive wear in hydraulic machinery", Wear Vol. 20, No. 1, 1972, pp. 29 - 50.

Tullis, J. P., "Hydraulics of pipelines: pumps, valves, cavitation, transients", New York: Wiley, 1989.

Tsuguo N., "Estimation of repair cycle of turbine due to abrasion caused by suspended sand and determination of desilting basin capacity", 1999, Proc., International seminar on sediment handling technique, NHA, Kathmandu.

Veerapen, J. P., B. J. Lowry, and M. F. Couturier, "Design methodology for the swirl separator", Aquacultural Engineering Vol. 33, No. 1, 2005, pp. 21 - 45.

Versteeg, H. K., and W. Malalasekera, "An Introduction to Computational Fluid Dynamics (The Finite Volume Method)": Longman Scientific and Technical, 1995.

Walley, S. M., and J. E. Field, "The contribution of the Cavendish Laboratory to the understanding of solid particle erosion mechanisms", Wear Vol. 258, No. 1 - 4, 2005, pp. 552 - 566.

W. A. Stauffier, "The abrasion of hydraulic plant by sandy water", 1956, Schweizer Archiv. Angew. Wiss. Technik., 24, pp 3-30. Also shorter version in Metal Prog., January 1956.

Yust, C. S., and R. S. Crouse, "Melting at particle impact sites during erosion of ceramics", Wear Vol. 51, 1975, pp. 193 - 196.

Zhang, Y., E. P. Reuterfors, B. S. McLaury, S. A. Shirazi, and E. F. Rybicki, "Comparison of computed and measured particle velocities and erosion in water and air flows", Wear Vol. 263, No. 1 - 6, 2007, pp. 330 - 338.

Zhao, K., C. Gu, F. Shen, and B. Lou, "Study on mechanism of combined action of abrasion and cavitation erosion on some engineering steels", Wear Vol. 162 - 164, No. Part 2, 1993, pp. 811 - 819.

Zhong, Y., and K. Minemura, "Measurement of erosion due to particle impingement and numerical prediction of wear in pump casing", Wear Vol. 199, No. 1, 1996, pp. 36 - 44.

Appendix A

This appendix presents the auto generated hydraulic turbine report during simulation analysis at best efficiency point. The performance results obtained for the turbine rotor were used to plot the hydraulic performances of a turbine discussed in Chapter 7. This also includes the different blade loading charts, blade geometry plots and contour plots.

Title

Hydraulic Turbine Rotor Report at Best Efficiency Point (BEP)

Author: Hari P. Neopane

Date: 2010/01/13 11:37:10

Contents

1. File Report

Table 1: File Information for SST without particle_001	
Case	SST without particle_001
File Path	C:/Documents and Settings/haripra.old/Desktop/16 final/Without particle/SST without particle Rotating Frame/SST without particle_001.res
File Date	13 January 2010
File Time	09:18:30 AM
File Type	CFX5
File Version	11.0
Fluids	Water
Solids	None
Particles	None

2. Mesh Report

Table 2: Mesh Information for SST without particle_001		
Domain	Nodes	Elements
R1	95988	87320

Table 3: Mesh Statistics for SST without particle_001	
Domain	Maximum Edge Length Ratio
R1	9684.12

3. Physics Report

Table 4: Domain Physics for SST without particle_001				
Name	Location	Type	Materials	Models
R1	Passage 3	Fluid	Water	Turbulence Model = SST Turbulent Wall Functions = Automatic Buoyancy Model = Non Buoyant Domain Motion = Rotating
S1	Passage	Fluid	Water	Turbulence Model = SST Turbulent Wall Functions = Automatic Buoyancy Model = Non Buoyant Domain Motion = Stationary

S2	Passage 2	Fluid	Water	Turbulence Model = SST Turbulent Wall Functions = Automatic Buoyancy Model = Non Buoyant Domain Motion = Stationary

Table 5: Boundary Physics for SST without particle_001

Domain	Name	Location	Type	Settings
R1	R1 to R1 Periodic 1 Side 1	PER1 Passage 3	Interface	Mass And Momentum = Conservative Interface Flux Turbulence = Conservative Interface Flux
R1	R1 to R1 Periodic 1 Side 2	PER2 Passage 3	Interface	Mass And Momentum = Conservative Interface Flux Turbulence = Conservative Interface Flux
R1	R1 to R1 Periodic Side 1	PER1 2 OUTBlock	Interface	Mass And Momentum = Conservative Interface Flux Turbulence = Conservative Interface Flux
R1	R1 to R1 Periodic Side 2	PER2 2 OUTBlock	Interface	Mass And Momentum = Conservative Interface Flux Turbulence = Conservative Interface Flux
R1	R1 to S2 Side 1	INFLOW Passage 3	Interface	Mass And Momentum = Conservative Interface Flux Turbulence = Conservative Interface Flux
R1	R1 Outlet	OUTBlock OUTFLOW	Outlet	Flow Regime = Subsonic Mass And Momentum = Average Static Pressure Relative Pressure = 1 [atm] Pressure Averaging = Average Over Whole Outlet
R1	R1 Blade	BLADE 3	Wall	Wall Influence On Flow = No Slip
R1	R1 Hub	OUTBlock HUB, Passage HUB	Wall	Wall Influence On Flow = No Slip
R1	R1 Shroud	OUTBlock SHROUD, Passage SHROUD	Wall	Wall Influence On Flow = No Slip

S1	S1 Inlet	INFLOW	Inlet	Flow Direction = Cylindrical Components Unit Vector Axial Component = 0 Unit Vector Theta Component = -0.9165 Unit Vector r Component = -0.4 Flow Regime = Subsonic Mass Flow Rate = 540 [kg s^-1] Mass And Momentum = Mass Flow Rate Turbulence = Medium Intensity and Eddy Viscosity Ratio
S1	S1 to S1 Periodic 1 Side 1	PER1 Passage	Interface	Mass And Momentum = Conservative Interface Flux Turbulence = Conservative Interface Flux
S1	S1 to S1 Periodic 1 Side 2	PER2 Passage	Interface	Mass And Momentum = Conservative Interface Flux Turbulence = Conservative Interface Flux
S1	S2 to S1 Side 2	OUTFLOW Passage	Interface	Mass And Momentum = Conservative Interface Flux Turbulence = Conservative Interface Flux
S1	S1 Blade	BLADE	Wall	Wall Influence On Flow = No Slip
S1	S1 Hub	HUB	Wall	Wall Influence On Flow = No Slip
S1	S1 Shroud	SHROUD	Wall	Wall Influence On Flow = No Slip
S2	R1 to S2 Side 2	OUTFLOW Passage 2	Interface	Mass And Momentum = Conservative Interface Flux Turbulence = Conservative Interface Flux
S2	S2 to S1 Side 1	INFLOW Passage 2	Interface	Mass And Momentum = Conservative Interface Flux Turbulence = Conservative Interface Flux

S2	S2 to S2 Periodic 1 Side 1	PER1 Passage 2	Interface	Mass And Momentum = Conservative Interface Flux Turbulence = Conservative Interface Flux
S2	S2 to S2 Periodic 1 Side 2	PER2 Passage 2	Interface	Mass And Momentum = Conservative Interface Flux Turbulence = Conservative Interface Flux
S2	S2 Blade	BLADE 2	Wall	Wall Influence On Flow = No Slip
S2	S2 Hub	HUB 2	Wall	Wall Influence On Flow = No Slip
S2	S2 Shroud	SHROUD 2	Wall	Wall Influence On Flow = No Slip

4. Tabulated Results

The first table below gives a summary of the performance results for the turbine rotor. The second table lists the mass or area averaged solution variables and derived quantities computed at the inlet, leading edge (LE Cut), trailing edge (TE Cut) and outlet locations. The flow angles Alpha and Beta are relative to the meridional plane; a positive angle implies that the tangential velocity is the same direction as the machine rotation.

Table 6: Performance Results		
Rotation Speed	-62.8318	[radian s^-1]
Reference Diameter	0.9850	[m]
Volume Flow Rate	11.0270	[m^3 s^-1]
Head (LE-TE)	214.8660	[m]
Head (IN-OUT)	216.8290	[m]
Flow Coefficient	0.1836	
Head Coefficient (IN-OUT)	0.5551	
Shaft Power	21894500.0000	[W]
Power Coefficient	0.0955	
Total Efficiency (IN-OUT) %	93.6583	

Table 7: Summary Data							
Quantity	Inlet	LE Cut	TE Cut	Outlet	TE/LE	TE-LE	Units
Density	997.0000	997.0000	997.0000	997.0000	1.0000	0.0000	[kg m^-3]
Pstatic	1559540.0000	1353300.0000	208617.0000	203652.0000	0.1542	-1144680.0000	[Pa]
Ptotal	2397140.0000	2395050.0000	294253.0000	277153.0000	0.1229	-2100790.0000	[Pa]
Ptotal (rot)	387806.0000	386660.0000	351069.0000	253295.0000	0.9080	-35591.6000	[Pa]
U	51.2049	46.7384	30.9449	25.5322	0.6621	-15.7934	[m s^-1]
Cm	10.4949	11.5194	12.2979	9.7932	1.0676	0.7784	[m s^-1]
Cu	-39.5827	-43.6257	0.4033	-1.7434	-0.0092	44.0290	[m s^-1]
C	41.0781	45.6422	13.7646	11.2940	0.3016	-31.8777	[m s^-1]
Distortion Parameter	1.0030	1.0444	1.0835	1.1949	1.0375	0.0391	
Flow Angle: Alpha	75.1921	52.6567	-12.1631	11.4885	-0.2310	-64.8197	[degree]
Wu	11.6222	3.1143	31.3542	23.7888	10.0679	28.2399	[m s^-1]
W	15.7712	13.1874	33.7696	26.1468	2.5608	20.5822	[m s^-1]
Flow Angle: Beta	-48.9092	-33.7478	-69.5526	-66.8545	2.0610	-35.8048	[degree]

5. Blade Loading Charts

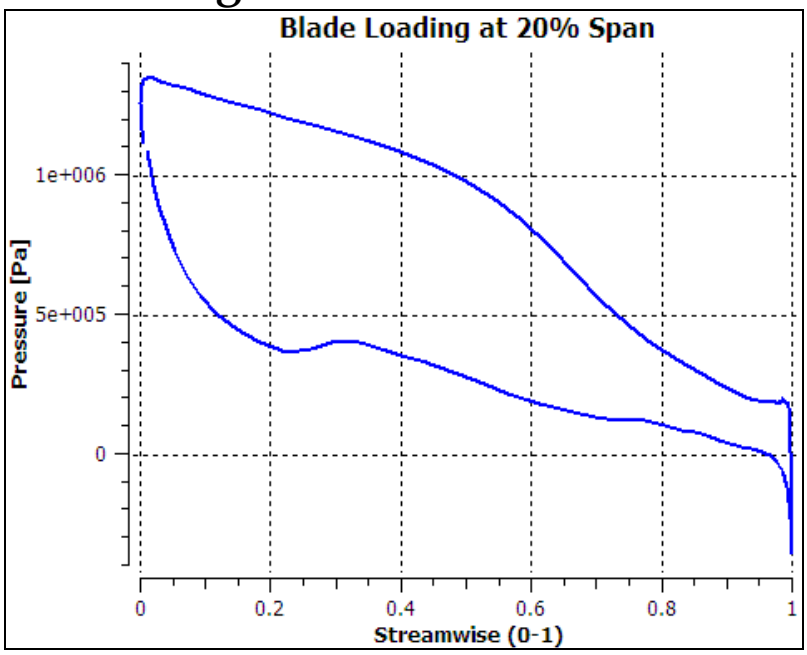

Chart 1: Blade Loading at 20% Span

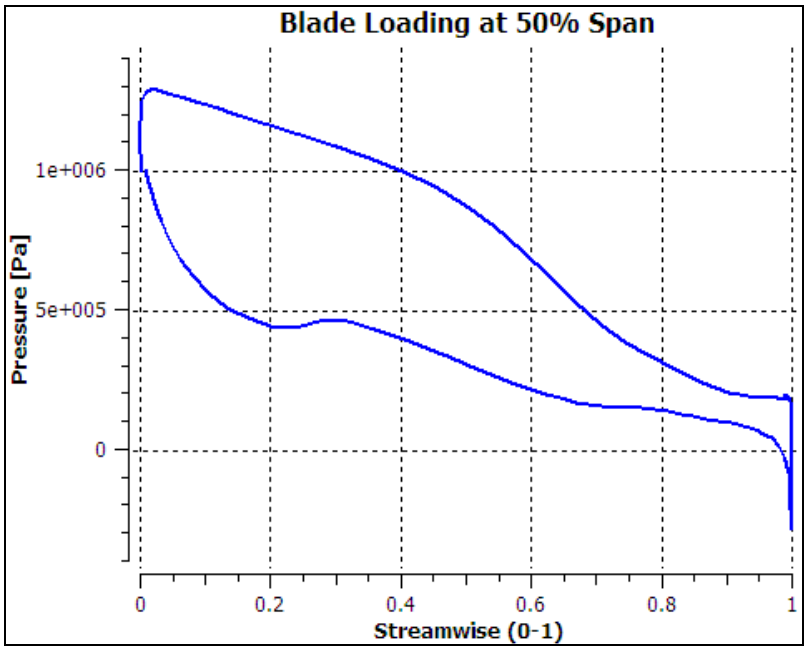

Chart 2: Blade Loading at 50% Span

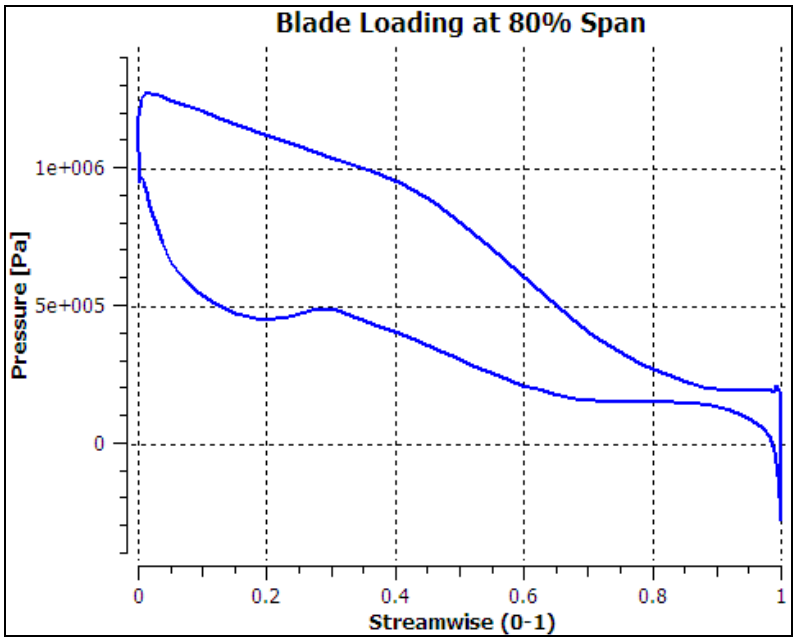

Chart 3: Blade Loading at 80% Span

6. Streamwise Charts

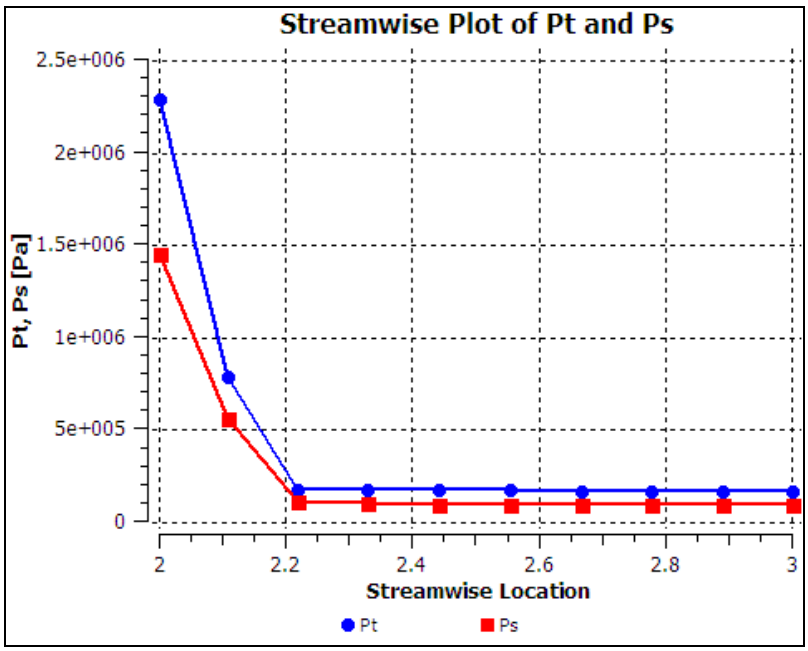

Chart 4: Streamwise Plot of Pt and Ps

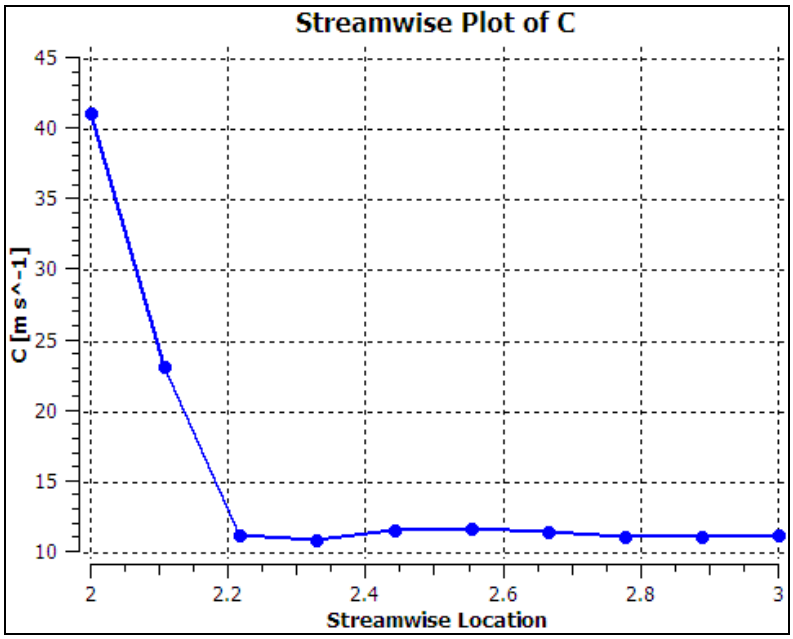

Chart 5: Streamwise Plot of C

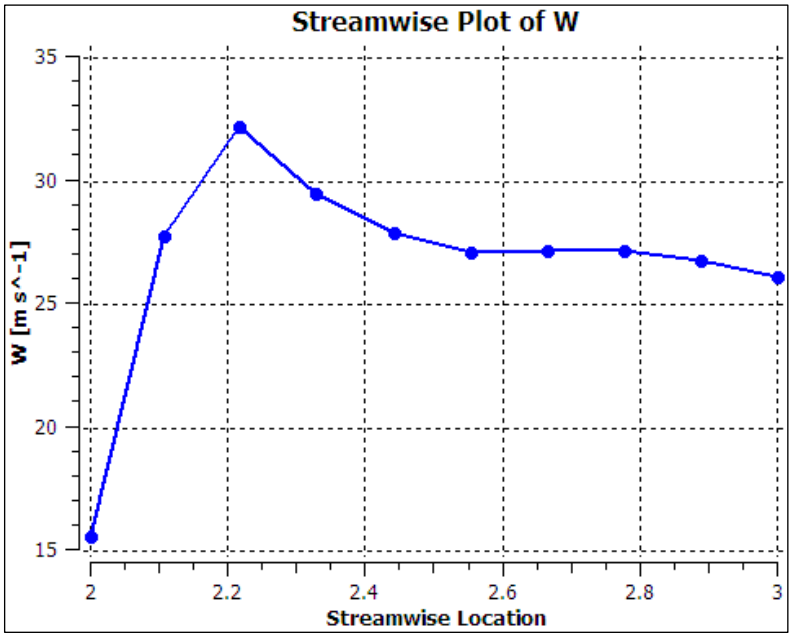

Chart 6: Streamwise Plot of W

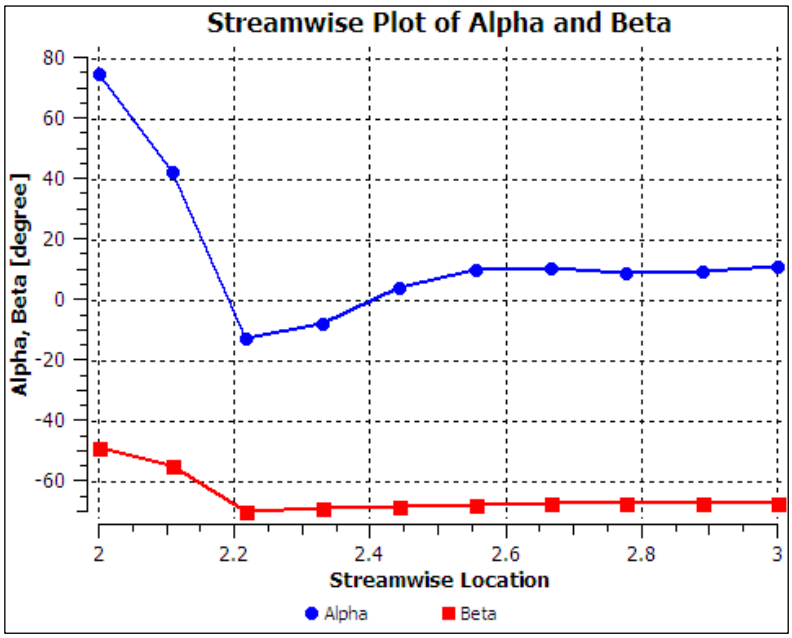

Chart 7: Streamwise Plot of Alpha and Beta

7. Spanwise Charts

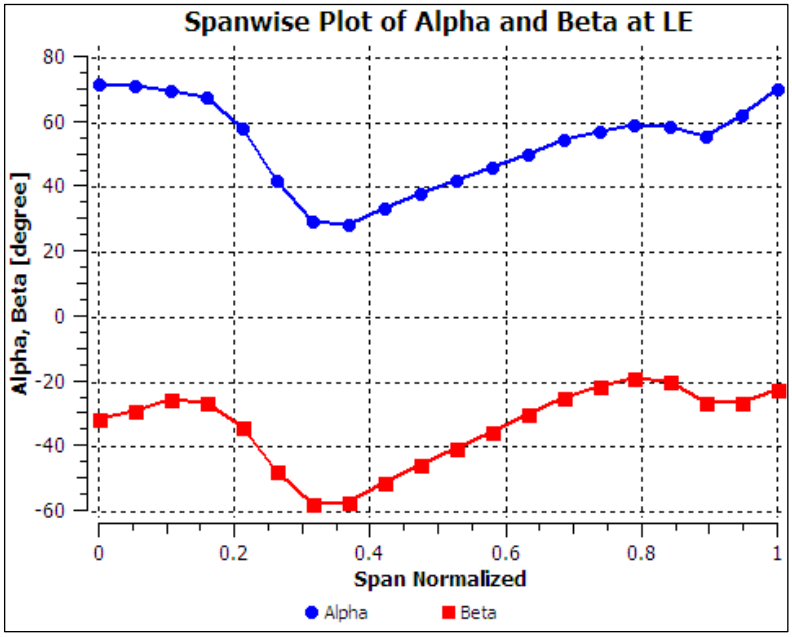

Chart 8: Spanwise Plot of Alpha and Beta at LE

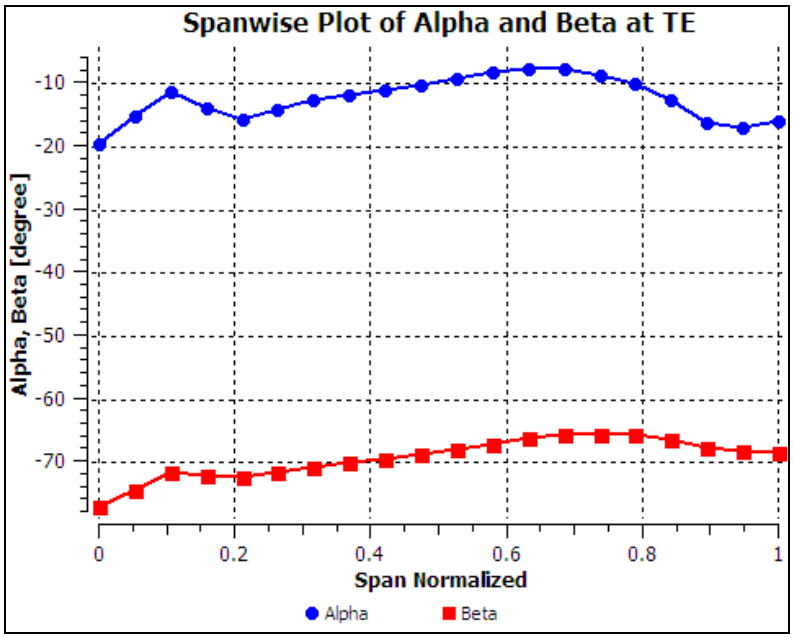

Chart 9: Spanwise Plot of Alpha and Beta at TE

8. Blade Geometry Plots

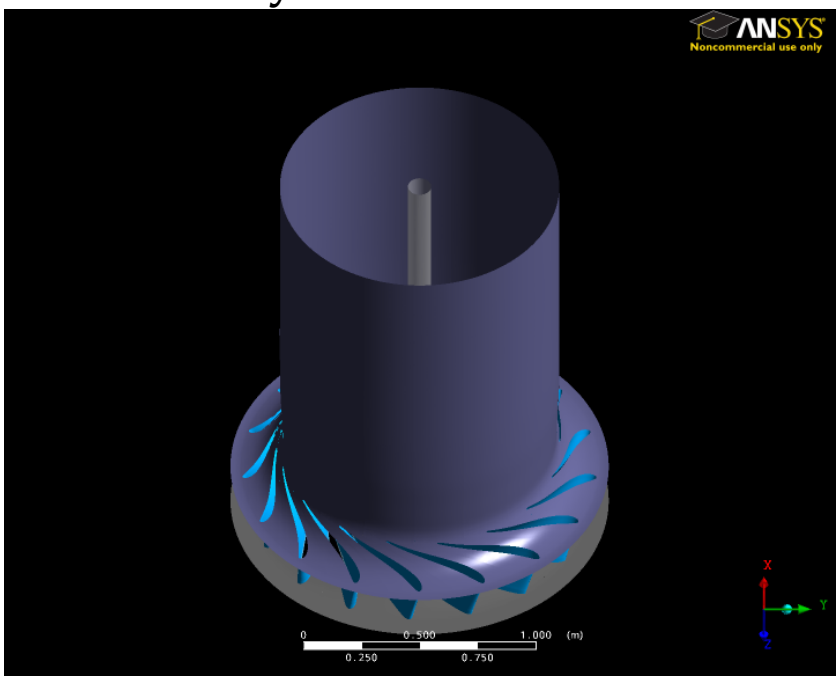

Figure 1: Isometric 3D View of the Blade, Hub and Shroud

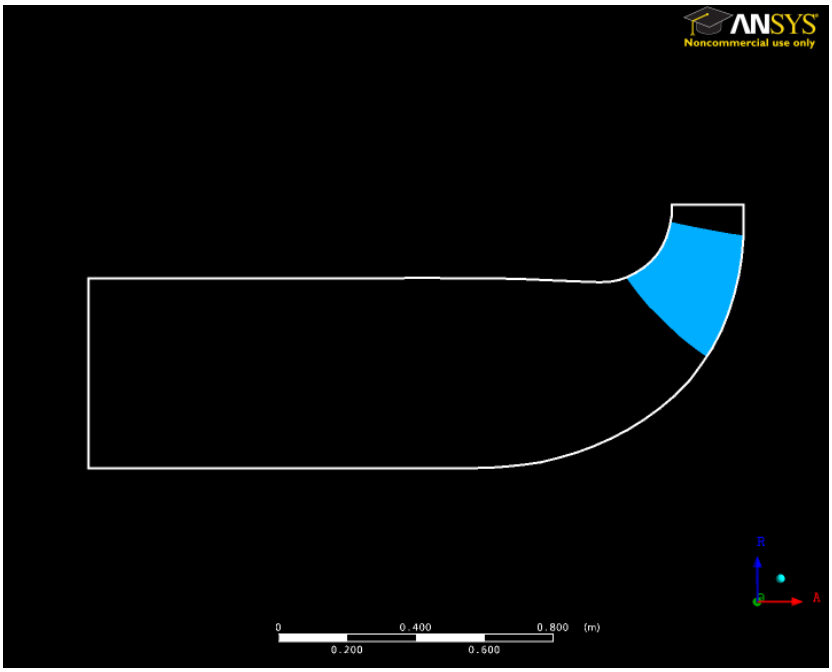

Figure 2: Meridional View of the Blade, Hub and Shroud

9. Blade Mesh Plot

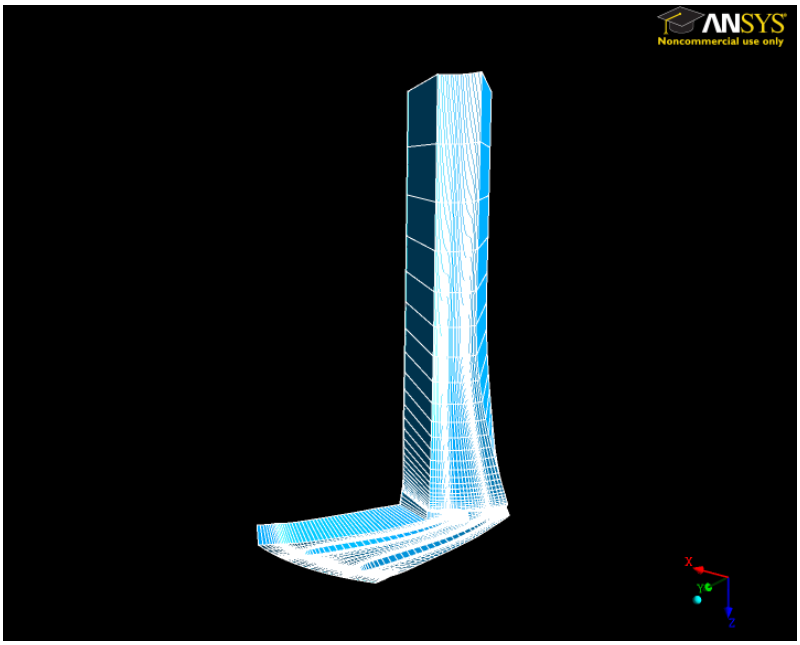

Figure 3: Mesh Elements at 50% Span

10. Blade to Blade Plots

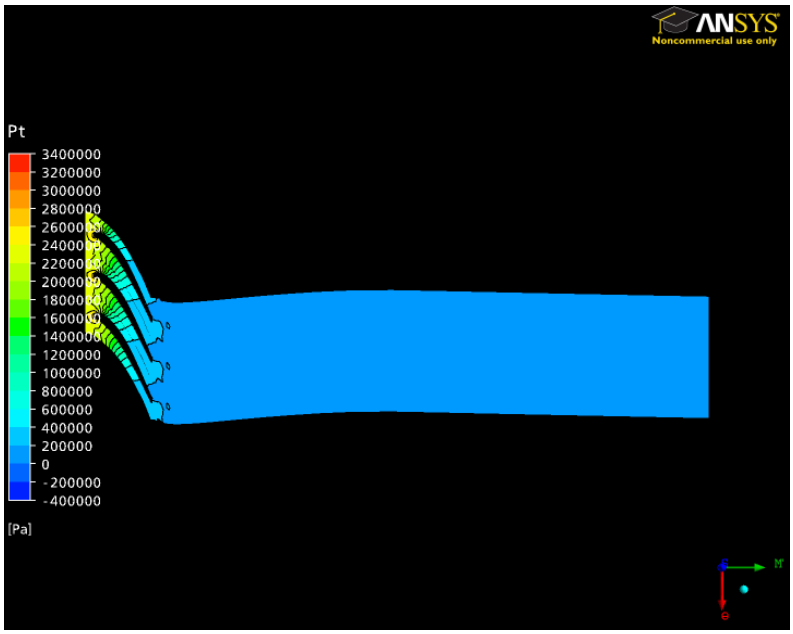

Figure 4: Contour of Pt at 50% Span

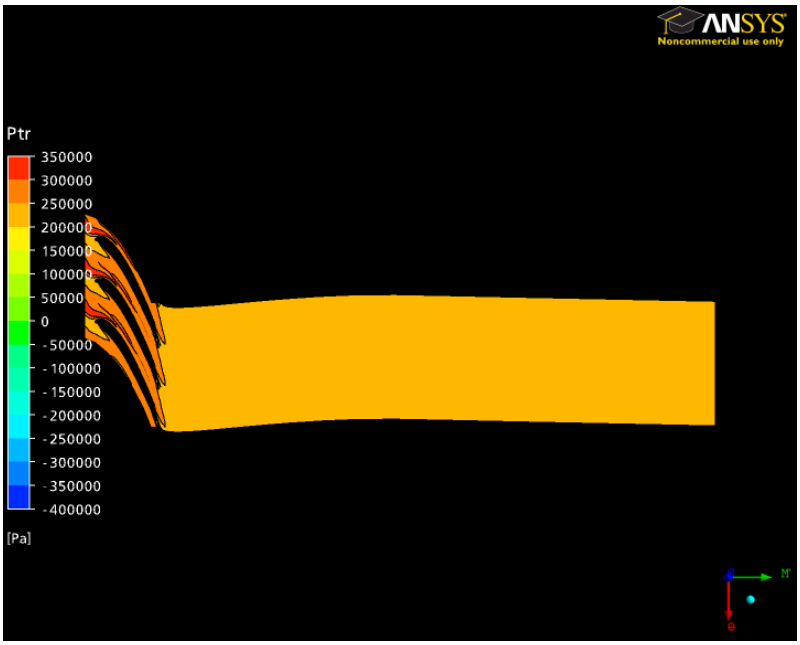

Figure 5: Contour of Ptr at 50% Span

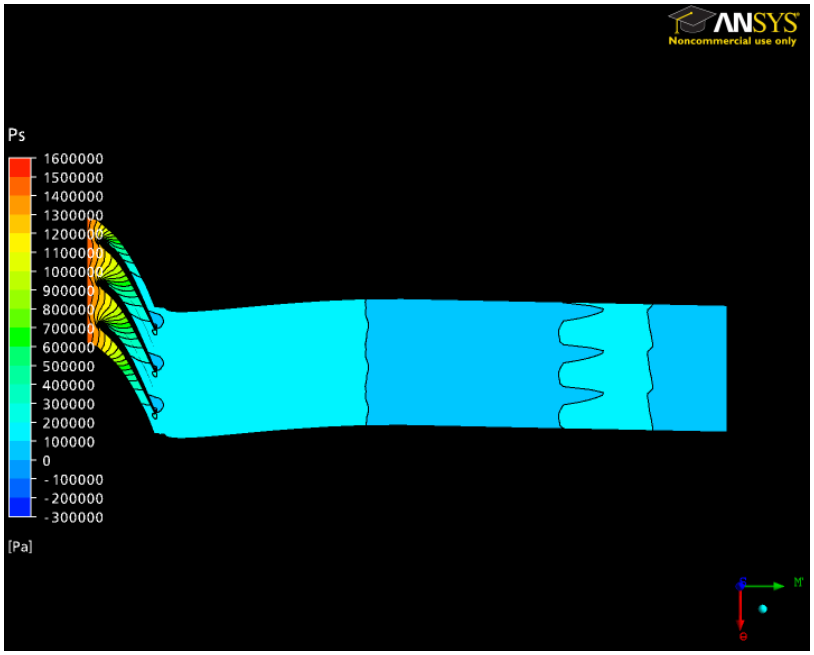

Figure 6: Contour of Ps at 50% Span

Figure 7: Contour of W at 50% Span

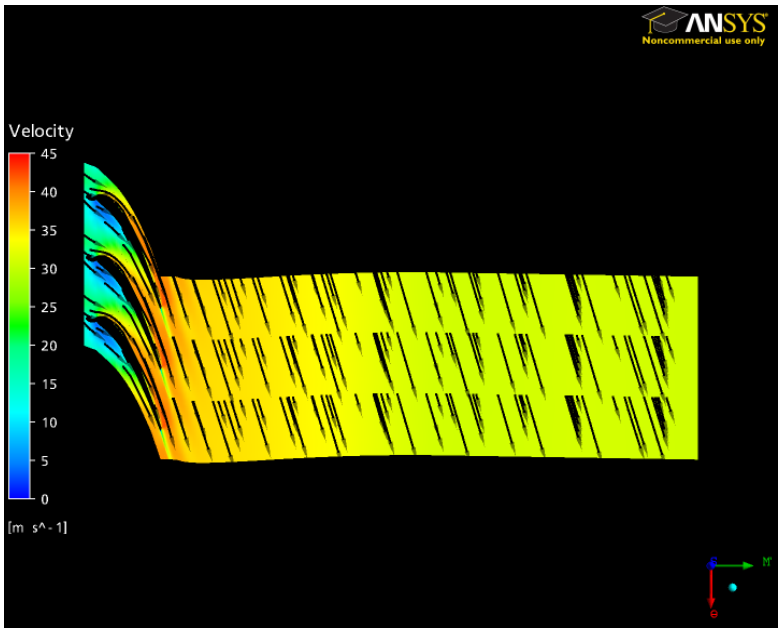

Figure 8: Velocity Vectors at 20% Span

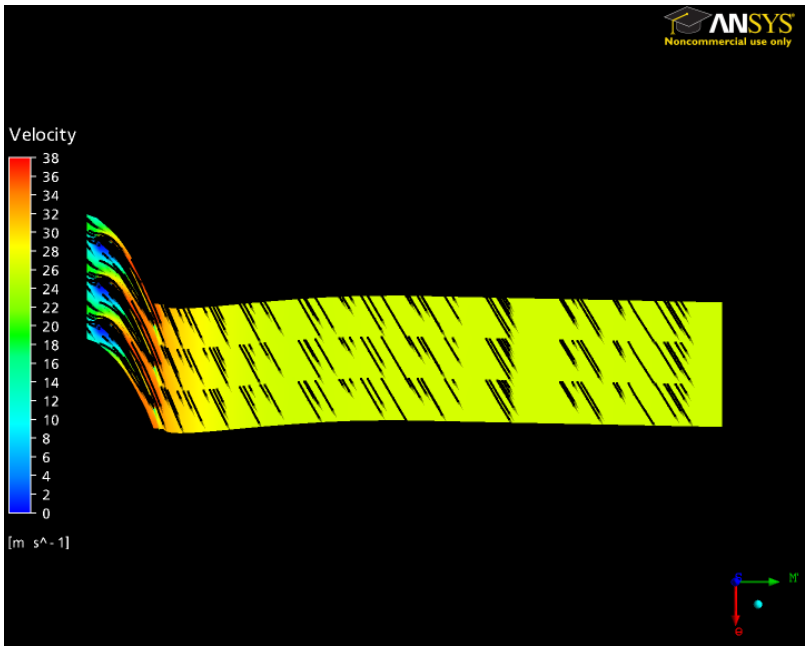

Figure 9: Velocity Vectors at 50% Span

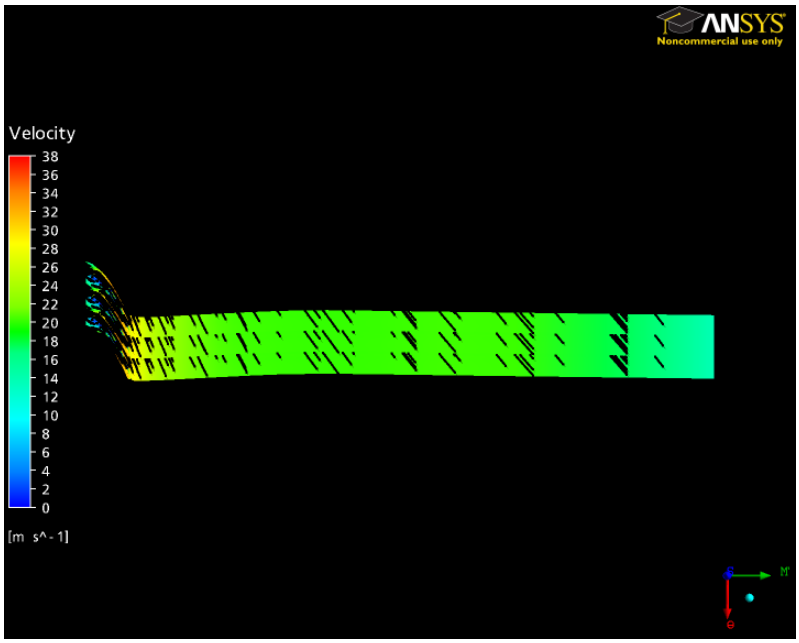

Figure 10: Velocity Vectors at 80% Span

11. Meridional Plots

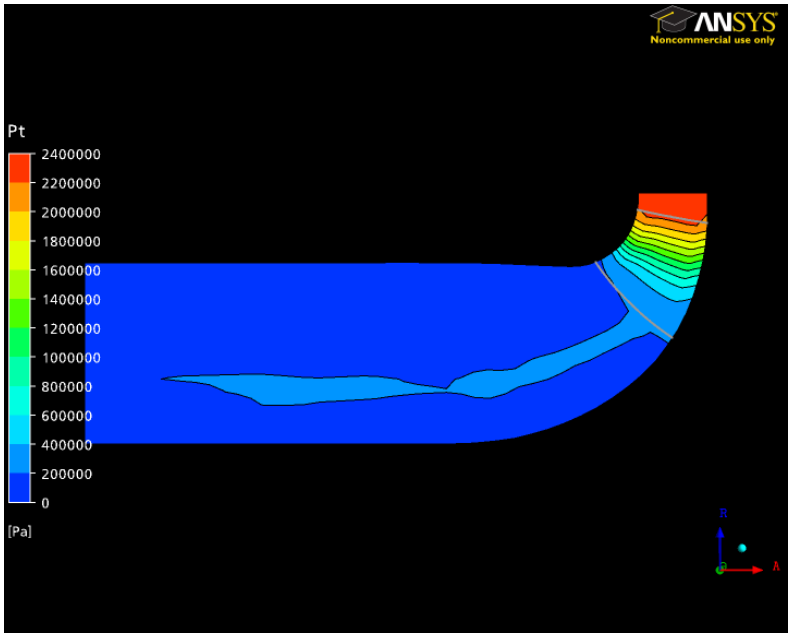

Figure 11: Contour of Mass Averaged Pt on Meridional Surface

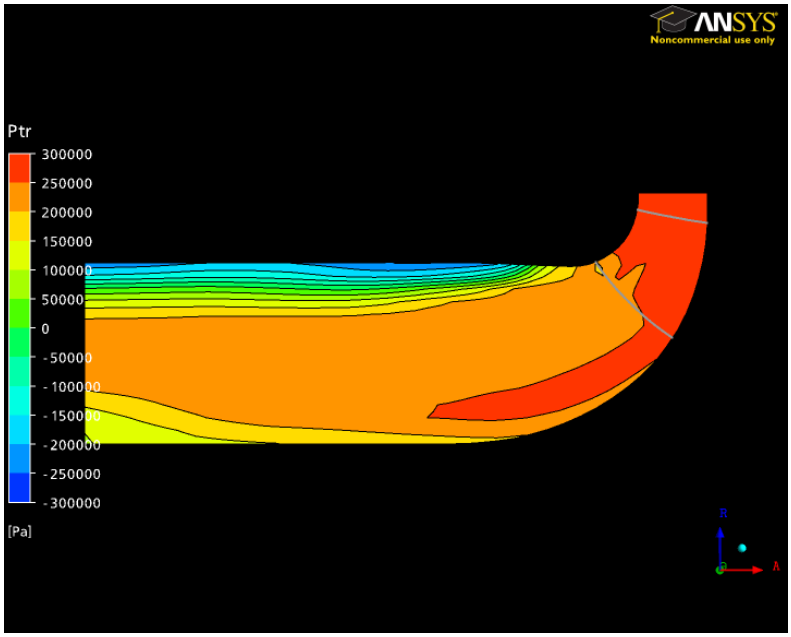

Figure 12: Contour of Mass Averaged Ptr on Meridional Surface

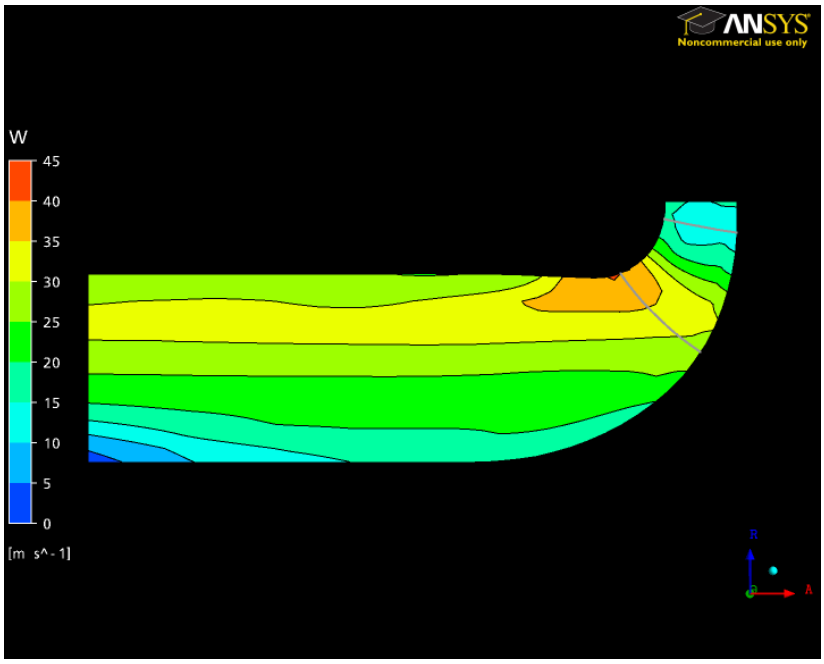

Figure 13: Contour of Mass Averaged W on Meridional Surface

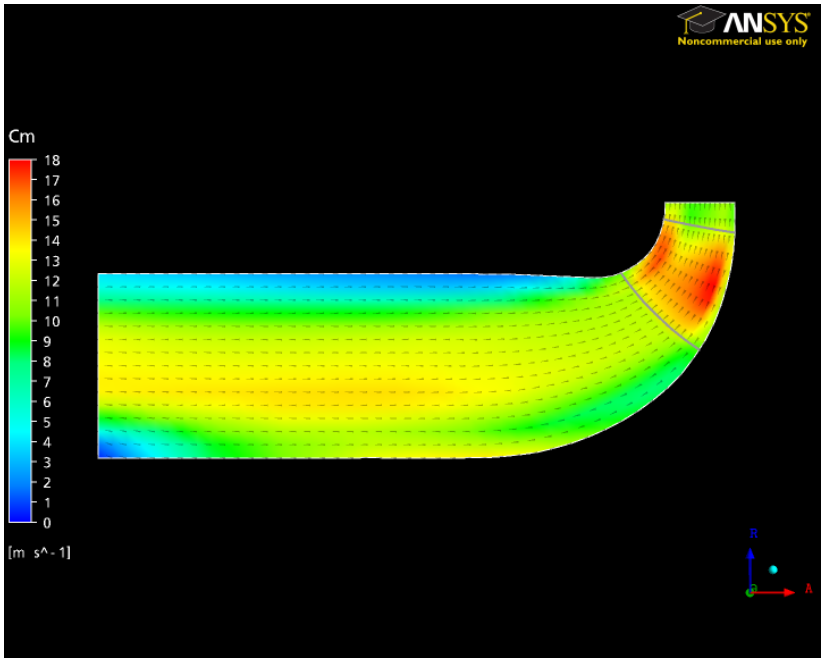

Figure 14: Vector of Area Averaged Cm on Meridional Surface

12. Circumferential Plots

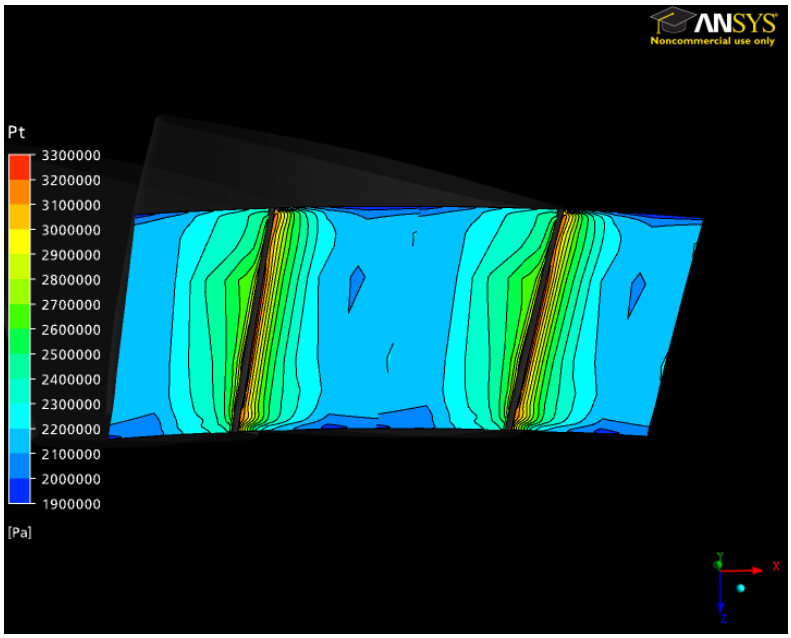

Figure 15: Contour of Pt at Blade LE

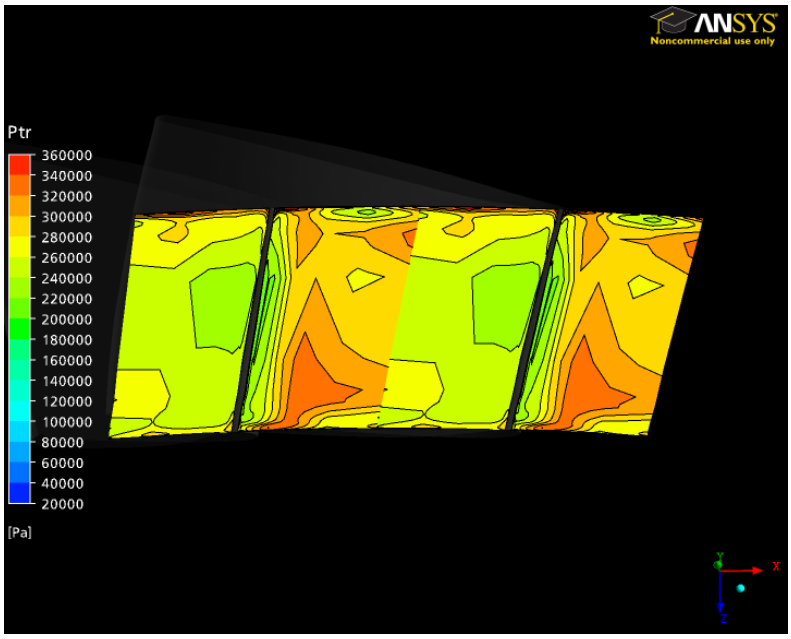

Figure 16: Contour of Ptr at Blade LE

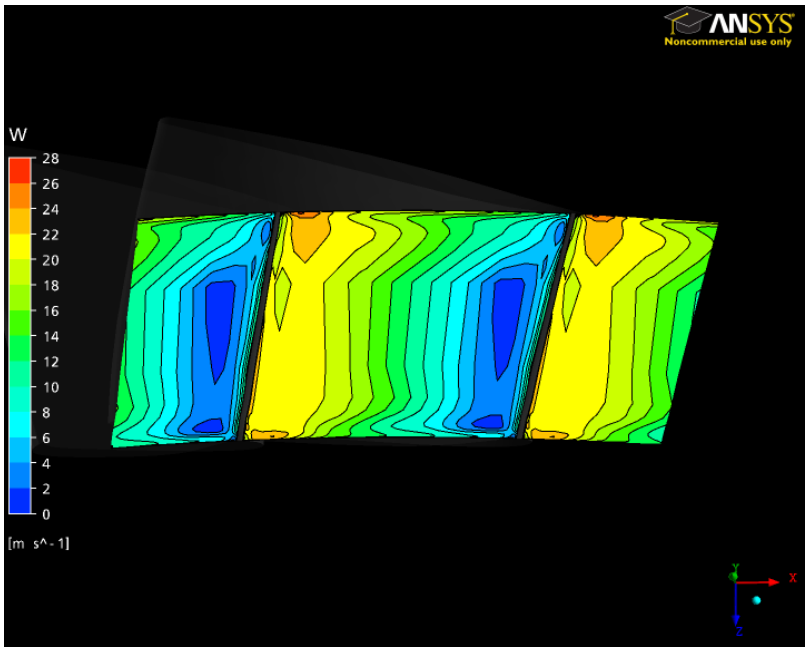

Figure 17: Contour of W at Blade LE

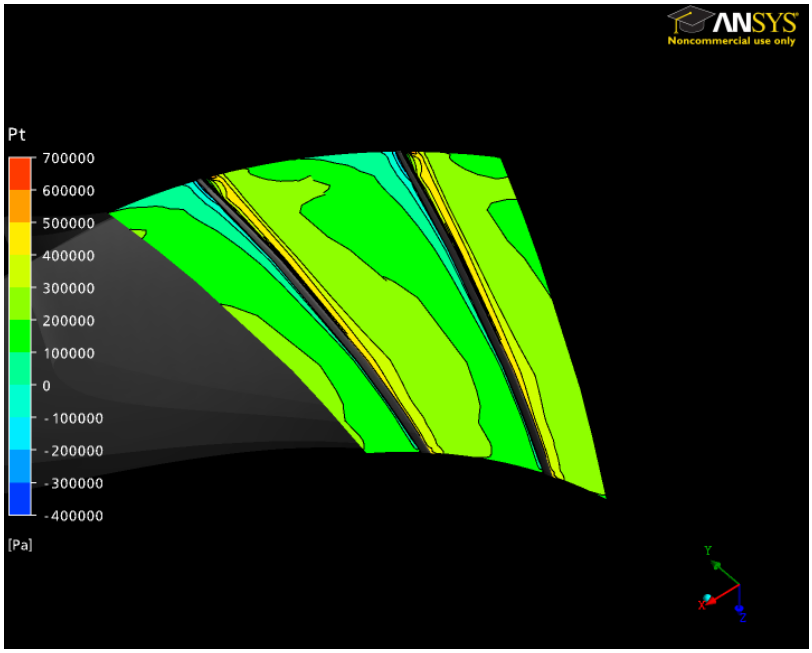

Figure 18: Contour of Pt at Blade TE

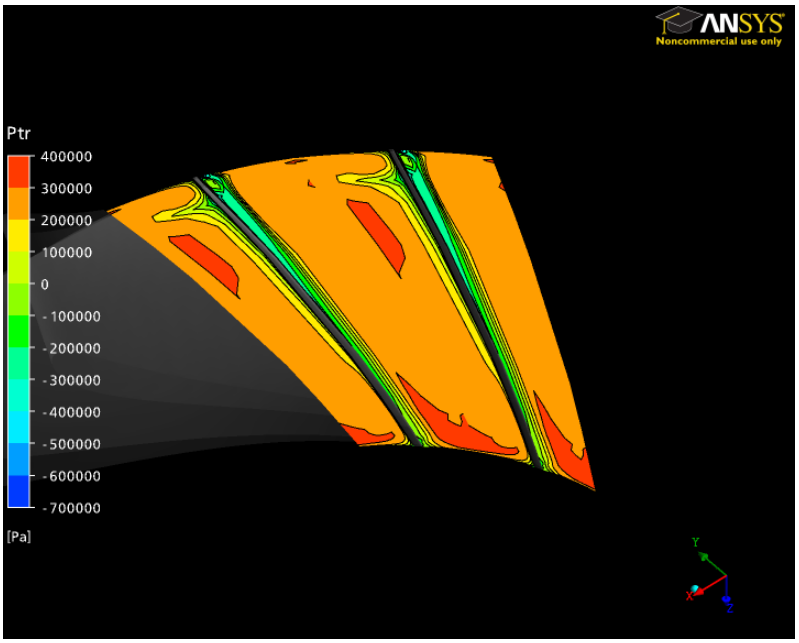

Figure 19: Contour of Ptr at Blade TE

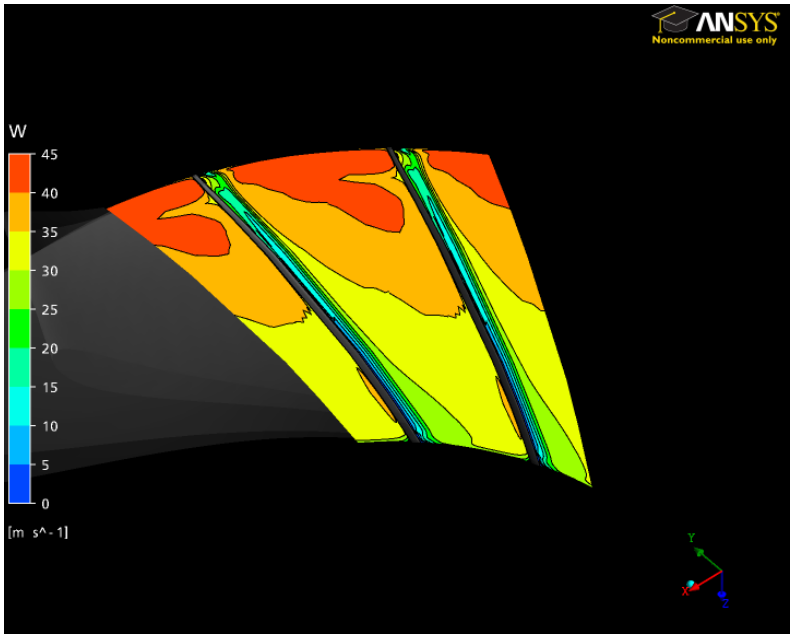

Figure 20: Contour of W at Blade TE

13. Streamline Plot

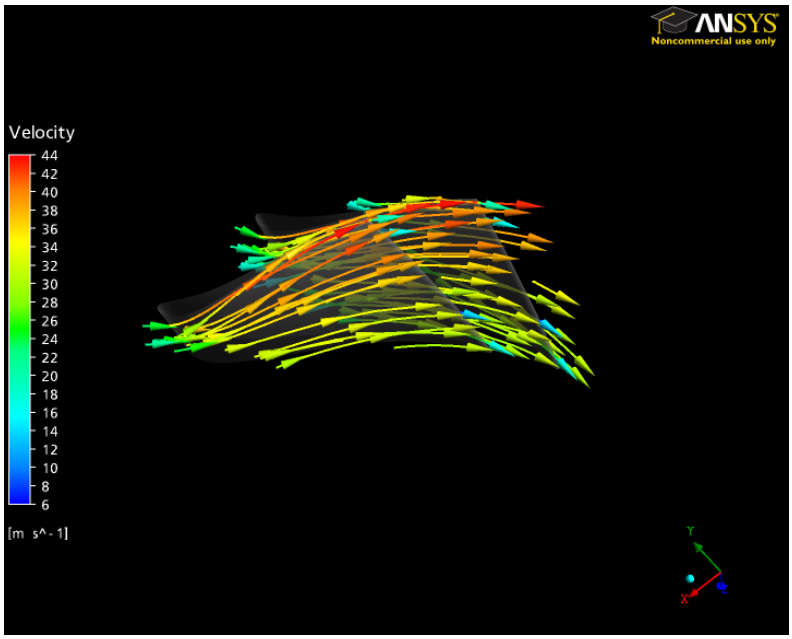

Figure 21: Velocity Streamlines at Blade TE

Chart 10

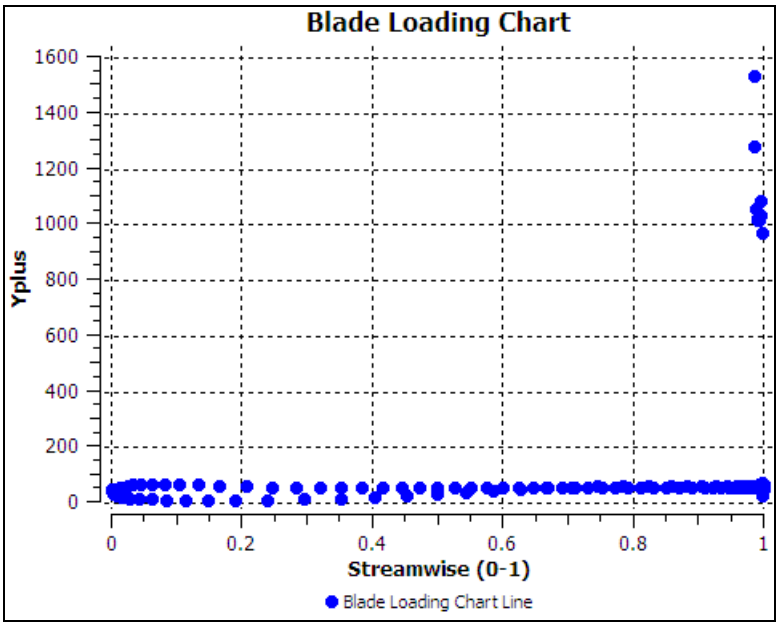

Appendix B

This appendix presents the part of auto generated hydraulic turbine rotor report during simulation analysis at full load operating condition. The performance results obtained for the turbine rotor were used to plot the hydraulic performances of a turbine discussed in Chapter 7.

Title: Hydraulic Turbine Rotor Report at Full Load

Author: Hari P. Neopane

Date: 2010/01/13 11:51:47

Contents

1. File Report

Table 1: File Information for 685 SST without particle after corecting_001	
Case	685 SST without particle after corecting_001
File Path	C:/Documents and Settings/haripra.old/Desktop/22 final/685 SST without particle after correcting/685 SST without particle after corecting_001.res
File Date	13 January 2010
File Time	11:40:03 AM
File Type	CFX5
File Version	11.0
Fluids	Water
Solids	None
Particles	None

2. Mesh Report

Table 2: Mesh Information for 685 SST without particle after corecting_001		
Domain	Nodes	Elements
R1	131425	119952

Table 3: Mesh Statistics for 685 SST without particle after corecting_001	
Domain	Maximum Edge Length Ratio
R1	1703.81

3. Physics Report

Table 4: Domain Physics for 685 SST without particle after corecting_001				
Name	Location	Type	Materials	Models
R1	Passage 3	Fluid	Water	Turbulence Model = SST Turbulent Wall Functions = Automatic Buoyancy Model = Non Buoyant Domain Motion = Rotating
S1	Passage	Fluid	Water	Turbulence Model = SST Turbulent Wall Functions = Automatic Buoyancy Model = Non Buoyant Domain Motion = Stationary
S2	Passage 2	Fluid	Water	Turbulence Model = SST Turbulent Wall Functions = Automatic Buoyancy Model = Non Buoyant Domain Motion = Stationary

Table 5: Boundary Physics for 685 SST without particle after corecting_001				
Domain	Name	Location	Type	Settings
R1	R1 to R1 Periodic 1 Side 1	PER1 Passage 3	Interface	Mass And Momentum = Conservative Interface Flux Turbulence = Conservative Interface Flux
R1	R1 to R1 Periodic 1 Side 2	PER2 Passage 3	Interface	Mass And Momentum = Conservative Interface Flux Turbulence = Conservative Interface Flux
R1	R1 to R1 Periodic Side 1	PER1 2 OUTBlock	Interface	Mass And Momentum = Conservative Interface Flux Turbulence = Conservative Interface Flux
R1	R1 to R1 Periodic Side 2	PER2 2 OUTBlock	Interface	Mass And Momentum = Conservative Interface Flux Turbulence = Conservative Interface Flux
R1	R1 to S2 Side 1	INFLOW Passage 3	Interface	Mass And Momentum = Conservative Interface Flux Turbulence = Conservative

				Interface Flux
R1	R1 Outlet	OUTBlock OUTFLOW	Outlet	Flow Regime = Subsonic Mass And Momentum = Average Static Pressure Relative Pressure = 1 [atm] Pressure Averaging = Average Over Whole Outlet
R1	R1 Blade	BLADE 3	Wall	Wall Influence On Flow = No Slip
R1	R1 Hub	OUTBlock HUB, Passage HUB	Wall	Wall Influence On Flow = No Slip
R1	R1 Shroud	OUTBlock SHROUD, Passage SHROUD	Wall	Wall Influence On Flow = No Slip
S1	S1 Inlet	INFLOW	Inlet	Flow Direction = Cylindrical Components Unit Vector Axial Component = 0 Unit Vector Theta Component = -0.9165 Unit Vector r Component = -0.4 Flow Regime = Subsonic Mass Flow Rate = 685 [kg s^-1] Mass And Momentum = Mass Flow Rate Turbulence = Medium Intensity and Eddy Viscosity Ratio
S1	S1 to S1 Periodic 1 Side 1	PER1 Passage	Interface	Mass And Momentum = Conservative Interface Flux Turbulence = Conservative Interface Flux
S1	S1 to S1 Periodic 1 Side 2	PER2 Passage	Interface	Mass And Momentum = Conservative Interface Flux Turbulence = Conservative Interface Flux
S1	S2 to S1 Side 2	OUTFLOW Passage	Interface	Mass And Momentum = Conservative Interface Flux Turbulence = Conservative Interface Flux

S1	S1 Blade	BLADE	Wall	Wall Influence On Flow = No Slip
S1	S1 Hub	HUB	Wall	Wall Influence On Flow = No Slip
S1	S1 Shroud	SHROUD	Wall	Wall Influence On Flow = No Slip
S2	R1 to S2 Side 2	OUTFLOW Passage 2	Interface	Mass And Momentum = Conservative Interface Flux Turbulence = Conservative Interface Flux
S2	S2 to S1 Side 1	INFLOW Passage 2	Interface	Mass And Momentum = Conservative Interface Flux Turbulence = Conservative Interface Flux
S2	S2 to S2 Periodic 1 Side 1	PER1 Passage 2	Interface	Mass And Momentum = Conservative Interface Flux Turbulence = Conservative Interface Flux
S2	S2 to S2 Periodic 1 Side 2	PER2 Passage 2	Interface	Mass And Momentum = Conservative Interface Flux Turbulence = Conservative Interface Flux
S2	S2 Blade	BLADE 2	Wall	Wall Influence On Flow = No Slip
S2	S2 Hub	HUB 2	Wall	Wall Influence On Flow = No Slip
S2	S2 Shroud	SHROUD 2	Wall	Wall Influence On Flow = No Slip

4. Tabulated Results

The first table below gives a summary of the performance results for the turbine rotor. The second table lists the mass or area averaged solution variables and derived quantities computed at the inlet, leading edge (LE Cut), trailing edge (TE Cut) and outlet locations. The flow angles Alpha and Beta are relative to the meridional plane; a positive angle implies that the tangential velocity is the same direction as the machine rotation.

Table 6: Performance Results		
Rotation Speed	-62.8318	[radian s^-1]
Reference Diameter	0.9835	[m]
Volume Flow Rate	13.9743	[m^3 s^-1]
Head (LE-TE)	205.9170	[m]
Head (IN-OUT)	216.2730	[m]
Flow Coefficient	0.2338	
Head Coefficient (IN-OUT)	0.5554	
Shaft Power	25261500.0000	[W]
Power Coefficient	0.1110	
Total Efficiency (IN-OUT) %	85.4894	

Table 7: Summary Data							
Quantity	Inlet	LE Cut	TE Cut	Outlet	TE/LE	TE-LE	Units
Density	997.0000	997.0000	997.0000	997.0000	1.0000	0.0000	[kg m^-3]
Pstatic	1872070.0000	1758220.0000	277735.0000	198927.0000	0.1580	-1480490.0000	[Pa]
Ptotal	2490610.0000	2485050.0000	471754.0000	376068.0000	0.1898	-2013290.0000	[Pa]
Ptotal (rot)	877233.0000	872237.0000	821108.0000	550511.0000	0.9414	-51128.8000	[Pa]
U	51.2055	46.7381	30.8987	25.3838	0.6611	-15.8394	[m s^-1]
Cm	13.2556	14.3394	15.5960	12.5494	1.0876	1.2566	[m s^-1]
Cu	-32.2993	-34.6462	9.6645	7.5696	-0.2789	44.3107	[m s^-1]
C	35.2618	37.7048	19.7635	16.2150	0.5242	-17.9412	[m s^-1]
Distortion	1.0042	1.0434	1.0745	1.2007	1.0297	0.0310	

Parameter							
Flow Angle: Alpha	65.0771	66.6155	-39.2267	-30.0992	-0.5889	-105.8420	[degree]
Wu	18.9062	12.0921	40.5654	32.9534	3.3547	28.4733	[m s^-1]
W	23.2236	19.2514	43.5515	35.3219	2.2622	24.3000	[m s^-1]
Flow Angle: Beta	-56.2440	-39.9337	-70.7207	-70.9315	1.7710	-30.7870	[degree]

Appendix C

ALTERNATIVE DESIGN OF A FRANCIS TURBINE FOR SAND LADEN WATER

Hari Prasad Neopane[1], Ole Gunnar Dahlhaug[2], and Bhola Thapa[3]

This paper is presented at the Hydro Sri Lanka 07, International Conference on small Hydropower, held in Kandy, Sri Lanka, 22 - 24 October 2007. The paper has also published in the proceedings for this symposium.

ABSTRACT

The main objective of this paper is to propose an alternative design of a Francis turbine for minimizing the sand erosion effect in sand laden river. To achieve this objective, one erosion model for hydraulic machinery has been selected and all technical and managerial aspects have been considered in this study. Hydraulic turbine components operating in sand-laden water subjected to erosive wear. Erosion reduces efficiency and life of turbine. It also causes problem in operation & maintenance. Himalayan rivers carry large amount of hard abrasive particles. Withdrawal of the clean water from the river for power production is expensive due to design, construction and operation of sediment settling basins. Even with the settling basins, 100 % removal of fine sediments is impossible and uneconomical. The design of the Francis turbine can be done in two main stages. The first step is the initial design, based on empirical data and the Euler's turbine equation. The second step is a three dimensional CFD analysis for fine tuning of the design, normally based on the assumption of uniform flow field from the guide vanes cascade towards the runner blade inlets. The hydraulic design strategy for the Francis turbine has played the major role in the design. The main objectives in the design of the medium head Francis turbines are to reduce the pressure pulsation, avoid cavitations, to reduce sand erosion and to gain maximum efficiency. The ideal goal is to design a runner that has the widest possible operating range for head variations beyond the normal design head, and that would require the minimal maintenance. The initial step is the most important. The basic hydraulic design of the runner is done during this stage, and the balancing of the pressure distribution on the blades by controlled parameters gives the designer an important feeling, which assists in evaluating the result of the CFD analysis. This feeling is very useful in helping to make the right changes in the geometry and to improve the performance of the runner. The CFD analysis is also important in the study of the model turbine behaviour and forms the basis for final tuning of the prototype Francis runners.

1 CONVENTIONAL DESIGN OF FRANCIS TURBINE

1.1 THE IMPORTANCE OF THE RUNNER

The hydraulic energy of the water is converted into mechanical shaft energy in the turbine runner at the expense of the interaction between flow and the runner blades constituting a rotating cascade of profiles. Runner is one of the most important components of the turbines. Francis turbine is a reaction type of turbine where the specific energy in front of the runner consists of partly pressure energy and partly kinetic energy. For the high head type of the Francis turbine approximately 50 % of the energy is converted into kinetic energy in front of the runner and there is a pressure drop through the runner of approximately 50 % of the total energy drop through the turbine. So, the design of the runner is very important.

1.2 INPUT PARAMETER

The main input parameter of the design is the net head (H_e), which is calculated from the available head after deducting the friction losses on the penstock, flow at the full load (Q) and available submersion. The available submersion is the distance between the centerline of the turbine and the tailrace. For the purpose of this research work, the input parameters have been selected based upon the 12 MW Jhimruk Hydro Power Plant, [Flow at the full load (Q) = 7.05 m^3/s, net head (H_n) = 201.5 m, and available submersion = 0 m], which is located in western part of Nepal.

1.3 CALCULATIONS OF THE DIMENSIONS OF THE RUNNER

The development of hydraulic turbines is aimed towards two goals: to achieve the maximum efficiency and to avoid cavitation damage with the highest possible circumferential speed and meridional velocity in the runner for the given submergence of the turbine.

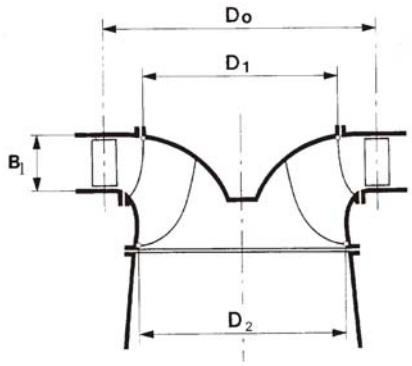

Figure 1.1 Main dimension of the runner

For high head runners the cavitation problems are most likely to occur at the outlet section of the blades. In order to study the cavitation a careful study of the blade loading must be done. For such study, the curvature of shroud and crown as well as curvature of the blades, the blade angles and the blade leaning are the important parameters. The empirical relation for the outlet angle and peripheral velocity is given by [8]:

$13^0 < \beta_2 < 22^0$ lowest values for the highest head
$35 < U_2 < 43$ highest values for the highest head

For maximum efficiency, maximum peripheral speed at the outlet of the runner, U_2 = 40 m/s at the ring for moderate setting assumed. In some case, the noise and vibrations problems are likely to increase with the speed. To avoid the noise and vibrations problem, higher values of peripheral velocity couldn't be used. U_2 >43 m/s is not recommended. If the higher values of U_2 is chosen the blade outlet angle should be reduced. Assume, β_2 = 17 ^{0}. The lower values of β_2 is also not recommended due to welding constraints. From the maximum efficiency point of view, no swirl at the outlet i.e. C_{2u}= 0 m/s has been selected. The meridional velocity at the outlet of the runner at best efficiency with no rotation in draft tube will get a normal value in this case. (See the outlet velocity vector diagram). Then the following meridional velocity will be obtained:

$$C_{m2} = U_2 \cdot \tan\beta_2 \quad = \quad 12.2 \text{ m/s} \qquad (1.1)$$

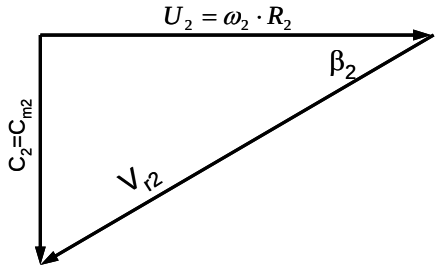

Figure 1.2 Outlet velocity diagram

The ratio between the full load flow and the best efficiency flow

$$\kappa = \frac{Q}{Q^*} = 1.1 \; - \; 1.3 \qquad [\text{ - }] \qquad (1.2)$$

We choose $\kappa = 1.2$

So, $Q^* = \frac{Q}{1.2}$ = 5.875 m^3/s, (* denotes the best efficiency point)

The outlet diameter may now be found by assuming C_{m2} to be constant across the outlet area across the runner outlet diameter:

$$D_2 = \sqrt{\frac{4 \cdot Q^*}{(\pi \cdot C_{m2})}} = 0.808\ m \tag{1.3}$$

The speed of the turbine will then be according to the chosen values of U_2 and β_2

$$n = \frac{60 \cdot U_2}{\pi \cdot D_2} = \frac{60 \cdot 40}{\pi \cdot 0.808} = 946 \text{ rpm} \tag{1.4}$$

This will not normally be a synchronous speed and an adjustment of the speed has to be made by adjusting the circumferential speed U_2 and the diameter. We want to keep the velocity triangle the same at the outlet therefore the outlet blade angle β_2 is constant.

In order not to increase the necessary submergence of the turbine, the speed should be reduced to nearest synchronous speed.

The synchronous speed is found by checking the formula

$$n = \frac{3000}{Z} \qquad \text{[rpm]} \tag{1.5}$$

Where Z = number of the pairs of the poles in the generator for an electric grid with a frequency of 50 Hz.

If Z= 3, then $n = 1000\ rpm$ and ω = 104.71 rad/s
If Z = 4, then $n = 750\ rpm$ and ω = 78.53 rad/s

Using an empirical equation for calculation of the Net Positive Suction Head [4],

$$NPSH = \frac{\left(a \cdot C_{2m}{}^2 + b \cdot U_2{}^2 \right)}{2 \cdot g} \qquad \text{[m]} \tag{1.6}$$

Where a and b are constant and depends upon the speed number (Ω)

$$\Omega = \underline{\omega}^* \cdot \sqrt{\underline{Q}^*} \qquad \text{[-]} \tag{1.7}$$

If $\Omega < 0.55$ then $a = 1.12, b = 0.055$
If $\Omega > 0.55$ then $a = 1.12,\ b = 0.1 \cdot \Omega^*$

$\Omega = 0.51$ for $n = 1000\ rpm$
$\Omega = 0.38$ for $n = 750\ rpm$

In both case $\Omega < 0.55$ and thus $a = 1.12$ and $b = 0.055$

If the outlet angle β_2 shall be unchanged as well as the best efficiency flow Q* the velocity vector diagram will be homogeneous and the following equation will be valid.

$$\frac{\pi \cdot D_2^{\,2}}{4} \cdot C_{m2} = Q^* \qquad [m^3/s] \qquad (1.8)$$

$$U_2 = \frac{n \cdot \pi \cdot D_2}{60} \qquad [m/s] \qquad (1.9)$$

Then from simplification of above (1.8) and (1.9) equations we get

$$D_2 = \sqrt[3]{\frac{240 \cdot Q^*}{\pi^2 \cdot n \cdot \tan \beta_2}} \qquad [m] \qquad (1.10)$$

For determining the required submergence of the runner the following equation has been used [5],

$$h_s = h_b - h_{va} - NPSH \qquad [m] \qquad (1.11)$$

NPSH is depends on turbine parameters. It is also a requirement for the turbine design and has been denoted as a required net positive suction head for turbine. The NPSH of the power plant has been included the necessary submergence of the runner ($-h_s$) the barometric pressure (h_b) and the vapor pressure (h_{va}) which ultimately depends upon the water temperature.

The practical experience shows that for not exceed the cavitation limits, the difference of the barometric pressure and the vapor pressure in the above equation is around -10 m. then the above equation becomes,

$$h_s = 10 - NPSH \qquad [m] \qquad (1.12)$$

Before going to choose the best synchronous speed of the runner we have to calculates the outlet diameter, outlet peripheral velocity of the runner and required submergence by changing the outlet blade angles as shown in the following tabular form,

	n = 1000 rpm		
β_2	D_2	U_2	h_s
15	0.81	42.41	-2.42
16	0.79	41.5	-2.89
17	0.77	40.31	-3.21

	n = 750 rpm		
β_2	D_2	U_2	h_s
15	0.89	34.95	1.58
16	0.87	34.16	1.26
17	0.85	33.5	0.94

From the above result we can choose the best parameter of the outlet of the runner. The selection of the parameters depends upon the fulfillment of the main objective of the Francis runner, which have been defined in the beginning. So the best outlet parameters and appropriate speed of the runner are as follows:

$\beta_2 = 17^0$ $D_2 = 0.85$ m $U_2 = 33.5$ m/s $C_{m2} = 12.2$ m/s n = 750 rpm.

The inlet dimensions may now be found by means of the Euler turbine equation. The energy converted by the runner will be

$$E_1 - E_2 = U_1 \cdot C_{u1} - U_2 \cdot C_{u2} = g \cdot H \cdot \eta_h \qquad [m^2/s^2] \qquad (1.13)$$

The hydraulic efficiency η_h is the ratio of the available energy which is transfer to and converted to mechanical energy by the runner and the net energy drop from the upstream to down stream side of the turbine. (Mechanical losses, friction losses and leakage losses are not taken into consideration in the hydraulic efficiency.) That is:

$$\eta_h = \frac{U_1 \cdot C_{u1} - U_2 \cdot C_{u2}}{g \cdot H} \qquad [\,-\,] \qquad (1.14)$$

Principally every turbine is designed according to the available discharge Q, net head H_n and a chosen optimal rotational speed n. These parameters however, differ over wide ranges from one site to the other. For this variability it is very useful to have similarity relations at hand for comparison means. In the following it is therefore, introduced some ratio parameters which are designated as reduced quantities.

$$\underline{c} = \frac{c}{\sqrt{2 \cdot g \cdot H_n}} \quad \text{as reduced absolute velocity} \qquad [\,-\,] \qquad (1.15)$$

$$\underline{u} = \frac{u}{\sqrt{2 \cdot g \cdot H_n}} \quad \text{as reduced peripheral velocity} \qquad [\,-\,] \qquad (1.16)$$

$$\underline{v} = \frac{v}{\sqrt{2 \cdot g \cdot H_n}} \quad \text{as reduced relative velocity} \qquad [\,-\,] \qquad (1.17)$$

Velocity diagrams based on dimensional values of the velocities are valid for only one single value of the net head H_n. If reduced velocities however, present the corresponding velocity diagrams, these diagrams keep a similar shape. The velocity diagrams based on reduced velocities are therefore beneficial because these diagrams are valid for any value of H_n.

Additional useful reduced quantities are:

$$\underline{h} = \frac{h}{H_n} \quad \text{is the reduced head} \qquad [\,-\,] \qquad (1.18)$$

$$\underline{Q} = \frac{Q}{\sqrt{2 \cdot g \cdot H_n}} \quad \text{is the reduced discharge} \qquad [\,-\,] \qquad (1.19)$$

$$\underline{\omega} = \frac{\omega}{\sqrt{2 \cdot g \cdot H_n}} \quad \text{is the reduced angular velocity} \qquad [\,-\,] \qquad (1.20)$$

By using dimensionless reduced parameters the above equation yields

$$\eta_h = 2 \cdot \left(\underline{u_1} \cdot \underline{c_{u1}} - \underline{u_2} \cdot \underline{c_{u2}} \right) \qquad [\,-\,] \qquad (1.21)$$

Assume that the hydraulic efficiency of 96 % and the approximately 50 % of the energy in front of the runner is converted to kinetic energy, i.e.

$$\frac{C_1^{\,2}}{2\cdot g} = 0.5\cdot H_n \quad \Rightarrow \quad \frac{C_1^{\,2}}{2\cdot g\cdot H_n} = 0.5 \quad \Rightarrow \quad \underline{C_1} \cong 0.7 \qquad [\,-\,]$$

By drawing the inlet velocity vector diagram, will try to obtain the stagnation point on the blade inlet tip and the inlet angle so the relative velocity does not lead to separation and possible inlet cavitations. (Especially for low head turbines)

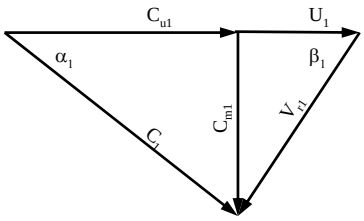

Figure 1.3.The inlet velocity diagram

Besides the assumption that $\underline{C_1} \cong 0.7$ .Now will use Eq. (2.21) when assume the hydraulic efficiency of the runner to be 96 % and no swirl conditions at the outlet of the runner. The following equation yields:

$$\underline{u_1}\cdot\underline{c_{u1}} = 0.48 \qquad [\,-\,] \qquad (1.22)$$

The inlet velocity diagram clearly illustrates that the smallest variation of the inlet flow angle with variation in the guide vane angle is obtained if the angle between the absolute and relative velocity in close to 90 ^{0} at best efficiency point of operation.

Using the following empirical relation for calculation of the reduced dimensionless circumferential speed of the blade inlet [8]

$$0.7 < \underline{u_1} < 0.75 \qquad [\,-\,] \qquad (1.23)$$

The reduced dimensionless circumferential speed of the blade inlet then from experience may be chosen to 0.71, for a low specific speed and then

$$\underline{c_{u1}} = \frac{0.48}{0.71} = 0.68 \qquad [\,-\,] \qquad (1.24)$$

The inlet diameter of the runner can now be found by the absolute value of U_1

$$U_1 = 0.71\cdot\sqrt{2\cdot g\cdot H} = 44.6 \qquad [\mathrm{m/s}] \qquad (1.25)$$

The inlet diameter of the runner will then be

$$D_1 = \frac{U_1 \cdot 60}{n \cdot \pi} = 1.137 \qquad \text{[m/s]} \qquad (1.26)$$

The meridional velocity at the inlet may from experience be chosen approximately 10 % [8] lower than at the outlet of the runner in order to obtain a slight acceleration of the meridional flow. (However, this choice will be different for different manufacturers due to the philosophy of blade shape etc,) Thus,

$$C_{m1} = 0.9 \cdot 10.3 = 9.3 \qquad \text{[m/s]} \qquad (1.27)$$

Then the height of the blade at the inlet =B_1, can now be found by means of equation of continuity as follows,

$$B_1 = \frac{Q^*}{\pi \cdot D_1 \cdot C_{m1}} = 0.176 \qquad \text{[m]} \qquad (1.28)$$

The inlet blade angle = β_1 can be found from the following relation (see the above inlet velocity triangle)

$$\tan \beta_1 = \left(\frac{C_{m1}}{U_1 - C_{1u}} \right) \quad \Rightarrow \quad \beta_1 = 77^o \qquad \text{[degrees]} \qquad (1.29)$$

Note: In this preliminary calculation the displacement of the blade thickness has been neglected. By taken the blade thickness into consideration the blade angles must be corrected due to increased relative velocity or meridional velocity.

2 EROSION MODELS AND ALTERNATE DESIGN OF RUNNER

The mathematical models of erosion are useful for design of turbine components, sediment settling basin and optimization of hydropower plant operation in Sand-laden River. Most often, individual particle dynamics are used for developing erosion models. Empirical and statistical relations are also often developed from experiments and field experiences. As erosion studies are heading toward numerical modeling and simulations, the importance of analytical models are increasing day by day. Truscott [6] has found that the most often quoted expression for erosion is

$$Erosion \propto velocity^n \qquad (2.1)$$

2.1 EROSION MODELS FOR HYDRAULIC MACHINERY

The erosion models are basically developed for specific purpose or condition. For example, Bitter's model is developed for dry condition, hence it is not clear whether this equation realistically predict erosion rate for wet condition or not. Few researchers have presented models specifically for hydraulic machinery. Truscott [9] presented the equation of Bergeron (1952) to predict the erosion rate of pump with simplified assumptions such as pure sliding of spherical particles over the surface. He presented equation for erosion as:

$$Erosion \propto \frac{V_{char}^3}{D} \cdot \left(\rho_p - \rho\right) \cdot D_p^3 \cdot p \cdot K \tag{2.2}$$

Where V_{char} is the characteristic velocity of liquid, D is the characteristic dimension of the machine, ρ_p is density of particle, D_p is diameter of particle, p is number of particles per unit surface area, ρ is density of liquid and K is experimental coefficient depending upon nature of abrasive particles. This equation is proportional to experimental coefficient, which is dependent on abrasive nature of particles. Karelin et al. [10] established the equation for surface erosion based on impact effect of particles considering kinetic energy of single particle.

They have anticipated deviation on erosion estimated by equation due to uncertainties like non-homogeneous particles, variable concentration, continuous alteration and pulsation of velocities and pressure, non-uniform flow distribution and so on. On the contrary to laboratory tests, Tsuguo [11] established the relationship of factors concerning erosion of turbines based on 8 years erosion data of 18 hydropower plants. The repair cycle of turbine is determined according to calculation of turbine erosion from equation, which gives erosion rate in term of loss of thickness per unit time.

$$W = \lambda \cdot c^{x} \cdot f^{y} \cdot k_1 \cdot k_2 \cdot k_3 \cdot V_{char}^{z} \tag{2.3}$$

Where λ is turbine coefficient at eroded part; c is the concentration of suspended sediment, V is relative velocity. The term f is average grain size coefficient on the basis of unit value for grain size 0.05 mm. The terms k_1 and k_2 are shape and hardness coefficient of sand particles and k_3 *i*s abrasion resistant coefficient of material. The x, y and n are exponent values for concentration, size coefficient and velocity respectively. The value of x and y are close to the unity and any deviation of this linear proportionality is determined from plot of wear versus parameter. The values of z are proposed for different turbine components based on relation between relative velocity and erosion. Minimum value of z is proposed as 1.5 for Pelton bucket and maximum value is 3 for Francis turbine runner. Equation 2.3 has been chosen for calculation of outlet dimensions of modify turbine runner.

As, $W \propto V_r^3$ and also assume all the coefficients in equation 2.3 has a constant values, and

$$W = k_1 \cdot V_r^3 \qquad (2.4)$$

Where, $k_1 = 0.3 - 0.5$. For the discussion, the constant, k_1 is chosen to be 0.3.

3 RESULTS AND DISCUSSION

The main erosion of the Francis turbine occurs at the outlet of the guide vanes and at the outlet of the runner. In order to reduce the erosion rate of the turbine, the absolute velocity at the inlet of the runner and the relative velocity at the outlet of the runner have to be reduced. In this study, the flow and head are kept constant while the speed, inlet peripheral velocity and outlet runner blade angle has been changed according to Table 3.1

Table 3.1 Variable input parameters

Speed	rpm	n	750	600	500	433	375	333	300	275
Inlet peripheral Velocity, reduced	-	$\underline{U_1}$	0.71	0.74	0.77	0.8	0.83	0.86	0.89	0.92
Outlet blade angle	degree	β_2	17	19	21	23	25	27	29	31

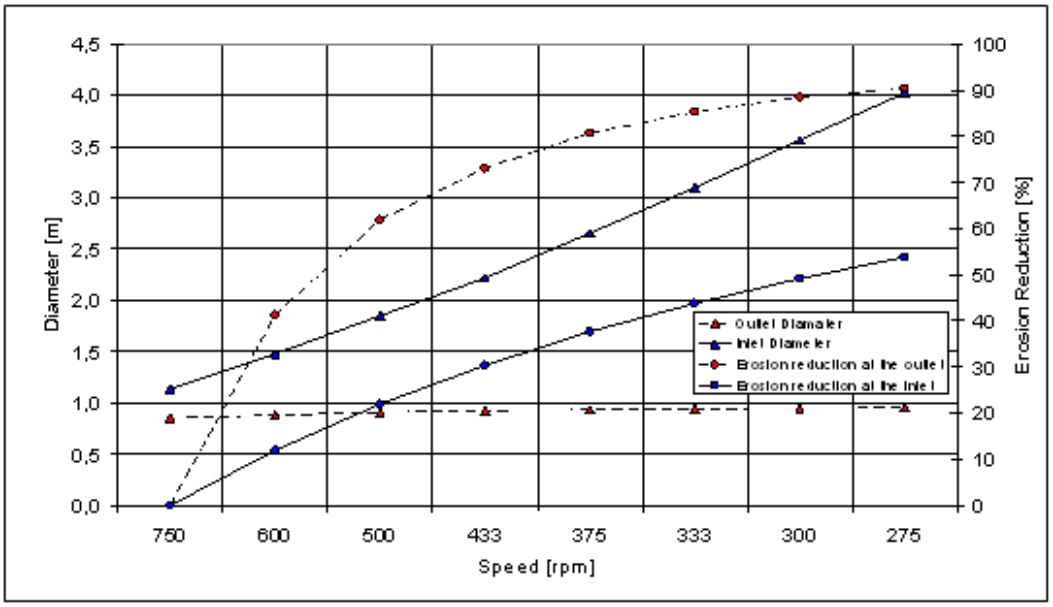

Figure 3.1 Results from the new design of the Francis runner

The results show that the outlet diameter changes relatively little while the inlet diameter changes drastically. The reduction of the erosion at the outlet is more than at the inlet. This is shown in Figure 3.1. The inlet angle of the turbine has changed so that the design looks more like a pump-turbine. This means that the turbine will be larger than the traditional design. The reduction of the erosion is linked to the reduction of the velocity and therefore the size of the turbine increases. This result in a higher price of the turbine, but it will reduce the maintenance costs during its lifetime.

It has been shown from the above calculation that the design of the runner can decrease the sand erosion. If a Francis turbine designer combines the hydraulic design and coating of the critical parts, a significant reduction of erosion can be achieved.

4 CONCLUSION

The reduction of the erosion is linked to the reduction of the velocity and therefore the size of the turbine increases. This result in higher price of the turbine, but it will reduce the maintenance costs during its lifetime.

It has been shown from the above calculation that the design of the runner can decrease the sand erosion. However, if a Francis turbine designer combines the hydraulic design and coating of the critical parts, a significant reduction of erosion can be achieved.

5 FURTHER WORK

This paper is a part of the PhD study of the author. Only few aspects of sand erosion investigation are presented in this paper. CFD analysis has not done yet. The modification in the conventional design of the runner has played significant role for increasing manufacturing cost, reducing repair and maintenances cost, and increase the life and efficiency of the runner. Hence, detail technical, managerial and economical consideration is needed along with experimental and computational fluids dynamics analysis. The author is expected to explore more about it and will be presented in PhD thesis.

REFERENCES

[1] T. R. Bajracharya, C. B. Joshi, R. P. Saini and O. G. Dahlhaug, Efficiency improvement of hydro turbines through erosion resistant design approach, ICPS Conference Proceedings (2004), IOE/TU/IITB/IIIE

[2] T. R. Bajracharya, C. B. Joshi, R. P. Saini, O. G. Dahlhaug, Sand erosion of Pelton nozzles and buckets: A case study of Chilime Hydropower Plant, Wear (2007) doi: 10.1016/j.wear.2007.02.021

[3] B. S. Mann, High-energy particle impact water resistance of hard coating and their application in hydro turbines, Wear (2000), 140-146

[4] B. Thapa, Ole G. Dahlhaug, Sand erosion in hydraulic turbines and wear rate measurement of turbine materials, CD ROM proceedings of international Conference-Hydro Africa 2003

[5] T. R. Bajracharya T. R., D. Sapkota, R. Thapa, S. Poudel, C. B. Joshi, R. P. Saini, O. G. Dahlhaug (2006), Correlation Study on Sand Led Erosion of Buckets and Efficiency Losses in High Head Power Plants, Proceedings of First National Conference on Renewable Energy Technology for Rural Development 12-14th October Kathmandu, Nepal.

[6] B. Acharya, B. Karki, and L. Lohia, (2005), Study on the Sand Erosion Led Damages of the Pelton Turbine Component and their effects (A Case Study of Chilime Hydroelectric Project), BE Thesis, Department of Mechanical Engineering, Pulchowk Campus, Institute of Engineering, Tribhuvan University

[7] B. Thapa, R. Shrestha, P. Dhakal, (2004) Sediment in Nepalese hydropower projects, Proc, Int. Conf. on the great Himalayas: climate, health, ecology, management and conservation, Kathmandu

[8] H. Brekke: Hydraulic Turbines, Design, Erection and Operation, NTNU, Trondheim, 2000.

[9] G. F. Truscott, A literature survey on abrasive wear in hydraulic machinery, Wear (20), Elsevier (1972) pp 29-49

[10] V. Y. Karelin, Fundamentals of hydro-abrasive erosion theory, Imperial College press (2002) pp 1-52

[11] N. Tsuguo, Estimation of repair cycle of turbine due to abrasion caused by suspended sand and determination of desiting basin capacity, Proceedings of International seminar on sediment handling techniques, NHA, Kathmandu (1999)

LIST OF SYMBOLS AND ABBREVIATIONS

α	Guide vane blade angle	degrees	k_3	Abrasion resistance coefficient	-
a	Constant (used in equation 1.6)	-	K	Experimental coefficient	-
A	Cross sectional area of pipe	m^2	λ	Turbine coefficient	-
b	Constant (used in equation 1.6)	-	k	Capacity ratio	-
B	Height of the runner	m	n	Speed	rpm
β	Blade angle	degrees	NPSH	Net Positive Suction Head	m
c	Concentration of the sediments	ppm	ω	Angular velocity	rad/s
C	Absolute velocity at the inlet	m/s	$\underline{\omega}$	Angular velocity, reduced value	-
$\underline{C}$	Absolute velocity, reduced value	-	Ω	Speed number	-
D	Diameter	m	p	Number of particles	$1/m^2$
E	Energy	m^2/s^2	ρ	Density	kg/m^3
η_h	hydraulic efficiency	-	Q	Flow rate	m^3/s
f	Grain size coefficient	-	$\underline{Q}$	Flow rate, reduced value	-
g	Gravity	m/s^2	U	Peripheral velocity	m/s
H	Head	m	$\underline{U}$	Peripheral velocity, reduced value	-
h	Head	m	V	Relative velocity	m/s
$\underline{h}$	Head, reduced value	-	$\underline{V}$	Relative velocity, reduced value	-
H_n	Net head	m	V_{char}	Characteristic velocity	m/s
k_1	Shape constant	-	Z	Number of generator pole pairs	-
k_2	Hardness constant	-	W	Erosion rate	-

SUB-SYMBOLS

b	Refers to the atmospheric pressure	s	Refers to the suction head
h	Hydraulic	x	Concentration exponent
m	Refers to the meridional direction	y	Size exponent
n	Refers to the net value	z	Characteristic velocity exponent
p	Refers to a particle	0	Refers to the centerline of the stay vane shaft
u	Refers to the peripheral direction	1	Refers to the inlet of the turbine runner
va	Refers to the vapor pressure	2	Refers to the outlet of the turbine runner
r	Relative value	*	Refers to the best efficiency point of the turbine
		o	Refers to the full load of the turbine

Appendix D

AN INVESTIGATION OF THE EFFECT OF PARTICLE SHAPE AND SIZE IN HYDRAULIC TURBINES

Hari Prasad Neopane [1], Ole Gunnar Dahlhaug[2], and Bhola Thapa[3]

This paper is presented at the Waterpower XVI 09, International Conference, held in Spokane, USA, 27 - 30 July 2009. The paper has also published in the proceedings for this symposium.

ABSTRACT

Hydraulic turbine components operating in sand-laden water are subject to erosive wear. This wear is not only reduces efficiency and life of turbine but also causes problems in operation and maintenance. A test rig designed to insert different shapes and sizes (1 to 10 mm) of particles was built. The flow in the guide vane cascade was simulated in order to find the drag force of a particle in swirl flow. When a particle is flowing in swirl flow, drag force and centrifugal force are two major forces influencing the particle equilibrium. The equilibrium of these two forces provides the critical diameter of the particle. A particle larger than the critical diameter moves away from the centre and hits the wall, but a smaller particle flows along with the water. The critical diameter of the particle is such that the particle continues to rotate in the turbine. Different shapes and sizes of particles were tested with the same operating conditions and found that triangularly-shaped particles were more likely to hit the suction side of the guide vane cascade. Furthermore, it supports the concept of separation of particles from streamlines inside the test rig, and lead to the development of an operating strategy for a Francis turbine processing sand-laden water. A high-speed digital camera was used to capture images of particles. This study also permitted experimental verification of a given size and shape of a particle as it orbits in the turbine until either the velocity components are changed or the particle becomes smaller by fracturing due to impact against the outer wall.

1. INTRODUCTION

Sand erosion is caused by impacts of sand particles against the solid surface. These particles are contained in liquid flow medium and possess kinetic energy that is sufficient to damage even metallic surface. The process of material removal from a solid surface by a stream of impacting solid particles has been studied by a number of researchers, and considerable information has been documented on the mechanism of material removal processes. It has been well established that the erosion wear per impacting particle W is a function of the impacting velocity 'v' as well as the particle diameter 'd' as given by the equation $W = K \cdot v^a \cdot d^b$ (Sheldon et al., 1972). Similarly, several other authors have provided simple expressions, based on wear test results, for wear rate as a function of velocity, material hardness, and grain size or solids concentration (Truscott, 1972). The one most often quoted is: $Wear \propto (Vel.)^n$ Where, the index n may vary depending on the material and other factors involved; the most common value appears to be 3 (Truscott, 1972). Some more detailed analyses consider wear as affected by the forces and velocities acting on a particle in a liquid flow. Truscott, 1972, stated that wear is directly proportional to "abrasive power" of a particle impinging on a surface. Many equations have been developed and presented in literature relating wear rate based upon velocity of particles, but less information is found relating wear rate based upon the shape and size of the particles.

Furthermore, solid particles of different shapes and sizes play a significant role in many separation processes. Swirl flow is a primary mechanism for separation of particles that creates a centrifugal force in many separation processes including in a gap between the guide vane outlet and the runner inlet in a Francis turbine. The separation of particles of different shapes and sizes depends upon the variations in behaviour of the particles when subjected to the action of moving fluid. A particle falling in an infinitely large fluid under the influence of gravity will accelerate until the gravitational force is exactly balanced by the resistive force that includes buoyancy and drag. The constant velocity reached at that stage is called the terminal velocity. The resistive drag force depends upon an experimentally determined drag co-efficient. The drag co-efficient and terminal velocities are important design parameters for many separation processes (Gabitto et al., 2007).

Particles in water may range in size from a few manometers up to millimetres dimensions. Natural particles also have various shapes, including rods, plate, and spheres, with many variations in between, which make a treatment of particle size difficult. The discussion is vastly simplified if the particles are considered spherical. In this case only one size parameter is needed (the diameter) and hydrodynamic properties are much more easily treated. Of course, non-spherical particles also occur in natural water, and some way of characterizing them is essential. A common concept is that of the 'equivalent sphere' based on a chosen property of the particles (Gregory, 2006). For instance, an irregular particle has a certain surface area and the equivalent sphere could

be chosen as that having the same surface area. The surface area of sphere, with diameter d, is just $\pi \cdot d^2$.
So, if the surface area of the non-spherical particle is known, the equivalent spherical diameter can easily be calculated. For an object of a given volume, the sphere has minimum surface area and the volume (or mass) of a given particle must be equal to or less than that of the sphere. Another common definition of equivalent spherical diameter is based on sedimentation velocity. In this case, from the sedimentation velocity and density of particle, the diameter of a sphere of the same material that would settle at the same rate can be calculated. This is sometimes called the 'Stokes equivalent diameter'.

In this paper, the results of an experimental study of the effect of various shapes and sizes of different materials in swirl flow are reported. The main focus of the paper is to discuss the critical diameter of particles, and also support the concept of separation of particles from streamlines inside the test rig and to establish the operating strategy for a Francis turbine processing sand-laden water.

1.2 MOTION OF PARTICLE THROUGH FLUIDS

There are three forces acting on a particle moving through a fluid: 1) The external force, gravitational or centrifugal; 2) The buoyant force, which acts parallel with the external force but in the opposite direction; 3) The drag force, which appears whenever there is relative motion between the particle and the fluid.

1.1.2 EQUATIONS FOR ONE-DIMENSIONAL MOTION OF PARTICLE THROUGH FLUID

Consider a particle of mass m moving through a fluid under the action of an external force F_e. Let the velocity of the particle relative to the fluid be u, let the buoyant force on the particle be F_B and let the drag be F_D, then,

$$m \cdot \frac{du}{dt} = F_e - F_B - F_D \qquad \text{[N]} \qquad (1)$$

The external force can be expressed as a product of the mass and the acceleration a_e of the particle from this force,

$$F_e = m \cdot a_e \qquad \text{[N]} \qquad (2)$$

The buoyant force is, be Archimedes' law, the product of the mass of the fluid displaced by the particle and the acceleration from the external force. The volume of the particle

is $\frac{m}{\rho_p}$, the mass of fluid displaced is $\left(\frac{m}{\rho_p}\right)\cdot\rho$, where ρ is the density of the fluid. The buoyant force is then,

$$F_B = \frac{m\cdot\rho\cdot a_e}{\rho_p} \quad \text{[N]} \quad (3)$$

The drag force is

$$F_D = \frac{C_d\cdot U^2\cdot\rho\cdot A_p}{2} \quad \text{[N]} \quad (4)$$

Where C_d is the drag coefficient, A_p is the projected area of the particle in the plane perpendicular to the flow direction.

By substituting the forces into Eq. (1), we have

$$\frac{du}{dt} = a_e - \frac{a_e\cdot\rho}{\rho_p} - \frac{C_d\cdot U^2\cdot A_p\cdot\rho}{2\cdot m} = a_e\cdot\left(\frac{\rho_p-\rho}{\rho_p}\right) - \frac{C_d\cdot U^2\cdot A_p\cdot\rho}{2\cdot m}$$

[m/s²] (5)

Motion from gravitational force:

In this case, $a_e = g$ [m/s²]

$$\frac{du}{dt} = g\cdot\left(\frac{\rho_p-\rho}{\rho_p}\right) - \frac{C_d\cdot U^2\cdot A_p\cdot\rho}{2\cdot m} \quad \text{[m/s²]} \quad (6)$$

Motion in a centrifugal field:

$a_e = r\cdot\omega^2$ [m/s²]

$$\frac{du}{dt} = r\cdot\omega^2\cdot\left(\frac{\rho_p-\rho}{\rho_p}\right) - \frac{C_d\cdot U^2\cdot A_p\cdot\rho}{2\cdot m} \quad \text{[m/s²]} \quad (7)$$

In this equation, *u* is the velocity of the particle relative to the fluid and is directed outwardly along a radius.

1.2 TERMINAL VELOCITY

In gravitational settling, *g* is constant. Also, the drag always increases with velocity. The acceleration decreases with time and approaches zero. The particle quickly reaches a constant velocity which is the maximum attainable under the circumstances. This maximum settling velocity is called terminal velocity.

$$\frac{du}{dt} = g \cdot \left(\frac{\rho_p - \rho}{\rho_p} \right) - \frac{C_d \cdot U^2 \cdot A_p \cdot \rho}{2 \cdot m} = 0 \qquad [m/s^2] \qquad (8)$$

$$u_t = \sqrt{\frac{2 \cdot g \cdot (\rho_p - \rho) \cdot m}{A_p \cdot \rho_p \cdot C_d \cdot \rho}} \qquad [m/s] \qquad (9)$$

In motion from a centrifugal force, the velocity depends on the radius and the acceleration is not constant if the particle is in motion with respect to the fluid. In many practical use of centrifugal force, $\frac{du}{dt}$ is small. If $\frac{du}{dt}$ is neglected, then

$$u_t = \omega \cdot \sqrt{\frac{2 \cdot r \cdot (\rho_p - \rho) \cdot m}{A_p \cdot \rho_p \cdot C_d \cdot \rho}} \qquad [m/s] \qquad (10)$$

Motion of spherical particles:

If the particles are spheres of diameter D_p, then, $m = \frac{\pi \cdot {D_p}^3 \cdot \rho_p}{6}$ and, $A_p = \frac{\pi \cdot {D_p}^2}{4}$

Substitution of m and A_p into the equation for u_t gives the equation for gravity settling of spheres:

$$u_t = \sqrt{\frac{4 \cdot g \cdot (\rho_p - \rho) \cdot D_p}{3 \cdot C_d \cdot \rho}} \qquad [m/s] \qquad (11)$$

1.3 DRAG COEFFICIENT

Drag coefficient is a function of Reynolds number. The drag curve applies only under restricted conditions:

- The particle must be a solid sphere;
- The particle must be far from other particles and the vessel wall so that the flow pattern around the particle is not distorted;
- It must be moving at its terminal velocity with respect to the fluid.

Particle Reynolds number: $R_{e,p} = \frac{u \cdot D_p \cdot \rho}{\mu}$ [-] (12)

Where, u : relative velocity of particle, D_p : diameter of the particle, ρ : density of fluid, μ : viscosity of fluid.

Stokes' law applies for particle Reynolds number less than 1.0

$$C_d = \frac{24}{R_{e,p}} \quad [-] \quad (13)$$

From Eq. (4)

$$F_D = \frac{C_d \cdot {u_t}^2 \cdot A_p \cdot \rho}{2} = \frac{24}{R_{e,p}} \cdot {u_t}^2 \cdot \rho \cdot \frac{{D_p}^2 \cdot \pi}{4} \cdot \frac{1}{2} = \frac{24 \cdot \mu}{u_t \cdot D_p \cdot \rho} \cdot {u_t}^2 \cdot \rho \cdot \frac{{D_p}^2 \cdot \pi}{8} = 3 \cdot \pi \cdot \mu \cdot u_t \cdot D_p$$

$$F_D = 3 \cdot \pi \cdot \mu \cdot u_t \cdot D_p \quad [\text{N}] \quad (14)$$

From Eq. (11)

$$u_t = \sqrt{\frac{4 \cdot g \cdot (\rho - \rho_p) \cdot D_p}{3 \cdot C_d \cdot \rho}} = \sqrt{\frac{4 \cdot g \cdot (\rho - \rho_p) \cdot D_p}{3 \cdot \frac{24 \cdot \mu}{u_t \cdot D_p \cdot \rho} \cdot \rho}} = \sqrt{\frac{g \cdot (\rho_p - \rho) \cdot {D_p}^2 \cdot u_t}{18 \cdot \mu}}$$

$$U_t = \frac{g \cdot {D_p}^2 \cdot (\rho_p - \rho)}{18 \cdot \mu} \quad [\text{m/s}] \quad (15)$$

In the case of centrifugal, g is replaced by $r \cdot \omega^2$

For $1000 < R_{e,p} < 200{,}000$, use Newton's law

$$C_d = 0.44 \qquad [-] \qquad (16)$$

$$F_D = 0.055 \cdot \pi \cdot D_p{}^2 \cdot u_t{}^2 \cdot \rho \qquad [\mathrm{N}] \qquad (17)$$

$$u_t = 1.75 \cdot \sqrt{\frac{g \cdot D_p \cdot (\rho_p - \rho)}{\rho}} \qquad [\mathrm{m/s}] \qquad (18)$$

At higher relative velocities, the inertia of the fluid begin to dominate (the fluid must accelerate out of the way of the particle). Analytical solution of the Navier-Stokes equations is not possible under these conditions. However, experiments give the relationship between the drag co-efficient and particle Reynolds number in the form of the so- called standard drag curve. Four different regions are identified: the Stokes' law region, the Newton's law region in which drag coefficient is independent of Reynolds number, an intermediate region between the Stokes and Newton's regions; and the boundary layer separation region. The Reynolds number ranges and drag co-efficient correlations for these regions are given in Table 1, (Martin, 2008).

Table 1

Region	Stokes	Intermediate	Newton's law
$R_{e,p}$ *range*	< 0.3	$0.3 < R_{e,p} < 500$	$500 < \mathrm{Re},\ p < 2 \times 10^5$
C_d	$\frac{24}{R_{e,p}}$	$\frac{24}{R_{e,p}} \cdot \left(1 + 0.15 \cdot R_{e,p}{}^{0.687}\right)$	≈ 0.44

Several correlations have been proposed for C_d over the entire range, the one presented in equation (19) is that of Haider et al. (1989), which is claimed to fit the data with a root mean square deviation of 0.024.

$$C_d = \frac{24}{R_{e,p}} \cdot \left(1 + 0.1806 \cdot R_{e,p}{}^{0.6459}\right) + \left(\frac{0.4251}{1 + \frac{6880.95}{R_{e,p}}}\right) \qquad [-] \qquad (19)$$

1.4 PARTICLE IN SWIRL FLOW

When particles travel in swirling flow toward a turbine's outlet, which is located in the centre as shown in **Figure 1.1**, the particles will be exposed to two main forces. Centrifugal force (F_c) moves the particles away from the centre, while the drag force (F_D) pulls them toward the outlet, which is in the centre, or toward the runner in the case of a Francis turbine (Thapa et al., 2004). These two forces are given by the following equations.

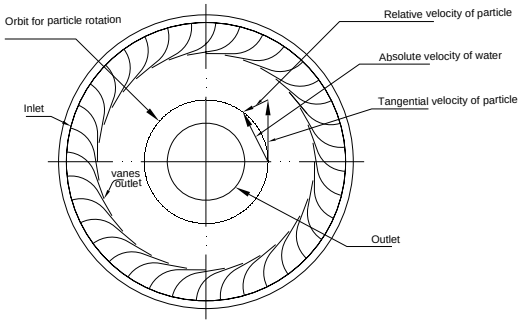

Figure1.1 Illustration of particle flow in spiral swirl

$$F_c = \rho_p \cdot \frac{\pi \cdot d^3}{6} \cdot r \cdot \omega^2 = \rho_p \cdot \frac{\pi \cdot d^3}{6} \cdot \frac{C_t^{\,2}}{r} \qquad [\mathrm{N}] \qquad (20)$$

$$F_D = \frac{1}{2} \cdot C_d \cdot \rho \cdot V_r^{\,2} \cdot A_p \qquad [\mathrm{N}] \qquad (21)$$

Following three conditions prevail in such case:

- Particle will stay at the orbit of radius r, if $F_c = F_D$
- Particle will strike outer wall, if $F_c > F_D$
- Particle will flow along with water towards the centre of the tank, if $F_c < F_D$

At equilibrium, these two forces balance each other and a particle of a given diameter will stay at an orbit of radius (r) until either the velocity component is changed or particles become smaller by fracture due to impact. The diameter of a particle (d) for the equilibrium condition is given by equation (22). This is called the critical diameter.

$$d_c = \frac{3}{4} \cdot C_d \cdot \left(\frac{\rho}{\rho_p}\right) \cdot \left(\frac{V_r}{C_t}\right)^2 \cdot r \qquad [\mathrm{m}] \qquad (22)$$

The drag force is caused by the relative velocity of particles in radial direction (i.e. towards the centre of the tank), and centrifugal force is caused by the velocity of particle in tangential direction (i.e. away from the centre of the tank).

2. DESCRIPTION OF TEST RIG AND TEST PROCEDURE

A test rig was developed and designed at the waterpower laboratory, Norwegian University of Science and Technology, Norway, to create strong swirl flow, similar to the flow between the guide vane outlet and the runner inlet of a turbine. There was a provision to introduce particles, with sizes ranging from 1 to 10 mm, into the swirl, and to observe the motion of the particles from Plexiglas windows located on the cover of the tank using a high-speed digital camera.

The experimental set up, as shown in **Figure2.1**, consisted of a main tank (1100 mm diameter and 700 mm height), 400 mm diameter inlet pipe and outlet cone with valve. The main tank and other components of the test rig were designed and dimensioned for 50 m of head in order to carry out the experiment in high velocity. The main tank consisted of two compartments with a 250 mm diameter opening at the centre of the plate. This plate divides the main tank into two compartments. Thirty-six curved vanes, which resemble guide vanes of a Francis turbine, with a radius of 100 mm toward the inlet and a 90mm straight section toward the outlet, were fixed at a pitch circle diameter of 900mm to the middle plate in such a way that the inlet velocity direction should be almost in the radial direction and the outlet would be 10 ^{0} to the tangent. These vanes were located in between the upper part of the middle plate and the bottom part of a 50mm thick, 950 mm diameter transparent Plexiglas plate. From this arrangement, the swirl flow in between the Plexiglas and the middle plate could be clearly observed. The edge of the Plexiglas was made uniform to ensure uniform flow.

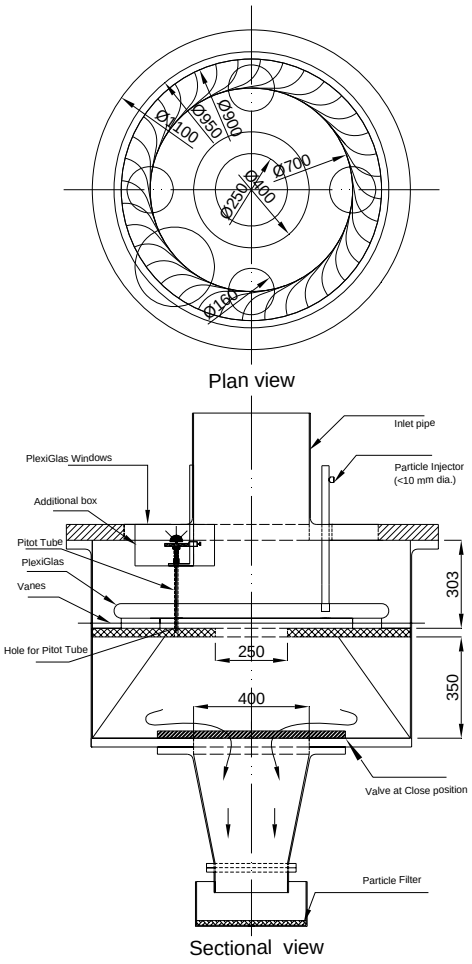

Figure2.1 The experimental set up

The top cover of the tank was fitted with five transparent windows of Plexiglas. Four of those transparent windows of 160 mm diameter were located at 90 ^{0}, 180 ^{0}, 270 ^{0} and 360 ^{0}

respectively at the pitch circle diameter 700 mm to observe the motion of the particles, and the fifth window of 275 mm diameter was located at 315 ^{0} at 700 mm pitch circle diameter to measure the velocity of the flow (after inserting a Pitot tube) and to observe the velocity of particle. The particle injection point was located at 279 mm from the centre of the tank. The particle was released at the bottom of the Plexiglas through a 15 mm diameter pipe and valves arrangement. Particles up to 10 mm in diameter were tested in this experiment.

A manometer was fitted into the injection pipe and valves arrangement in order to measure the inlet pressure of the tank in the swirl flow field. There were two additional manometers located in the system. One was connected to an air-bleeding valve located at 390mm from the centre of the tank for measuring the inlet pressure, and another was fitted at the outlet of cone for measuring the pressure at the outlet. The flow rate was calculated with the help of an ultrasonic flow meter fitted in the inlet pipe.

The main purpose of this experiment was to determine the velocity of the particle that would flow along with water in the given flow condition. To achieve this, firstly, the operating condition was set at a certain velocity level by controlling the valve opening. Then the particle was injected and the motion of the particle was observed through the Plexiglas windows with the help of the high-speed camera. The particle image was saved and analysis was performed based upon the time required to move the particle from one fixed location to another fixed location. Location of the particle was identified based upon the radial and angular position of particle inside the test rig. In order to calculate the correct location of the particle inside the test rig, radial and angular markings were inscribed on the middle plate at diameters of 219 mm, 239 mm, 259 mm, 279 mm, 299 mm, 309 mm and 22.5 degrees interval respectively. Using these markings, six different circles and eight different angular lines could be clearly observed in the middle plate.

3. RESULTS AND DISCUSSION

Velocities of particles of different sizes and shapes are shown in **Figures 3.1 and 3.2.** The velocity of the particle will increase if the operating head increases. The size of the particle is inversely proportional to the velocity of the particle, and it also depends upon the shape of the particle. Different shapes of particles were tested, and it was determined that spherically-shaped particles had higher settling velocities than particles with other shapes.

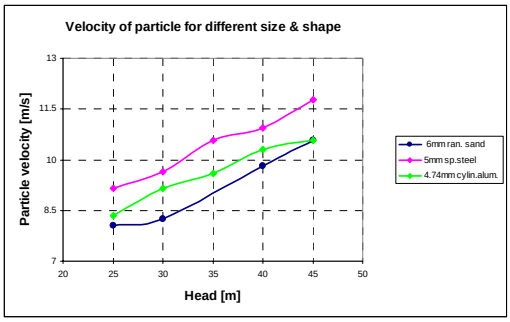

Figure 3.1 Velocity of particle for different sizes and shapes

Many natural particles are not usually in spherical shape. These particles will tend to have lower settling velocities because both decreases in sphericity and increases in angularity tend to decrease settling velocities. Furthermore, larger cross-sectional areas tend to be directed perpendicular to the transport path. Separation of flow is more likely to occur for non-spherical particles, and less spherical particles may rotate, follow wobbling paths, etc.

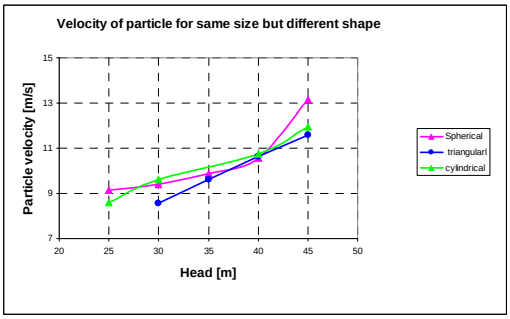

Figure 3.2 Velocity of particle for same sizes but different shapes

If centrifugal force and drag force on the particle are equal, the particle will rotate exactly at the injecting radius, but if those forces do not balance each other, there will two possibilities. The particle either moves toward the inner radius and ultimately sinks or moves toward the outer radius and ultimately hits the sides of the vanes. The equilibrium condition was observed for a given particle after manipulating the flow velocity, providing verification that the different forces were balanced in the test rig. This also revealed that the particle with a given diameter would stay at the orbit of the injecting radius until either the velocity components were changed or the particle became smaller by fracturing due to impact with the outer wall. Different shapes of particles were tested with the same operating conditions as shown in **Figure 3.3,** and it was determined that triangularly-shaped particles were more likely to hit the suction side of the guide vane cascade. The radius at which the particle is moving, called rotation radius. This rotation radius also varied with different shapes of particles, which further supports the influence of shape factor for particle velocity calculation.

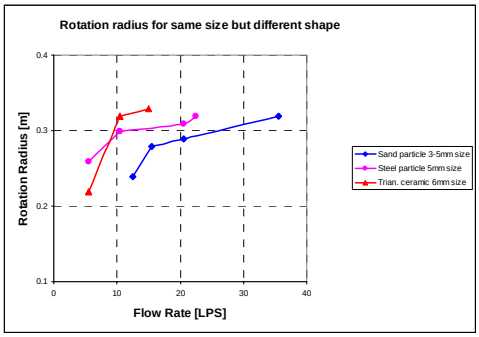

Figure 3.3 Rotation radius for particles of the same size but different shapes

Drag co-efficient was also calculated and plotted versus different shapes, sizes and particle Reynolds number as shown in **Figures 3.4 and 3.5.**

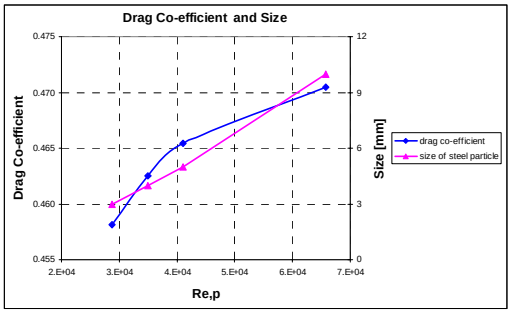

Figure 3.4 Drag co- efficient and size

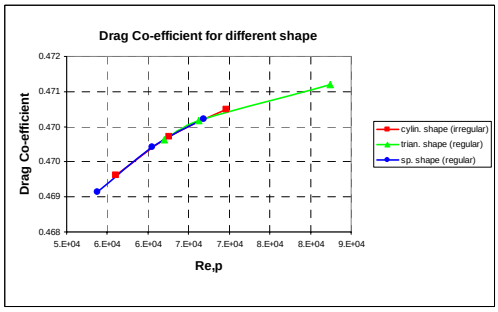

Figure 3.5 Drag co- efficient & shapes

The drag co-efficient, C_d is a non-dimensional number that depends on the shape of the particle, the fluid kinematic viscosity and grain size. It has been found that the effect of the shape of non-spherical particles on their drag co-efficient can be defined in terms of its sphericity. Moreover, shape affects drag co-efficient far more in the Intermediate and Newton's law regions than in the Stokes' law region. However, the variation of drag co-efficient in the Newton's law region is not so significant, but the influence of size and shape of the particle has been clearly demonstrated. The result shows that the triangularly-shaped particles have a higher drag co-efficient than other shapes because the angular particles also tend to have lower settling velocity than the spherical ones.

4. CONCLUSIONS

The equilibrium between centrifugal force and drag force holds true in the case of particle movement in swirl flow. The concept of particle separation due to high velocity and acceleration in swirl flow is not only correlated for guide vane outlets and runner vane inlets, but also correlated for other turbine components like flow through stay vanes, guide vane cascades, runner vanes of reaction turbines and Pelton buckets. Direct application of this concept leads to an operating strategy for Francis turbines that process sand-laden water. For example, guide vane position could be manipulated to maintain the velocity ratio in such a way that particles of a given size should flow along with the water without striking the wall. This means that the guide vane opening should be adjusted to maintain a velocity ratio, which would be appropriate to the characteristic diameter of the particles. This will keep the particles in the orbit without striking the wall and, thus, the effect of sand erosion can be minimized.

Furthermore, the particle velocity and drag co-efficient not only depend on particle size but are also sensitive to the shape of the particle along with other variables. The reduction of the erosion is also linked to the reduction of particle velocity.

REFERENCES

1. Brekke H. (2002) “Design of hydraulic machinery working in sand laden water,” In: Duan C.G. and Karelin V.Y. (eds), “Abrasive erosion and corrosion of hydraulic machinery,” pp 155-181, Imperial college press, London.
2. Chevallier, P. and A. B. Vannes (1995). "Effects on a sheet surface of an erosive particle jet upon impact." Wear 184(1): 87-91.
3. Doby, M. J., A. F. Nowakowski, et al. (2007). "Numerical and experimental examination of swirl flow in a cylindrical container with rotating lids." Minerals Engineering 20(4): 361-367.
4. Gabitto, J. and C. Tsouris (2008). "Drag co-efficient and settling velocity for particles of cylindrical shape." Powder Technology 183(2): 314-322.
5. Gregory, J. (John), Particles in water properties and processes, University college London England, 2006, CRC press, Taylor & Francis Group, p. 9-10
6. Haider, A. and O. Levenspiel (1989). "Drag coefficient and terminal velocity of spherical and nonspherical particles." Powder Technology 58(1): 63-70.
7. Jie Zhang , Particle Technology - Study Notes.
8. K. Harris January 21, 2003, “Sediment transport processes in coastal environments,” Lecturer notes.
9. Martin Rhodes, 2008 “Introduction to Particle Technology,” second edition, p. 29-42.
10. Neopane, Hari Prasad, Ole G. Dahlhaug and Bhola Thapa, 22-24 Oct.2007, “Alternative Design of a Francis Turbine for Sand Laden Water.” Proc. International Conference on Small Hydropower - Hydro Sri Lanka.
11. Sheldon, G. L. and A. Kanhere (1972). "An investigation of impingement erosion using single particles." Wear 21(1): 195-209.
12. Truscott, G. F. (1972). "A literature survey on abrasive wear in hydraulic machinery." Wear 20(1): 29-50.
13. Tabakoff, W., A. Hamed, et al. (1983). "Investigation of gas particle flow in an erosion wind tunnel." Wear 86(1): 73-88.
14. Tabakoff, W. (1995). "High-temperature erosion resistance of coatings for use in turbomachinery." Wear 186-187(Part 1): 224-229.
15. Thapa, B. (2004). “Sand erosion in hydraulic machinery.” Trondheim, Norwegian University of Science and Technology, Faculty of Engineering Science and Technology, Department of Energy and Process Engineering. 2004:105.
16. Thapa B. and Brekke H. (2004) “Effect of sand particle size and surface curvature in erosion of hydraulic turbine,” IAHR symposium on hydraulic machinery and systems, Stockholm.
17. Zhao, K., C. Gu, et al. (1993). "Study on mechanism of combined action of abrasion and cavitation erosion on some engineering steels.” Wear 162-164 (Part 2): 811-819.

LIST OF SYMBOLS AND ABBREVIATIONS

F_D	Drag force	N	A_p	Projected area	m^2
a	Constant	-	C_D	Drag co-efficient	-
A	Cross sectional area of pipe	m^2	r	radius	m
b	Constant	-	U_t	Terminal velocity	m/s
m	Maas of the particle	kg	$R_{e,p}$	Particle Reynolds number	-
F_e	External force	N	μ	Viscosity of fluid	Ns/m^2
F_B	Buoyant force	N	ω	Angular velocity	rad/s
C_t	Absolute velocity at the inlet	m/s	F_c	Centrifugal force	N
d_c	Critical dia. of particle	m	C_d	Drag co-efficeint	-
Dp	Diameter of particle	m	ϱ_p	Density of particle	kg/m^3
g	Gravity	m/s^2	ϱ	Density of fluid	kg/m^3
H	Head	m	Q	Flow rate	m^3/s
h	Head	m	U	Peripheral velocity	m/s
W	Erosion rate	-	u	Relative velocity of particle	m/s
V_r	Relative velocity	m/s	a_e	acceleration	m/s^2
d	Diameter of particle	m	π	pi	Const.
n	Refer to exponential factor	-			

Appendix E

NUMERICAL PREDICTION OF PARTICLE SHAPE FACTOR EFFECT ON SEDIMENT EROSION IN FRANCIS TURBINE BLADES

Hari Prasad Neopane[1], Ole Gunnar Dahlhaug[2], and Mette Eltvik[3]

This paper is presented at the Hydropower'10, the 6th International Conference on Hydropower, held in Trømso, Norway, 1 - 3 February 2010. The paper has also published in the proceedings for this symposium.

ABSTRACT

Hydraulic turbine components operating in sand-laden water are subject to abrasive and erosive wear. This wear not only reduces the efficiency and life of a turbine but also causes problems in operation and maintenance. The prediction of the erosion on a Francis turbine blade will be described based upon the two different shapes of particles at two operating conditions, namely, best efficiency (BEP) and full load, for which the results of experimental tests are available for discussion, comparison and validation. A numerical simulation is based on the Lagrangian particle tracking multiphase model that is available in ANSYS CFX, which is capable of modelling dispersed phases, which are discretely distributed in a continuous phase. The modelling involves the separate calculation of each phase with source terms generated to amount for the effects of the particles on the continuous phase. It is found that erosion on a turbine blade is strongly dependent on the shape of the particle. The predicted erosion rate density is in good agreement with the particle velocity obtained from experiments.

1. INTRODUCTION

Hydraulic turbine components operating in sand-laden water are subject to sediment erosion. This type of erosion is not only reduces efficiency and the life of a turbine but also causes problems in operation and maintenance (Brekke, 2002; Neopane, 2009). Suspended sediments in water are subjected to kinetic energy, the force of gravity, viscosity, turbulence, centrifuge and cavitation. The sediment erosion is a result of the mechanical wear of components. This is due to the dynamic action of sediment flowing along with water impacting against the solid surface. Therefore, sediment flowing along with water passing through the turbine is the root caused of sediment erosion in turbine components (Naidu, 1999). The sediment content in rivers may cause abrasion on different components of hydraulic turbines. The erosion intensity depends on the sediment type, its characteristics (particle shape, size and concentration etc.), the operating conditions of the machine (flow rate, head and rotation speed etc.), and the hydraulic design itself, as well as the material used for the turbine component (Finnie, 1972; Truscott, 1972; Thapa and Brekke, 2004). Various researchers have conducted experiments to study the effect of these parameters on erosive wear, but most of these experiments are on small-size samples in different types of test rigs to simulate the flow conditions in the turbine, but actual flow conditions and the phenomenon of erosive wear are too complex to simulate (Padhy and Saini, 2008).

Particle characteristics are an important but relatively poorly researched aspect of the erosion problem (Stachowiak et al., 2006). It is impossible to isolate hardness completely from other features of the particle such as its shape. Even if the particle is hard but relatively blunt then it is unlikely to cause severe erosive wear. A blunt particle has a mostly curved surface approximating a spherical shape, while a sharp particle consists of flat areas joined by corners with small radii, which are critical to the process of wear (Stachowiak et al., 2006). The sediment wear increases rapidly with the flow velocity, and is often reported as being approximately $\propto$ (velocity)^3, or $\propto$ (pump head)$^{3/2}$, from both theoretical considerations and test results (Truscott, 1972). The actual value of the index, for any given conditions and the actual mechanism of the erosive wear is not yet clearly understood. Hence, a simple, reliable and generalized model for erosion is not yet developed for engineering purposes. Many erosion models are developed for a specific purpose or condition (Thapa, 2004). Most of the common expressions for erosive wear are based upon the experimental experience so that a multidimensional study approach is needed to investigate the relationship between sediment movement and sediment erosion mechanism inside the hydraulic machines (Naidu, 1999). There is a pressing need to study sediment erosion and develop more realistic empirical relations based upon the combined experimental, numerical and field experiences with respect to the influencing factors is increasing day by day.

Traditionally, manufacturers of hydraulic turbines have only relied on empirical data and experience gathered from site to investigate the component damage due to silt abrasion between outages. This information is very helpful, but for new hydropower projects involving the risk of sand abrasion, it is desirable to numerically study the abrasive

mechanism during the design process in order to predict and quantify, the zones, where there is a high risk of erosion damage (Vu and Alain, 2000).
The main objective of this paper is to investigate the relationship between the different shapes of particle movement and the tendency of erosion inside the Francis turbine blades. Then establish the operating strategy for a Francis turbine operating in sand-laden water. In order to achieve the main objective, numerical simulations are carried out based upon the commercial Computational Fluid Dynamics (CFD) code, namely CFX on a Francis turbine of Cahua Hydropower plant. The prediction of the erosion on turbine blade will be described based upon the two different shapes of particles at two operating conditions, namely, best efficiency (BEP) and maximum load. Here the results of the experimental tests are available for discussion, comparison and validation.

1.1 CAHUA HYDROPOWER PLANT (HPP)

Cahua HPP is a Run-of-River hydropower plant in Peru. It is located 200 km north of Lima, by the Pativilca River. The power plant has two low head vertical Francis turbines and total installed capacity of 43 MW with a gross head of 215 m and a mass flow of 22 m^3/s. The average annual output is 280 GWh. Both Francis turbines composed of 20 stay vanes, 20 guide vanes and 17 runner blades. The power plant was completed in 1967 and purchased by SN Power Norway in 2003.

The sediment study conducted in this power plant indicated that, the sediment concentration exceed 120,000 tons of sediment only after six weeks of operation. The average content of quartz particles in the sediment is found to about 35 % and feldspar is found to about 30 %, which are harder than the turbine material, is main reason of excessive sediment erosion in the hydraulic machinery operating in this power plant.

2. CFD METHODOLOGIES

The numerical unsteady simulations are carried out with the commercial software ANSYS CFX. There are a number of different solution methods which are used in CFD codes. The most common, and the one on which ANSYS CFX is based, known as the finite volume technique. In this technique, the region of interest is divided into small sub-regions, called control volumes. The equations are discretized and solved the incompressible Unsteady Reynolds Averaged Navier-Stokes (URANS) equations in their conservative form iteratively. As a result, an approximation of the value of each variable at specific points throughout the domain can be obtained. In this way, one derives a full picture of the behaviour of the flow. To provide closure to the time averaged Navier-Stokes equations, it is necessary to utilize a turbulence closure model. The two equations turbulence models, $k-\varepsilon$ and SST were tested.

The $k-\varepsilon$ model has proven to be stable and numerically robust and has a well-established regime of predictive capability. For general-purpose simulations, the $k-\varepsilon$ model offers a good compromise in terms of accuracy and robustness; however, it can lack prediction accuracy for complex flow. Such complexities include rapid variations in flow area, flows with boundary layer separation, flows with sudden changes in the mean strain rate, flows in rotating fluids, flows over curved surfaces etc.

A Reynolds Stress model may be more appropriate for flows with sudden changes in strain rate or rotating flows, while the SST model may be more appropriate for separated flows. Hence, the Shear stress turbulence (SST) model was utilized as default closure model. Furthermore, the discretization of the equations was made with the Forward Euler implicit scheme, second order time, and in high resolution advection scheme. The assumed convergence criterion for residuals was RMS of 10^{-4}.

2.1 PARTICLE TRANSPORT THEORY

Particle transport modelling is one type of multiphase model, where particulates are tracked through the flow in a Lagrangian way, rather than being modelled as an extra Eulerian phase. The full particulate phase is modelled by just a sample of individual particles. The tracking is carried out by forming a set of ordinary differential equations in time for each particle, consisting of equations for position, velocity, temperature, and masses of species. These equations are then integrated using a simple integration method to calculate the behaviour of the particles as they traverse the flow domain. While setting up the Lagrangian way particle model, the following assumptions are implied:

- Particle-particle interactions are neglected due to the low particle concentrations experienced.
- The particles are spherical. The physical properties of each phase are constants.
- The mean flow is steady. The turbulent flow is locally isotropic.
- The geometry modification caused by the removal of wall by the sand particles, are neglected.

2.2 PARTICLE TRAJECTORIES COMPUTATION

To evaluate the particle trajectories, its velocity and finally erosion due to the particle movement, it is necessary to develop equation of motion for that particle. Consider a discrete particle travelling in a continuous fluid medium. The forces acting on the particle, which affect the particle acceleration, are due to the difference in velocity between the particle and fluid, as well as to the displacement of the fluid by the particle. The equation of motion for such a particle was derived by Basset, Boussinesq and Oseen (BBO) for a rotating reference frame.

$$m_P \frac{dU_P}{dt} = F_D + F_B + F_R + F_{VM} + F_P + F_{BA} \quad (2.1)$$

Where, F_D is drag force acting on the particle, F_B is buoyancy force due to gravity, F_R is forces due to domain rotation (Centripetal and Coriolis forces) , F_{VM} is virtual (or added) mass force. This is the force to accelerate the virtual mass of the fluid in the volume occupied by the particle. This term is important when the displaced fluid mass exceeds the particle mass, such as in the motion of bubbles, F_P is pressure gradient force. This is the force applied on the particle due to the pressure gradient in the fluid surrounding the particle caused by fluid acceleration. It is only significant when the fluid density is comparable to or greater than the particle density and, F_{BA} is basset force or history term which accounts for the deviation in flow pattern from a steady state. This term is not implemented in ANSYS CFX.

A moving fluid exerts an aerodynamic force which is sum of the drag force (acts in opposite direction to the fluid motion) and lift force (acts normal to the fluid motion). CFX gives consideration to pressure gradient forces of the surrounding fluids and gravitational effects. The lift force effect is simply ignored for the computational ease. Furthermore, virtual mass force, basset force and other forces are normally neglected in view of the large differential density between phases. The equation for the rate of change of velocity within CFX is derived directly from Newton's second law. The velocities are obtained by simply integrating the force balance in a Lagrangian frame of reference.

$$m_P \cdot \frac{dU_P}{dt} = \frac{1}{2} \cdot C_D \cdot \rho_F \cdot A_F \cdot \left|U_F - U_P\right| \cdot \left(U_F - U_P\right) + \frac{\pi}{6} \cdot d_p{}^3 \cdot \left(\rho_P - \rho_F\right) \cdot g - \frac{m_F}{\rho_F} \cdot \nabla P \quad (2.2)$$

In the simplest form of equation of motion, the main term on the right hand side is the drag force that includes the consideration of both skin and form effects. The total drag force is most conveniently expressed in terms of the non dimensional drag coefficient, as defined by the Schiller- Naumann correlation. ANSYS CFX modifies this to ensure the correct limiting behaviour in the inertial regime by taking,

$$C_D = \max\left(\frac{24}{R_e} \cdot \left(1 + 0.15 \cdot R_e{}^{0.687}\right),\ 0.44\right) \quad (2.3)$$

However, this correlation has been developed based upon spherical shape of the particle; the trajectories of the non-spherical particles can be modelled through the application of shape factors, allowing non-uniform drag distribution and bounce characteristics to be classified.

2.3 RESTITUTION COEFFICIENT FOR PARTICLES

The parallel and perpendicular restitution co-efficient describe the action of particles when they hit a wall. The reflected velocity of the particle is lower than the incoming velocity due to energy transfer. Energy is dissipated as heat, noise and target material deformation. This effect is described by the momentum based restitution coefficient. The coefficient values of one described an elastic collision, while values less than one describe an inelastic collision. The parallel coefficient is usually equal to one. The perpendicular coefficient will depend on the particle material. Particle that bounces off walls will have a perpendicular coefficient close to one, while particles that stick to walls will have a perpendicular coefficient of zero. In this simulation, the perpendicular and parallel coefficients of restitutions are chosen equal to 0.9 and 1 respectively.

2.4 TABAKOFF EROSION MODEL

In general, the Tabakoff model provides more scope for customization with its larger number of input parameters. The choice of one model over another is largely simulation-dependent. The erosion model can be set on a per-boundary or per-domain basis. When enabled for the domain, the domain settings will apply for all boundaries that do not explicitly have erosion model settings applied to them. The Tabakoff model requires the specification of five parameters. The k_{12} constant, 3 reference velocities and the angle of maximum erosion γ_0 must all be specified. The erosion rate E is determined from the following relations:

$$E = k_1 \cdot f(\gamma) \cdot V_p{}^2 Cos^2\gamma \cdot \left[1 - R_T{}^2\right] + f\left(V_{P\,N}\right) \tag{2.4}$$

$$f(\gamma) = \left[1 + k_2 \cdot k_{12} \cdot Sin\left(\gamma \cdot \frac{\pi/2}{\gamma_0}\right)\right]^2 \tag{2.5}$$

$$R_T = 1 - k_4 \cdot V_P \cdot Sin\gamma \tag{2.6}$$

$$f\left(V_{P\,N}\right) = k_3 \cdot \left(V_P \cdot Sin\gamma\right)^4 \tag{2.7}$$

$$k_2 = \begin{cases} 1.0 & if\ \gamma \le 2 \cdot \gamma_0 \\ 0.0 & if\ \gamma > 2 \cdot \gamma_0 \end{cases} \tag{2.8}$$

Here E is the dimensionless mass (mass of eroded wall material divided by the mass of particle). V_P is the particle impact velocity. γ is the impact angle in radians between the

approaching particle track and the wall, γ_0 being the angle of maximum erosion. k_1 to k_4, k_{12} and γ_0 are model constants and depend on the particle/wall material combination. The overall erosion rate of a wall due to a particle is computed from the following relation:

$$Erosion\ Rate = E \cdot \dot{N} \cdot m_p \qquad (2.9)$$

Here m_p is the mass of the particle and $\dot{N}$ is its number rate. The overall erosion of the wall is then the sum over all particles. This gives an erosion rate in kg/s, and an erosion rate density variable in the res file and post-processor in kg/s/m^2. Furthermore, this erosion rate is only a qualitative guide to erosion, unless precise values for the model constants are known.

2.5 NUMERICAL MODEL

To achieve a result with second order accuracy and sufficient numerical stability, the high-resolution scheme was applied for discretization of the grid. Turbo Grid 11.0 was selected for meshing because this is a highly automated hexahedral mesh generator, specially designed for turbo machinery. Grids generation is relied on three different factors; namely, number of cells, Reynolds number and turbulence model desired. Two equations turbulence model were chosen initially for grids generation but the SST model gave the most realistic results, and it was decided to continue the simulation with this model only. For setting up a new simulation in ANSYS CFX, the mesh files were imported and merged together to form computational domains as shown in Figures 2.1 and 2.2.

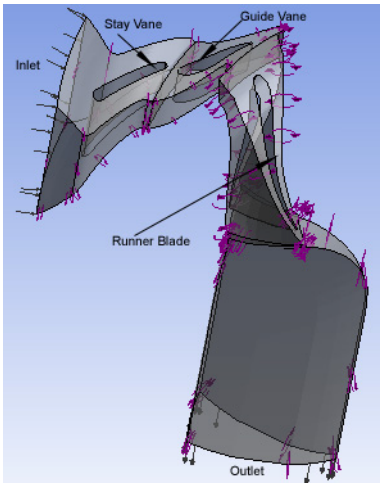

Figure 2.1 Computational Model at BEP

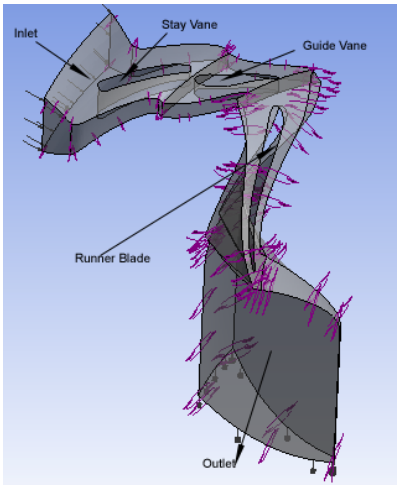

Figure 2.2 Computational Model at Full Load

The key steps of the numerical modelling process mainly include:

(a) Component definition: The component definition panel is used to import meshes and to select the rotation speed of each component and set a tip clearance.
(b) Physics definition: All the physical settings, including fluid type, simulation type, inlet and outlet boundary conditions, interface types and solver parameters are set in this panel. The selection of boundary template, which provides quick setup of the most common turbo machinery boundary conditions, has to be specified in this stage. For this simulation mass flow inlet, pressure static outlet is selected per passage basis.
(c) Interface definition: The frozen rotor interface was selected as the interface default type and set the convergence control to physical timescale with a value of $1/\omega$ [rev/min]. Generally the interfaces are automatically created using the region information from the component definition panel.
(d) Boundary definition: Boundary conditions are also automatically created using the region information from the component definition panel and information from the physics definition panel.
(e) Final Operation: The final operation panel is used to enter in to the general mode of operation for applying other CFX features including sand properties definition and particle tracking etc.
(f) Defining the properties of Sand: The material properties of sand particles used in the simulation needs to be defined in general mode. Heat transfer and radiation modelling are not used in this simulation, so the only property that needs to be defined is the density of sand.

To calculate the effect of particles on continues fluids, between 100 and 1 000 particles are usually required. However, if accurate information about the particle volume fraction or local forces on the wall boundaries is required, then a much larger number of particles need to be modelled. After creating a domain, full coupling or one-way coupling between the particle and continues phase has to be chosen. Full coupling is needed to predict the effect of particles on the continuous phase flow field but has the higher CPU cost than one-way coupling. One-way coupling simply predicts the particle paths during post processing based on the flow field, but without affecting the flow field. To optimize CPU usage, the two sets of identical particles were created. The first set will be fully coupled and between 100 and 1,000 particles will be used. This allows the particles to influence the flow field. The second set will use one-way coupling but a much higher number of particles will be used. This provides a more accurate calculation of the particle volume fraction and local forces on the wall.

Sand particles are uniformly injected at the stay vane inlet with the same conditions as the fluid. The particles will follow through the domains and exit at the outlet. The sand particles are defined as solid particles and the size distribution is uniform in diameter. The turbulence dissipation force is activated, and the Schiller Naumann model is chosen to calculate the drag force acting on the particle.

2.6 BOUNDARY CONDITIONS

If all residual are below their targeted criteria then convergences of equations will prevail. To improve the convergences of simulation and to obtain a conversion of solution with less numbers of iterations in relatively short interval of time, only one set of blades was considered in this simulation analysis. In the post processing, there is a provision to assemble all components of turbine. The two most interesting operating points are at the best point efficiency and full load, with guide vane angle of 16 and 22 respectively. To study the effect of different shape of the particle for predicting erosion rate density, the simulations were carried out at same concentration rates for both operating conditions.

2.6.1 INLET AND OUTLET

When setting boundary conditions, ANSYS CFX best practices guide for Turbo machinery recommended specifying a total inlet pressure and mass flow outlet. This will give a more appropriate calculation of the flow field than with the mass flow inlet condition for those machines drawing fluid directly from a static reservoir. This may be valid for hydraulic pump simulation but in the case of radial turbine, the mass flow inlet and a total pressure outlet was found more appropriate and robust than the total inlet pressure and mass flow outlet. In addition, this provides better performance of turbine, when looked at pressure distribution, y+ values, power output, head and flow rate. Thus, the inlet condition was set as mass flow rate per passage with velocity components. The outlet pressure in this case is arbitrary and is usually set at or close to zero to reduce round off error. In this simulation, this was chosen equal to 1 atm. The detail boundary condition with appropriate value is presented in Table 2.1.

Table 2.1: Boundary conditions

Variable	Value
Water density	997 kg/m^3
Quartz particle density	2.65 gm/cm^3
Diameter of the particle	0.1 to 0.2 mm
Inlet mass flow rate of water at BEP	540 kg/s
Inlet mass flow rate of water at Full Load	685 kg/s
Total pressure outlet	1 [atm.]
Inlet mass flow rate of particle	0.05 kg/s per passage
Inlet flow direction at Stay vanes (α, r, θ)	0 , -0.4 , -0.9165

2.6.2 WALL

The covers, hub, shroud and vanes were defined as smooth walls with no-slip condition. Fluid velocities near the wall will then be decreased by the wall friction. The runner has an angular velocity 600 rpm, while the stay vane and guide vane are stationary domains.

A periodic boundary condition was set to couple two adjacent blades. This simplified the computational model.

3. RESULTS AND DISCUSSIONS

Figure 3.1 and 3.2 shows the prediction of erosion rate density along the blade surface at 16 ^{0} guide vane angle which is at maximum efficiency point. It can be clearly seen from the figures that maximum erosion occurs in the blade profile with shape factor of 0.5. The particles shape factor assumed to be spherical by default in ANSYS and its value is equal to 1. If the particle is deviated from spherical shape then shape factor value is less than 1. ANSYS CFX always calculates the diameter of the particle from the mass of the particle divided by its density, assuming it is spherical. A cross sectional area factor can be included to modify the assumed spherical cross section area to allow for non-spherical particles. This affects the drag force calculated by ANSYS CFX. The surface area factor is analogous to the cross sectional factor.
For non-spherical particle, it is the ratio of the surface area to the surface area of spherical particle with the same equivalent diameter. This affects both mass transfer and heat transfer correlation.

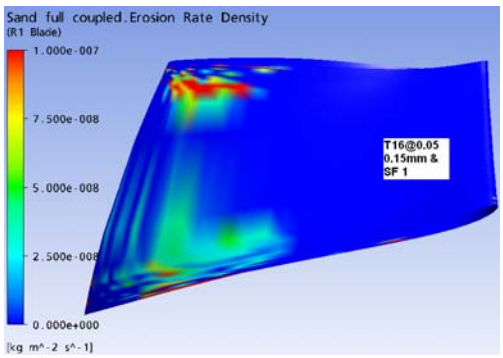

Figure 3.1 Erosion rate at BEP @ SF 1

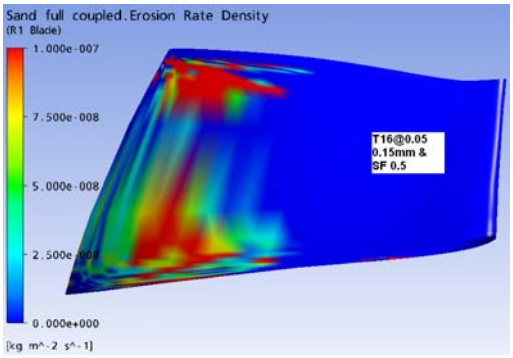

Figure 3.2 Erosion rate at BEP @ SF 0.5

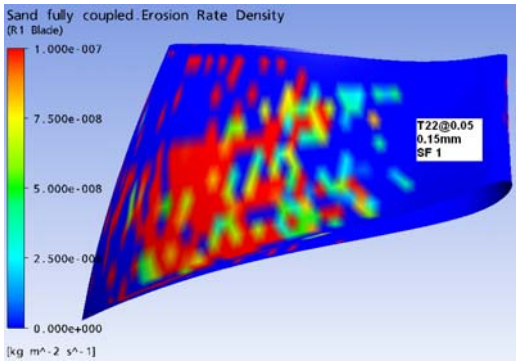

Figure 3.3 Erosion rate at Full Load @ SF 1

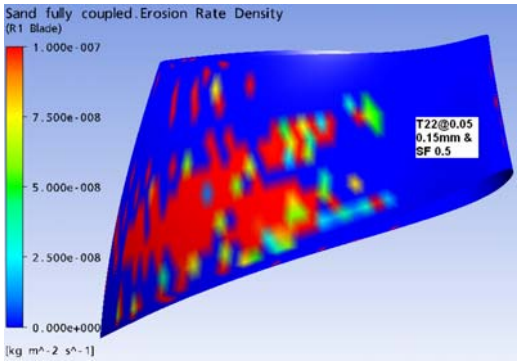

Figure 3.4 Erosion rate at Full Load @ SF 0.5

Similarly, Figure 3.3 and 3.4 shows the prediction of erosion rate density along the blade surface at 22 ^{0} guide vane angle which is at full load condition. It can also be clearly seen from the figures that maximum erosion occurs in the blade profile with shape factor 0.5. A similar erosion pattern is observed in each case. However, the blade profile area is highly affected and larger intensity of erosion rate is clearly observed in the case of non-spherical shape of the particle. The erosion rate density of pressure side is more than of the suction side of the blade. This is even more in larger the guide vane opening. The erosion rate density is more towards the outlet as compare to the inlet of the blade. This may be due to the blade profile tail vortex flow, which leads to increasing the erosion rate density in the blade outlet.

To validate simulation result, a test rig, was developed and designed at the Waterpower Laboratory, Norwegian University of Science and Technology, Norway. The velocity of particle was calculated in highly swirl conditions similar to turbine flow in curved path, and found that the size of the particle is inversely proportional to the velocity of the particle, and it also depends upon the shape of the particle. Different shapes of particle were tested, and it was determined that spherically shaped particle had higher velocity than particle with other shapes. Generally the erosion rate density will increase when the velocity of particle increase. However, this has not occurred in this simulation analysis because of shape factor of the particle.

In general, many natural particles are usually in non-spherical shape. These particles will tend to have lower velocities because both decreases in spheroid and increases in angularity tend to decrease velocities. The impact area of these particles on the eroded surface is relatively larger and tends to be directed perpendicular to the transport path. As a result, higher co-efficient of drag, higher rotational motion and more separation of flow likely to occur and hence more erosion rate is found.

4. CONCLUSIONS

The operation of turbine at full load not only caused poor efficiency but also increased turbulence and higher relative velocity of flow at outlet of the blade. This also creates strong swirl flow in turbine. The role of operating conditions on erosion rate density clearly demonstrated in simulation analysis. It has been shown that predicted erosion rate density is in good agreement with the experiments. It has been found that erosion process is strongly depended on the shape of the particle. Furthermore, the significant reduction of erosion rate can be achieved by operating turbine in best efficiency point as far as possible.

REFERENCES

1. ANSYS: CFD online, http://www.cfd-online.com/[Accessed on 31 August 2009]
2. ANSYS Turbo Grid Release 11.0. Users guide, 2006.

3. ANSYS CFX Release 11.0 Solver Theory Guide, 2006.
4. Brekke Hermod, 2002. Design of hydraulic machinery working in sand laden water. Abrasive erosion and corrosion of hydraulic machinery, London.
5. Bergeron S. Y., T. C. Vu, and A. P. Vincent, 2002. Silt erosion in hydraulic turbines: The need for real-time numerical simulations.
6. Doby M. J., A. F. Nowakowski, E. Nowak, and T. Dyakowski, 2007. Numerical and experimental examination of swirl flow in a cylindrical container with rotating lids. Minerals Engineering 20(4): 361 - 367.
7. Forder A., M. Thew, and D. Harrison, 1998. A numerical investigation of solid particle erosion experienced within oilfield control valves. Wear 216(2): 184 - 193.
8. Finnie I., 1972. Some observations on the erosion of ductile metals. Wear 19: 81 - 90.
9. Gabitto J. and C. Tsouris, 2008. Drag coefficient and settling velocity for particles of cylindrical shape. Powder Technology 183(2): 314 - 322.
10. Liu X.B., L.D. Zhang, Z. Liang, and L.J. Cheng, 1996. Numerical prediction of silt abrasive erosion in hydraulic turbine. Fluids Engineering Division Conference Volume 1, ASME.
11. Mack R., P. Drtina, and E. Lang, 1999. Numerical prediction of erosion on guide vanes and in labyrinth seals in hydraulic turbines. Wear. 233 - 235: 685 - 691.
12. Neopane Hari P., Ole G. Dahlhaug, and Thapa Bhola, 2009. Experimental examination of the effect of particle size and shape in hydraulic turbines. Waterpower XVI, Spokane, Washington, USA.
13. Naidu D. B. K. S., 1999. Developing silt consciousness in the minds of hydro power engineers. Silting problems in hydro power plants, New Delhi, India.
14. Ole G. Dahlhaug and Thapa Bhola, 2004. Sand erosion in Francis turbine: a case study from Jhimruk power plant, Nepal. 22nd IAHR Symposium on Hydraulic Machinery and System, Stockholm, Sweden.
15. Padhy M. K. and R. P. Saini, 2008. A review on silt erosion in hydro turbines. Renewable and Sustainable Energy Reviews 12(7): 1974 - 1987.
16. Stachowiak G. W. and A. W. Batchelor, 2006. Abrasive, erosive and cavitation Wear. Engineering Tribology (3 Edition). Burlington, Butterworth-Heinemann: 501 - 551.
17. Thapa Bhola and Brekke Hermod, 2004. Effect of sand particle size and surface curvature in erosion of hydraulic turbine. IAHR symposium on hydraulic machinery and systems, Stockholm.
18. Thapa Bhola, 2004. Sand erosion in hydraulic machinery, PhD thesis, Norwegian University of Science and Technology, Faculty of Engineering Science and Technology, Department of Energy and Process Engineering, 2004: 105.
19. Truscott G. F., 1972. A literature survey on abrasive wear in hydraulic machinery. Wear 20(1): 29 - 50.
20. Zhang Y., E. P. Reuterfors, B. S. McLaury, S. A. Shirazi, and E.F. Rybicki, 2007. Comparison of computed and measured particle velocities and erosion in water and air flows. Wear 263(1 - 6): 330 - 338.